STATE OF CALIFORNIA • DEPARTMENT OF TRANSPORTATION
TECHNICAL REPORT DOCUMENTATION PAGE
TR0003 (REV 10/98)

1. REPORT NUMBER	2. GOVERNMENT ASSOCIATION NUMBER	3. RECIPIENT'S CATALOG NUMBER
CA17-2755		

4. TITLE AND SUBTITLE	5. REPORT DATE
Nonlinear Time History Analysis or Ordinary Standard Bridge	May 16, 2017
	6. PERFORMING ORGANIZATION CODE
	OSU, UCF

7. AUTHOR	8. PERFORMING ORGANIZATION REPORT NO.
Kevin R. Mackie, Michael H. Scott, Karryn Johnsohn, Munaf Al-Ramahee, Michael Steijlen	

9. PERFORMING ORGANIZATION NAME AND ADDRESS	10. WORK UNIT NUMBER
Oregon State University, School of Civil and Construction Engineering, 101 Kearney Hall, Corvallis, OR 97331	
University of Central Florida, Department of Civil, Environmental, and Construction Engineering, 12800 Pegasus Dr. #211, Orlando, FL 32816	11. CONTRACT OR GRANT NUMBER
	65A0559

12. SPONSORING AGENCY AND ADDRESS	13. TYPE OF REPORT AND PERIOD COVERED
California Department of Transportation	Final Report
Division of Engineering Services	7/1/2015 – 4/30/2017
1801 30th Street, MS #9-2/5i	14. SPONSORING AGENCY CODE
Sacramento, CA 95816	913

15. SUPPLEMENTARY NOTES

Prepared in cooperation with the State of California Department of Transportation.

16. ABSTRACT

Reliable seismic response models are necessary to support the assessment and design of California highway bridges. To this end, similar results for nonlinear static and dynamic time history response should be obtained between disparate software packages. This requires transparency of the element and constitutive model formulations implemented in the software. Models of four ordinary standard bridges (OSBs) are created using the CSiBridge and OpenSees software packages, both widely used for bridge engineering applications. Similar distributions of mass and stiffness are achieved from each software package, as evidenced by agreement in modal analyses for models with simple roller abutments as well as models with nonlinear abutments. A series of benchmark problems show that the software packages are able to produce similar results for lumped and distributed plasticity frame elements. Further calibration and matching of constitutive models show that similar nonlinear static responses are attained for each OSB; however, the cyclic behavior of the constitutive models differ significantly, leading to discrepancies in dynamic response. Sensitivity analysis based on the direct differentiation method available in OpenSees shows the effect of modeling parameters on the response of each OSB. The most significant parameters were found to be the stiffness and strength of the abutment models.

17. KEY WORDS	18. DISTRIBUTION STATEMENT
Nonlinear analysis, Earthquake loading, Sensitivity analysis, Ordinary bridges, Constitutive models, Finite element formulations, Benchmarks, Verifications	No restrictions

19. SECURITY CLASSIFICATION (of this report)	20. NUMBER OF PAGES	21. COST OF REPORT CHARGED
None	266	

Reproduction of completed page authorized.

Nonlinear Time History Analysis of Ordinary Standard Bridges

by

Kevin R. Mackie (Co-Principal Investigator)
University of Central Florida

Michael H. Scott (Principal Investigator)
Oregon State University

Karryn Johnsohn
Oregon State University

Munaf Al-Ramahee
University of Central Florida

Michael Steijlen
University of Central Florida

FUNDING AGENCY ACKNOWLEDGMENT

DISCLAIMER STATEMENT

EXECUTIVE SUMMARY

Nonlinear Time History Analysis of Ordinary Standard Bridges was a joint effort by research teams from Oregon State University and the University of Central Florida. The objectives of this study were two-fold: 1) To assess the ability of disparate software packages, namely CSiBridge and OpenSees, to give similar results for nonlinear time history analysis of four ordinary standard bridges (OSBs); and 2) To assess the sensitivity of nonlinear time history response of the OSBs with respect to material properties and modeling assumptions. The four OSBs each have two-span continuous superstructures. Two of the OSBs (OSB1 and OSB2) have integral bents, with OSB1 having a two-column bent and OSB2 having a single-column bent. The other two OSBs (OSB3 and OSB4) have isolation bearings between the superstructure and bent/abutments, with a similar breakdown of columns per bent (OSB3 has a two-column bent, for example). The technical content of the report is broken down into four parts followed by modeling recommendations.

The first part addressed benchmarking implementations of lumped and distributed plasticity in cantilever columns. It was demonstrated that both CSiBridge and OpenSees can be used to correctly implement a lumped plasticity approach for 2D and 3D analysis of simple steel and concrete cross sections, relative to the exact solution based on Euler-Bernoulli assumptions. OpenSees can be used to correctly implement the distributed plasticity approach, again relative to the reference solution. In both the lumped and distributed plasticity cases, the explicit consideration of the cross section with associated uniaxial constitutive models is beneficial in accounting for axial-moment interaction, as well as excitation about an arbitrary axis for the cross section. The discrepancies that arise from the series arrangement of the elements in the lumped approach can be approximately corrected, particularly for the initial stiffness and yield force. However, this creates issues with the post-yield hardening and softening behaviors, as well as cyclic response.

The second part utilized the approximately corrected lumped plasticity approaches to compare the nonlinear static and nonlinear time history analysis (NTHA) of the four OSBs, as implemented in CSiBridge and OpenSees. Constitutive models of the columns were standardized, as possible, followed by the elements and springs governing the isolation bearings and abutment boundaries. Sectional analysis, nonlinear static analysis of the column hinge elements, and pushover analysis of the bents were performed for OSB1 and OSB2. Cyclic analysis on the isolator elements was performed for OSB3 and OSB4. Modal analysis and NTHA were performed for all OSBs under two different boundary conditions: an original configuration based on the Caltrans CSiBridge models and a second based on making the boundary conditions simple rollers. Care was taken to enforce the common model basics in the two implementations, and it was demonstrated that the two software implementations could be used to generate nominally similar responses for the OSBs. However, it was shown that the agreement in terms of trends and magnitudes was highly dependent on the abutment boundaries and the cyclic response of the column concrete constitutive model.

The third part utilized a set of OpenSees models based on distributed plasticity for the four OSBs to perform sensitivity analyses. Pushover and NTHA model predictions were first compared with those in the previous part, followed by sensitivity analyses using

the direct differentiation method (DDM) for parameters such as the column reinforcing details, abutment strengths, isolator strengths, and superstructure stiffness. The sensitivity analyses revealed that the stiffness and strength of abutment gap models have a significant influence on the nonlinear static and dynamic response of all OSBs. Although they receive predominant attention in the literature, reinforcing details and modeling assumptions for the columns have less influence on the response of OSB1 and OSB2; however, the influence is not insignificant. As expected for OSB3 and OSB4, the stiffness and strength of the isolators have a large influence on the dynamic response. Depending on the boundary conditions at the abutments, the assumed stiffness of the superstructure can have a seemingly large influence on the bridge response.

Contents

List of Figures

List of Tables

16

17

Chapter 1

Project Summary

General purpose finite element tools such as Perform, SAP2000, CSiBridge, OpenSees, etc. have put nonlinear time history analysis (NTHA) within an engineer's reach for the assessment of ordinary bridge response to seismic loading. While these tools predict structural response more accurately compared to response spectrum or nonlinear static methods, it has been observed that the response is extremely sensitive to modeling details as well as the algorithms employed to find a numerical solution to the nonlinear equations of dynamic equilibrium. Furthermore, these tools can give significantly different results due to inherent modeling assumptions and mathematical formulations of element response that are not readily apparent. Without modeling guidance and safeguards against numerical instabilities, NTHA can give results that are incomplete or that controvert engineering judgment.

1.1   Introduction

NTHA has been used successfully for simulating the seismic response of special bridges in California. The vast majority of California bridges, however, are ordinary bridges, e.g., two-span overpasses, for which traditional methods, such as response spectrum and static pushover analysis, are employed. These traditional methods result in conservative estimates of the effect of cyclic energy dissipation and degradation. To achieve confident results for a variety of earthquake scenarios, the idealized model should also contain a realistic representation of the geometry, boundary conditions, gravity load, mass distribution, and energy dissipation for all major components of the bridge.

If a simple linear elastic model of a bridge structure is used, the corresponding analysis will only accurately capture the static and dynamic behavior of the system when stresses in all elements of the bridge do not exceed their elastic limit. Beyond that demand level, the forces generated by a linear elastic analysis will differ considerably from the actual force demands on the structure; however, the displacements are shown to be a reasonable estimate of the actual displacements. Such a linear model will fail to capture the effects of many sources of inelastic response of the bridge such as the effects of the surrounding soil at different shear strain levels, cyclic yielding of structural components, opening and

closing of superstructure expansion joints, engagement, yielding and release of restrainers, and the complex nonlinear abutment behavior. Both linear and nonlinear modeling are supplementary tools that allow the trained designer and analyst to verify results against known ranges and established structural behavior during past earthquakes.

Nonlinear modeling and analysis allows more accurate determination of stresses, strains, deformations, forces, and displacements of critical components. It provides a mechanism for incorporating realistic material behavior beyond the elastic limit, loss of stiffness due to nonlinear geometric (P-Δ) effects, and contact nonlinearity. Results from nonlinear analysis can then be utilized for the final design of the bridge subsystems or for evaluation of its global capacity and ductility. However, the resulting response values are potentially sensitive to small variations in the input parameters. To obtain an accurate representation of the nonlinear behavior of the bridge structure, it is necessary for the design engineer to have a clear understanding of basic nonlinear analysis concepts and to have guidance on parameter selection and the consequences of choices, as inferred from suitable parametric sensitivity studies, made at the input level.

Unfortunately, the additional level of sophistication of the nonlinear model will also increase the computational effort required for the analysis, as well as the difficulty in the interpretation of results. The accurate estimation of the peak demand and response of the bridge structure under dynamic excitation requires the use of a suite of ground motions, and will therefore further increase the complexity of the analysis process and size of the output data. Therefore, three (3) important considerations arise in nonlinear analysis in addition to parameter selection: 1.) understanding the balance between model complexities and the corresponding gain in accuracy of the results (i.e., when is nonlinear analysis needed), and 2.) making both input and output readily accessible and understandable (i.e., user interface to nonlinear models), and 3.) ensuring that the element and material formulations in a given software are understood relative to the linear and nonlinear responses (i.e., whether or not the numerical results are reliable).

In general, the modeling assumptions should be independent of the computer program used to perform the static and dynamic analysis; however, mathematical models are often limited by the capabilities of the computer program utilized. Therefore, the proposed work involves proper parameter selection and input into OpenSees and CSiBridge/SAP2000. However, the guidance on how similar results can be produced between these two software packages, or potentially any other general purpose structural analysis software, will provide more general insight and illustrate the consequences of analytical formulations on response.

1.2 Background Research

Previous work on NTHA of ordinary bridges was formalized into PEER report 2008/03 "Guidelines for Nonlinear Analysis for Bridge Structures in California" [2]. This report provides detailed written guidelines on the construction of three-dimensional (3D) models that utilize one-dimensional elements (frames, links, and hinges) in both OpenSees and SAP2000.

The report contains information on modeling options, analysis options, and guidelines on model construction for both nonlinear static and nonlinear dynamic analysis. Different static pushover patterns, eigenvalue or Ritz-vector analysis options, nonlinear abutment models, damping and time history integrator parameter selection, and response spectrum analysis are illustrative of the broad scope and depth of information available. The primary findings and recommendations are presented in easy to follow tables and cut-away views of an idealized bridge. The components required to be modeled using nonlinear elements are suggested for each analysis type (primarily abutments and piers), and recommendations are made on the accuracy of results. For example, fiber hinges should be used for nonlinear 3D NTHA in SAP.

Bias factors with respect to stiffness and strength degrading materials in OpenSees showed that SAP may not yield conservative results for all ground motions (bias factors ranged between 1 and 3). Another contribution of the report is the calibration of parameters against known solutions (for a simple cantilever column case) and against OpenSees models. These calibration practices are particularly important to have when formulation of individual elements may result in incorrect 3D response that can be knowingly accounted for *a priori* (for example, 3D response of some SAP plastic hinge models have incorrect stiffness and yield values).

While the guidelines allow direct implementation in SAP, direct software tools, guidelines, and input files are not provided for NTHA using OpenSees. In addition, multiple ground motion inputs were considered in the analyses; however, no constructs were provided for performing parameter variation or sensitivity studies directly in OpenSees. Parameter studies are best performed with the computational control provided by the linkage of OpenSees with the Tcl scripting language as manual perturbation of parameters and continual save/run/visualize actions in SAP2000 can be overly cumbersome.

To follow up on the modeling and analysis recommendations made in the 2008/03 PEER report, Caltrans sponsored additional studies on "Parametric Study of Ordinary Standard Bridges using OpenSees and CSiBridge" under contract #65A0445 [18] and "Guidelines for Nonlinear Seismic Analysis of Ordinary Bridges: Version 2.0" under contract #65A0454 [22]. The same four ordinary standard bridges considered in this report (OSB1 through OSB4) were studied in #65A0445, whereas three representative bridges (Jack Tone Road Overcrossing, La Veta Avenue Overcrossing, and Jack Tone Road Overhead) were considered in #65A0454. La Veta is one of the bridges analyzed in the original study [2].

Recently completed work by researchers at University of California, San Diego (UCSD) led to the development of a graphical user interface (GUI) for a set of OpenSees-based tools, named MSBridge. The GUI allows rapid model building for a broad range of typical bridge configurations, and graphically displays output. The interface was used to generate numerous time history responses and compare with equivalent static analysis. The four OSB bridges were analyzed under several ground motions and three different abutment conditions (roller, elastic-perfectly-plastic gap, and elastic-perfectly-plastic gap with elastomeric bearings models). However, the work did not interpret results obtained via MSBridge, e.g., through parametric studies that could be used as a tool for establishing reasonable bounds

on bridge response to seismic loading. Simple examples that highlighted and explained the differences between basic structural elements and nonlinear material models in MSBridge, which uses distributed plasticity and plastic hinge formulations, and CSiBridge, which uses concentrated plasticity formulations, were not presented.

Modeling issues related to abutments, expansion joints, and soil-structure interaction (SSI), all of which were outside the scope of the 2008/03 PEER report, were first addressed with #65A0454. The v2.0 guidelines were intended to expand upon the original guidelines in the PEER report by incorporating soil-structure interaction effects, revisiting nonlinear component models, a look into numerical integrators and algorithms, and a more comprehensive ground motion selection and scaling treatment for bridges. The primary refinements were in the nonlinear spring models of the abutments (backfill springs oriented perpendicular to the backwall), SSI in pile shafts, shear key models, and in-span hinge models. Transverse response and interaction at the abutment were neglected (beyond the shear key and springs normal to backwall). The study included several different skew angles when considering the dependence of response quantities on the properties of the shear keys and backfill springs.

Sensitivity of column ductility, deck displacement/rotation, and unseating to shear key and backfill properties were presented, showing larger displacement demands for the brittle shear key case and smaller backfill resistance. Results highlighted the importance of abutment boundary properties on quantifying bridge response. A reduced-order model was used to study pile SSI effects that included an option for pinned column-to-pile cap connection. Global bridge displacement demands were relatively insensitive compared to reference boundary condition cases, but provided useful estimates of pile curvature distributions. The consideration of foundation models is important in the case where nonlinear behavior moves into the foundation and impacts the kinematic and force demands on the bents.

The algorithm and integrator studies reviewed existing methods available in OpenSees. Ground motion selection and scaling comparisons were drawn between conditional mean spectrum, unconditional spectrum, and spectral acceleration (at first mode), with respect to a reference case (using larger number of motions). Small differences were observed in the different response parameters except for local measures using the selection and scaling techniques, the unconditional method suggested for use as slightly conservative in case of the local measures.

1.3 Current Research Approach

The research presented in this report addresses two broader needs. The first need is for sensitivity and parametric studies that relate to understanding the role of uncertain parameters on the nonlinear static and dynamic response of common bridges. Based on previous work, this has not been rigorously performed for California bridges. The second need is implementation efficacy, or better quantification of behavior of common bridges using commercial software. This includes the ability to easily obtain similar results between two software packages and it requires a thorough understanding of the finite element formulations, constitutive models, and solution algorithms implemented in each package.

Addressing these needs should relate back to the use of nonlinear analysis tools for typical bridges as opposed to special projects only. These two needs should also relate to the cost of design and broader performance-based impacts that can be demonstrated using NTHA tools over more conventional linear elastic or response spectrum methods. The structures selected for demonstration should be reflective of a range of ordinary standard bridges. Hence the effects of multiple bents, multiple-column bents, skew, superstructure elevation, curves, bearings, abutments, expansion joints, and potentially soil-structure compliance are not included in this research; however, this research should form the basis for further investigation of these nonstandard features.

The research presented here is not intended to minimize the importance of, or need for additional, experimental studies to quantify the response of bridge components and sub-assemblies under seismic loads. The research emphasis here is complementary in two ways: 1.) it provides a basis for judgments on what the most important model and model parameters are within the nonlinear load-resisting response mechanisms, and 2.) it emphasizes the distinct differences in being able to standardize nonlinear static vs nonlinear dynamic responses and the significant effect of the latter on predicted nonlinear time history response metrics.

Chapter 2

Literature Review

Nonlinear time history analysis (NTHA) of highway bridges has been a widely studied topic due to the adoption of performance-based earthquake engineering (PBEE) methodologies, the development of advanced finite element models, and the steady increase of computational power. While computing resources enable a large number of analyses to be carried out quickly, a significant amount of uncertainty persists in the modeling of nonlinear bridge response to seismic loading. This uncertainty lies in the numerical formulations and software implementation of the finite element response and variability, or randomness, of structural properties, among other factors. While the ability to account for such uncertainties is an advantage of PBEE [16], there are barriers to its adoption by practicing engineers. Expert knowledge may be required to perform detailed nonlinear dynamic analyses that account for uncertainties. In addition, inconsistencies can arise when using different software tools to carry out these analyses. Modeling decisions regarding abutment response and soil-structure-interaction are among the largest and most dominant sources of uncertainty.

2.1 Current State of NTHA

Kunnath [16] discusses the I-880 viaduct testbed project, which aims to validate the PEER performance-based earthquake engineering (PBEE) methodology and identify its strengths and drawbacks. The I-880 viaduct was designed with the PBEE methodology, and a simulation model was constructed based on this design. Force-based nonlinear beam column elements with fiber sections were used to consider the spread of plasticity along the pier columns. Elastic beam elements were used to model the bent cap and the longitudinal box girders. Soil-structure interaction (SSI) was also considered using six uncoupled elastic zero-length elements to represent all degrees of freedom provided by the soil-foundation system. To determine the spring constants for these six degrees of freedom, three-dimensional linear elastic finite element models were created for the piles and soil under each bent. Radiation damping was omitted when considering SSI. The shear keys, restrainers, and bearing pads were modeled using discrete zero-length elements. In the transverse direction, the shear key is modeled using elastic-perfectly-plastic gap elements. Member masses were distributed and

lumped at 1/3 points.

Fenves and Ellery [11] investigated the failure mechanism of the Route 14/Interstate 5 Separation and Overhead bridge during the Northridge, California earthquake and examined modeling and analysis recommendations for earthquake engineering of highway bridges. To this end, the authors developed a nonlinear inelastic model of the selected bridge. The superstructure and bent caps are modeled using linear elastic beam-column elements. The pier columns are modeled using inelastic beam-column elements using a fiber cross section model. The soil backfill and support conditions at the abutments are modeled with nonlinear spring elements in conjunction with gap elements. The authors considered soil-structure interaction by implementing bilinear springs along the length of the shaft (p-y springs) to represent the nonlinear force-deformation relationship for the shaft and soil. Radiation damping was omitted when considering SSI. After simulation of earthquake forces, the authors determined that the most likely cause of collapse was the shear failure of one of the piers. The nonlinear model was also compared to two three-dimensional linear models, a compression model, where the intermediate hinge is assumed closed, and a tension model, where the intermediate hinge is assumed open. The authors concluded that the compression model adequately represents the displacement demands on the bridge.

Choi et al. [6] modeled four bridges to develop fragility curves for bridges in the Central and Southeastern United States. Though the current research is not concerned with fragility curves, the bridge modeling assumptions are of interest. The authors modeled the deck and prestressed girders as one linear beam-column element with the assumptions that the girders and deck are composite and that they will remain elastic under longitudinal seismic loads. The column cross-sections were modeled as a series of fiber elements. In these models, the authors chose to treat the compressive strength of concrete and the yield strength of steel as random variables to take into account material uncertainty and variability. Abutment effects were modeled to account for both passive and active action. In modeling the pile foundations, linear translational and rotational springs were used in combination. Pounding effects were also considered utilizing trilinear compression only elements in tandem with a gap representative of the expansion joint.

Erhan and Dicleli [10] compare the seismic performance of integral and conventional bridges using finite-element modeling. The authors modeled the longitudinal deck and prestressed girder superstructure as a single segmented linear 3D beam element assuming full composite section properties. In the transverse direction, at abutment and pier locations, the deck was modeled as a rigid bar between edge girders. This rigidity simulates the interactions between the axial deformation of the columns and torsional rotation of the bridge deck, and the interaction between the in-plane rotations of the deck and displacements of the bearings. The column piers and the foundation piles were modeled using nonlinear concentrated plasticity hinge elements, calibrated with prescribed moment-curvature relationships. Reinforced concrete abutments were modeled as a grid of frame elements using nonlinear springs and dashpots. Mass of the superstructure was assigned, based on tributary areas, at the nodes of the superstructures segments. The substructures tributary masses were assigned at the joints between the cap beam and the columns. Pounding and shear key effects were also

simulated. The cyclic soil-pile interaction was modeled based on hysteresis behavior using nonlinear link elements. Dashpots were utilized to model the damping effects of the pile impacting the surrounding soil. Through a sensitivity study, the authors determined that friction at the interface of abutments and backfill soil is negligible in the seismic response of bridges.

Hajihashemi et al. [13] investigated the effect of two support modeling conditions on the seismic response of bridge structures. The first was a basic support condition where the base of each column was fixed in both rotation and translation; the bridge ends were fixed against rotation and vertical translation while lateral and transverse translation were supported by linear springs. The second was a nonlinear support condition where all fixities remained the same as the basic configuration except that the lateral and transverse translation were supported by nonlinear springs based on a detailed soil-structure analysis. From the results, the author concluded that the basic support condition resulted in a conservative seismic response when compared to the nonlinear support condition. While the nonlinear support condition produces relatively realistic results, the basic support condition requires considerably less modeling effort as soil-structure interaction need not be considered.

Kunde and Jangid [15] investigated the effects of deck and column flexibility on the seismic response of isolated bridges. To this end, three numerical models were constructed. The first model considered flexibility in both the superstructure and the columns. The second model considers flexibility in the columns only while the third model excludes flexibility of both the superstructure and the columns. After comparison of the different models responses, the authors conclude that three models were comparable with computational efficiency increasing from the first to the third model. Though the models were comparable, the third model underestimates deck accelerations and peak responses diverge as the flexibility of the deck and columns increase.

Rahmani et al. [24] developed a 3D continuum model of the Meloland Road overpass. This model utilized several nonlinear finite elements, including eight-node brick elements and four-node shell elements to represent the response of the foundation system. The pile columns were modeled as nonlinear elastoplastic elements. The remainder of the bridge structure is modeled using elastic elements, as they are capacity-protected by design. After analysis of the bridge model and comparison to the actual response of the bridge during two earthquakes, the authors concluded that for complete bridge systems, continuum modeling is potentially an effective tool for detailed analysis, but requires high-performance computing to perform a timely analysis.

Aviram et al. [3] generated finite-element spine models of six typical California reinforced concrete box girder bridges to develop practical modeling recommendations for the nonlinear analysis of these bridges under seismic ground motions. Recommendations were developed for modeling the superstructure, cap beams, pier columns, abutments, expansion joints, soil-structure interaction, and damping. Two software packages were employed to aid in the development of these recommendations, SAP2000, and OpenSees. The SAP2000 and OpenSees models used similar modeling assumptions for the superstructure, cap beam, and abutment system, but the column bent models used differing assumptions. The OpenSees

model utilized a distributed plasticity model while the SAP2000 model utilized a lumped plasticity model. Upon comparison, the results, of the NTHA for these two packages, were found to disagree, despite the fact that the two models agreed for eigenvalue and pushover analyzes. The authors stated differences in element formulation between modeling software as the cause of the discrepancy and found the discrepancy between results to increase with intensity. Due to these discrepancies, the authors recommend further research.

Salveson and Fell [25] investigated the adequacy of existing design codes in the state of California concerning abutment shear keys. To this end, linear elastic bridge models were created with and without nonlinear shear key elements. A rate-independent force-deformation model was used to simulate the nonlinear response of bridge shear keys. This model considered gap effects along with realistic deformations models. After comparison of the results, the authors noted that linear shear key models yield conservative results when compared to their nonlinear counterparts. The authors suggested more rigorous and complete research efforts to develop and validate more accurate bridge shear key models.

Kwon and Elnashai [17] utilized soil-structure interaction to derive fragility curves for bridges in the Central and Eastern United States. Two different modeling software packages were utilized. The bridge structure was modeled in Zeus-NL with the substructure elements modeled as fiber sections. The authors modeled embankments, abutments, and foundations in OpenSees by implementing a soil mesh, matching realistic soil material models. The results of these models showed the embankment and abutment system have highly nonlinear behavior.

In a study conducted by Erhan and Dicleli [9], five structural models were constructed with gradual simplifications in soil-pile and soil-abutment interactions. The most sophisticated of these models considered free field effects, local soil-pile interaction, global soil-pile interaction and radiation damping while the simplest model entirely excludes nonlinear soil-bridge interaction. The authors concluded, after comparing the results from the five models, that the seismic response of bridges is considerably affected by soil-bridge modeling assumptions, especially for higher intensity ground motions. Though the simplified models produce a similar response to the most complex model for low-intensity ground motions, the authors recommend caution when utilizing simplified models with high-intensity ground motions as these models may not consistently capture the highly nonlinear bridge behavior at higher intensity ground motions. This finding is consistent with Aviram et al. [3].

Jeremic et al. [14] discussed the response of highway bridges concerning the effect of soil-foundation-structure interaction. To this end, a finite element model of the I-880 Viaduct was developed. The inelastic seismic response of both the soil and the structural components was included. The superstructure is modeled using elastic elements, the pier columns are modeled using inelastic fiber beam elements, and the soil-foundation-structure interaction is modeled using equivalent zero-length springs. Elastic soil properties were utilized in a three-dimensional finite element model of the pile group foundation system to determine the foundation spring stiffnesses. The authors compared the seismic response of the I-880 Viaduct with and without soil-foundation-structure interaction; the results demonstrated that under moderate to severe ground motions the inclusion of soil-foundation-structure

interaction increased displacement demand, conversely under mild ground motions the inclusion decreased displacement demand. From this comparison, the authors concluded that the effect of soil-foundation-interaction could have either a beneficial or an adverse effect on the seismic response of the structure dependent on the intensity of the ground motion input.

Zhang et al. [31] investigated soil-structure-interaction concentrating on the application of the Lysmer-Kuhlemeyer transmitting/absorbing boundary. To this end, the authors developed a two-dimensional nonlinear OpenSees model of the Humboldt Bay Bridge using fiber beam-column elements for the pier columns and foundation piles, and linear elastic beam-column elements for the superstructure. The nonlinear soil domain model incorporates liquefaction effects and effective stresses. The model uses four-node, finite elements for various soil layers. Viscous dampers, tangential and normal to the soil boundaries, are used to model a modified Lysmer transmitting/absorbing boundary. After comparison of linear elastic soil to elastoplastic constitutive behavior, soil nonlinearity is determined to significantly affect wave propagation through the soil foundation.

Aviram et al. [1] performed a sensitivity study on the effect of abutment modeling on the seismic response of bridges. Three abutment models were considered, listed in order of complexity: spring, simplified and basic. The spring abutment considers the response of elastomeric bearing pads, concrete shear keys, wing walls, abutment back wall, abutment piles and soil backfill material. The simplified abutment simplifies the spring model considering only the gap and embankment fill response. The basic abutment only restrains vertical translation. The results of the study indicate that the nonlinear behavior of abutments does not control the nonlinear response of long bridges as significantly as it does for short bridges. Therefore, the authors recommend the use of the basic abutment for long spans only and recommend the spring abutment for short spans. The simplified model also underestimates displacement in the transverse direction.

Mackie and Stojadinovic [19] performed a sensitivity study on the influence of two different abutment models on the seismic response of short and medium length bridges using Probabilistic Seismic Demand Analysis. The test bridge was modeled after typical new California highway overpasses consisting of two equal spans with seat-type abutments and a single column bent. The first abutment model considers back wall passive pressure, wall shear strength, and pile group stiffness and strength in the longitudinal direction. In the transverse direction, this model considers resistance from wing walls, shear keys, and pile groups. The second abutment model derives soil stiffness per unit length from cross-section geometry, soil shear moduli, and unit weight. The unit length stiffness is assumed to apply in both the transverse and longitudinal directions. After sensitivity studies had been performed, the authors concluded that the participating length of the abutment, which affects the participating mass, is the most critical abutment modeling parameter and that both abutment modeling approaches are adequate.

Scott and Ryan [27] presented calibration techniques to account for differences between section moment-curvature and element moment-rotation response for two hinge integration methods: modified Gauss-Radau and two-point Gauss-Radau. The modified Gauss-Radau integration results in a bilinear response and is calibrated by satisfying simple constraints.

The two-point Gauss-Radau hinge integration results in a trilinear moment-rotation response and thus a secant approximation is used to obtain the desired bilinear response. After comparing the calibrated models to their uncalibrated counterparts, the authors conclude that uncalibrated plastic hinge models over predicted the lateral load capacity.

Dameron et al. [8] investigated and modeled significant foundation nonlinearities as part of the San Diego-Coronado Bay Bridge retrofit project by developing a nonlinear finite-element model of the bridge. The model including nonlinear representations for the following components: expansion joint gaps, pier columns, pile groups, abutments and isolation bearings. In modeling the foundation, three foundation configurations were developed for comparison: linear, approximate nonlinear and detailed nonlinear. After comparison of the three different foundation models, the authors recognized that the detailed and approximate nonlinear foundation models were similar, but the linear model showed a significant deviation in displacements compared to the nonlinear model, especially after the initial ground motion pulse.

Shamsabadi et al. [28] considered the lateral response of seat type abutments by developing nonlinear numerical simulation models. A log-spiral hyperbolic model and a detailed finite-element model were developed to simulate clayey silt and silty sand. Full-scale abutment tests were performed and used to validate these models. From the results, extended hyperbolic force displacement curves were developed. The effects of unloading/reloading, gap formation between the backfill and backwall, wingwalls, shear keys and abutment piles were not considered in this study. After comparison of the two models to the full-scale abutment test, the authors noted that the finite-element model nearly identically matches the experimental test results and the log-spiral hyperbolic model yielded slight variation from the experimental results.

Shamsabadi et al. developed a simple hyperbolic force-displacement equation via limit-equilibrium methods using mobilized logarithmic-spiral failure surfaces coupled with a modified hyperbolic soil stressstrain behavior [30]. The model incorporates soil-pile characteristics to estimate the nonlinear abutment backfill force. This equation applies to all soil types, given that the required soil characteristics can be determined, and was validated with eight field experiments. In applying the equation, the authors concluded that the bridge superstructures may unseat under a high-velocity pulse if abutment seat width is inadequate

Mutobe and Cooper [20] assessed the performance of friction pendulum bearings slated for installation in the 11 span Benicia-Martinez Bridge as part of a seismic retrofit. The authors created a finite-element model in ADINA that included the nonlinear behavior of both the bridge structure and the friction pendulum bearings. The friction pendulum bearing model was validated with other finite element models and compared to laboratory results of building structures as no experimental data were available for bridge structures at the time. The authors recommend additional research into the effect of friction pendulum bearings on the seismic response of buildings.

Nielson and DesRoches [21] investigated the modeling parameters that significantly affect the seismic response of multi-span simply supported steel girder bridges. The authors created several nonlinear 3D bridge models. Nonlinearity of the abutments, bearings, columns and

bent caps was considered in the bridge model. After comparison of several bridge models, the authors concluded that loading direction, damping ratio, and fixed bearing stiffness most greatly influence the seismic response of this bridge type.

Shamsabadi et al. [29] aimed to improve current seismic analysis procedures and guidelines by comparing the predictions of finite element models to multiple sets of seismic response records. Comparisons were made for three types of California bridges: standard ordinary non-skewed, skewed bridge and non-standard long-span bridge. Shell elements were used to model the deck and abutment walls. The finite element models included nonlinear foundation-soil-interaction effects at abutment and pile foundations, and abutment shear keys effects. After initial comparison to the seismic response records, the models were calibrated to predict better the actual seismic response. From the results, the authors concluded, given accurate modeling of the abutment and pile foundations, that the models could predict seismic response.

2.2   Knowledge Gaps in NTHA

While the current state of research in NTHA of highway bridges encompasses a wide range of modeling approaches, element and constitutive model formulations, and solution strategies, significant knowledge gaps remain.

- The difference in simulated response when using similar bridge models in separate software packages

- The effect of cyclic degradation of structural components on the dynamic response of bridges

- Modeling errors associated with the choice of nonlinear constitutive or element models and errors with respect to known benchmark solutions

- Ranking and prioritization of the modeling parameters that have the most significant influence on bridge response during earthquake loading

The benchmark tests of finite element formulations typically employed in bridge analysis and NTHA simulations of four ordinary standard bridges (OSBs) summarized in the following chapters will address these knowledge gaps.

In addition, it should be recognized that the above list is not exhaustive, and there are several other knowledge gaps worthy of further study; however, they are not addressed directly in this report. These include:

- Numerical integrators and nonlinear algorithms, including accuracy and stability, for solving nonlinear time history equations of motion

- The sensitivity of response to the choice of damping model and the corresponding need for more information on other non-classical damping models

- The difference between characterizing idealized new construction versus existing bridges that exhibit environmental and potentially mechanical degradation

- Lack of information to relate predictions from NTHA to useful acceptance criteria based on the performance of the bridge system as a whole

- Effect of ground motion uncertainty on NTHA response predictions

- Propagation of ground motion uncertainty, model uncertainty, and parameter uncertainty through NTHA.

Chapter 3

Benchmark Problems

We begin by illustrating some simple theory of nonlinear structural element formulations, specifically cantilever columns, as well as how CSiBridge and OpenSees are able/unable to implement them. With a homogeneous steel cross section, a closed form solution is quickly derived with which to validate both software platforms, so in the first section we restrict ourselves to strictly two-dimensional (2D) steel sections. The second section introduces the complication of coupled lateral response in three-dimensional analysis, but retaining the simplicity of a homogeneous circular steel cross section. This section has perfect circular symmetry and therefore it is easier to establish errors or approximations with the numerical implementations.

Finally, there should be no loss of generality when moving to the concrete sections, because it will be shown it is the element formulation that causes the issues, and is illustrated in more detail in the third section of the document. The fiber cross sections yield the same sectional behaviors (i.e., moment-curvature relation) as long as the constitutive models input are consistent between software; however, this does not always lead to consistent element-level results.

This document is intentionally limited to nonlinear static (i.e., pushover) response analysis. There are many basic behaviors that a model should capture and can be studied in this series of case studies. However, for the purposes of NTHA, obviously the cyclic unloading/reloading behaviors and numerical stability of different materials/elements are important, but will be studied further in Chapters 4 and 5.

3.1   2D system (steel rectangular cross section)

A steel cantilever column has a rectangular cross section and is loaded with an axial and lateral load as shown in Figure 3.1. The axial force is held constant while the lateral load is monotonically increased (here load control is adopted with load factor λ). It is assumed throughout the document that the shear deformations are negligible (the shear area is assumed to be large in the software implementations). The dimensions, material properties, and applied load are shown in Table 3.1.
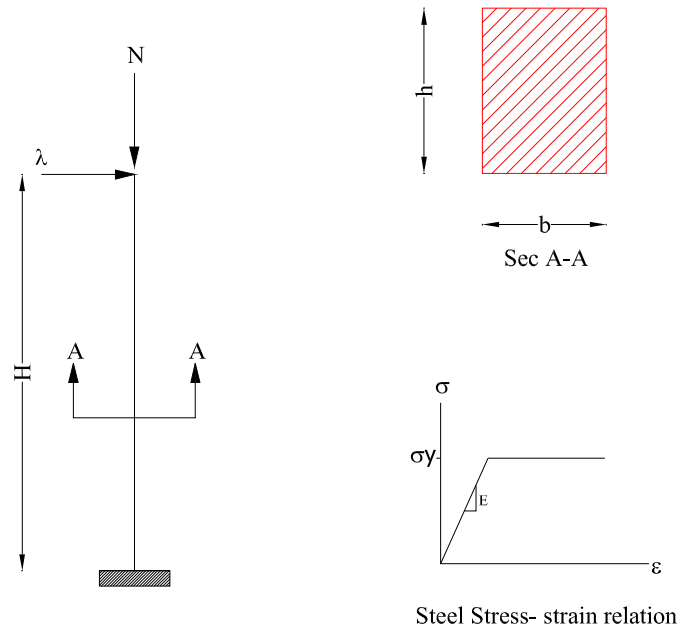
Figure 3.1: Geometry, cross section, and material of the 2D steel case study

Table 3.1: Rectangular 2D steel column properties

$H = 240$ in	$b = 15$ in	$h = 20$ in	$\sigma_y = 50$ ksi
$E = 29000$ ksi	$N = 1000$ kip	$\lambda = $ variable	
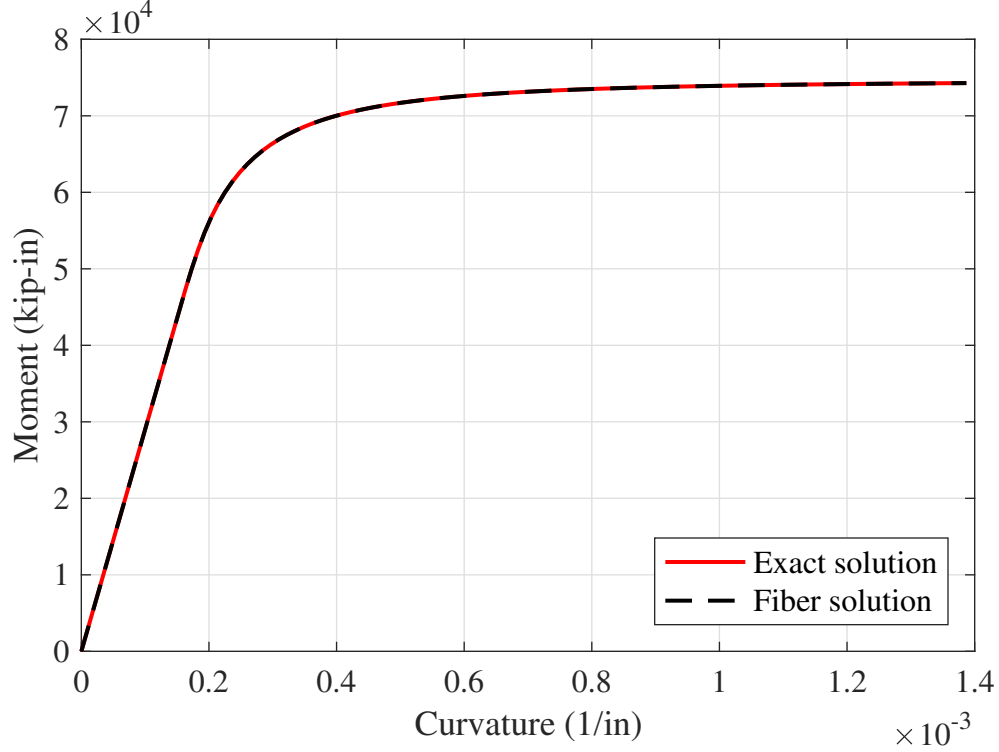
Figure 3.2: Moment-curvature results for 2D steel section

3.1.1 Moment-Curvature Relation

The moment-curvature relationship was calculated based on both an exact (theoretical) solution and a numerical solution with a fiber section, as shown in Figure 3.2. The cross section was divided into 50 layers (50 x 2) in CSiBridge to get the fiber solution (there are still some minor differences between the two solutions because of the use of discrete areas in the fiber section and the midpoint integration rule).

3.1.2 Case A

Case A represents the common implementation of a beam/column under lateral load where the plasticity is concentrated at a hinge location. Using this lumped hinge assumption, it is possible to derive the closed-form or analytical solution under this assumption (as well as the numerical results using implementations in both CSiBridge and OpenSees). To obtain the analytical solution, an elastic beam in series with a zero-length hinge was considered as shown in Figure 3.3 below. The solution procedure is:

$$u_3(i) = u_{(3_2)}(i) + u_{(3_1)}(i)$$
$$u_3(i) = (\lambda_i H^3)/3EI + \theta_i H \quad (3.1)$$
$$u_3(i) = (\lambda_i H^3)/3EI + \phi_i l_p H$$

34

where H = total height, λ_i = load at each step, ϕ_i = curvature at each step (the total curvature), and l_p = plastic hinge length (assumed to be 10 in). The curvature ϕ_i can be found from moment-curvature curve once M_i is determined (for the monotonically increasing case study).

Implicit in the formulation above is that the plastic curvature is constant over the plastic hinge length, which is obviously not a correct assumption. Similarly, there are two other important assumptions. The first assumption relates to the length of the column that contributes to the elastic deformations. Initially here the full height H is assumed, which will lead to an over prediction of the elastic displacement because of the contribution of the hinge. Later in this section, methods of correcting this oversight are introduced (i.e., by considering $H - l_p$). The second assumption is that the location of the integration point that corresponds to the hinge is at the base of the column ($x = 0$). The implication is that the yield moment and therefore the yield load are correct; however, the initial stiffness and post-yielding stiffness are not correct. Later in this section, an appropriate correction will also be made (i.e., that the location of the integration point is at some point l_h above the base).

Figure 3.5 shows the load-displacement curve from the analytical solution. Due to the simplicity of the case study, the plastic moment (and therefore plastic load) is exact. However, as mentioned above, the initial elastic stiffness is small (solution is more flexible), because the deformations accumulate simultaneously in both elements. Comparisons with solutions from the two software (CSiBridge and OpenSees) are shown later because there are several different modeling choices that can be made.

The Case A solution shown in Figure 3.5 is of course also somewhat dependent on the selected value of the plastic hinge length, as with any method that must account for the difference between rotation and curvature. In this section, the plastic hinge length is kept constant between all implementations and was obtained as half of the cross section dimension. The larger the assumed plastic hinge length, the larger the discrepancy will be between the true/exact stiffness and the one predicted using the analytical solution of Case A.

3.1.3 Case B

Case B represents the exact solution in the sense that plastic curvature is allowed to form anywhere along the length of the beam-column. In addition, the plastic curvature is exactly integrated at all locations to yield the correct displacement field. As with Case A, only the analytical solution is derived here, the results from implementing in different software are shown along with the modeling assumptions in a later section.

The procedure for the analytical solution for the problem shown in Figure 3.4 is:

$$M(x) = -\lambda_i H + \lambda_i x$$

$$\theta(x) = \int \phi(x)dx$$

$$u_2(H) = \int_0^H \theta(x)dx$$

(3.2)

35
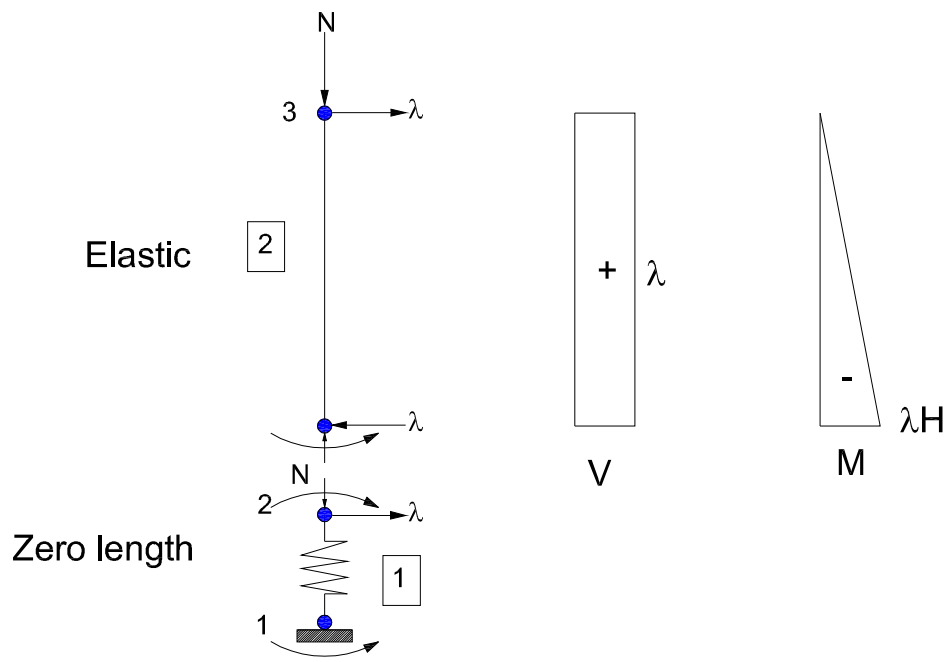
Figure 3.3: Details of the elements and internal forces for Case A
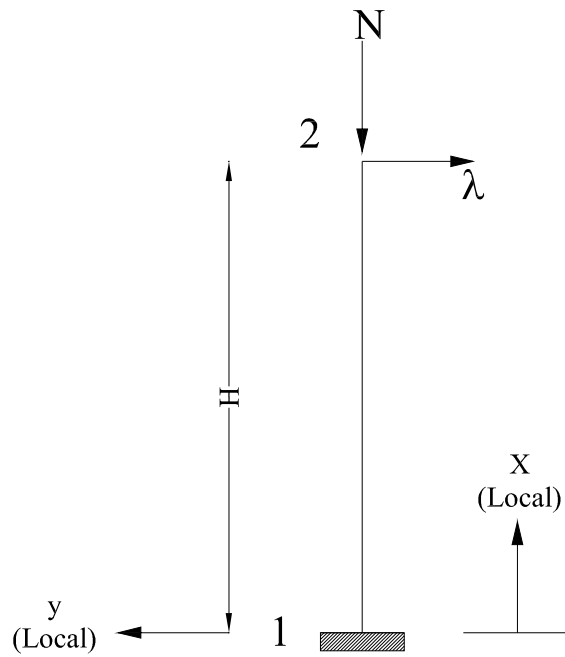
Figure 3.4: Details of the element for Case B
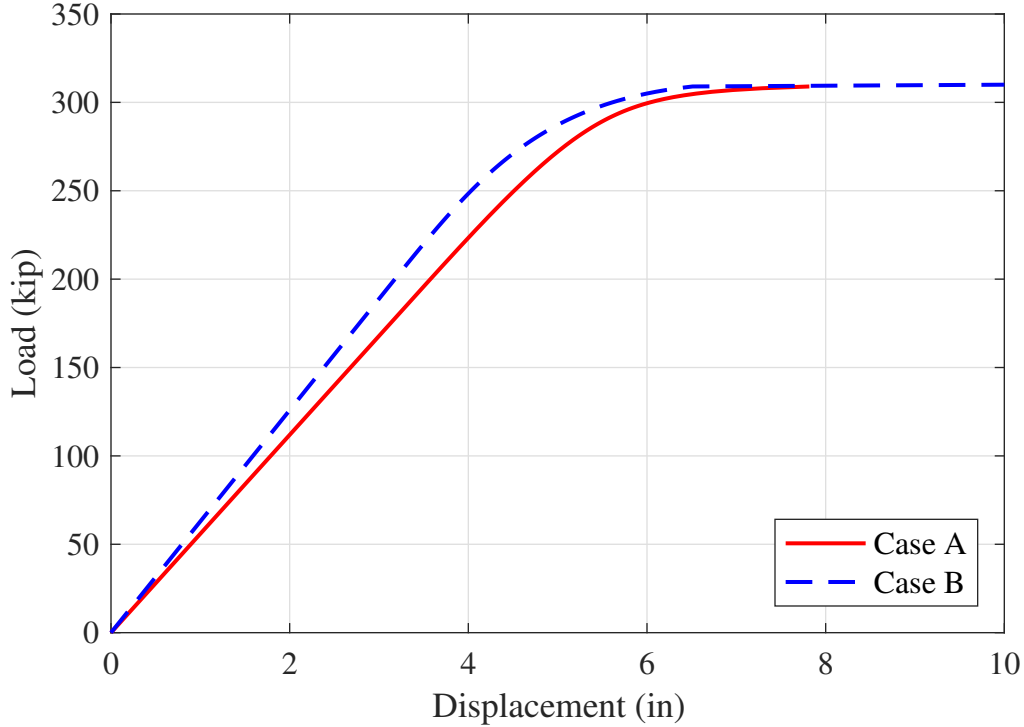
Figure 3.5: Comparison of Case A and Case B analytical solutions

The curvature $\phi(x)$ is obtained from the moment-curvature diagram. Both $\theta(x)$ and $u_2(H)$ can be calculated using numerical integration (the trapezoid rule was used). There is no longer any assumption about the plastic curvature, it may be linearly or nonlinearly varying in the plastic hinge region and is defined explicitly by the shape of the moment-curvature relation. The resulting load-displacement curve for Case B is shown in Figure 3.5.

The comparison of the two cases is shown below in Figure 3.5. As can be seen, the common observation that a series representation of a hinge and column is more flexible than considering the true response is upheld. However, because of the series system, the forces are the same in the hinge and column, and therefore the yield moment is preserved. As with the elastic stiffness, the post-yielding stiffness would also not the same in the two approaches (here it is less apparent because an elastic-perfectly-plastic material was selected). Note that both analytical solutions are exact under the assumptions of the element(s), the deviation from these using software implementations is explored next.

3.1.4 Case C Software implementations

Showing that Case A is Fiber hinge model in CSiBridge

The problem in Case A was modeled using CSiBridge V17.3.0. A single frame element is used along the full height of the column. At the base of the column, a frame hinge (Fiber P-M2-
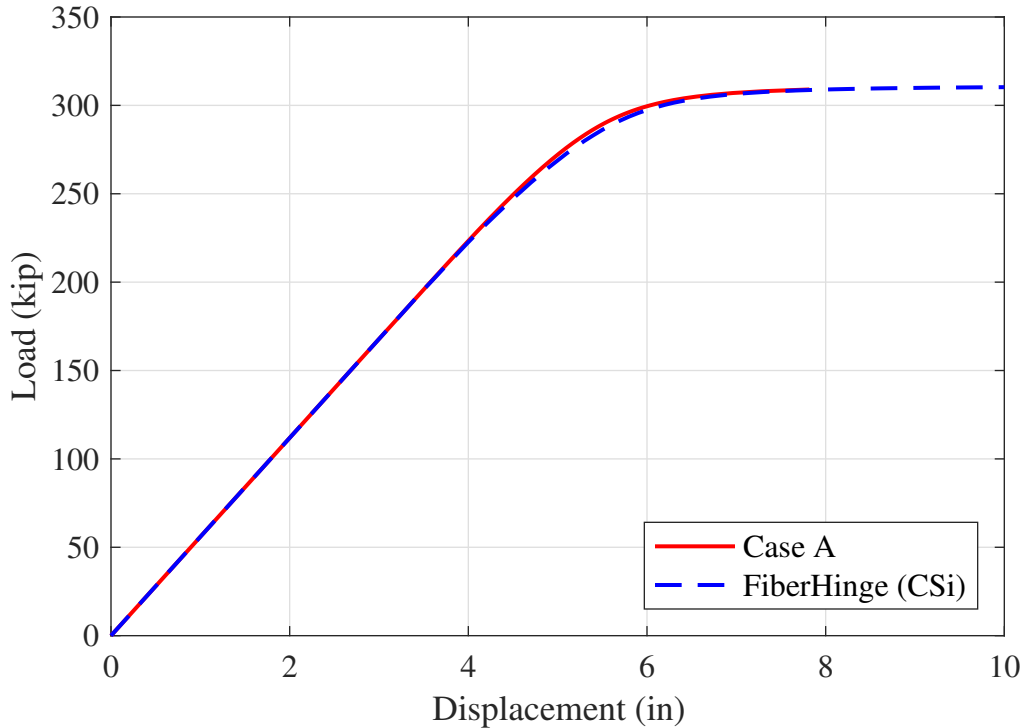
Figure 3.6: Comparison of Case A with CSiBridge

M3) with a plastic hinge length of 10 in was defined. The steel cross section discretization was 50 by 50 fibers. Nonlinear analysis with displacement control was adopted. As can be seen in Figure 3.6, the CSiBridge results give an excellent match with the analytical solution for case A.

Showing that Case A is OpenSees elasticBeamColumn with zeroLength element

The problem was also modeled in OpenSees to show consistent results can be obtained, meaning the limitation is with the formulation of the elements, not the software implementation. An elasticBeamColumn element of length H was used with a zeroLength element at the base of the cantilever. This modeling approach was adopted because the zeroLengthSection does not have a plastic hinge length associated with the element. The ElasticMultiLinear material was used to define the points on the backbone of the moment-rotation relation used in the rotational degree of freedom of the zeroLength element. The moment-rotation backbone was obtained from a sectional analysis using the zeroLengthSection element and a section discretization similar to that used in the CSiBridge Fiber hinge. Figure 3.7 below shows the comparison results between Case A and OpenSees.

As would be expected, both the OpenSees and CSiBridge implementations are able to match the Case A analytical results within a close numerical tolerance.
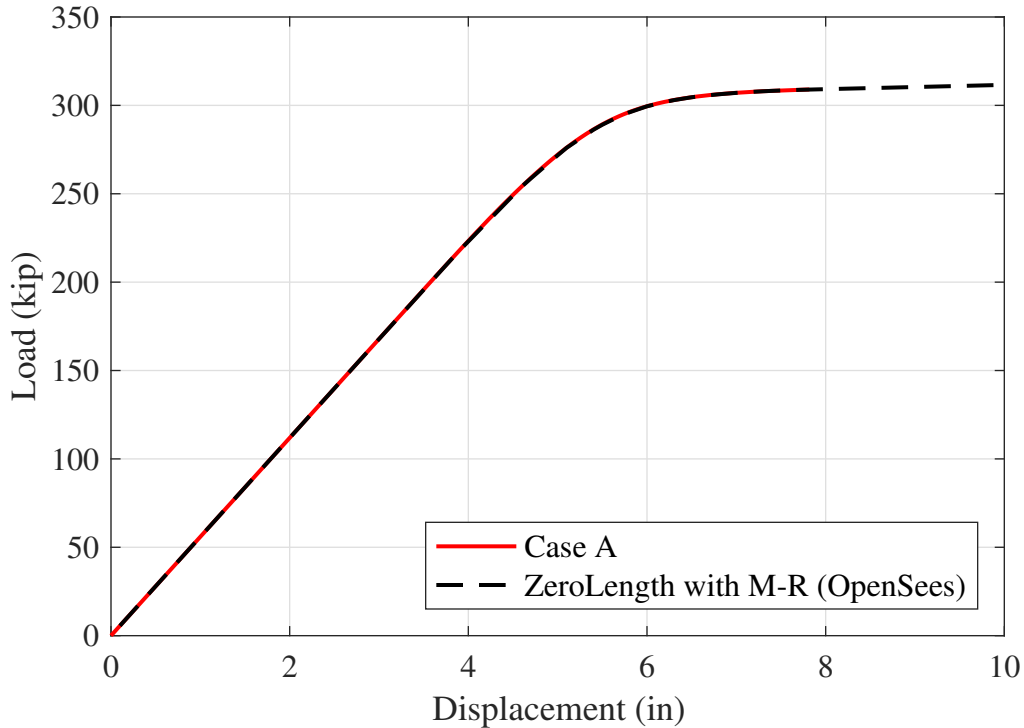
Figure 3.7: Comparison of Case A with OpenSees

Showing that Case B is OpenSees forceBeamColumn

The column in Case B was modeled using OpenSees with two types of elements to compare the results with the exact solution. The first is the forceBeamColumn in OpenSees, which is based on the iterative force-based formulation. A single forceBeamColumn (formerly nonlinearBeamColumn) column element was used to model the column. The Lobatto integration rule with five integration points was used. Figure 3.8 compares the results between Case B and forceBeamColumn element implementation in OpenSees. A second element may be introduced to improve the prediction of the curvature distribution along the length of the column, but the force-displacement relation remains very close to the true solution even with the single element.

Showing that Case B is OpenSees beamWithHinges

The beamWithHinges element in OpenSees contains a hinge section at both ends of an elastic element, and was used to construct the same column shown in Case B. A plastic hinge with length 10 in at both ends (i and j nodes) of the element was created with the same fiber section discretization as the previous implementations (forceBeamColumn in OpenSees, zeroLengthSection in OpenSees, and Fiber hinge in CSiBridge). From Figure 3.9 a good match between the exact solution and beamWithHinges element implementation can be noticed. The slight discrepancy between the yield and plastic force is due to the selected
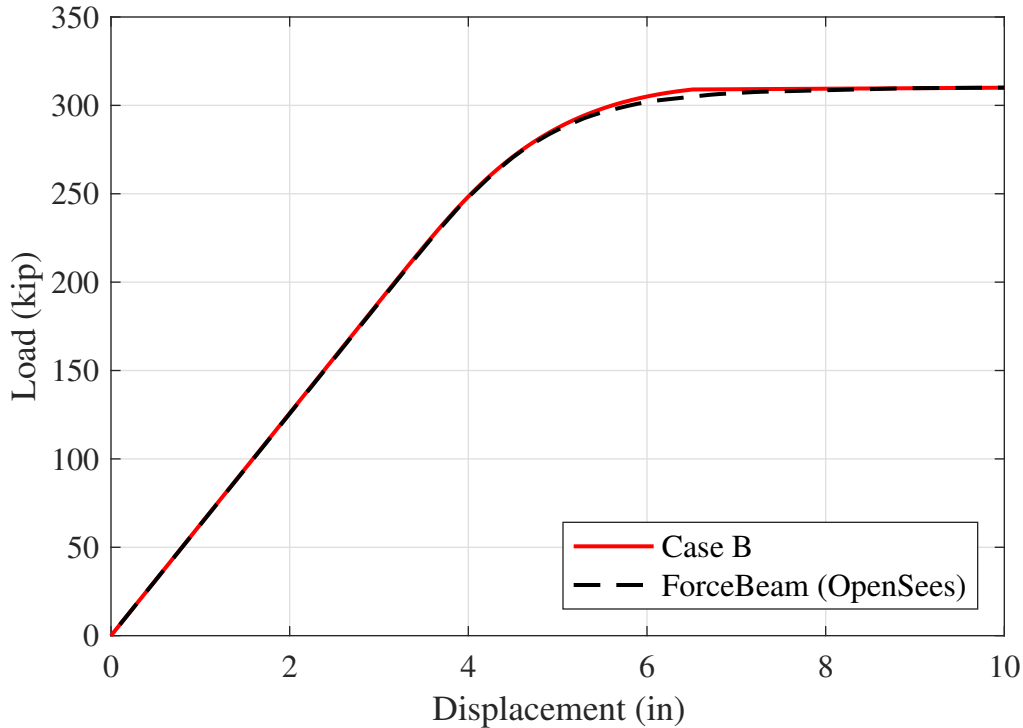
Figure 3.8: Comparison of Case B with OpenSees (forceBeamColumn)

value of the plastic hinge length.

3.1.5   Case D Corrections to Software Implementations

In order to adjust the Fiber hinge model in CSiBridge to match or be close to the exact solution (meaning Case B), two methods of adjustment in CSiBridge were introduced. These are both commonly accepted forms of improving the response of lumped-plasticity models. It is just demonstrated here that with a 2D homogeneous steel section, both methods of correction have the desired outcome.

Introduce a rigid-plastic hinge

This method of correction was implemented by introducing an Interaction hinge type (P-M2-M3) in the CSiBridge software at the lower end of the column instead of the Fiber hinge. The type of hinge is a moment-rotation hinge and the surface data was introduced depending on FEMA 356, equation 5-4, although obviously the values on the moment-rotation backbone given as defaults are not directly relevant for bridge analysis. The Caltrans hinge appears to be conceptually similar in implementation. The parameters of this type of hinge are shown in Figure 3.10. The results of this method of correction are shown in Figure 3.11.

From this figure, it can be seen that this method can partially correct the numerical results. The elastic slope (stiffness) exactly matches the closed-form solution but the post-
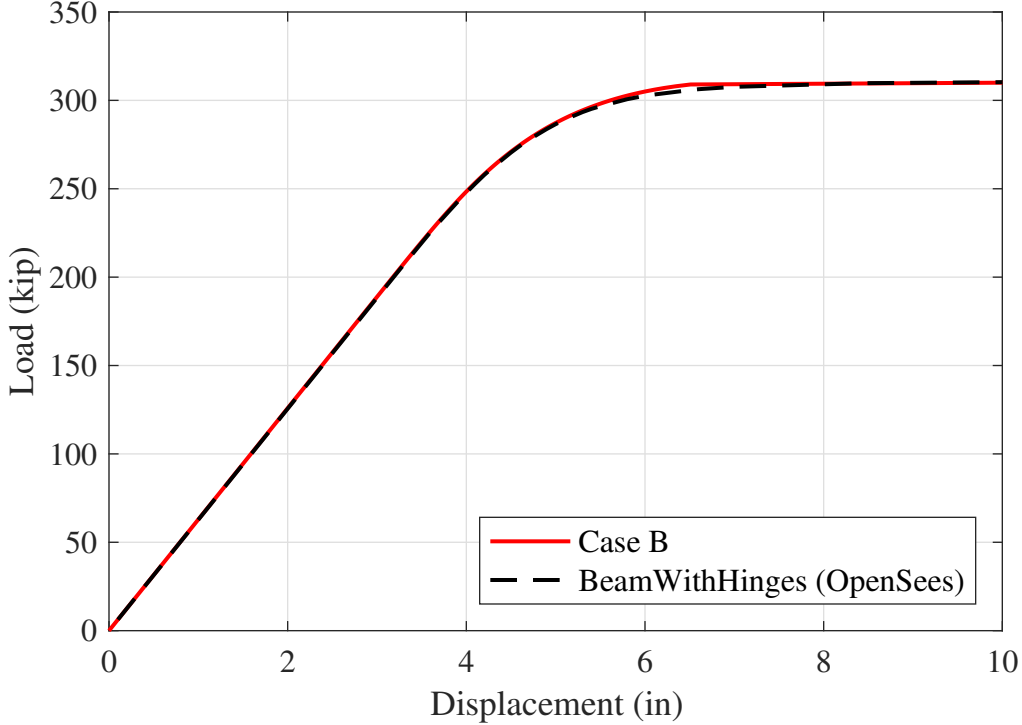
Figure 3.9: Comparison of Case B with OpenSees (beamWithHinges)

yielding slope is not correct. As the hinge does not contribute to the deformations prior to yielding, both the elastic stiffness and the yield force (or yield moment) are preserved. However, there are limitations on the type of nonlinear and yielding behaviors that can be achieved due to the use of the discrete points on the backbone curve (there is no discretized fiber cross section), in addition to the unloading-reloading behavior during cyclic analysis.

Introduce a rigid element in the hinge region

In this method, the column is split into two different frame elements. The element at the base is a rigid element ($EI = \infty$) with length of l_p (10 in), i.e., there is a new node at $x = l_p$. It is not necessary for the multiplier to be infinite, similar results can be obtained with multipliers in the range of 3 to 10. A frame hinge type (Fiber P-M2-M3) is introduced at the bottom of the rigid element (at $x = 0$). The remaining length ($H - l_p = 230$ in) was modeled as an elastic beam (frame element without any frame hinges). The details of this method are shown in Figure 3.12.

The results of this correction method are shown in Figure 3.13. The initial stiffness is approximately correct (it is shown through an analytical solution below that the stiffness is actually not exact, but very close), and generally there is a better match between the corrected case and exact solution from Case B. There is the added benefit of being able to use the fiber cross section that was not possible with the rigid-plastic hinge correction.

Due to the location of the hinge at the base of the column, the yield moment and therefore
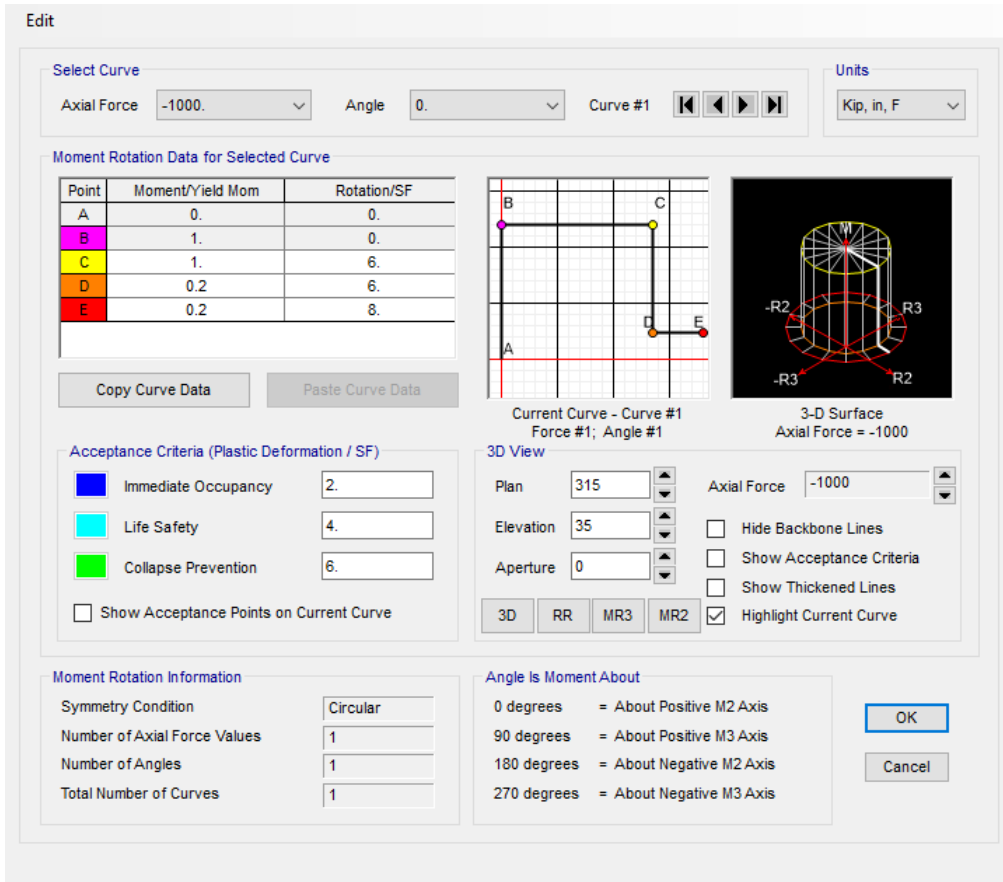
Figure 3.10: Rigid-plastic hinge data
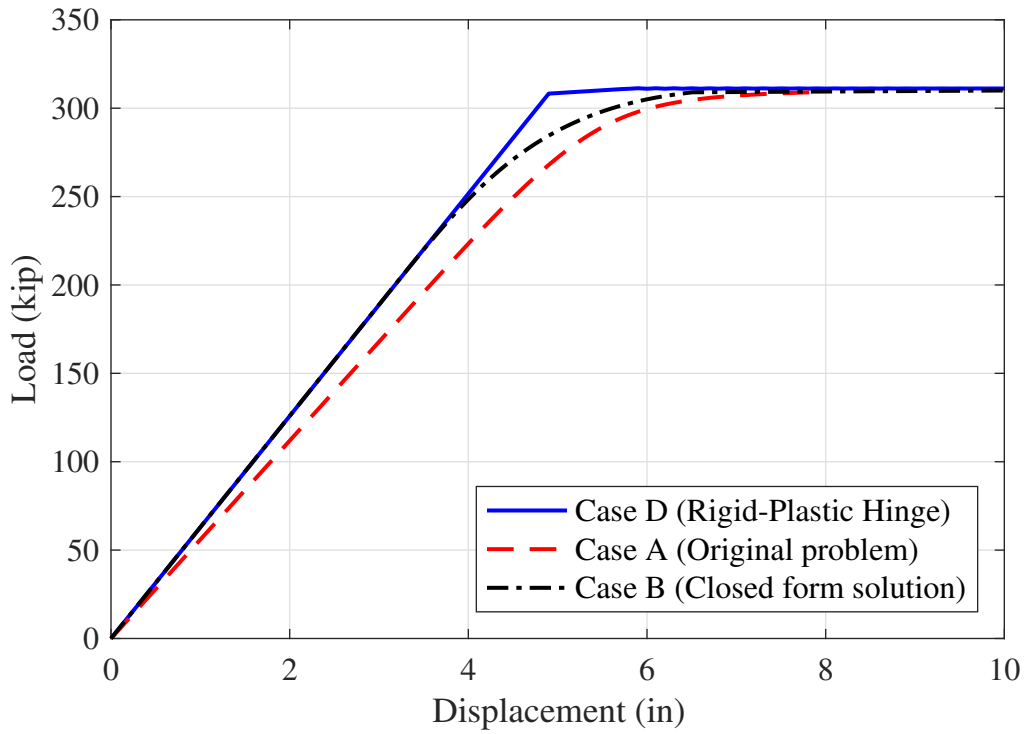
Figure 3.11: Correction of Case A using rigid-plastic hinge in CSiBridge
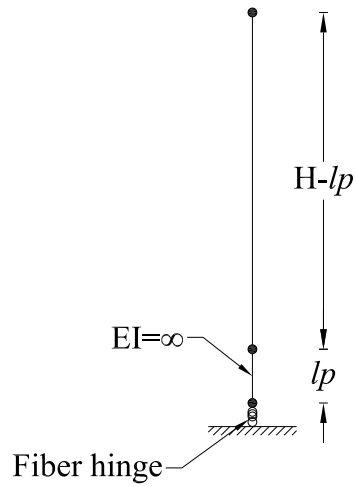
Figure 3.12: Details of the rigid element
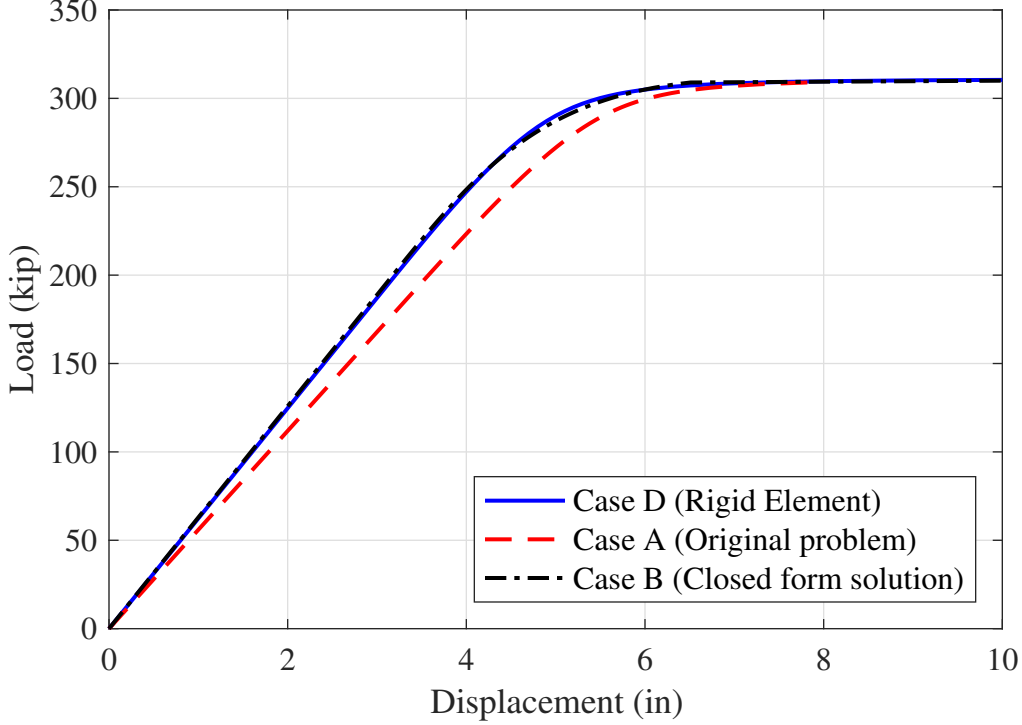
Figure 3.13: Rigid beam correction of Case A

yield force should also be exact. However, as with the other methods of correcting response, the post-yield stiffness is also only approximately correct.

Effect of fiber hinge location

It is of course not necessary in CSiBridge (or conceptually) to locate the hinge at the base of the rigid element. It may be beneficial to locate near the midpoint, as suggested in previous work (Aviram et al., 2008). To study the effect of the fiber hinge location on the monotonic behavior of the 2D steel cantilever column, and to establish whether the results in Figure 3.13 are correct, different locations of the hinge were studied using both an analytical solution and CSiBridge software implementation. As derived in Case A, the solutions procedure is:

$$
\begin{aligned}
u_3(i) &= u_{(3_2)}(i) + u_{(3_1)}(i) \\
u_3(i) &= (\lambda_i(H - l_p)^3)/3EI + \theta_i(H - x_h) \\
u_3(i) &= (\lambda_i(H - l_p)^3)/3EI + \phi_i l_p(H - x_h)
\end{aligned}
\tag{3.3}
$$

where H = total height, λ_i = load at each step, ϕ_i = curvature at each step (the total curvature), x_h = location of the hinge ($x_h = 0, 5, 10$ in) as shown in Figure 3.14, and l_p = plastic hinge length (assumed to be 10 in). The curvature ϕ_i can be found from moment-curvature curve once M_i is determined (for the monotonically increasing case study).

As with the derivation in Case A, it is assumed that the plastic curvature is constant over the plastic hinge length. The presence of the rigid element removes the elastic deformation

44
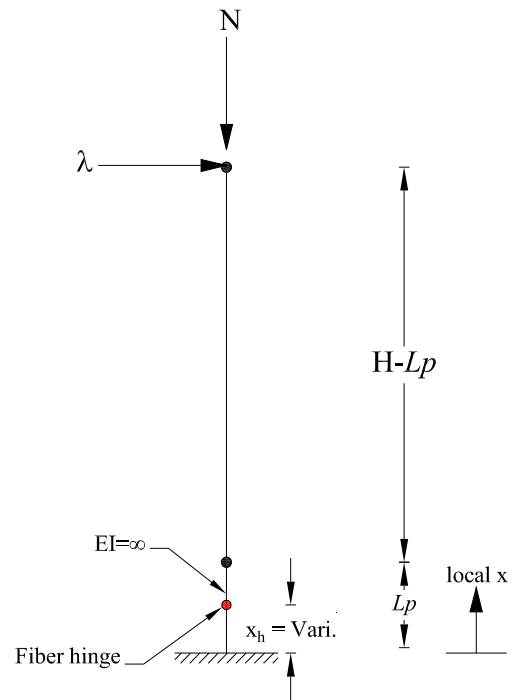
Figure 3.14: Location of the fiber hinge
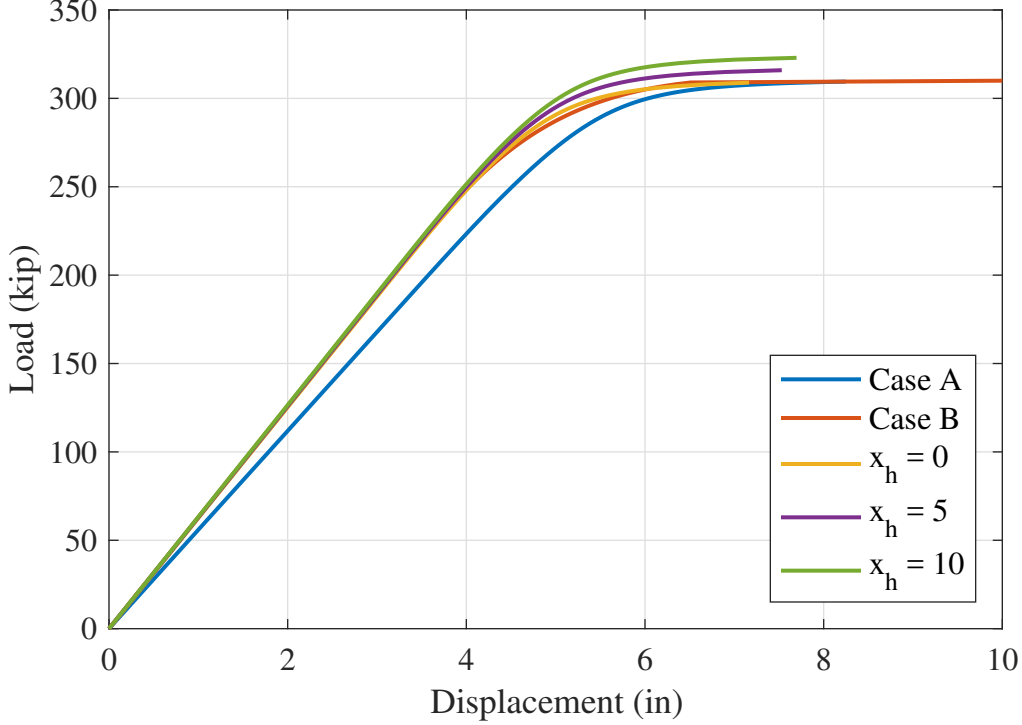
Figure 3.15: Comparison of analytical solutions using different fiber hinge locations

in the plastic hinge region. However, the additional dimension x_h is still needed to define the location of the integration point used for evaluating the curvature and moment. Setting l_p to zero and x_h to zero degenerates the solution into that previously defined in Case A. An additional assumption is made that the location of the integration point also defines the location of the lumped rotation due to the constant plastic curvature over l_p.

The effect of moving the location of the hinge on the new analytical solution is shown in Figure 3.15. The elastic stiffness for each of the hinge locations ($x_h = 0$, 5, 10 in) is approximately equal to the exact stiffness (Case B). It can be shown that the exact elastic stiffness can be derived by setting x_h equal to $H - \sqrt{H^2 - l_p H + l_p^2/3}$. In addition, due to the preservation of the location of the peak moment at the hinge location, the $x_h = 0$ in location preserves the yield force. The yield force is progressively overestimated as the location of the hinge is increased. The optimal location of the hinge for purposes of initial stiffness therefore, by definition, will lead to an overestimate of the yield force.

Moreover, the problem is repeated in CSiBridge using several locations of the hinge ($x_h = 0$, 5, 10 in), to be consistent with the analytical solution. The results from CSiBridge are shown in Figure 3.16. It can be seen that both the stiffness and strength are consistent between Figure 3.15 and Figure 3.16. The location of the hinge at the bottom of the rigid element ($x_h = 0$ in) provides the best match with the actual solution (Case A that is).
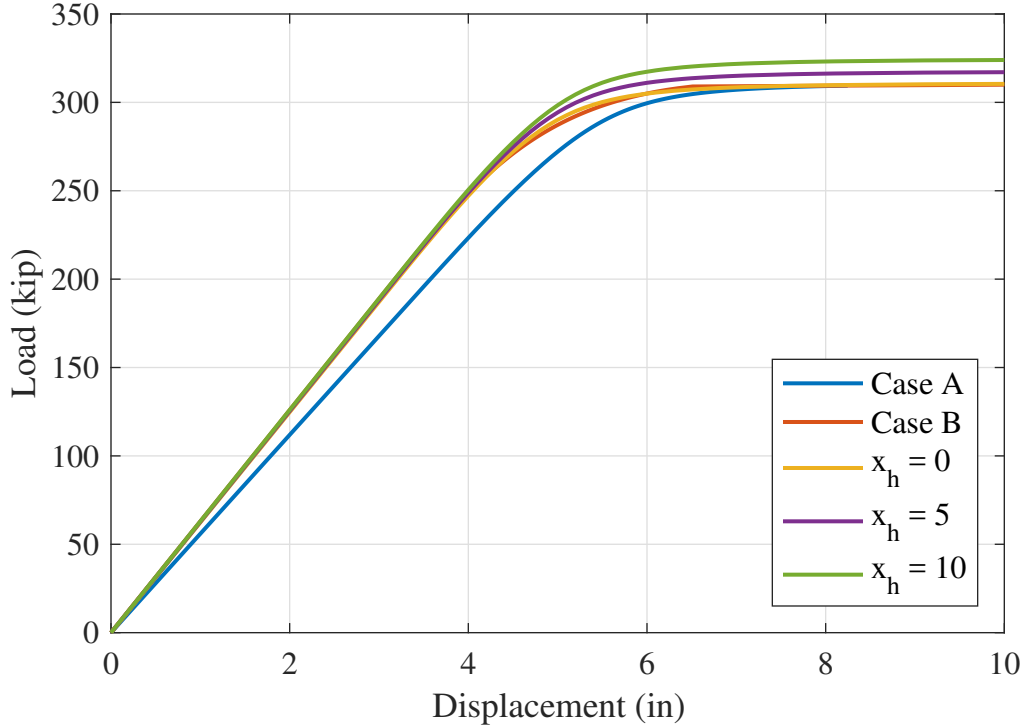
Figure 3.16: Comparison of CSiBridge results of different fiber hinge locations

Table 3.2: Circular 3D steel column properties

$H = 240$ in	$D = 20$ in	$\sigma_y = 50$ ksi
$E = 29000$ ksi	$N = 1000$ kips	$\lambda z, \lambda y =$ variable

3.2 3D system (circular steel cross section)

A steel circular cantilever column is loaded with an axial and two equal lateral loads in the local z and y directions as shown in Figure 3.17. The axial force is held constant while the lateral load is monotonically increased (here load control is adopted with load factor λz and λy).

Because of the circular symmetry of the cross section, the load-displacement (defined as the vector combination of loads in y and z directions, and the vector combination of displacements in the y and z directions) behavior is always the same regardless of the combinations of loads in each of the lateral directions (i.e., factors λy and λz).

The dimensions, material properties, and applied load are shown in Table 3.2.

3.2.1 Moment-Curvature Relation

The moment-curvature diagram was plotted from a numerical solution with a fiber section in CSiBridge, as shown in Figure 3.18. The cross section was divided into 50 layers in
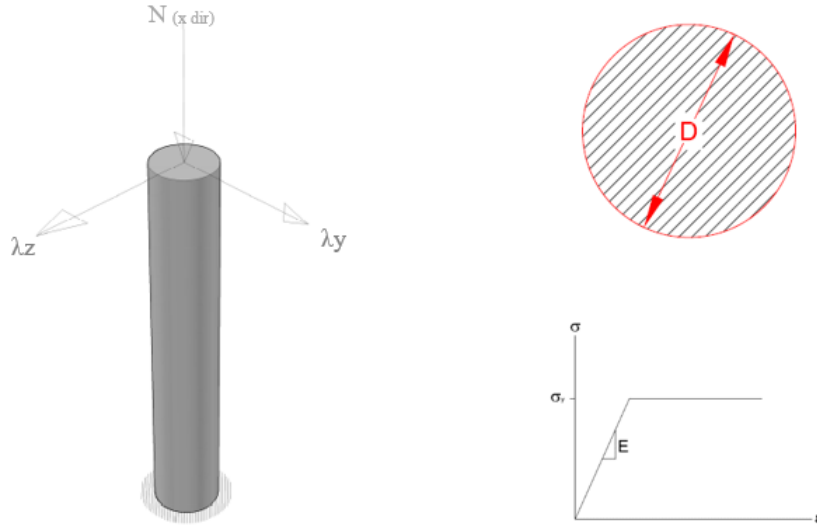
Figure 3.17: Geometry, cross section, and material of the 3D case study

the tangential direction and 40 layers in the radial direction, as shown in Figure 3.19. As discussed in past research [4], there are other discretizations of circular cross sections that yield the same results with more optimal placement of the fibers in the core.

In theory, due to the circular symmetry of the cross section, any vector combination of moments Mz and My will produce the same curve as Figure 3.18. However, the numerical implementation may yield slightly different responses due to only a single axis of symmetry in the patch discretization or a non-standard starting angle paired with a coarser section discretization.

3.2.2   Cases A and B

Similar to the procedure followed in the 2D case study, the analytical solutions were derived for Case A (series system containing an elastic beam and a zero-length hinge) and Case B (single beam with ability for plasticity to spread along the height). The results are shown in Figure 3.20 and exhibit similar characteristics to those shown previously in Figure 3.5. To make all the subsequent plots comparable, the vertical axis (ordinate) is always the vector combination (square root sum of the squares) of loads in the y and z directions. Similarly the horizontal axis (abscissa) is always the vector combination of the displacements in the y and z directions.
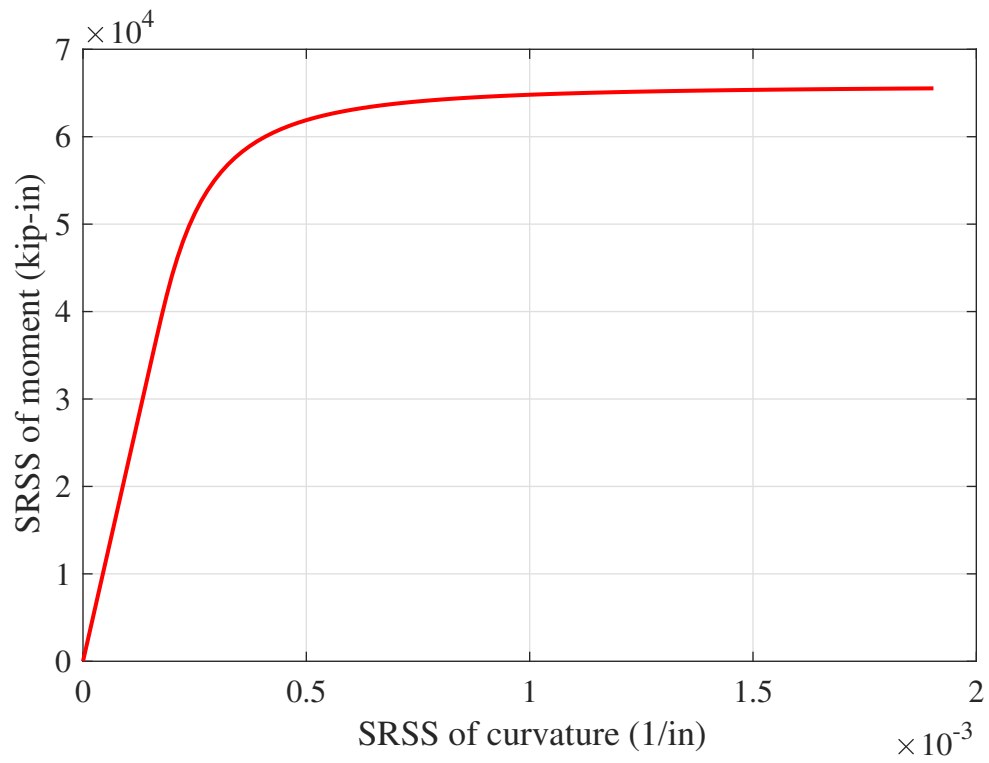
Figure 3.18: Moment curvature for the 3D circular steel section
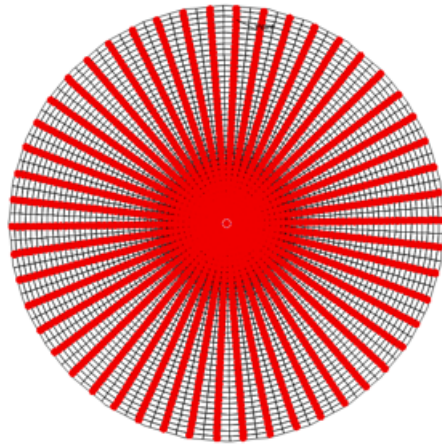
Figure 3.19: Fiber distribution of circular steel cross section in CSiBridge
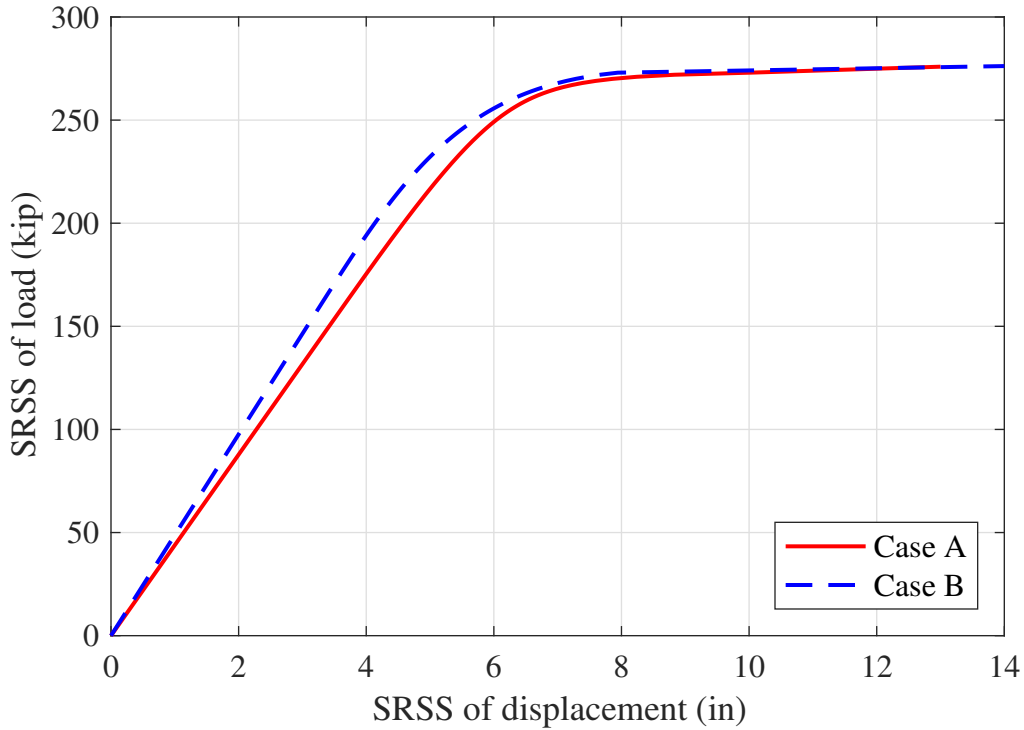
Figure 3.20: Comparison of Case A and Case B for 3D steel circular column

3.2.3 Case C Software implementations

Showing that Case A is Fiber hinge model in CSiBridge

As in the 2D case, the 3D case study was modeled using CSiBridge V17.3.0 using a single frame element. At the base of the column, a frame hinge type (Fiber F-M2-M3) with a plastic hinge length of 10 in was inserted (the plastic hinge length is again not the intent of this study, and is used consistently between implementations in this section). Nonlinear analysis with displacement control was carried out. As can be seen in Figure 3.21, the CSiBridge analysis results show an acceptable match with the analytical solution from Case A.

Showing that Case A is OpenSees elasticBeamColumn with zeroLength element

The problem was modeled in OpenSees by using the elasticBeamColumn element in series with a coupledZeroLength element at the lower end of the cantilever. The moment-rotation relation was obtained from the moment curvature relation by multiplying the curvature by the plastic hinge length (l_p) to get the rotation and then used as input in Opensees. The backbone was specified using an ElasticMultiLinear material and the coupling between lateral responses was enabled by the circular yield surface of the coupledZeroLength element. Figure 3.23 below shows the comparison of results between Case A and OpenSees.
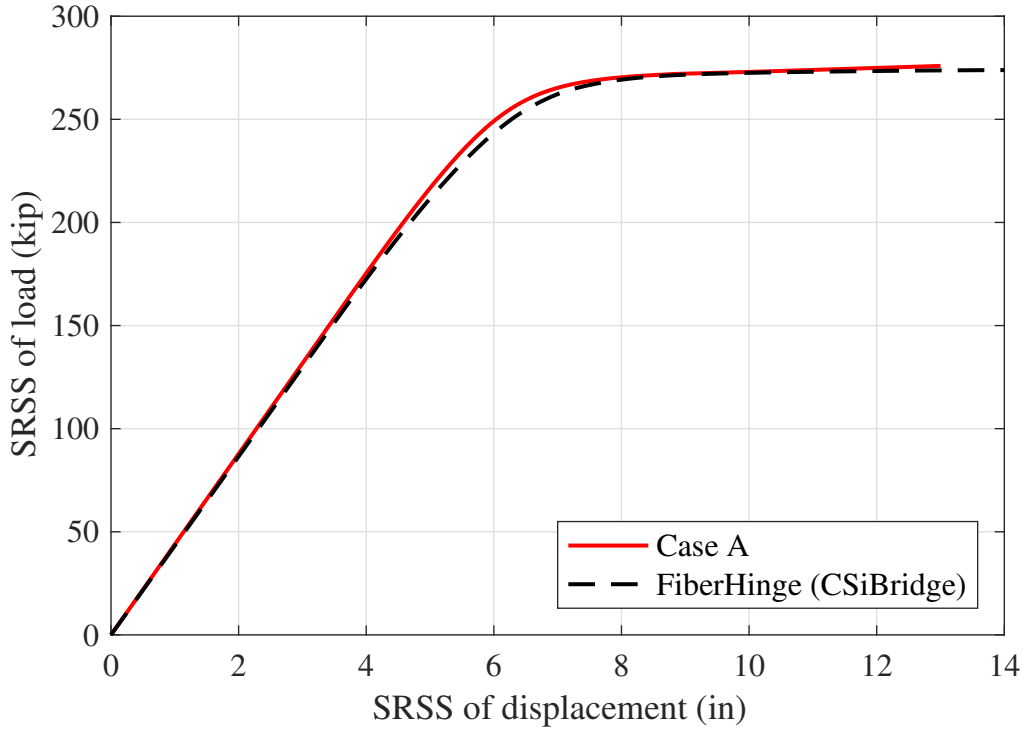
Figure 3.21: Comparison of Case A with CSiBridge for 3D case
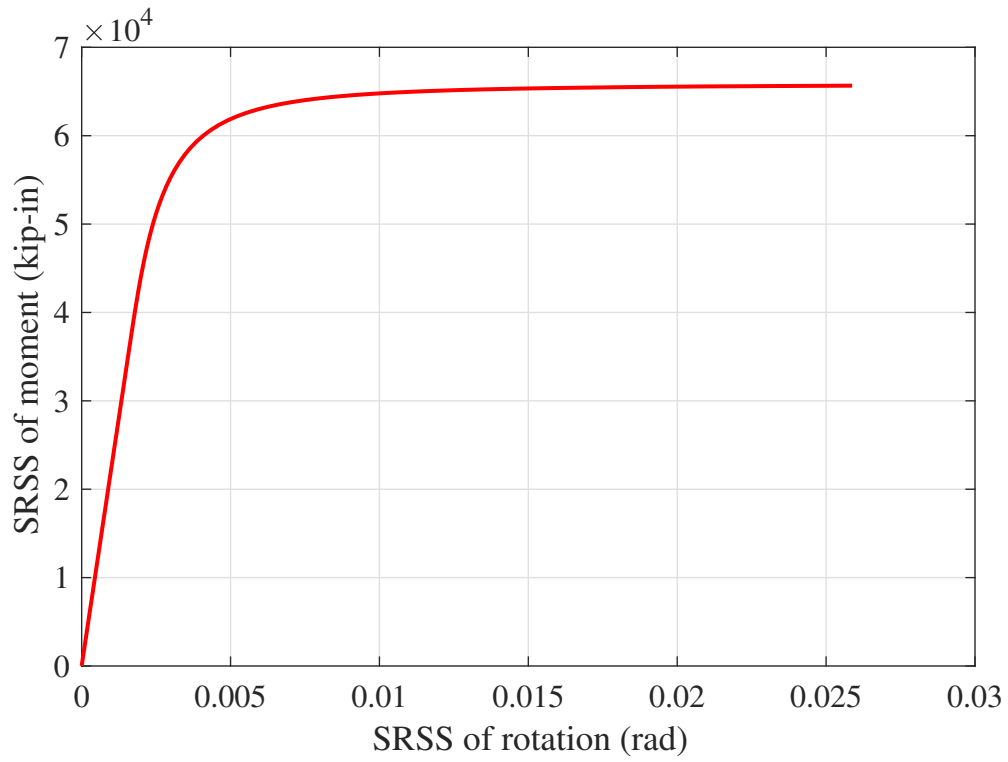
Figure 3.22: Hinge moment rotation from CSiBridge for 3D case

51
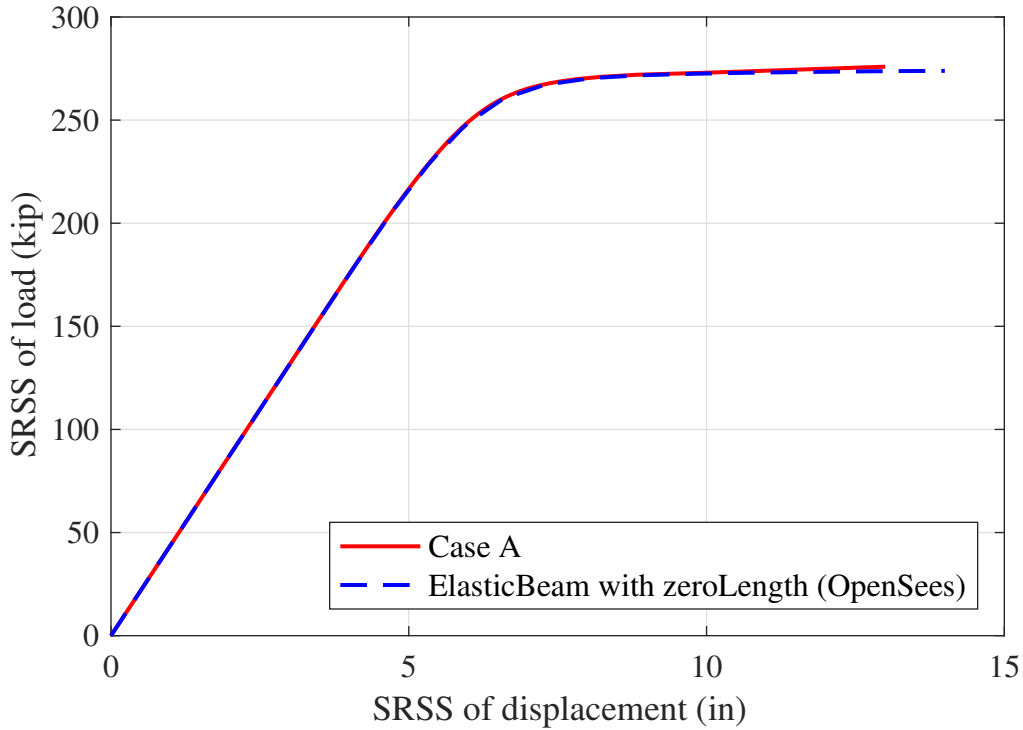
Figure 3.23: Comparison of Case A with CSiBridge for 3D case

Showing that Case B is OpenSees forceBeamColumn

Similar to the 2D case, it was possible to model the exact solution (Case B) using OpenSees with two types of elements. The first is the forceBeamColumn element. A single forceBeam-Column element was used to model the column (with similar stipulations that more elements or integration points may be warranted in different situations), which is based on the iterative force-based formulation. The same Lobatto integration rule with 5 integration points was used. Figure 3.24 compares the results between the exact solution and forceBeamColumn element in OpenSees, with good agreement.

Showing that Case B is OpenSees beamWithHinges

Two hinge sections at both ends of an elastic element were used to define this beamWith-Hinges model. A plastic hinge with length 10 in at both nodes i and j of the element were created with the same fiber section as the previous implementations (meaning force-BeamColumn and a sectional analysis comparable to the CSiBridge discretization shown in Figure 3.18). From Figure 3.25, a good match between the exact solution and beamWith-Hinges implementation is evident. As with the 2D case study, the slight discrepancy between the two curves in the yielding region is due to the assumed plastic hinge length.
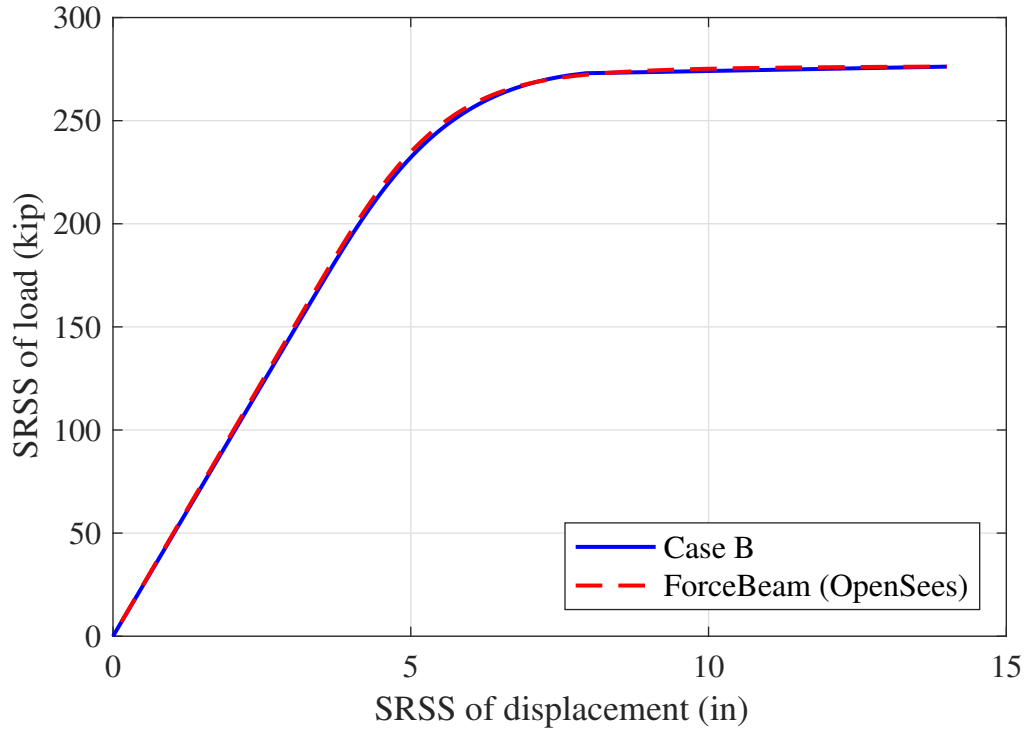
Figure 3.24: Comparison of Case B with OpenSees (forceBeamColumn) for 3D case
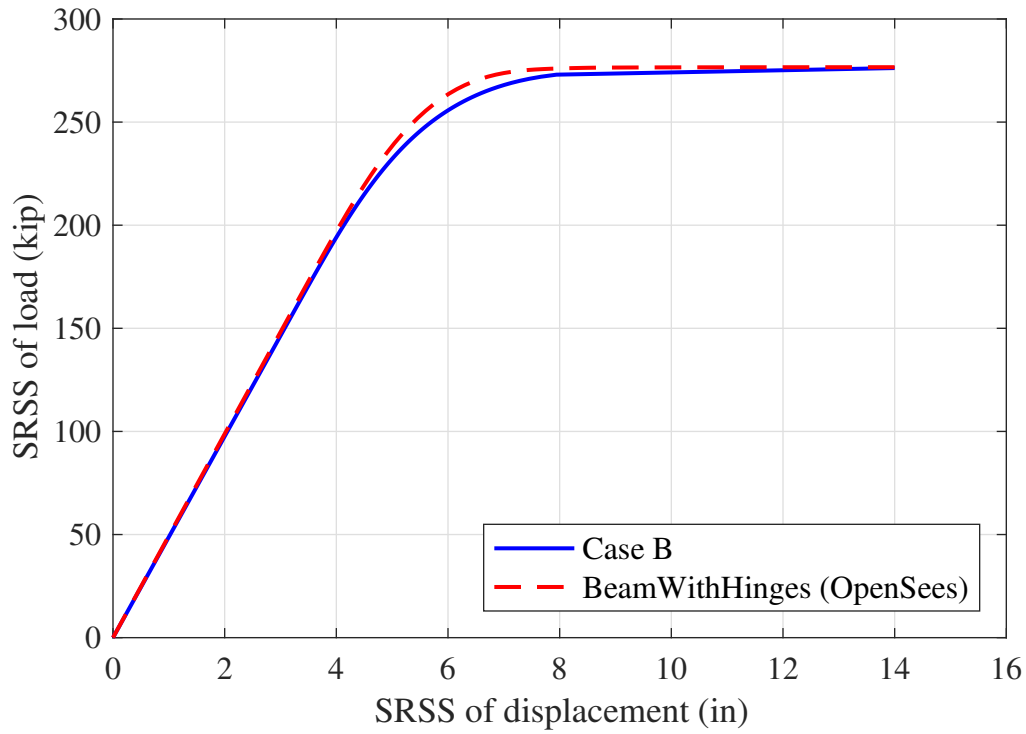
Figure 3.25: Comparison of Case B with OpenSees (beamWithHinges) for 3D case

53
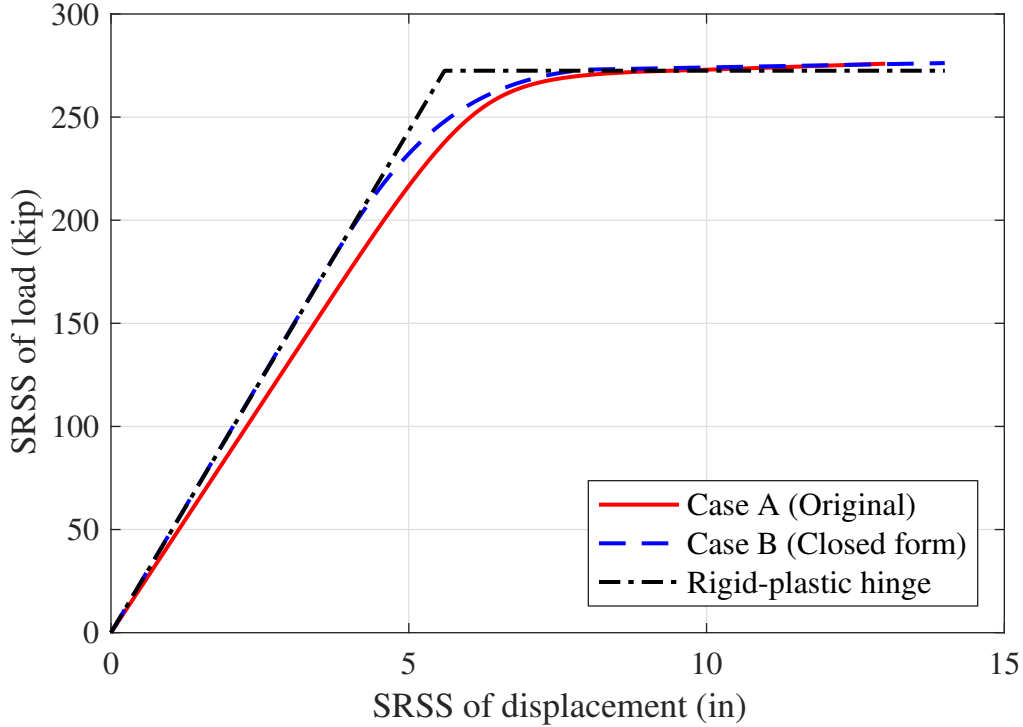
Figure 3.26: Adjustment of Case A by introducing rigid-plastic hinge in CSiBridge

3.2.4 Case D (Methods of Corrections)

Two methods of adjusting the response obtained from CSiBridge were once again introduced to more closely reproduce the exact (Case B) solution.

Introduce a rigid-plastic hinge

This method of correction introduces an Interaction hinge type (P-M2-M3) in CSiBridge in place of the Fiber hinge. The same hinge properties that was defined previously in the 2D case study were used here. The results of this method of correction are shown in Figure 3.26. From this figure, it can be seen that this method partially corrects the response.

The Interaction hinge is able to capture the coupling of the yield surface due to bidirectional loading. The initial elastic stiffness should match the exact solution and the yield load is preserved. However, as with the 2D case study, the post-yielding slope is not correct and the Interaction hinge removes the ability to study more explicit nonlinearities in the cross section enabled by the fiber discretization.

Introduce a rigid element

Similar to the 2D, the column is split into two different frame elements in this method of correction. A new node at $x = l_p$ was introduced to define the rigid element ($EI = \infty$) with length of l_p (10 in) at the base. It is not necessary for the multiplier to be infinite, similar
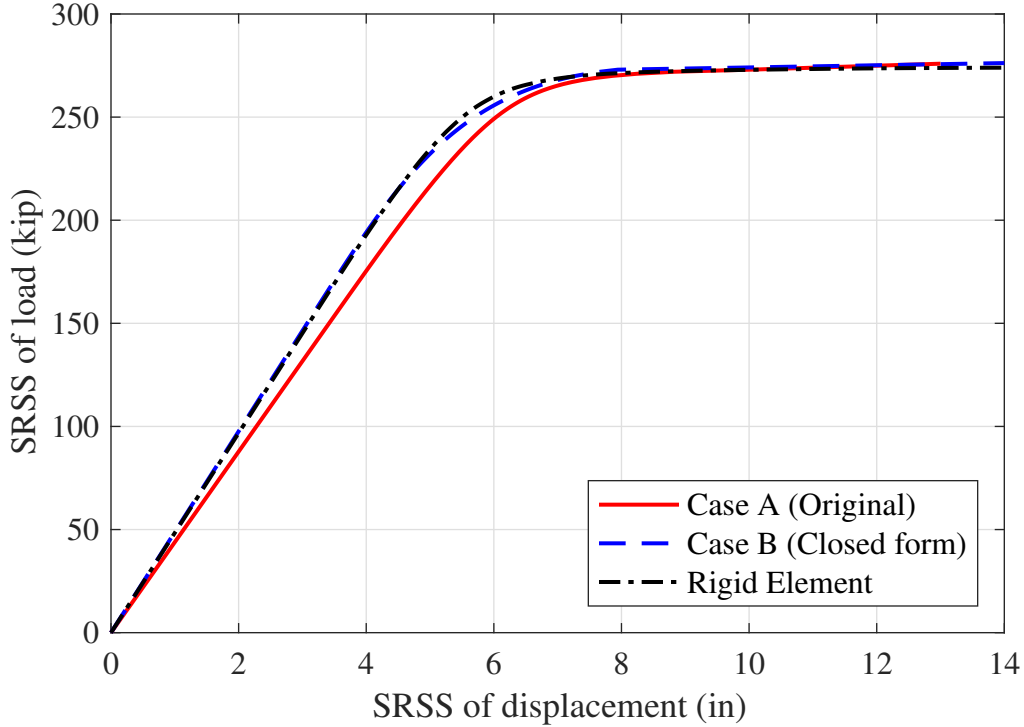
Figure 3.27: Correction of Case A using rigid element in CSiBridge

results can be obtained with multipliers in the range of 3 to 10. A frame hinge type (Fiber P-M2-M3) is introduced at the bottom of the rigid element (at $x = 0$). The remaining length $(H - l_p = 230$ in) was modeled as an elastic beam (frame element without any frame hinges). The details of this method are shown in Figure 3.12.

The result of this correction is shown in Figure 3.27. The initial stiffness is approximately correct, and generally there is a better match between the corrected case and exact solution from Case B. There is the added benefit of being able to use the fiber cross section that was not possible with the rigid-plastic hinge correction as mentioned before. However, as with the other methods of correcting response, the post-yield stiffness is also only approximately correct.

3.3   3D system (circular reinforced concrete section)

To generalize the analytical solutions and computer implementations of the previous sections, the response of a 3D reinforced concrete (RC) column with circular cross section is studied in this section. The RC cantilever column setup is similar to the previous 3D steel cantilever, as shown in Figure 3.28.

The circular RC section contains 8 #8 rebars. The section therefore exhibits many axes of symmetry. The properties of the cross section and constituent materials are shown in Table 3.3.
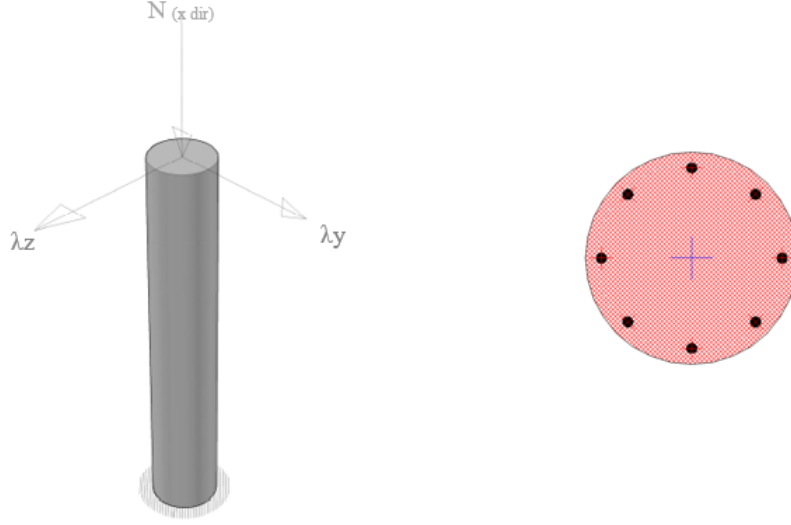
Figure 3.28: Loading and cross section of 3D reinforced concrete case study

Table 3.3: Circular 3D reinforced concrete column properties

$H = 240$ in	$D = 20$ in	$\sigma_y = 50$ ksi	$E_s = 29000$ ksi
$f'_c = 4$ ksi	$E_c = 3605$ ksi	$N = 135$ kips	$\lambda y, \lambda z = $ variable

The column was loaded with an axial load and two equal lateral loads in the local y and z directions, as shown in Figure 3.28. The axial load was held constant with a magnitude of 135 kips, which represents around 10% of the nominal axial resistance of a section at zero eccentricity P_o=1355.8 kips). The lateral load is monotonically increased (here load control is adopted with load factor λy and λz).

The elastic no tension (ENT) material was used to model the concrete and an elastic-perfectly-plastic (EPP) material was used to model the reinforcement. The purpose of the selection of these specific uniaxial materials is not to make the most realistic RC section; however, to ensure that both the OpenSees and CSiBridge sectional behaviors are identical without concern over the shape of the nonlinear portions of the stress-strain curves.

3.3.1 Moment-Curvature Relation

The moment curvature was plotted from OpenSees with a fiber section, as shown in Figure 3.29. The cross section was divided into 50 layers in the tangential direction and 30 layers in the radial direction for the core and 50 layers in the tangential direction and 5 layers in the radial direction for the cover.

The discrete regions of stiffness in the moment-curvature relation correspond to the yielding of the rebars as the neutral axis shifts.
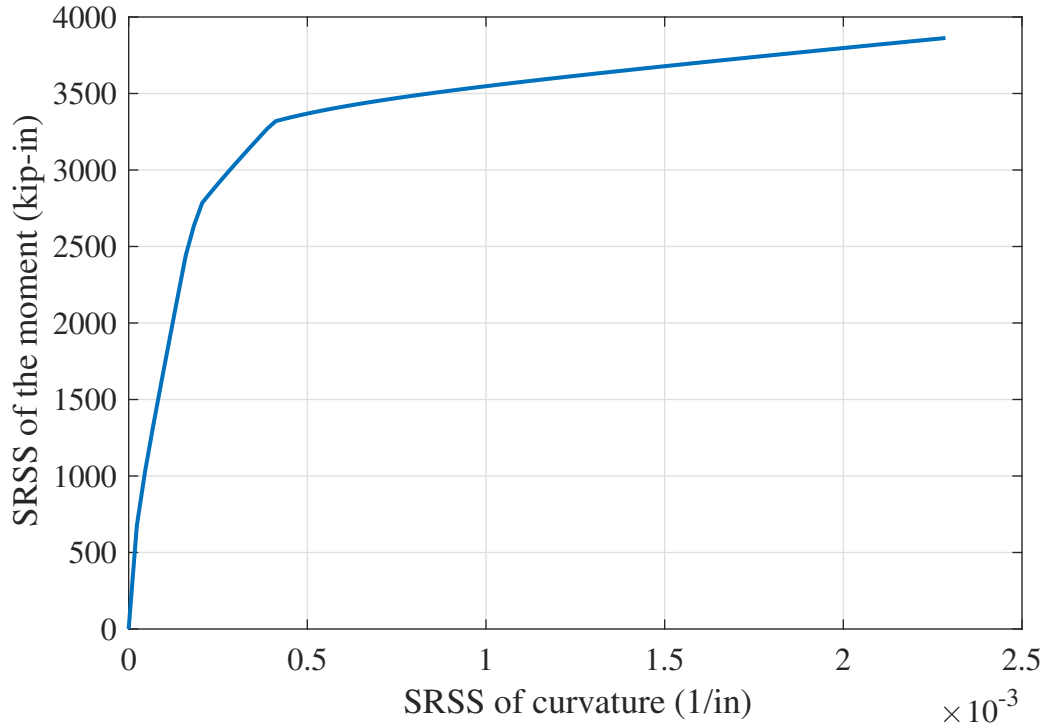
Figure 3.29: Moment curvature for the 3D RC section

3.3.2 Cases A and B

Similar to the procedure followed in the steel section 3D case study, the analytical solutions were derived for Case A (series system containing an elastic beam and a zero-length hinge) and Case B (single beam with ability for plasticity to spread along the height).

However, unlike the steel analyses, the elastic element properties for RC analysis are not uniquely defined. Initially, the properties for the elastic element were obtained from a CSiBridge analysis (for consistency of Case A solution). The modulus of elasticity was assumed to be equal to the modulus elasticity of concrete (3605 ksi) while the moment of inertia was $I = 7754$ in^4 (for comparison $I_g = 7854$ in^4).

Here, the plastic hinge length was assumed to be equal to the diameter of the column ($l_p = 20$ in). For comparison, the Caltrans SDC v1.7 [5] plastic hinge length equation is:

$$l_p = 0.08L + 0.15f_y d \tag{3.4}$$

which yields an estimate of 26.7 in for the RC case study column.

The results of Case A and Case B are shown in Figure 3.30. As mentioned in the 3D circular steel section case, the vertical axis (ordinate) is always the vector combination (square root sum of the squares) of loads in the y and z directions while the horizontal axis (abscissa) is always the vector combination of the displacements in the y and z directions.

Similar characteristics of the two solutions can be noted, mainly the location of the hinge guarantees that the nominal loads are equal. The stiffness (no clearly defined elastic and

57
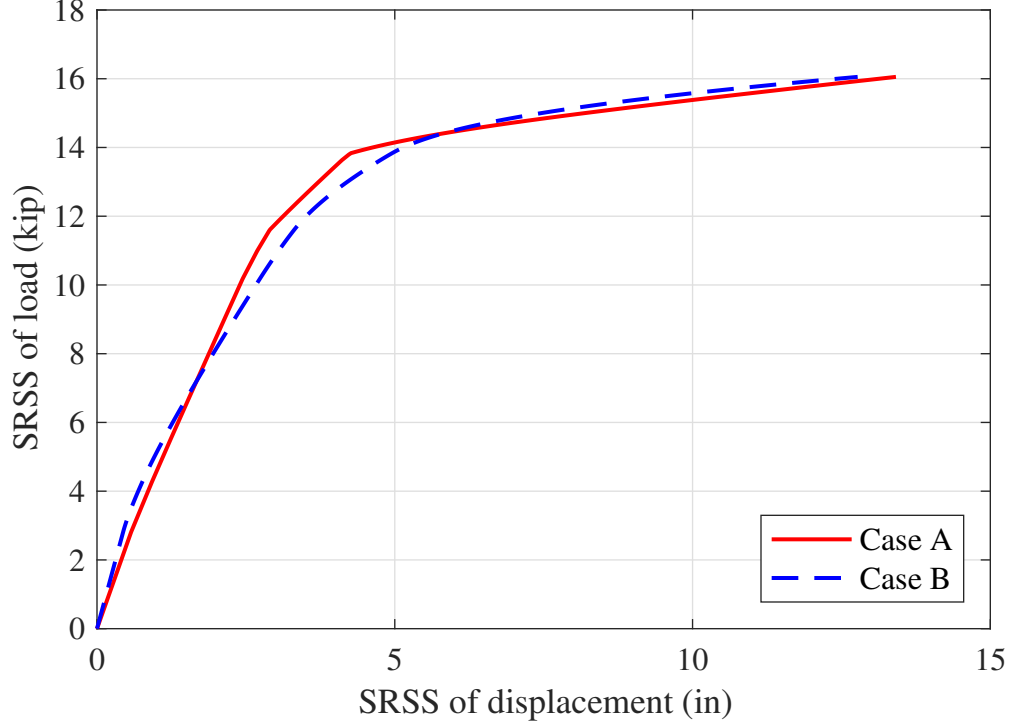
Figure 3.30: Comparison of Case A and Case B for 3D RC circular column

hardening regions now) are not correct, the series solution will always be more flexible. However, an important distinction with the steel results is that the RC Case A solution does not appear as poor of an approximation due to the large EI utilized by the CSiBridge frame element.

The moment of inertia of any reinforced concrete section depends mainly on the load level and stress distribution. As the load level increases, the moment of inertia decreases from the gross moment of inertia (I_g) until reaching the fully cracked moment of inertia (I_{cr}). Several values of the moment of inertia were investigated in the calculations of Case A to study its effect on the column behavior.

ACI 318-14 [7] section 6.6.3.1.1 suggests a value of $0.7I_g$ for the effective moment of inertia, which is independent of any parameters or load level. Paulay and Priestley (1992) [23] suggested a range of effective moment of inertias depending on the estimate of the axial load that includes the permanent gravity load plus the axial load from seismic overturning effects, as shown in Table 3.4. The original reference used axial force P in compression as the positive sign convention.

The Caltrans SDC [5] section 5.6.11 stipulates that the cracked flexural stiffness can be estimated by:

$$E_c \times I_{eff} = \frac{M_y}{\phi_y} \tag{3.5}$$

Where M_y = the moment capacity of the section at first yield of the reinforcing steel (M_y = 2419 k-in) and ϕ_y = the curvature of the section at first yield of the reinforcing steel (ϕ_y=

Table 3.4: Effective Moment of Inertia [23]

Axial load level	Effective moment of inertia range	Recommendation
$P > 0.5 f'_c A_g$	0.70-0.90 I_g	0.80 I_g
$P = 0.2 f'_c A_g$	0.50-0.70 I_g	0.60 I_g
$P = -0.05 f'_c A_g$	0.30-0.50 I_g	0.40 I_g
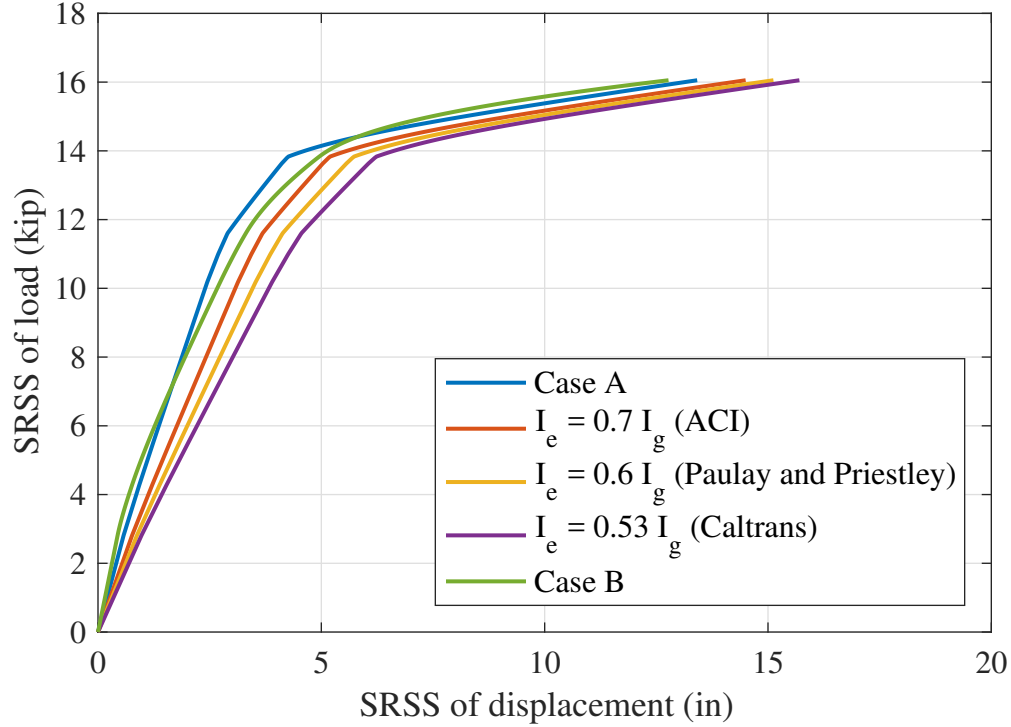
Figure 3.31: Effect of the moment of inertia reduction factor on RC column behavior

0.00016). The above equation gives an effective moment of inertia $I_{eff} = 4186$ in^4 which represents about 53% of the I_g.

Figure 3.31 shows the force-displacement comparison using different values of equivalent moment of inertia, including the one initially adopted from CSiBridge in the calculation of Case A. As can be seen, Case A (I from CSiBridge) has a different behavior compared to the 3D steel section case. Specifically, the stiffness of the column is over predicted after cracking because it is based on approximately the uncracked stiffness of the column ($I_{CSi} = 0.987\,I_g$) and not an appropriate composite or cracked stiffness. The member stiffness needs to be reduced to account for the inelastic cracking and softening that occurs as the neutral axis shifts. While any selection of I_{eff} is approximate (because it is not changed continuously with load level), it can be seen that the softening of I_{eff} yields the same trends between Case A and Case B as observed in the steel case study, e.g., Figure 3.21.
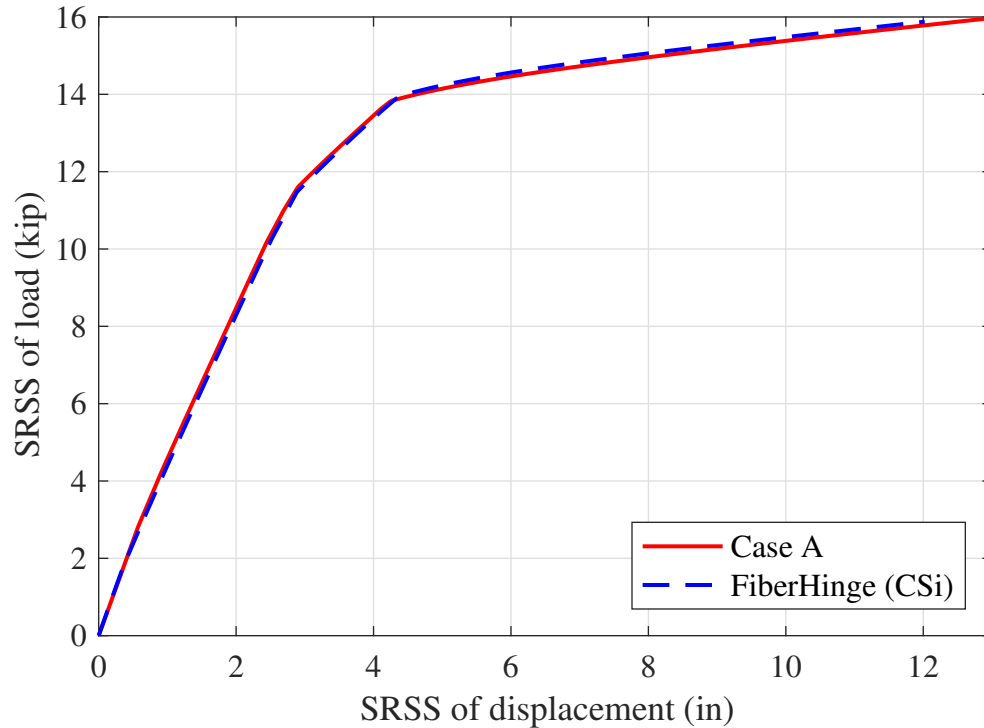
Figure 3.32: Comparison of Case A with CSiBridge for RC section of 3D case

3.3.3 Software implementations

Showing that Case A is Fiber hinge model in CSiBridge

Similar to the 3D case for the steel section, the 3D case study was modeled using CSiBridge V17.3.0 using a single frame element. At the base of the column, a frame hinge type (Fiber F-M2-M3) with a plastic hinge length of 20 in was inserted. Nonlinear analysis with displacement control was carried out. As can be seen in Figure 3.32, the CSiBridge analysis results show an acceptable match with the analytical solution from Case A.

Showing that Case B is OpenSees forceBeamColumn

Similar to the steel section in the 3D case, a single forceBeamColumn element was used to model the column (with similar stipulations that more elements or integration points may be warranted in different situations), which is based on the iterative force-based formulation. The same Lobatto integration rule with 5 integration points was used. Figure 3.33 compares the results between the exact solution and forceBeamColumn element in OpenSees, with a good match.
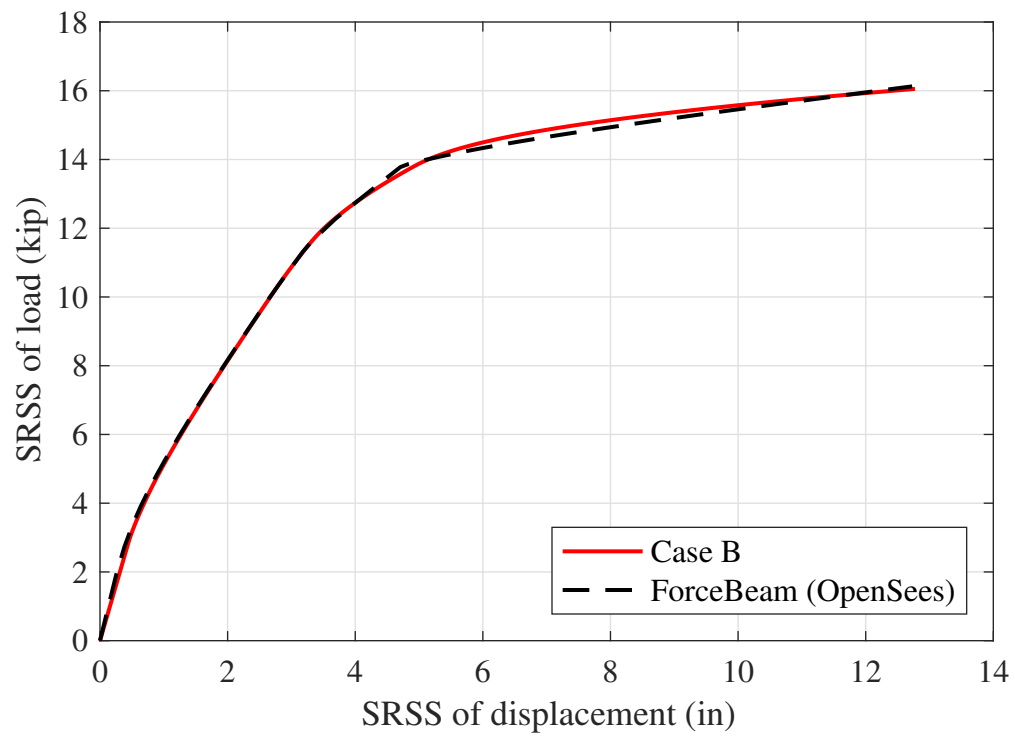
Figure 3.33: Comparison of Case B with forceBeamColumn element for RC section of 3D case
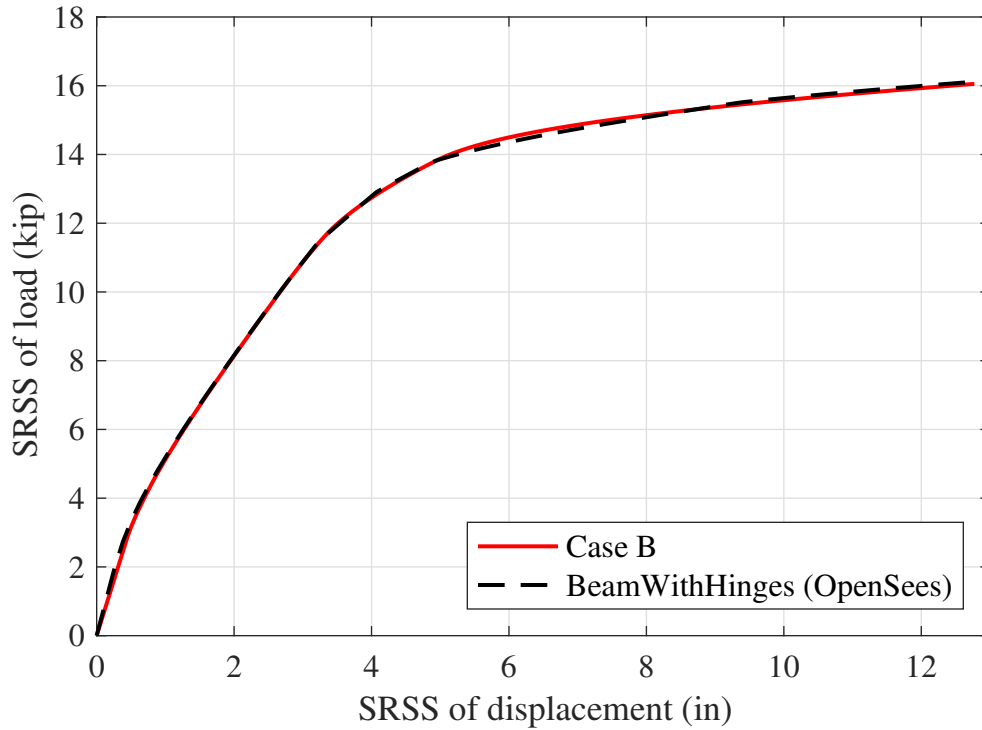
Figure 3.34: Comparison of Case B with beamWithHinges element for RC section of 3D case

Showing that Case B is OpenSees beamWithHinges

Two hinge sections at both ends of the column were used to define this beamWithHinges model. Also a fiber section was used to define the interior part of the column with length of $(H - 2l_p)$. Figure 3.34 shows the comparison between Case B and beamWithHinges and a good match between the two cases can be shown.

Correction of Fiber hinge by introducing a rigid element

A new node at $x = l_p$ was introduced to define the rigid element ($EI = \infty$) with length of l_p (20 in) and split the column into two different frame elements in this method of correction. The remaining length ($H - l_p = 220$ in) was modeled using an elastic beam (frame element without any frame hinges). A frame hinge type (Fiber P-M2-M3) is introduced at the bottom of the rigid element (at $x = 0$). The details of this method are shown in Figure 3.12. Here, the effective moment of inertia was used in both Case A (numerical solution) and in CSiBridge to be consistent with the outcomes of Figure 3.31. A modifier of 0.6 was used for the effective moment of inertia which represents the average of the values suggested by ACI 318-14 and Caltrans SDC.

Figure 3.35 shows the results of this method. It can be seen that the stiffness of the corrected case is under predicted due to the effect of the modifier before the cracking stage. The location of the hinge guarantees the nominal load is approximately correct. However,
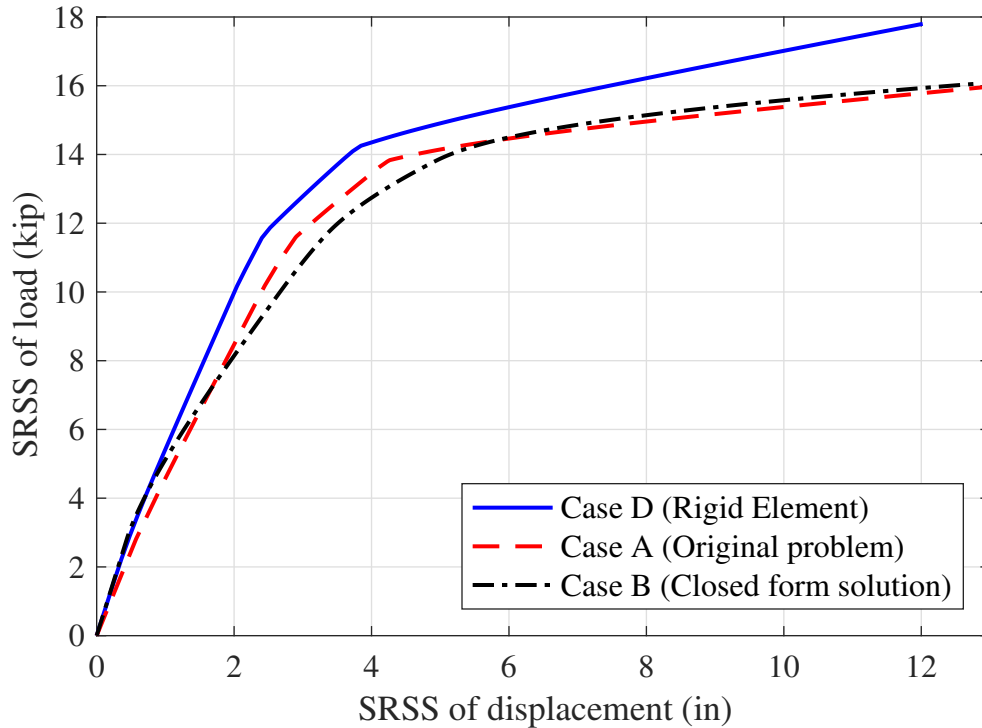
Figure 3.35: Correction of Case A using rigid element in CSiBridge

as mentioned previously, the effective moment of inertia is not changed continuously with load level and the presence of the rigid element result in the post-yielding stiffness being over predicted.

3.4 3D system (circular reinforced concrete section) in double curvature

In this section, the same reinforced concrete column is reanalyzed with double curvature. The rotation about y and z axes at the top end of the column were restrained in addition to the previous cantilever boundary conditions. The column was loaded with an axial load and two equal lateral loads in the local y and z directions. The axial load was held constant with a magnitude of 135 kips. Nonlinear analysis with displacement control was carried out.

Based on the results and findings for the reinforced concrete column described previously in this chapter, two modeling approaches were adopted in CSiBridge. The first approach is similar to Case A, but now with a fiber hinge (Fiber F-M2-M3) at both the top and the bottom of the column. Both hinges were assigned a plastic hinge length of 20 in. The column was modeled as a single frame element (containing the two end hinges) with a modifier of 0.6 on the moment of inertia.

In the second approach, the response is corrected by introducing rigid elements in the plastic hinge regions. The length of the rigid element was selected to be consistent with
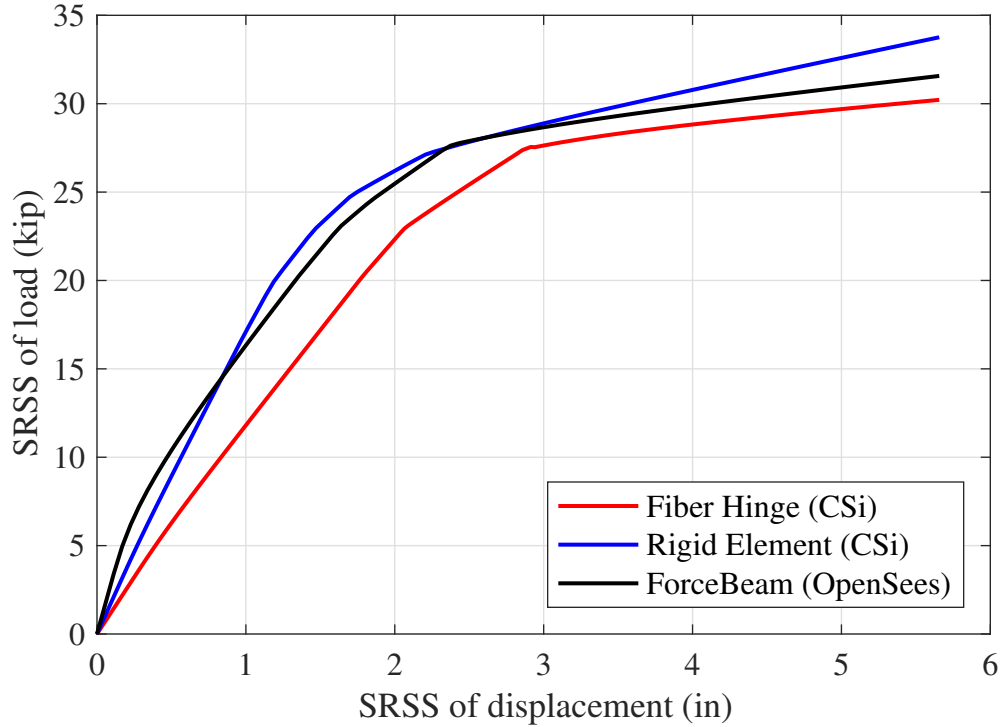
Figure 3.36: Comparison of CSiBridge and OpenSees results for double curvature case

the l_p (20 in) for both the top and the bottom of the column. This results in three frame elements being used in the column. The same effective moment of inertia from the single curvature case with a modifier of 0.6 was used.

The double curvature column was modeled in OpenSees using two forceBeamColumn elements. Each element contained 5 integration points (Lobatto integration rule). This is analogous to Case B in each of the two effective cantilever lengths, but results in a smaller integration point spacing than in the single cantilever case (because the overall column length remains unchanged).

Figure 3.36 compares the results between OpenSees and CSiBridge. The vertical axis represents the vector combination of loads in the y and z directions while the horizontal axis represents the vector combination of the displacements in the y and z directions. Similar to the single curvature case, the initial stiffness is under predicted in the corrected case (with rigid element at both ends of column); however, is limited to only the lower load levels. Near the nominal load capacity, the corrected stiffness is larger than that predicted by OpenSees. The post-yielding stiffness is over predicted once again.

3.5 Summary

This chapter demonstrated that the inelastic column responses predicted by both OpenSees and CSiBridge can be understood relative to the element formulations employed in each.

A sequence of analyses was performed with increasing complexity, starting with 2D steel columns, followed by 3D steel columns, and finally 3D reinforced concrete columns. Discrepancies in stiffness and strength are due to the series arrangement of hinge and frame elements, and the location of the plastic hinge relative to the peak column moment demands. Therefore, the same responses can be generated in both software packages as long as consistent modeling choices are made (i.e., selection of properties that govern the lumped plasticity elements). However, the extra step was taken to demonstrate a variety of common methods for approximately correcting the lumped plasticity approaches to better predict the response obtained when allowing plasticity to develop along the height of the columns. The most promising method is to introduce a rigid element over the plastic hinge region, while retaining the original position of the hinge itself. This enables the modeler to retain fiber cross sections, which is important for enabling both 2D and 3D responses to be correctly computed.

Numerous assumptions were made to simplify the modeling performed in this chapter. Specifically, the constitutive models were selected to be simple so as to ensure differences observed between software implementations were not due to the nonlinear backbone behaviors. Similarly, no attempt was made to include bond-slip springs, shear deformations, damage effects, etc. for similar reasons (it is not meant to imply that proper constitutive models and modes of deformation pertinent to the bridge at hand should be ignored).

Chapter 4

Benchmark Bridges – Description

To study more realistic bridges that contain a larger number of components and sources of nonlinearity, the four Ordinary Standard Bridges (OSBs) developed by Caltrans are employed. Three-dimensional (3D) bridge models were created based on drawings of the bridges and using the information already contained in the CSiBridge input files provided directly by Caltrans. The OpenSees models in the two benchmark chapters were specifically implemented to closely match the CSiBridge model responses, based on the lessons learned in Chapter 3, and do not reflect the more general modeling choices commonly made with OpenSees bridge models (see Chapter 6 for the models developed in OpenSees independently of the CSi ones).

To ensure that the commonalities identified by correcting the column responses from Chapter 3 were extended to the bridge level, two variants of each bridge model were created. The first entailed modifying the abutments in both the OpenSees and CSiBridge models to be simple rollers. The second entailed developing OpenSees models to mimic the assumed abutment boundary conditions already modeled in CSiBridge. The original abutment models are described for each bridge below, and referred to as the original abutment model. The simplified model of the abutment was generated by utilizing only a single roller (vertical single-point constraint) with a torsional restraint (rotation about the axis of the deck) and is referred to as the roller abutment model.

This chapter presents a detailed description of the four OSBs, the geometric and material properties, and the constitutive models employed in the OpenSees and CSiBridge implementations. The column constitutive models were subjected to both monotonic strain demands as well as cyclic strain demands to illustrate the differences in the OpenSees and CSiBridge realizations. The standardization of the inputs was largely achieved; however, unlike the simplified constitutive models utilized in Chapter 3, some differences remained in the constitutive models, particularly the unloading and reloading behaviors for concrete. In addition, the softening details did not necessarily match at all strain levels.

4.1 Ordinary Standard Bridge 1 (OSB1)

OSB1 is a two-span concrete bridge with a single two-column bent at the center. The clear column height is 18.5 ft (although this is not indicated on the drawings - but agreed upon based on discussions). Each span is 150 ft long. The bent contains two 5'-6" diameter circular reinforced concrete columns at 24' (center-to-center) spacing. The circular cross sections contain 36 #11 longitudinal bars and #8 at 6 in transverse spirals. The columns are founded on pile caps with potential foundation details for shallow or deep foundations. The connection at the pile cap to the column is a pipe pin.

The superstructure is a continuous cast-in-place (CIP) post-tensioned concrete box girder with five cells. The total depth and width of the superstructure are 6 ft and 47.5 ft, respectively. Each cell is 8 ft wide on center. The bent cap is integral with the superstructure, therefore, it has the same 6 ft height. The width of the bent cap is 8'-8". The abutments are standard seat-type abutments with 2" movement rating. Each abutment is founded on a pile cap and 7x2 pile group. The elastomeric bearings are 1'-6" square and 2.25 in high (one under each of the six webs). The backwall to stem wall interface contains a construction joint as does the exterior shear key to stem wall interface. The end diaphragm is also integral with the superstructure and has a 3 ft width.

The specified material properties are $f'_c = 3.6$ ksi for the abutments and bent pile cap, $f'_c = 4$ ksi for the bridge structural concrete, and $f_y = 60$ ksi. The jacking force (for the box girder) is 10940 kip using 270 ksi low relaxation strand.

4.1.1 CSiBridge

The CSiBridge OSB models were developed previously by Caltrans and no changes were made in this chapter. Modeling decisions specific to each bridge are listed here for consistent comparison between software implementations. The center of mass in the CSiBridge model is located at 20 ft above the column bases.

A rigid element with a length of 2.8 ft was introduced at the top of each column by multiplying the moments of inertia of the rigid element by a multiplier of 3. A frame hinge type (Fiber P-M2-M3) was introduced at the middle of the rigid element. The rigid offset (1.5 ft) between column top and the deck was modeled with a rigid zone factor of 0.5. This rigid offset within the top frame element containing the hinge forced the hinge to move to a location 18 in below the nodes defining the deck centerline (not at a distance 16.8 in below as would have been the case without the rigid offset).

The moment of inertia for the remaining length of the column was reduced by using a modifier of 0.35 in both directions and no frame hinge was introduced in this part of the column. The bottom end joint of the column was pinned. In CSiBridge, the column is assigned 3.6 ksi concrete. The gross elastic properties of the column cross section are listed in Table 4.1.

The concrete constitutive models employed were Mander-unconfined and Mander-confined. The parameters of the constitutive models are shown in Table 4.2 and Table 4.3 for unconfined and confined concrete, respectively. The steel constitutive models used were: simple

Table 4.1: OSB1 column material and section properties

Parameters	Value
Cross section area (ft^2)	23.76
Moment of inertia, I_{22} (ft^4)	44.92
Moment of inertia, I_{33} (ft^4)	44.92
Torsion constant (ft^4)	89.84
Youngs modulus (ksi)	3420
Shear modulus (ksi)	1425

(table-based input) for the longitudinal steel, and 270 ksi tendons (not utilized due to elastic modeling of the superstructure). The important parameters of the longitudinal steel model are shown in Table 4.4.

Table 4.2: OSB1 Mander-unconfined concrete model (3600Psi) parameters

Parameters	Value
Compressive strength (ksi)	3.6
Strain at compressive strength (in/in)	0.002219
Ultimate strain capacity (in/in)	0.005

Table 4.3: OSB1 Mander-confined concrete model (3600Psi) parameters

Parameters	Value
Tangent modulus of elasticity (ksi)	3.42
Secant modulus of elasticity (ksi)	0.754
Compressive strength of unconfined concrete (ksi)	3.6
Compressive strength of confined concrete (ksi)	5.055
Strain at strength of unconfined concrete (in/in)	0.002219
Ultimate strain capacity of unconfined concrete (in/in)	0.005
Strain at compressive strength of confined concrete (in/in)	0.00671

The superstructure (box girder) material was based on the elastic modulus of 3.6 ksi concrete and the section properties were selected to be non-prismatic. The nominal box girder cross-sectional properties are listed in Table 4.5. These values do not include the girder flare, or any other variation near the supports.

An infinite stiffness was used to define the material of the bent cap of the bridge. The frame elements for the bent cap utilized rectangular prismatic sections. The additional weight and mass due to the bent cap were included in the analysis. The bent cap cross-sectional properties are listed in Table 4.6.

For the bridge model containing the original abutment model, an infinite stiffness was used to define the material of the end diaphragm of the bridge. The frame elements for

Table 4.4: OSB1 simple steel model (A615Gr60) parameters

Parameters	Value
Young's Modulus (ksi)	29000
Yield stress (ksi)	60
Ultimate strength (ksi)	60
Strain at onset of strain hardening (in/in)	0.01
Ultimate strain capacity (in/in)	0.09
Final slope (Multiplier on E)	-0.1

Table 4.5: OSB1 superstructure material and section properties

Parameters	Value
Cross section area (ft^2)	83.34
Moment of inertia, I_{22} (ft^4)	444.01
Moment of inertia, I_{33} (ft^4)	15087.1
Torsion constant (ft^4)	1283
Youngs modulus (ksi)	3420
Shear modulus (ksi)	1425

Table 4.6: OSB1 bent cap material and section properties

Parameters	Value
Cross section area (ft^2)	52.00
Moment of inertia, I_{22} (ft^4)	156.00
Moment of inertia, I_{33} (ft^4)	325.48
Torsion constant (ft^4)	481.48
Youngs modulus (ksi)	∞
Shear modulus (ksi)	∞

the end diaphragm utilized rectangular prismatic sections. The additional weight and mass due to the end diaphragm were included in the analysis. The end diaphragm cross-sectional properties are listed in Table 4.7. The end diaphragm elements do not appear in the model with the roller abutments.

Table 4.7: OSB1 end diaphragm material and section properties

Parameters	Value
Cross section area (ft^2)	18.00
Moment of inertia, I_{22} (ft^4)	54.00
Moment of inertia, I_{33} (ft^4)	13.50
Torsion constant (ft^4)	67.50
Youngs modulus (ksi)	∞
Shear modulus (ksi)	∞

A single multilinear plastic link element was used to define the nonlinear properties of the longitudinal degree of freedom (U1) at each abutment. The force-deformation relation is elastic-plastic (compression only) with a yield displacement of -0.05 ft and yield force of -1555 kips, as shown in Figure 4.1. The effective stiffness for the linear analysis case for the longitudinal and transverse (local coordinates U1 and U3) directions are 31092 k/ft and 3780 k/ft, respectively. The effective stiffness for all analysis cases for the vertical degree of freedom (U2) is 1×10^6 k/ft. In addition, there is a restraint on the rotation about the vertical axis.
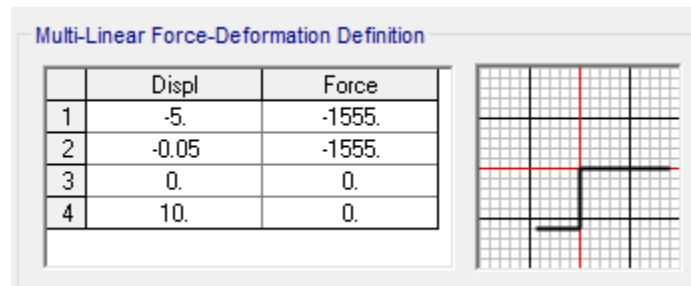
Figure 4.1: Properties of OSB1 abutment link in the longitudinal direction (kip-ft)

To more easily quantify the resultant behavior of the abutment elements and nonlinear behaviors, the load-displacement relationship of the abutment in OSB1 is shown in Figure 4.2. In the case of OSB1, the resultant force behaviors in each of the longitudinal, transverse and vertical directions, respectively, follow directly from the plastic link element behaviors.

The CSiBridge OSB1 abutment is consistent with the EPP-Gap model employed in the previous study [18] and in the MSBridge results presented in that report. However, the longitudinal gap is not consistent between the CSiBridge model, the MSBridge model, and the bridge plans.

70
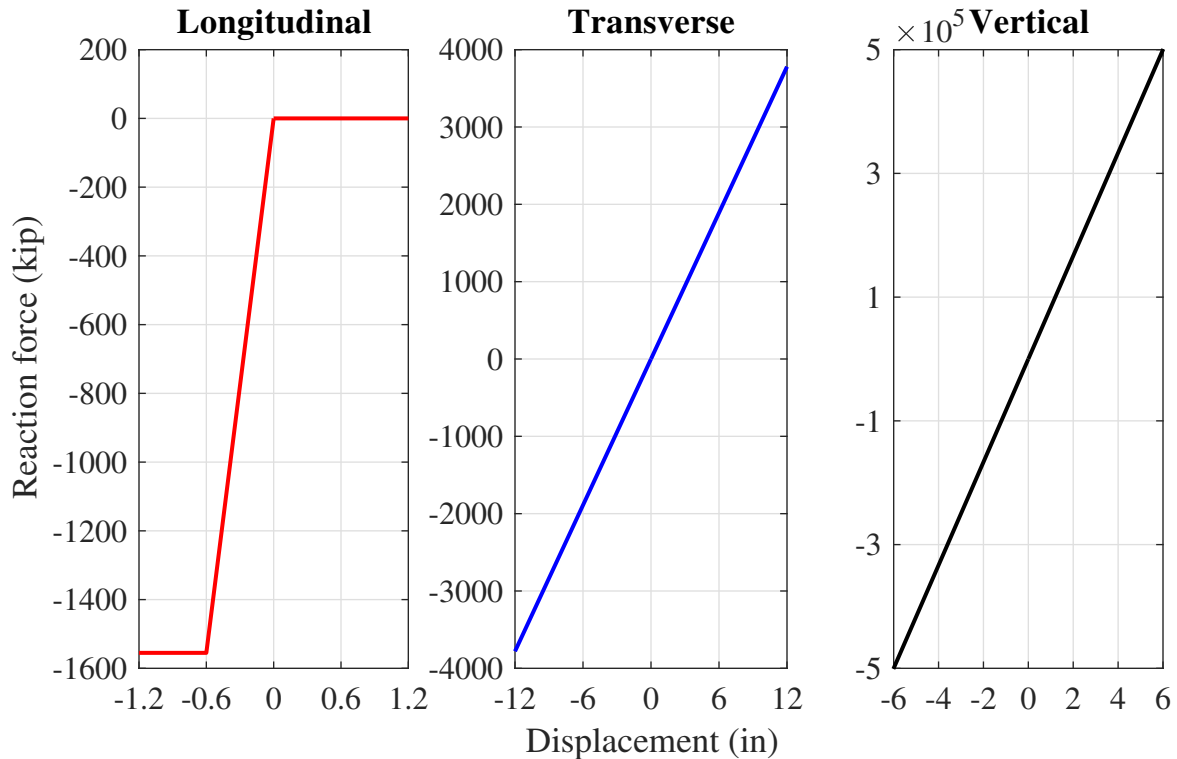
Figure 4.2: Abutment resultant load-displacement relationship for OSB1 in CSiBridge

4.1.2 OpenSees

The OpenSees OSB models developed for this project aim to imitate the CSiBridge models developed previously by Caltrans and subsequently used in this project. Modeling decisions specific to OSB1 are listed here for a consistent comparison between software implementations. The elastic material and section properties used for the columns, superstructure, bent cap, and end diaphragm were duplicated directly and therefore are not repeated here. The quantities were previously listed in Table 4.1, Table 4.5, Table 4.6, and Table 4.7, respectively. The elements assumed to remain elastic in the model were modeled using the elasticBeamColumn in OpenSees.

Due to the degrees of freedom associated with the zeroLengthSection in OpenSees, it was not possible to directly include a fiber-based cross section in the OpenSees model to match the CSi results. Therefore, two modeling strategies were adopted. The first was similar to that employed in Chapter 3, where the moment-curvature was run apriori with an assumed axial load, and the results were converted to a moment-rotation spring. The lumped spring was located at 15.6 in from the top of the elastic portion of the column. The spring itself was a CoupledZeroLength element to account for the circular yield surface, and the portions above and below the hinge were made stiff. The second approach used a forceBeamColumn element with a finite length specific to the hinge length, but using only a single integration point. To accommodate the particulars of the hinge assumptions in OSB1, it was necessary

71

to use the FixedLocation integration rule at the location specified above (since it is not in the center of the hinge element). The benefit of the latter approach is there is a fiber cross section at the single integration point, and therefore, the model accounts for axial load variations and is easier to implement. The second approach was adopted for the OSB1 results presented in the report.

The columns were modeled with stiff elasticBeamColumn elements to represent the rigid portions. The interior of the columns were modeled as elasticBeamColumns with the same property modifiers as implemented in the CSiBridge models. The bottom node of the columns were pinned. The fiber cross section discretization was created to match CSiBridge, with individual core concrete, cover concrete, and longitudinal reinforcing steel constitutive models. Due to the similarity of the constitutive models between the two software, Concrete04 was used for both the core and cover concrete with properties given in Table 4.8. Concrete04 does not model the linear descending branch of the unconfined concrete indicated in the CSiBridge manual and constitutive model dialog boxes, the stress immediately drops to zero at the specified ultimate strain.

Table 4.8: Concrete04 material properties employed for the OSB1 column

Parameter	Core	Cover
Compressive strength (ksi)	-5.08	-3.6
Strain at maximum strength	-0.0069	-0.0022
Crushing strength (ksi)	-4.66	-0.0
Strain at crushing strength	-0.0163	-0.0044
Tensile strength (ksi)	0	0.45
Elastic modulus (ksi)	4063	3420

The values for the ultimate strain and crushing strength of the confined concrete were taken directly from CSi for consistency. In addition, while the CSi manual indicates there is tension behavior in the confined concrete, it was not observed during the constitutive model tests presented in the next subsection, and therefore the tensile confined strength was set to zero.

The longitudinal steel reinforcement used the same table data to identify the tension and compression backbone points (symmetric). To allow for hysteretic behavior (albeit with the same initial stiffness throughout), the MultiLinear material was used. Due to the unloading and reloading rules of the material, it was not possible to include the full softening branch. Therefore, the material was wrapped in a MinMaxMaterial to ensure that the stress dropped to zero, in this case at a value of 0.10 in both compression and tension.

To define the nonlinear properties of the longitudinal degree of freedom at each abutment, a compression-only ElasticPPGap material in OpenSees was used. This material used a longitudinal gap, effective stiffness, and yield force of -0.0 ft, 31100 k/ft and -1555 k respectively. In the transverse and vertical directions, linear elastic behavior was assumed. The effective stiffnesses were 3780 k/ft and 1,000,000 k/ft, respectively, for the transverse and vertical direction. Torsion about the bridge deck at the bridge ends was also restrained.

The resulting model configuration can be seen in Figure 4.3.

(a) Perspective

(b) Profile

(c) Longitudinal
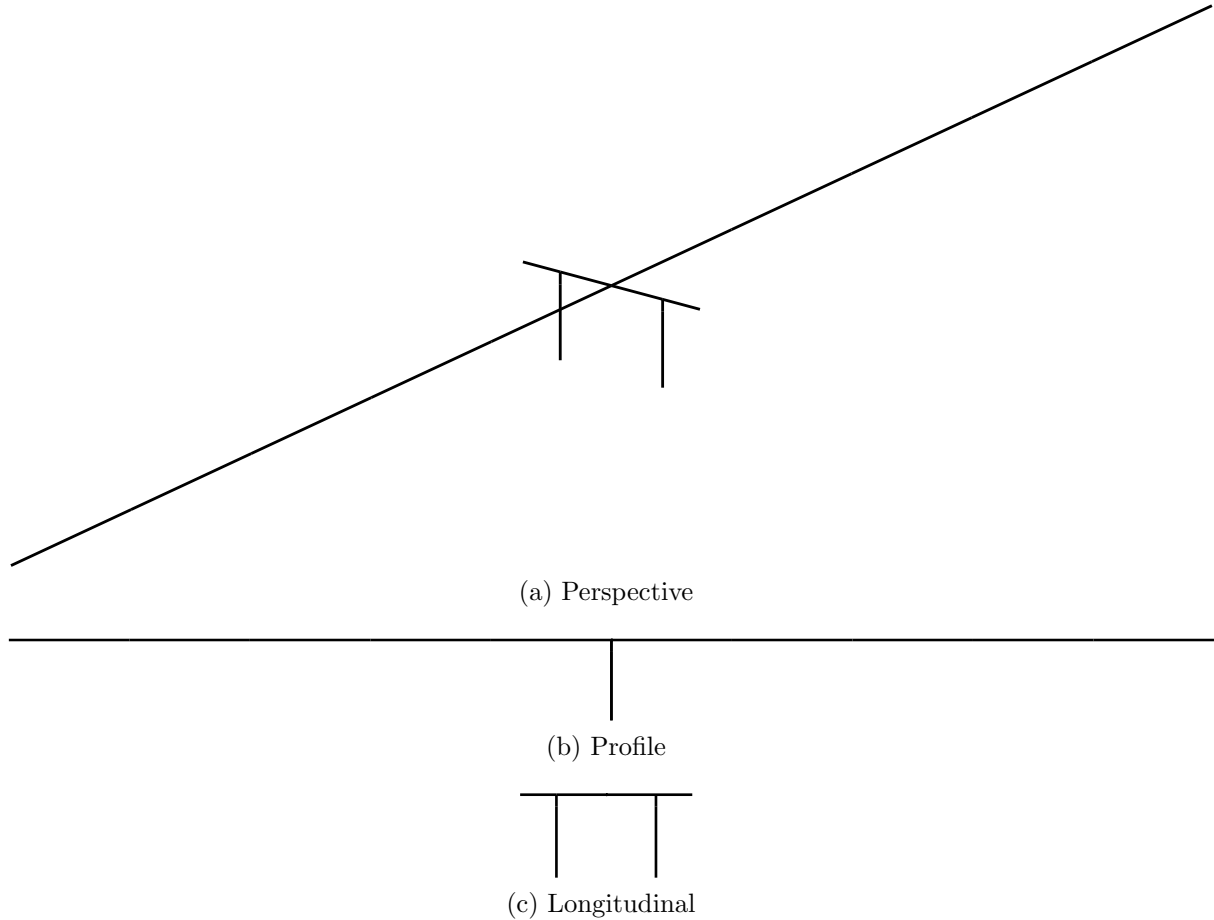
Figure 4.3: OpenSees model of OSB1

4.1.3 Column Constitutive Models

The column constitutive models were studied independently under monotonically increasing strains and cyclic strains. Comparative results are presented here for OSB1 models in OpenSees and CSiBridge for each of the longitudinal steel, cover concrete, and core concrete. The procedure for obtaining stress-strain relationships in OpenSees is direct (strain history desired is prescribed directly on a single fiber). However, in CSiBridge V17.3.0 the process was achieved through use of frame elements with creative use of properties.

A one-dimensional rigid truss element was used to obtain stress-strain relationships of the constitutive models. For the steel materials and unconfined concrete, a single fiber hinge of unit length and area was used to capture plastic behavior. For the confined concrete, the truss was split into two elements; the rigid element and an element of unit length with the cross section of the column's plastic hinge. The cross section of the column's plastic hinge
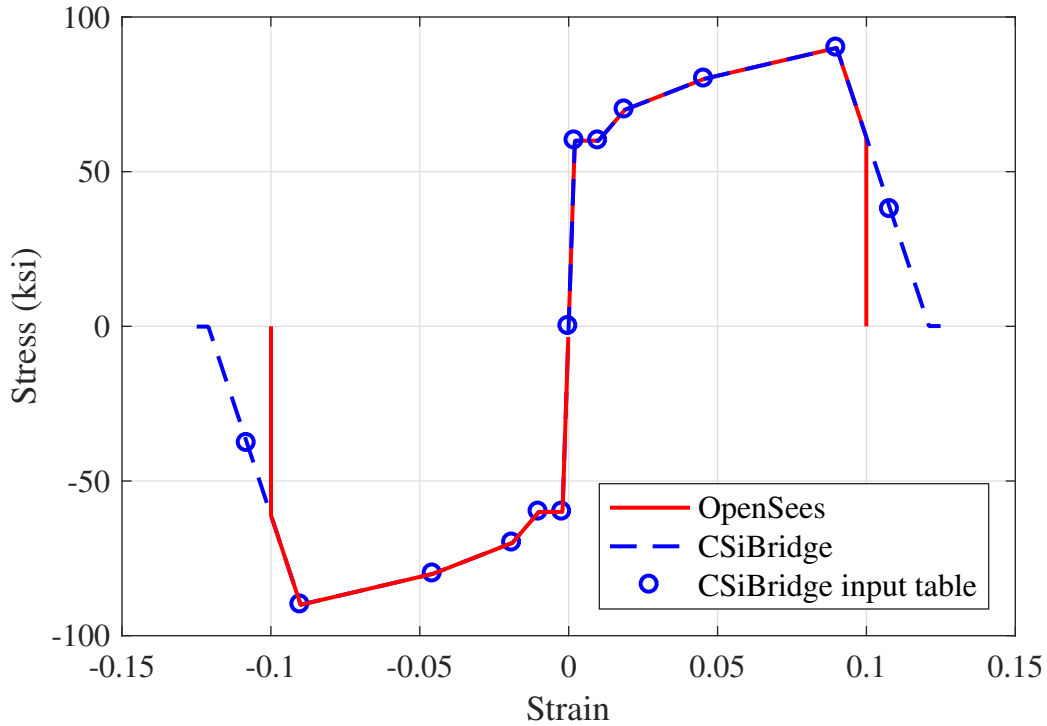
Figure 4.4: Steel monotonic stress-strain response for OSB1

was modified to have no cover concrete, and zero strength longitudinal bars. Thus leaving only the confined core concrete. The forces obtained from this model were normalized by the area of the core to obtain stress.

The steel monotonic and cyclic stress-strain responses are shown in Figures 4.4 and 4.5, respectively. Due to the table-based inputs associated with the steel models, clearly the responses are identical between the two software. The only distinction purposely introduced was that the OpenSees model gradually unloads to zero before being removed from the analysis (through the MinMaxMaterial) to eliminate spurious negative strength when unloading from the softening backbone. The cyclic results are also the same due to the assumptions of the Multilinear material in OpenSees.

The cover concrete (unconfined) monotonic and cyclic stress-strain responses are shown in Figures 4.6 and 4.7, respectively. The monotonic backbones are shown together with the predictions from the equations provided in the CSiBridge user manual. The cover compressive predictions are consistent for the monotonic case; however, the CSiBridge solution only matches the backbone in a piecewise linear way. It was verified that this piecewise linear behavior was not due to the convergence tolerance specified or the number of strain increments utilized in the history. The OpenSees compressive stress drops rapidly to zero after twice the strain at the peak compressive stress (due to Concrete04 material). However, the CSiBridge results continue to decrease linearly to zero, accommodating very large strains. The unconfined behavior does not appear consistent with the linear drop predicted by the equations and the figure shown in the constitutive model dialog boxes. The OpenSees model
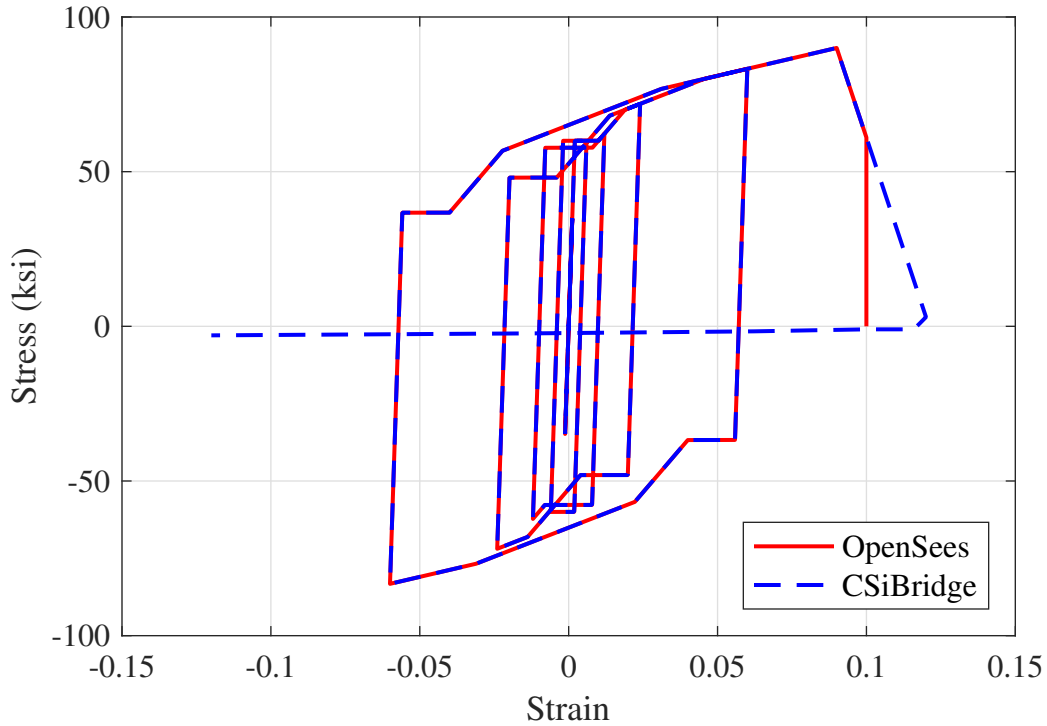
Figure 4.5: Steel cyclic stress-strain response for OSB1

has the ability to specify an exponential curve for the tension softening behavior, therefore, they are not identical as modeled here (OpenSees uses a parameter of 0.1 for the tension behavior).

The cyclic responses show a similar match for the portions of the tension and compression backbones; however, the unloading and reloading rules are not the same (CSiBridge here uses kinematic). In addition, there is spurious unloading and reloading through the lower-right quadrant for the CSiBridge model that dramatically increases the energy dissipation of the material. As with the monotonic case, it is possible to continue to increase the compressive strain well beyond the crushing strain (the linear softening in compression is evident from the figure).

The core concrete (confined) monotonic and cyclic stress-strain responses are shown in Figures 4.8 and 4.9, respectively. The monotonic backbones are shown together with the predictions from the equations provided in the CSiBridge user manual. There were convergence issues that prevented the softening portion of the CSiBridge from being obtained in the monotonic case, the results shown are based on a slightly relaxed convergence criterion. As with the unconfined case, there appears to be a linear softening portion that extends well beyond the crushing strain of the confined concrete. In addition, convergence problems prevented the CSiBridge cyclic case from running beyond the first few steps at low amplitude; therefore, only the OpenSees results are presented here. It is therefore unknown the difference in the energy dissipation capabilities at the constitutive model level.
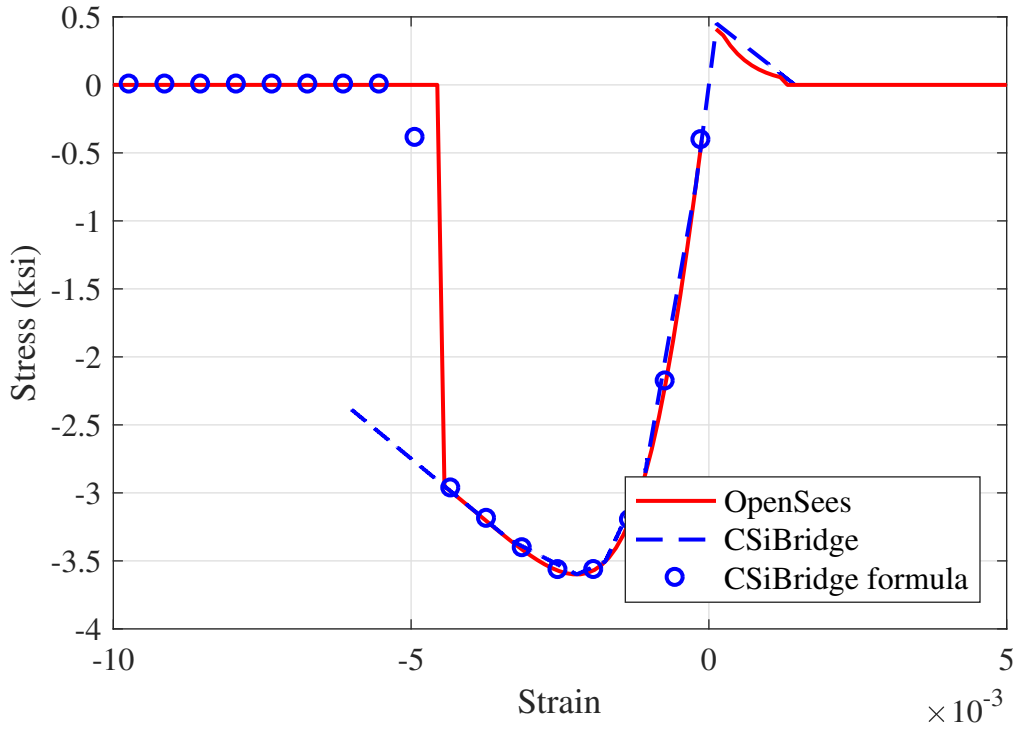
Figure 4.6: Cover concrete monotonic stress-strain response for OSB1
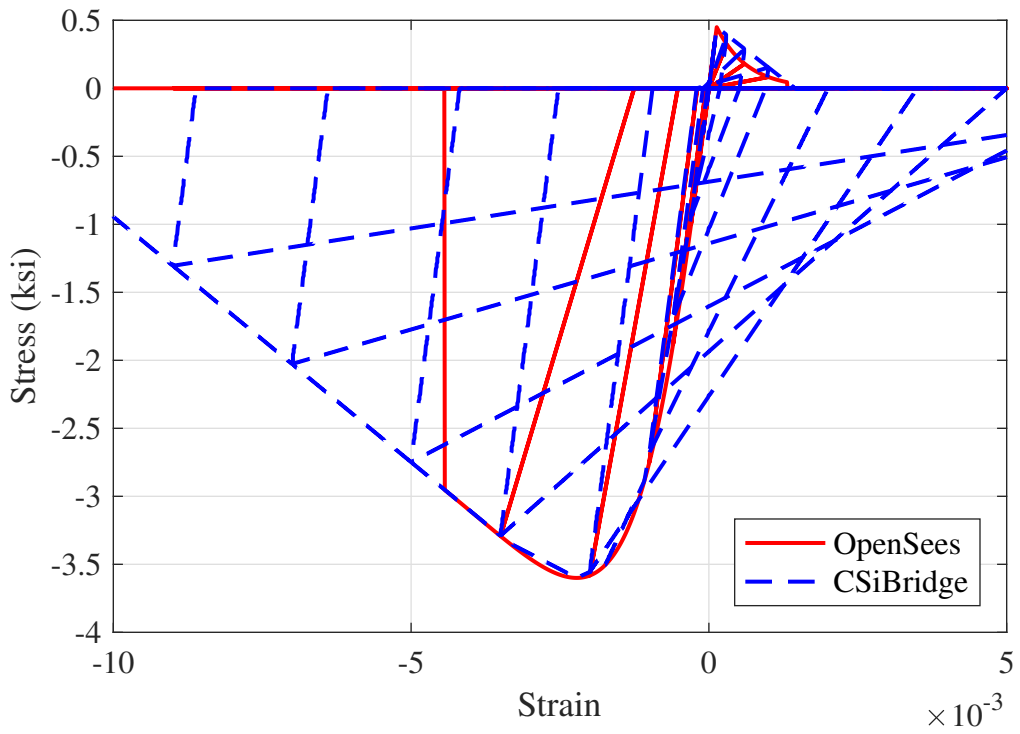
Figure 4.7: Cover concrete cyclic stress-strain response for OSB1
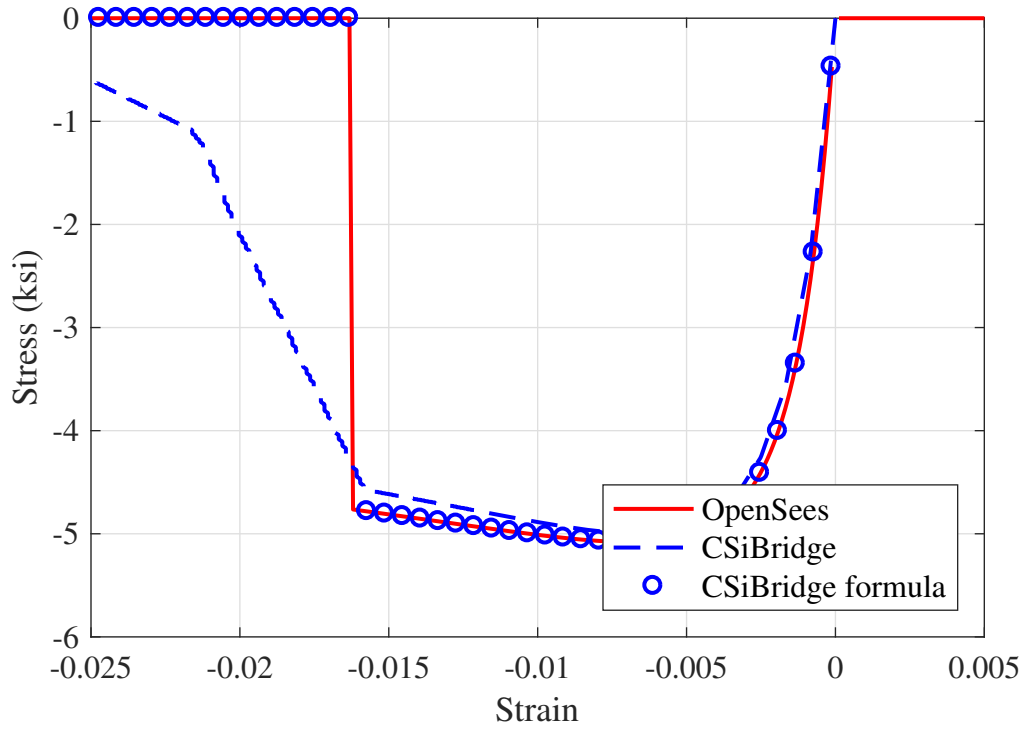
Figure 4.8: Core concrete monotonic stress-strain response for OSB1
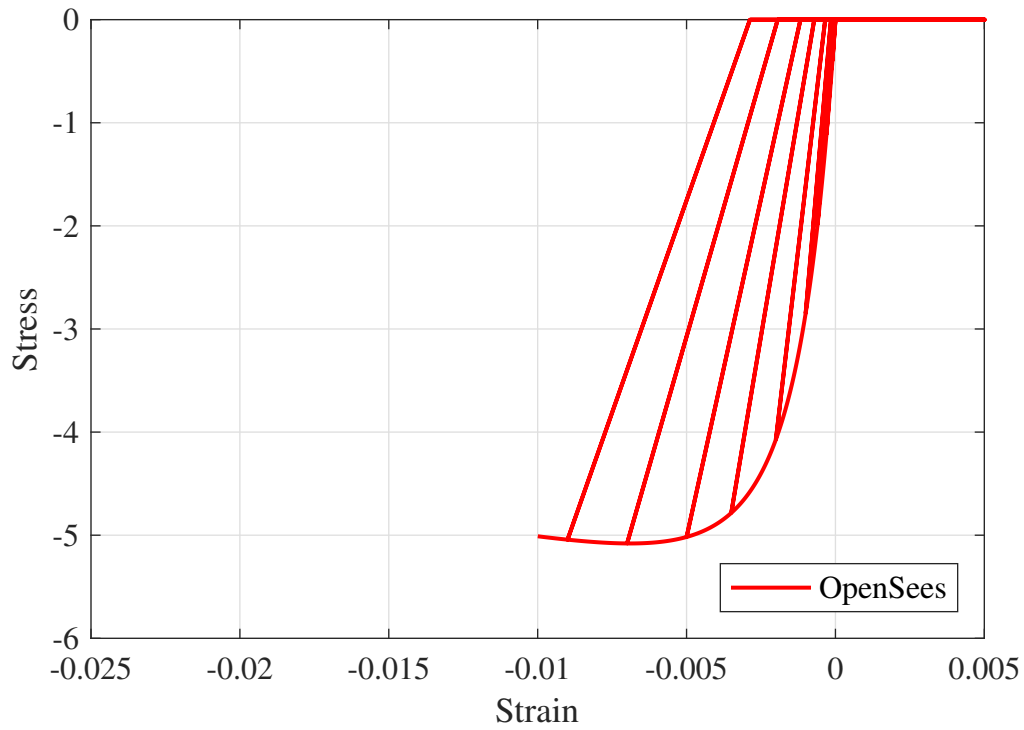
Figure 4.9: Core concrete cyclic stress-strain response for OSB1

77
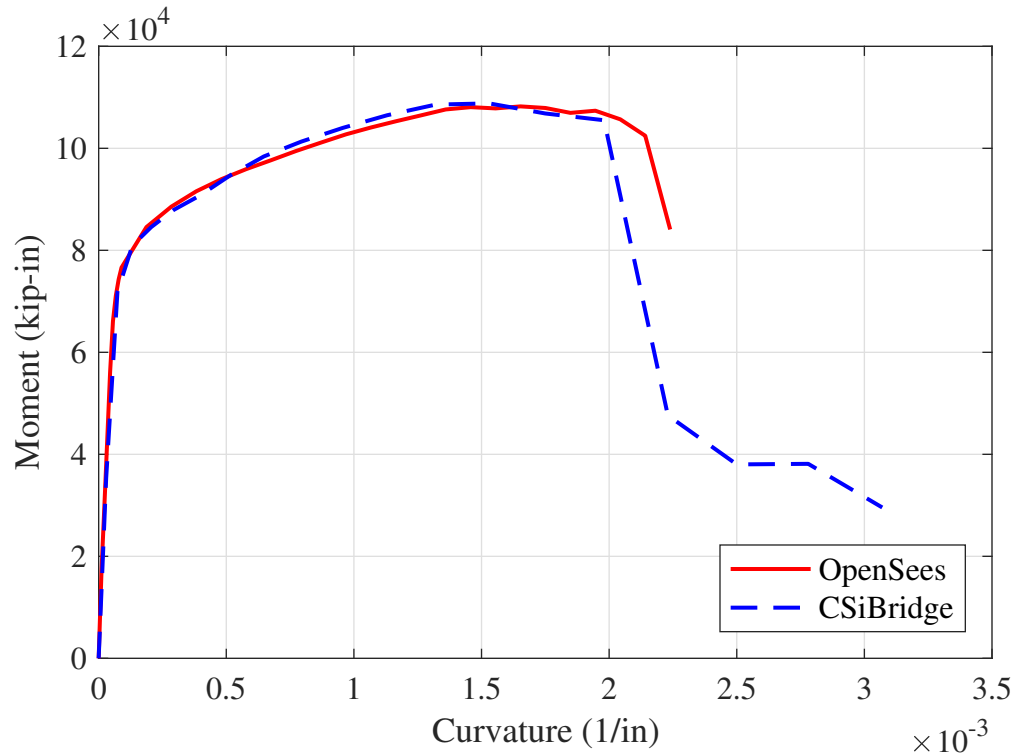
Figure 4.10: Moment-curvature response for OSB1

4.1.4 Moment-Curvature Analysis

The standardization of the column constitutive models was extended to the section level. Moment-curvature analysis was performed on the fiber cross section for OSB1. Here it is assumed that the axial load is zero. Due to the similarity of the monotonic stress-strain backbone curves of the constituent materials, it was anticipated that the sectional response curves between OpenSees and CSiBridge would be similar. The differences obtained are therefore due to the discretization of the cross section and minor constitutive model differences.

The moment-curvature response is shown in Figure 4.10. The results begin to diverge beyond the peak moment, although clearly the steel softening backbones are identical between the two software. By setting the maximum steel strain in OpenSees to 0.09 (at the peak strength), it is possible to make the moment-curvature points of rapid descent align. It is not clear what causes the sudden drop in the CSiBridge results that then stabilize; however, it is likely due to the residual capacity in the confined concrete observed in Figure 4.8.

4.1.5 Hinge Force-Deformation Analysis

The differences in the nonlinear static and nonlinear dynamic responses of the bridge systems presented in Chapter 5 are in part due to the performance of the hinge elements. This is compounded by the slight differences observed from the moment-curvature and stress-strain responses; however, it is evident there is an additional source of error introduced within the
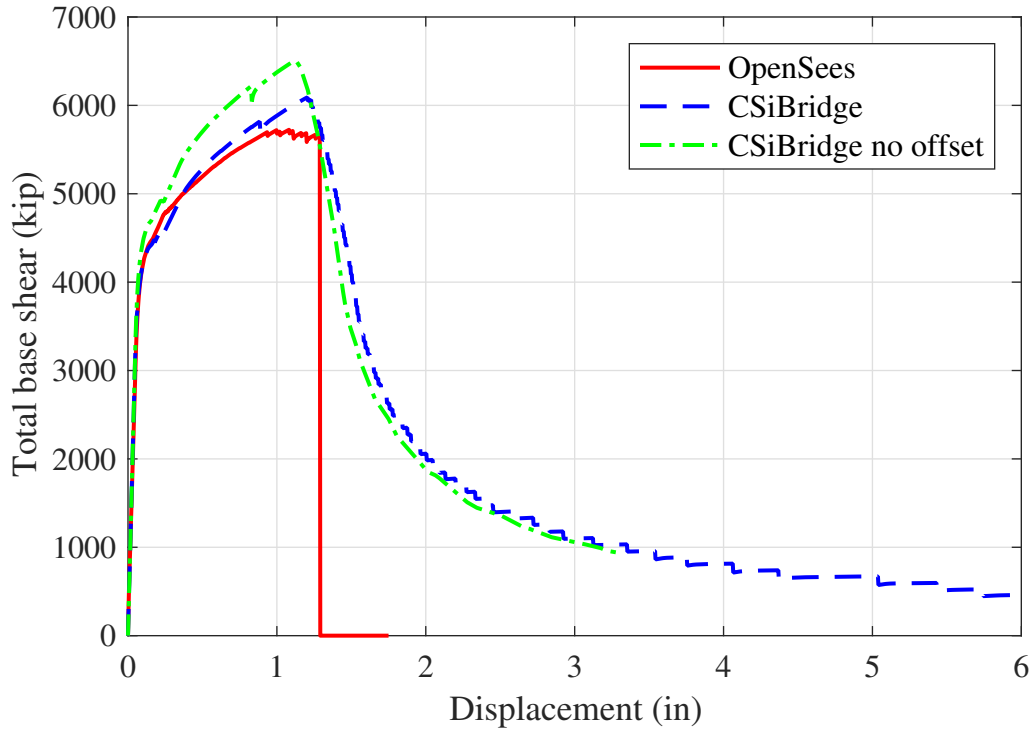
Figure 4.11: Column top hinge load-displacement response for OSB1

hinge elements themselves.

The column hinge at the top of the column was extracted from the overall bridge models in OpenSees and CSiBridge. This hinge was fully restrained at the base and then subjected to a monotonically increasing displacement at the top of the hinge in each lateral direction independently. The results are shown with an axial load of zero. The resulting force-displacement curve incorporates the modeling assumptions specific to the hinge, such as the rigid zone factor, rigid offset, location of the integration point, etc. Results from OSB1 are shown in Figure 4.11. The two CSiBridge cases shown are for the model as originally created, followed by a modified version where the rigid offset was removed. Both of these were used to attempt duplicating the responses in OpenSees.

Although the moment-curvature response is slightly more ductile in OpenSees, here the hinge pushover indicates a degradation of the strength near the peak force, as well as more brittle behavior than CSiBridge. This is due to the loss of concrete stress in Concrete04 once the ultimate strain is reached in compression. The location of the integration point also contributes to the hardening slope and peak strength; however, without a physical basis for moving it, the value reported in CSi as the absolute hinge location was utilized as described in the modeling section. The softening behavior prior to the peak shear force in OpenSees is also evident in the pushover curves of the whole bents presented in Chapter 5. It should be mentioned here that it is possible to get the hinge pushover and bent pushovers to agree; however, it requires removing the ultimate compressive strain limit (drop to zero stress) in concrete. Such an assumption leads to an increase in the predicted moment capacity and

ductility capacity, so the standardization of constitutive models to match the section level responses is maintained throughout.

4.1.6   MSBridge

The only modal information reported in [18] was 1.0, 1.0, and 0.82 sec for the first mode. Each value corresponds to a different type of abutment boundary, referred to as the "Roller model", "EPP-Gap model", and "EPP-Gap with bearings model", respectively.

In the EPP-Gap model in [18], a compression-only ElasticPPGap material in OpenSees was used for the longitudinal direction with gap of 0.14 in, stiffness of 2,591 kip/in, and yield force of -1,555 kip. For the transverse and vertical directions, an elastic material was used with stiffness of 315 kip/in and 83333 kip/in, respectively.

4.2   Ordinary Standard Bridge 2 (OSB2)

OSB2 is a two-span concrete bridge with a single column bent at the center. Each span is 150 ft long and the clear column height is 18.5 ft (clear column height similarly not specified on drawings but using 18.5 ft here by agreement). The column is 5'-6" diameter circular reinforced concrete section. The column section contains two rows of #11 longitudinal bars with 22 bars at each row (i.e., there are 22 bundles or a total of 44 bars) and #8 at 6" transverse spirals. The columns are founded on pile caps with details for a 5x5 pile group of 24" CIDH piles.

The superstructure is a continuous cast-in-place (CIP) post-tensioned concrete box girder with three cells. The total depth and width of the superstructure are 6 ft and 37.5 ft, respectively. The cells are 10'-8", 10'-2", and 10'-8" wide on center. The bent cap is integral with the superstructure. The dimensions of the bent cap are height of 6 ft and width of width of 8'-8". The abutments are standard seat-type abutments with 2" movement rating. Each abutment is founded on a pile cap and 6x2 pile group. The elastomeric bearings are 1'-6" square and 2.25 in high (one under each of the four webs). The backwall to stem wall interface contains a construction joint as does the exterior shear key to stem wall interface. The end diaphragm is also integral with the superstructure and has a 3 ft width.

The specified material properties are $f'_c = 3.6$ ksi for the abutments and bent pile cap, $f'_c = 4$ ksi for the bridge structural concrete, and $f_y = 60$ ksi. The jacking force is 8486 kip using 270 ksi low relaxation strand.

4.2.1   CSiBridge

Similar to OSB1, no changes were made to the CSiBridge model obtained from Caltrans. The center of mass in the CSiBridge model is located at 20 ft above the column bases. An inadvertent modeling choice was made for the column hinges that resulted in a much stiffer and more brittle bridge response than would otherwise have been anticipated. In Chapters 4

and 5, the original model was retained and a matched OpenSees model generated. However, a more representative model was created and used for study in Chapter 6.

A rigid element was introduced at the top and the bottom of the column with the same multiplier of 3 for the moments of inertia. The length of both the top and the bottom rigid element is 2.8 ft. A frame hinge type (Fiber P-M2-M3) is introduced at the middle of the rigid element (both at the top and bottom hinges). Unlike OSB1, no rigid offset was used in the OSB2 model, so the effective length of the columns is longer in OSB2. The inadvertent choice occurred due to the introduction of a separate element to model the rigid end regions with hinges. The default of 10% of the element length for the hinge length was retained which led to a plastic hinge length of 3.36 in.

The moment of inertia for the remaining length of the column was reduced by using a modifier of 0.35 in both directions and no frame hinge was introduced in this part of the column. The bottom of the column was fixed in all degrees of freedom. In CSiBridge, the column is assigned 4 ksi concrete. The gross elastic properties of the column cross section are the same as those shown for OSB1 in Table 4.1, except the elastic and shear moduli are 3605 ksi and 1520 ksi, respectively.

The constitutive models used in OSB2 were largely duplicates of those used in OSB1. Specifically, the longitudinal steel was identical to that shown in Table 4.4 and is not repeated here. The Mander model was once again used with the unconfined and concrete concrete; however, the parameters differed slightly due to the 4 ksi concrete. These updated parameters are shown in Tables 4.9 and 4.10 for unconfined and confined concrete, respectively.

Table 4.9: OSB2 Mander-unconfined concrete model (4000Psi) parameters

Parameters	Value
Compressive strength (ksi)	4
Strain at compressive strength (in/in)	0.002
Ultimate strain capacity (in/in)	0.005

Table 4.10: OSB2 Mander-confined concrete model (4000Psi) parameters

Parameters	Value
Tangent modulus of elasticity (ksi)	3.605
Secant modulus of elasticity (ksi)	0.961
Compressive strength of unconfined concrete (ksi)	4
Compressive strength of confined concrete (ksi)	5.4802
Strain at strength of unconfined concrete (in/in)	0.002
Ultimate strain capacity of unconfined concrete (in/in)	0.005
Strain at compressive strength of confined concrete (in/in)	0.005701

The total depth and width of the box girder are 6 ft and 27 ft respectively. The flange and web thickness of the box girder are 0.6 ft and 4 ft respectively. The bent cap is integral

with the superstructure. The depth and width of the bent cap cross section are 6 ft and 8.67 ft respectively with a total length of 37.5 ft. The superstructure's material and cross section properties are listed in Table 4.11.

Table 4.11: OSB2 superstructure material and section properties

Parameters	Value
Cross section area (ft^2)	70.8
Moment of inertia, I_{22} (ft^4)	310.9
Moment of inertia, I_{33} (ft^4)	7098
Torsion constant (ft^4)	777.43
Youngs modulus (ksi)	3420
Shear modulus (ksi)	1425

A rigid material was used to define the bent cap of the bridge by using an infinite modulus of elasticity. The frame elements for the bent cap utilized rectangular prismatic sections with properties listed previously in Table 4.6. No mass and weight contributions were added from the bent cap. Similarly, the end diaphragms were modeled as rigid with properties previously listed in Table 4.7. No mass and weight contributions were added from the end diaphragm.

In OSB2, two link elements in series are used to model the left and right abutments. The first link element connects to the deck end node, and is a gap link element with nonlinear properties for the longitudinal degree of freedom (U1). The effective stiffness for the linear analysis case is 2.4×10^6 k/ft while the gap and the stiffness for the nonlinear analysis case are -0.1667 ft and 120×10^3 k/ft respectively. The deck end node has restraints in U2, U3, and all rotational degrees of freedom. However, it appears the right abutment model has only the translational degrees of freedom restrained at the deck end node.

The second link element is a multilinear plastic link and it has nonlinear properties only in the longitudinal degree of freedom (U1) as shown in Figure 4.12. The nonlinear force-deformation relation is elastic-plastic (compression only) with a yield displacement of -0.05 ft and yield force of -1031 k. The node connecting the two link elements together has all degrees of freedom restrained except for U1 (longitudinal).

Multi-Linear Force-Deformation Definition

	Displ	Force
1	-8.3333	-1031.
2	-0.05	-1031.
3	0.	0.
4	0.05	0.
5	8.3333	0.
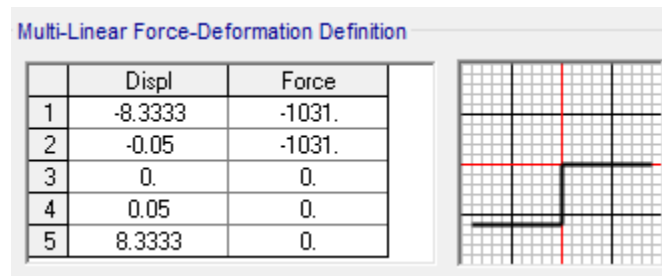
Figure 4.12: Properties of OSB2 abutment link in the longitudinal direction (kip-ft)

To more easily quantify the resultant behavior of the abutment elements and nonlinear behaviors, the load-displacement relationship of the abutment in OSB2 is shown in Fig-

ure 4.13. The transverse and vertical directions are restrained in the OSB2 model and therefore do not deform. The longitudinal direction is a series combination of the two link element behaviors.
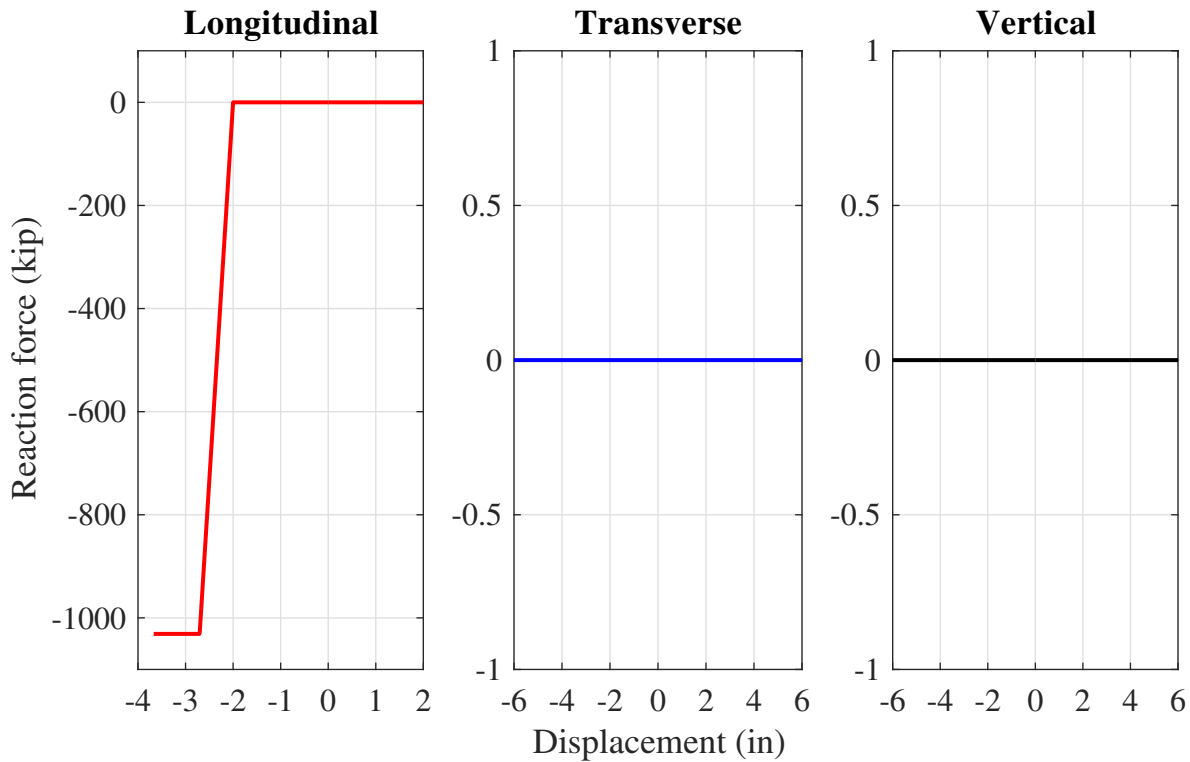
Figure 4.13: Abutment resultant load-displacement relationship for OSB2 in CSiBridge

4.2.2 OpenSees

The OpenSees OSB2 model followed directly the approach taken for OSB1 in imitating the CSiBridge models developed previously by Caltrans. Modeling decisions specific to OSB2 are listed here for a consistent comparison between software implementations. The elastic material and section properties used for the columns, superstructure, bent cap, and end diaphragm were duplicated directly and therefore are not repeated here. The elements assumed to remain elastic in the model were modeled using the elasticBeamColumn in OpenSees.

The same two plastic hinge modeling strategies mentioned with OSB1 were also adopted for OSB2. The first approach was the CoupledZeroLength element with a moment-rotation relationship determined from prior moment-curvature analysis. The implementation for OSB2 was simpler due to the absence of the rigid offset, so the hinge element of length 3.36 in was used directly in the center of the 2.8 ft rigid region at the top and bottom hinges. The second approach used a forceBeamColumn element with a finite length specific to the hinge length, but using only a single integration point. This approach was also simpler, with

a single Legendre integration point in the forceBeamColumn element. The second approach was again adopted for the results presented here.

The columns were modeled with stiff elasticBeamColumn elements to represent the rigid portions. The interior of the columns were modeled as elasticBeamColumns with the same property modifiers as implemented in the CSiBridge models. The bottom node of the column was fixed. The fiber cross section discretization was created to match CSiBridge, with individual core concrete, cover concrete, and longitudinal reinforcing steel constitutive models. Due to the similarity of the constitutive models between the two software, Concrete04 was again used for both the core and cover concrete with properties given in Table 4.12. The values for the ultimate strain and crushing strength of the confined concrete were taken directly from CSi for consistency.

Table 4.12: Concrete04 material properties employed for the OSB2 column

Parameter	Core	Cover
Compressive strength (ksi)	-5.51	-4.0
Strain at maximum strength	-0.0056	-0.002
Crushing strength (ksi)	-4.82	-0.0
Strain at crushing strength	-0.0153	-0.004
Tensile strength (ksi)	0	0.475
Elastic modulus (ksi)	4231	3605

To define the nonlinear properties of the longitudinal and transverse degree of freedom at each abutment, the ElasticPPGap materials in OpenSees were used. The longitudinal material used a gap, effective stiffness, and yield force of -0.167 ft, 21372 k/ft and -1031 k respectively. The transverse material used a gap, effective stiffness, and yield force of -0.083 ft, 1200 k/ft and -179.4 k respectively. In the vertical direction, the abutment was fixed. The resulting model configuration can be seen in Figure 4.14.

4.2.3 Column Constitutive Models

The column constitutive models were studied independently under monotonically increasing strains and cyclic strains. Comparative results are presented here for OSB2 models in OpenSees and CSiBridge; however, due to the similarity in the modeling assumptions made for OSB1 and OSB2, only the models that have different parameters are presented here (for OSB2, the steel model was the same, so it is omitted). The procedure for obtaining the stress-strain relationships in both software packages is also the same and not repeated here.

The cover concrete (unconfined) monotonic and cyclic stress-strain responses are shown in Figures 4.15 and 4.16, respectively. The monotonic backbones are shown together with the predictions from the equations provided in the CSiBridge user manual. The cover compressive predictions deviate slightly beyond the peak compressive stress, in addition to the previously observed match to the backbone in a piecewise linear way. The OpenSees model has the ability to specify an exponential curve for the tension softening behavior, therefore,

(a) Perspective

(b) Profile

(c)   Longitudinal
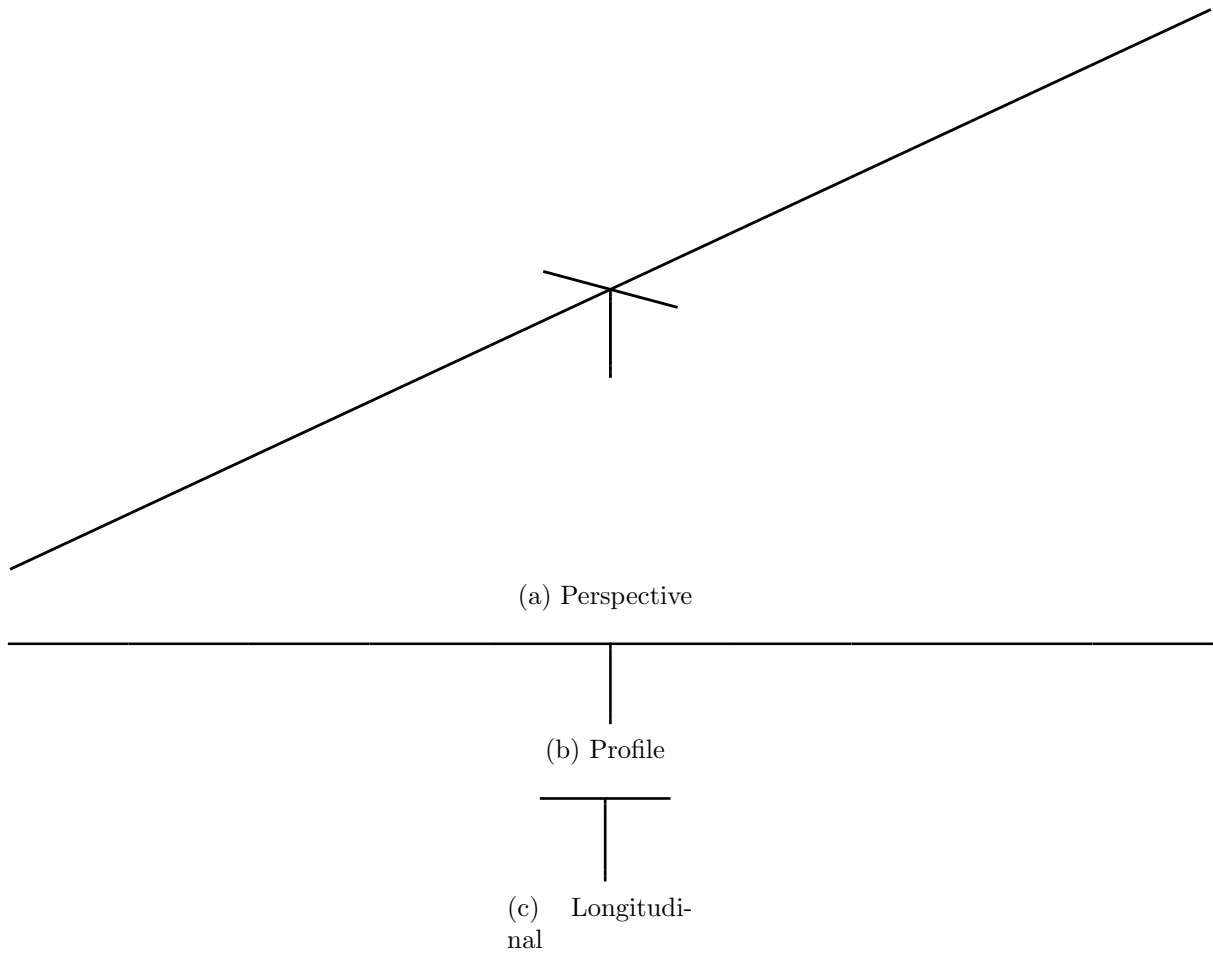
Figure 4.14: OpenSees model of OSB2
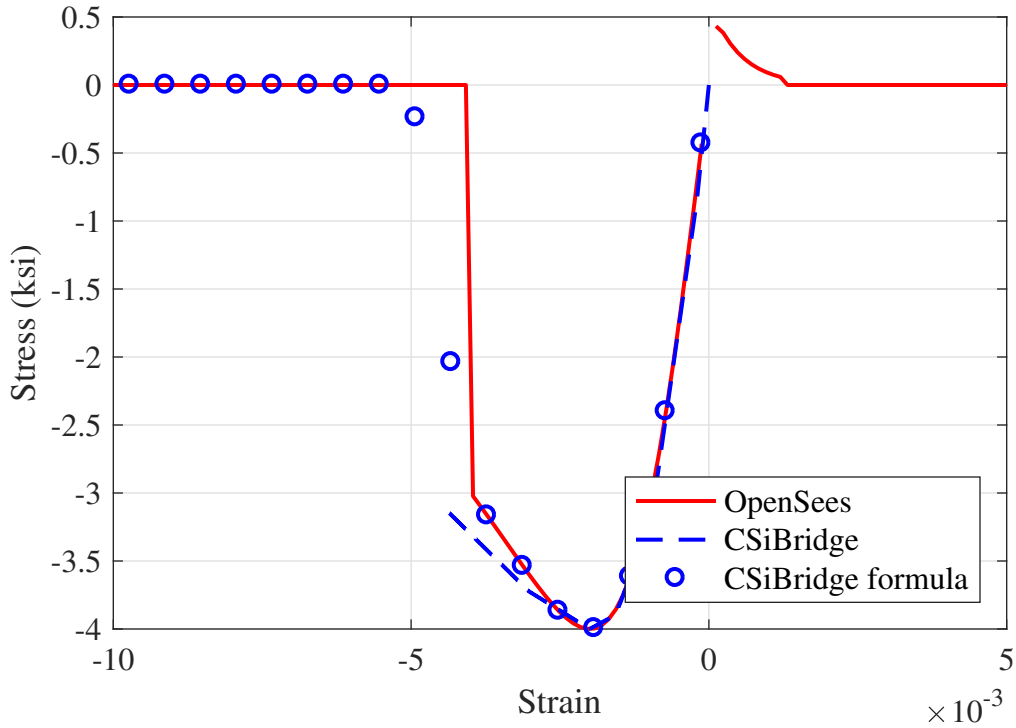
Figure 4.15: Cover concrete monotonic stress-strain response for OSB2

they are not identical as modeled here. The compressive stress drops rapidly to zero after twice the strain at the peak compressive stress. However, the CSiBridge results did not converge for the cover concrete case beyond the last point shown in the plot.

The cyclic responses show a similar match for the portions of the tension and compression backbones; however, the unloading and reloading rules are not the same (CSiBridge here uses kinematic). In addition, there is spurious unloading and reloading through the lower-right quadrant for the CSiBridge model that dramatically increases the energy dissipation of the material.

The core concrete (confined) monotonic and cyclic stress-strain responses are shown in Figures 4.17 and 4.18, respectively. The monotonic backbones are shown together with the predictions from the equations provided in the CSiBridge user manual. Convergence problems prevented the CSiBridge cyclic case from running beyond the first few steps at low amplitude; therefore, only the OpenSees results are presented here. It is therefore unknown the difference in the energy dissipation capabilities at the constitutive model level.

4.2.4 Moment-Curvature Analysis

The standardization of the column constitutive models was extended to the section level. Moment-curvature analysis was performed on the fiber cross section for OSB2. Here it is assumed that the axial load is zero. Due to the similarity of the monotonic stress-strain backbone curves of the constituent materials, it was anticipated that the sectional response

86
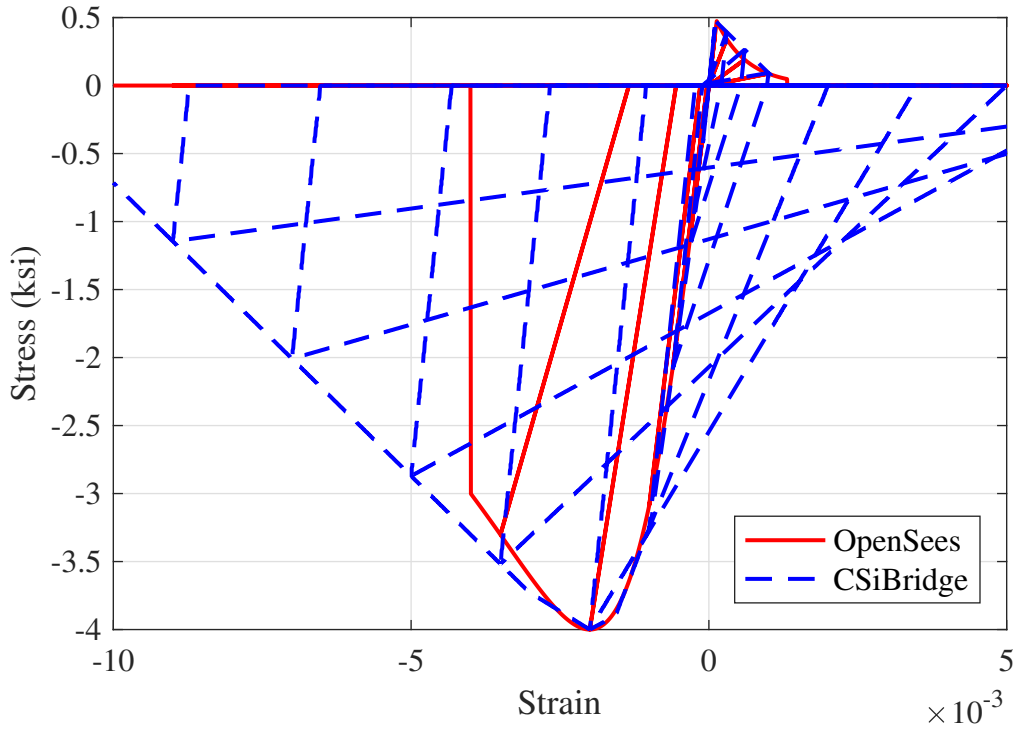
Figure 4.16: Cover concrete cyclic stress-strain response for OSB2
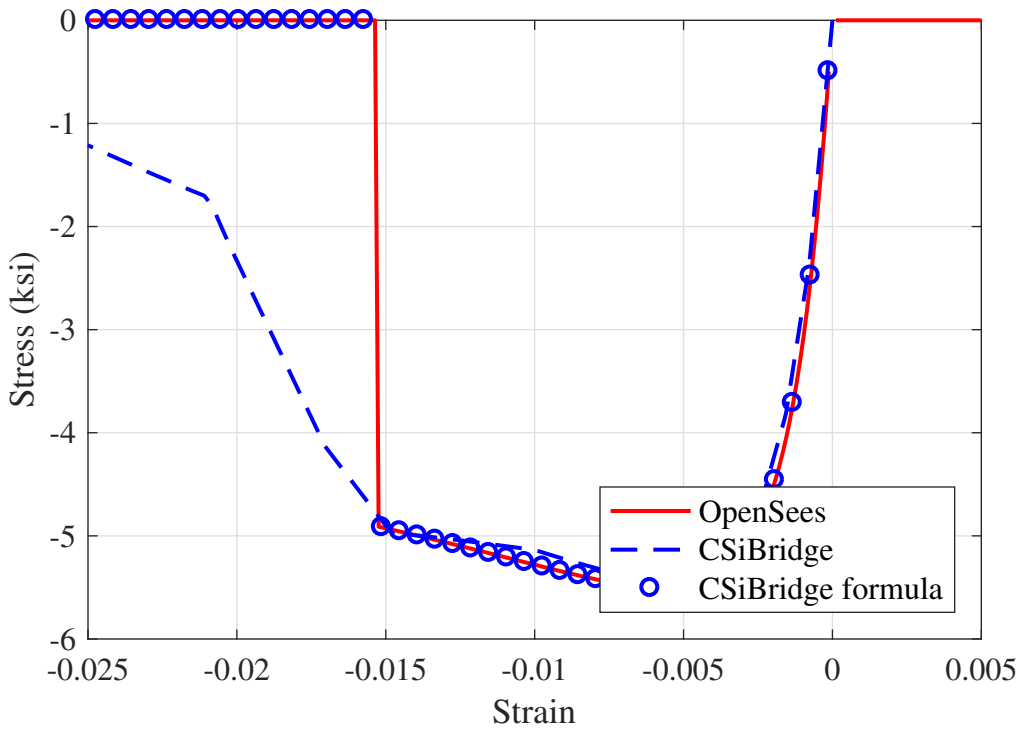
Figure 4.17: Core concrete monotonic stress-strain response for OSB2
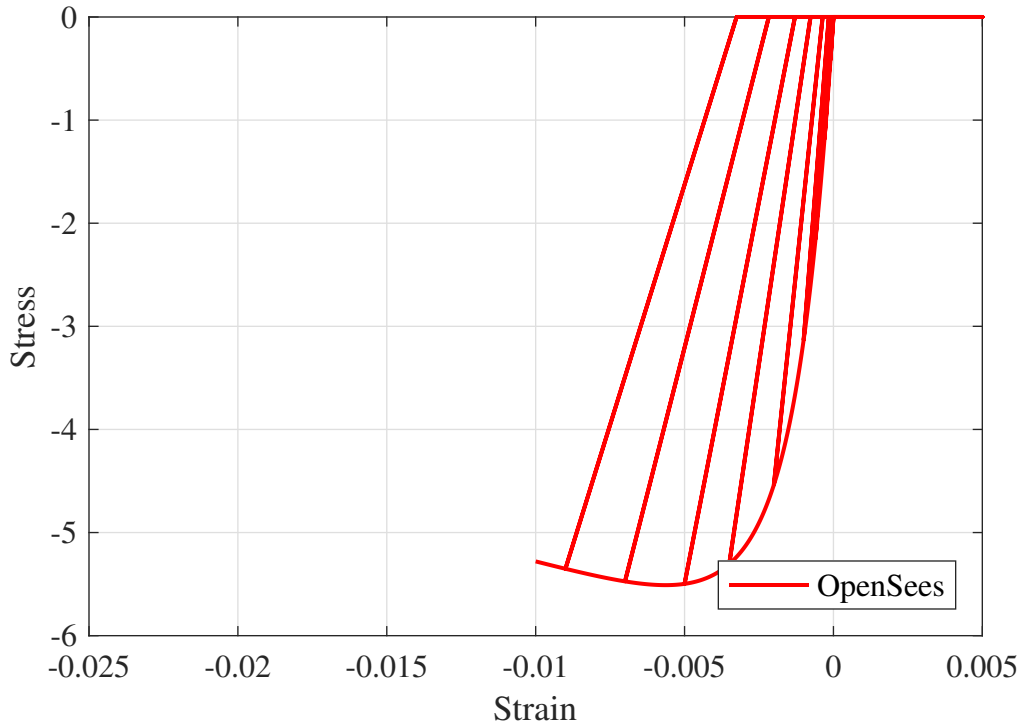
Figure 4.18: Core concrete cyclic stress-strain response for OSB2

curves between OpenSees and CSiBridge would be similar. The moment-curvature response is shown in Figure 4.19, with very similar overall behaviors as discussed previously for OSB1.

4.2.5 Hinge Force-Deformation Analysis

The differences in the nonlinear static and nonlinear dynamic responses of the bridge systems presented in Chapter 5 are in part due to the performance of the hinge elements. For OSB2, the hinge was more clearly defined, and therefore the differences observed during the hinge pushover were more due to the differences in confined concrete alone. The resulting force-displacement curves are shown in Figure 4.20. The two CSiBridge cases shown are for the model as originally created (labeled as 0.1 to indicate 10% of the rigid zone length) and what would have been achieved had the full plastic hinge length of 2.8 ft been used (labeled as 2.8).

The responses between OpenSees and CSiBridge agree for all except the peak strength, as was mentioned previously for OSB1. The stiffer and substantially more brittle response of the short hinges is what creates the rather unusual nonlinear static (pushover of the whole bridge system) and nonlinear dynamic results presented in Chapter 5. Therefore, care should be exercised when viewing those results relative to the modeling assumptions.
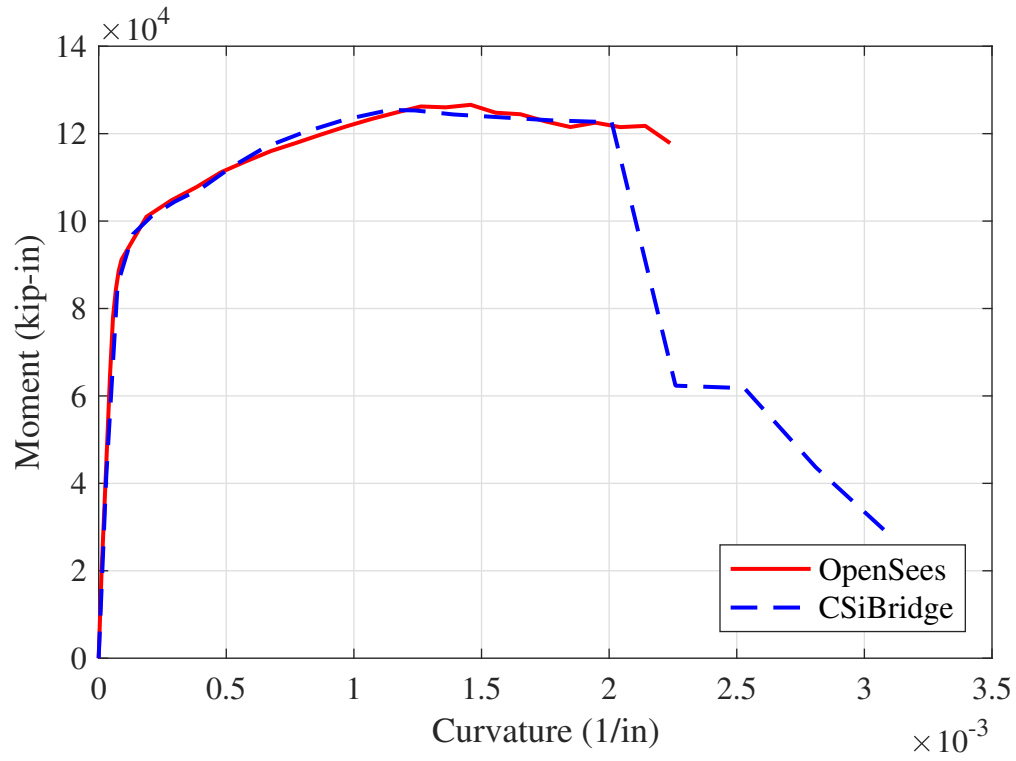
Figure 4.19: Moment-curvature response for OSB2
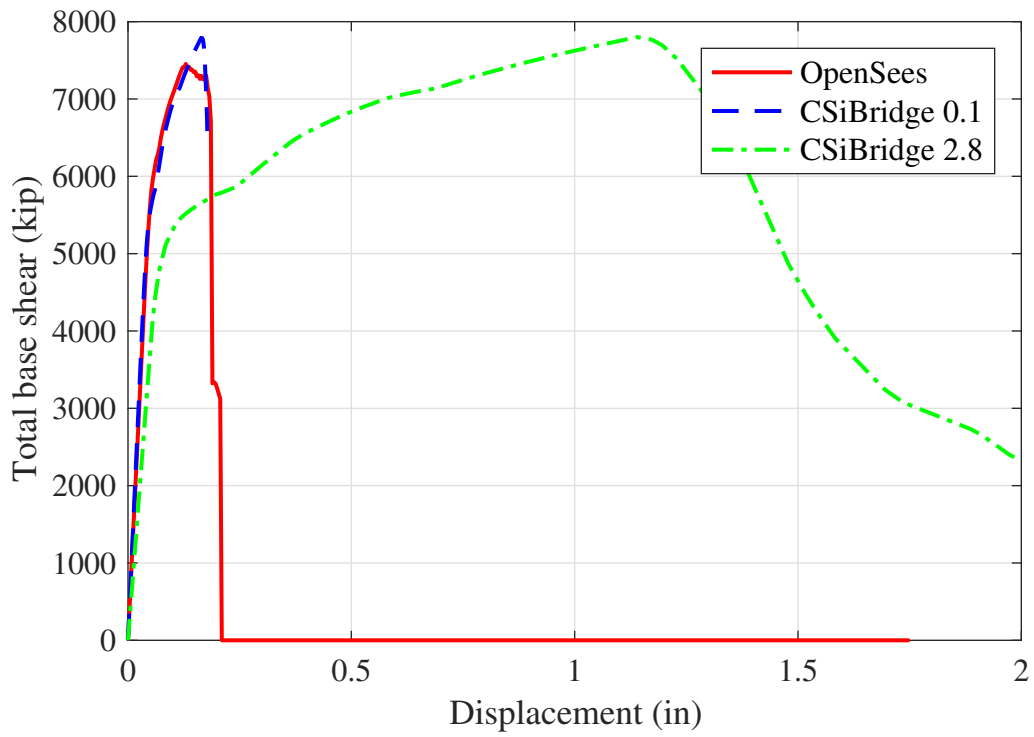
Figure 4.20: Column top hinge load-displacement response for OSB2

4.2.6 MSBridge

The only modal information reported in [18] was 0.69, 0.69, and 0.68 sec for the first mode. Each value corresponds to a different type of abutment boundary, referred to as the "Roller model", "EPP-Gap model", and "EPP-Gap with bearings model", respectively.

In the EPP-Gap model in [18], a compression-only ElasticPPGap material in OpenSees was used for the longitudinal direction with gap of 2 in, stiffness of 1,781 kip/in, and yield force of -1,031 kip. For the transverse direction, a compression-only ElasticPPGap material was used with gap of 1 in, stiffness of 100 kip/in, and yield force of -179.4 kip. The vertical direction had a single-point constraint.

4.3 Ordinary Standard Bridge 3 (OSB3)

OSB3 is a two-span concrete bridge with a single two-column bent at the center. The clear column height is 16 ft. Each span is 150 ft long. The bent contains two 5'-6" diameter circular reinforced concrete columns at 28.75' (center-to-center) spacing. The column section contains 22 bundled #11 longitudinal bars (i.e., 22 bundles or 44 total bars) and #8 at 6" transverse spirals. The precast columns are constructed in two parts with a 9" precast concrete shell (containing the reinforcement) and self-consolidating concrete in the center. There is a 2" clear concrete cover. The precast columns are connected to the pile cap using 4" galvanized pipes filled with UHPC. A 4x4 pile group is used consisting of 24" CIDH piles.

The connection between the precast columns and the superstructure is achieved using a precast column capitol (6' height) to which two isolation bearings are connected (there are two isolation bearings in series arranged in the longitudinal axis of the bridge atop each column). The bearings are then connected to a precast concrete "T-cap". The cap is transversely post-tensioned (1850 kip jacking force). The T-cap is inverted (4' wide at the top and 8' wide at the bottom). The T-cap accepts a coped prestressed wide flange girder on each side, with a moment-resisting connection created by vertical and horizontal reinforcement. The deck and diaphragm are cast in place.

The 5 precast prestressed girders are spaced at 9'-7" on center. The deck slab is 7.75 in thick. The girders are typical CA wide flange girders with depth 5'-6", bottom flange width 3'-9" and top flange width 4'. There are 50 0.6" diameter strands with 43.9 k/strand jacking force.

There is a standard diaphragm at the abutment that is 4' wide and connected to the PS girders. The diaphragm is seated on a total of two isolation bearings, each spaced at 14'-4.5" from the bridge centerline. The stem wall and backwall, with a 9" gap, are supported by a pile cap at 9x2 pile group of 16" class 140 piles. The backwall to stem wall interface contains a construction joint as does the exterior shear key to stem wall interface.

The specified material properties are $f'_c = 3.6$ ksi for the abutments, slabs, and bent pile cap, $f'_c = 4$ ksi for the bridge structural concrete and inverted T-cap, $f'_c = 5$ ksi for the SCC, $f'_c = 8$ ksi for the PC/PS girders, and $f_y = 60$ ksi. The isolation bearings at the bent and abutments are assumed to be lead rubber bearings; however, are only identified generically

through a typical force-deformation relationship in the plans. The models utilize properties of the isolators taken from [18]. At the bent, the values provided were yield strength 74.8 kip, initial elastic stiffness 74.8 kip/in, and post-yield stiffness ratio 0.1981. At the abutments, the values provided were different in each direction. The longitudinal direction had yield strength 37.4 kip, initial elastic stiffness 37.4 kip/in, and post-yield stiffness ratio 0.1981. The transverse direction had yield strength 35.57 kip, initial elastic stiffness 47.4 kip/in, and post-yield stiffness ratio of 0.156.

4.3.1 CSiBridge

The gross elastic properties of the column cross section are the same as those shown for OSB2, as are the details of the cross section (placement and number of longitudinal bars). The moment of inertia of the two columns was reduced by using a modifier of 0.35 in both directions. No hinges were inserted into the columns. The columns are fixed at the base.

A rubber isolator link with 1 ft length was used to connect the top of the columns and the bent cap with nonlinear properties for the longitudinal and transverse degrees of freedom (U2 and U3). Here, the local U1 direction of the link is in the direction along the axis of the column. The stiffness, yield force, and yield stiffness ratio of the link for the nonlinear analysis case in both U2 and U3 direction are 897.6 k/ft, 74.8 kip, and 0.198, respectively. The effective stiffness for the linear analysis case is 272.79 k/ft. The stiffness for all analysis cases for the U1 direction of the link is 144000 k/ft and 2×10^6 k/ft for all the rotational degrees of freedom.

An open box girder was used to model the superstructure of the bridge with a depth of 6.33 ft and width of 34 ft. The superstructure's material and cross section properties are listed in Table 4.13. The center of mass in the CSiBridge model is located at 17 ft above the column bases.

Table 4.13: OSB3 superstructure material and section properties

Parameters	Value
Cross section area (ft^2)	73.0
Moment of inertia, I_{22} (ft^4)	364.5
Moment of inertia, I_{33} (ft^4)	12727.1
Torsion constant (ft^4)	880.47
Youngs modulus (ksi)	3420
Shear modulus (ksi)	1425

The concrete material constitutive models used in OSB3 are identical to those used in OSB2. See Tables 4.9 and 4.10. The steel constitutive model was the same as OSB1 and OSB2, Table 4.4.

The abutment was modeled using two transverse arrays of elements. The cross section of the transverse elements is rectangular with 6.3 ft depth and 4 ft width. Two rubber isolator links were used to link the upper and lower transverse arrays. The stiffness, yield force, and

hardening stiffness ratio of each link used for the nonlinear analysis case in the U2 direction are 448.8 k/ft, 37.4 k, and 0.198, respectively. For the U3 direction, the stiffness, yield force, and hardening ratio of each link in the nonlinear analysis case are 569.12 k/ft, 35.57 k, and 0.1562, respectively. The effective stiffness for the linear analysis case for both U2 and U3 is 136.4 k/ft. The stiffness for all analysis cases for vertical degree of freedom (local U1) is 72000 k/ft and 1×10^6 k/ft for all the rotational degrees of freedom.

A multilinear plastic link was used to define the nonlinear properties of the longitudinal and transverse degree of freedom at each abutment. The link is attached at the center node of the top transverse array. For the longitudinal direction (local U2), the effective stiffness, yield force, and gap are 30864 k/ft, -1629 k, and -0.75 ft, respectively. For the transverse direction (local U3), the effective stiffness, yield force, and gap are 1200 k/ft, -179.4 k, and 0.083 ft, respectively. With this arrangement of isolator links and plastic link, the abutment behaviors are in parallel with the isolators.

The center node of the transverse array is located at the top of the stem wall (vertically). A body constraint for all degrees of freedom was used between this node and the deck end node for each abutment.

To more easily quantify the resultant behavior of the abutment elements and nonlinear behaviors, the load-displacement relationship of the abutment in OSB3 is shown in Figure 4.21. The resultant force in the figure is only for the multilinear plastic link. The displacement is of the center node on the top transverse array. Therefore, this figure is a direct representation of the link properties. The total abutment load-displacement relationship is shown in Figure 4.22. The resultant force in the figure is the summation of the two isolator reactions as well as the link force. As mentioned, the response is therefore the parallel combination of the three elements (two isolators and one abutment spring) in each degree of freedom.

4.3.2   OpenSees

The columns were modeled with the forceBeamColumn element in OpenSees. These elements used a fiber model consisting of core concrete, cover concrete, and longitudinal reinforcing steel. The section discretization and constitutive models employed were identical to those of OSB2. Two forceBeamColumn elements were used to model each column using the Lobatto integration rule with three integration points. The offset between column top and the deck center of gravity was modeled using an elasticBeamColumn element with stiff properties. The rigid elements were connected to the column elements via zero-length bidirectional sections in OpenSees that have the properties of the bent isolation bearings given previously. The bottom node of the column was fixed. Due to the use of fiber cross sections and the corresponding constitutive models, it is expected that the initial elastic stiffness of the OpenSees bents be higher than the corresponding CSiBridge bents.

The bent cap, end diaphragms, and superstructure were modeled with the elasticBeam-Column element in OpenSees. The material and geometric properties used for the bent cap, end diaphragms, and superstructure are given in Table 4.14, Table 4.15, and Table 4.13, respectively.
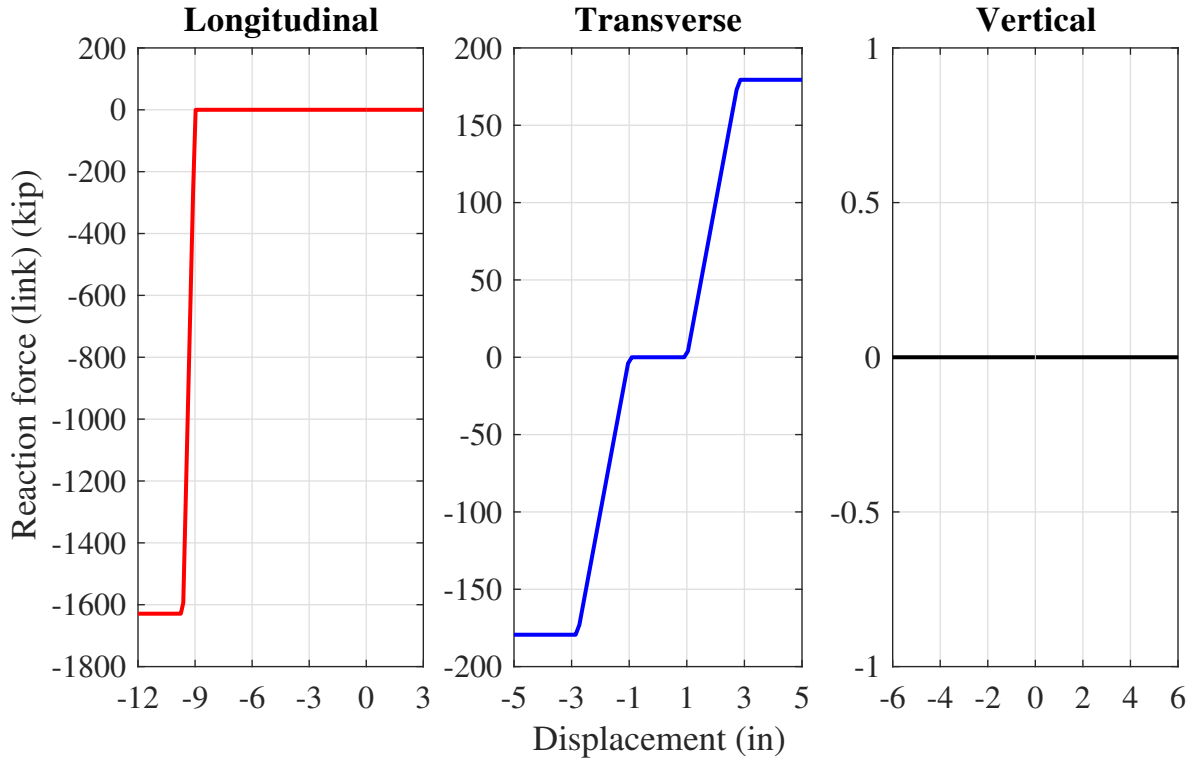
Figure 4.21: Abutment plastic link load-displacement relationship for OSB3 in CSiBridge

Table 4.14: OSB3 bent cap material and section properties used in OpenSees

Parameters	Value
Cross section area (ft^2)	76.00
Moment of inertia, I_{22} (ft^4)	254.04
Moment of inertia, I_{33} (ft^4)	912.00
Torsion constant (ft^4)	1166.04
Youngs modulus (ksi)	3605
Shear modulus (ksi)	1502

Table 4.15: OSB3 end diaphragm material and section properties used in OpenSees

Parameters	Value
Cross section area (ft^2)	25.33
Moment of inertia, I_{22} (ft^4)	84.68
Moment of inertia, I_{33} (ft^4)	33.78
Torsion constant (ft^4)	118.46
Youngs modulus (ksi)	3605
Shear modulus (ksi)	1502
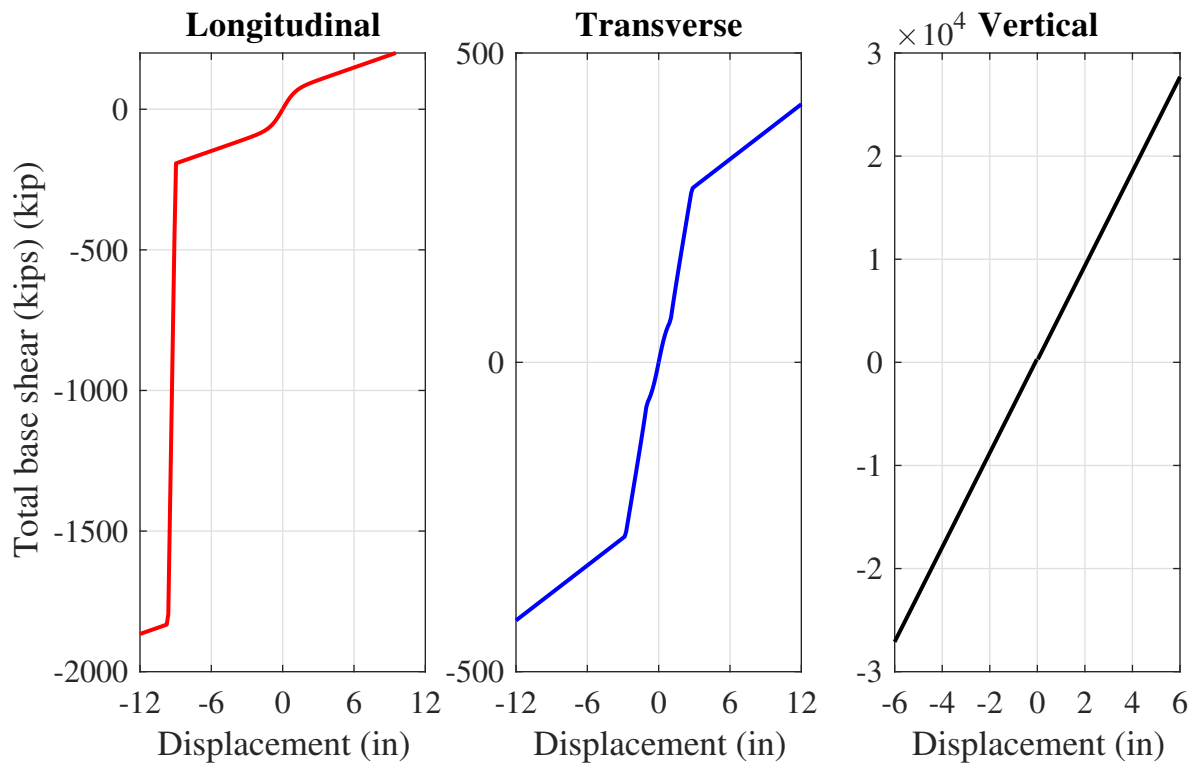
Figure 4.22: Abutment resultant load-displacement relationship for OSB3 in CSiBridge (includes isolators)

To define the nonlinear properties of the longitudinal and transverse degree of freedom at each abutment, compression-only ElasticPPGap materials in OpenSees were used. The longitudinal material used a gap, effective stiffness, and yield force of -0.75 ft, 30864 k/ft and -1629 k respectively. The transverse material used a gap, effective stiffness, and yield force of -0.083 ft, 1200 k/ft and -179.4 k respectively. In the vertical direction, the abutment was fixed. The abutment isolators were modeled with zero-length Elliptical sections (as the two orthogonal lateral directions did not have the same properties) and the properties of the abutment isolation bearings given previously. The resulting model configuration can be seen in Figure 4.23.

(a) Perspective

(b) Profile

(c) Longitudinal
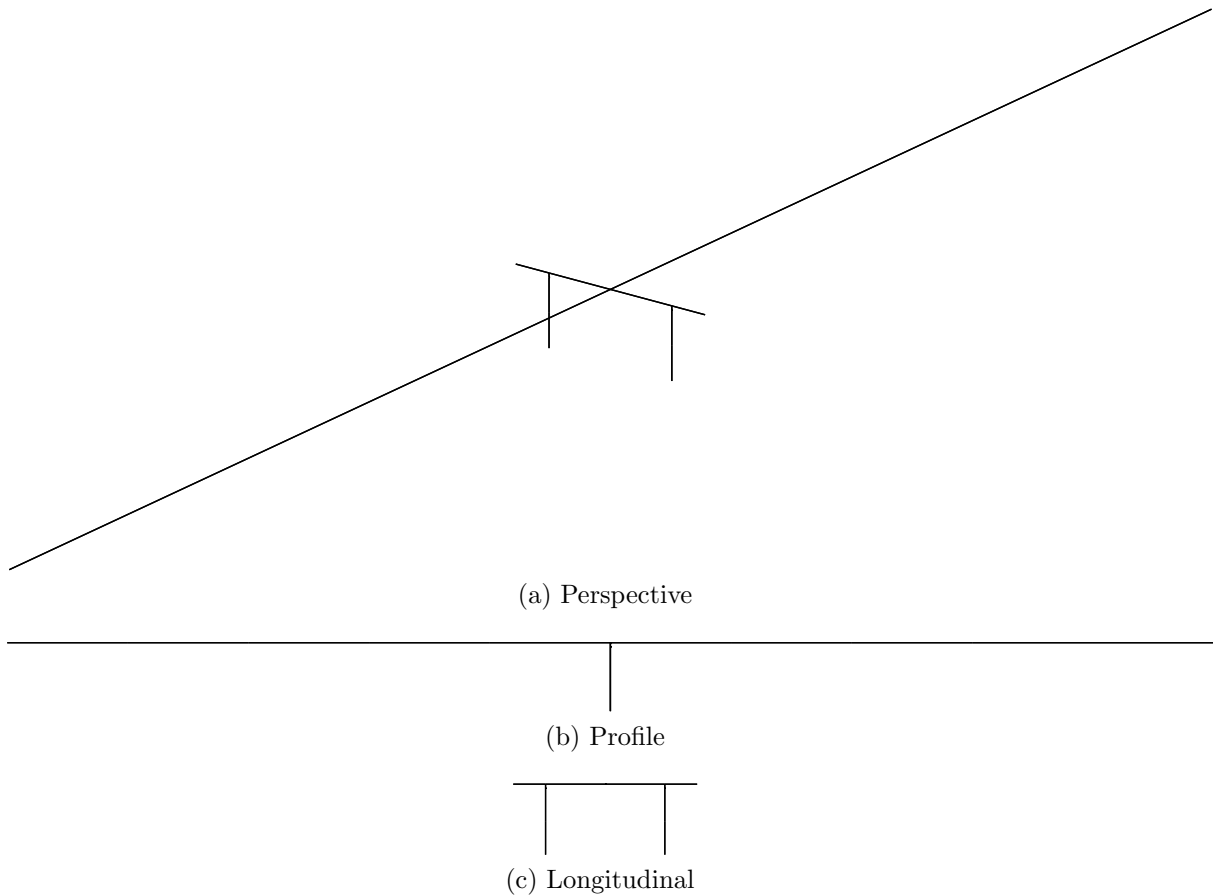
Figure 4.23: OpenSees model of OSB3

4.3.3 Isolation Bearing Models

As the column properties and constitutive models in OSB3 were the same as OSB2, the column constitutive model analysis was not repeated here. However, more importantly for the response of the isolated bridges are the element and material models associated with the isolation bearings at the bents and abutments, in addition to the abutment models
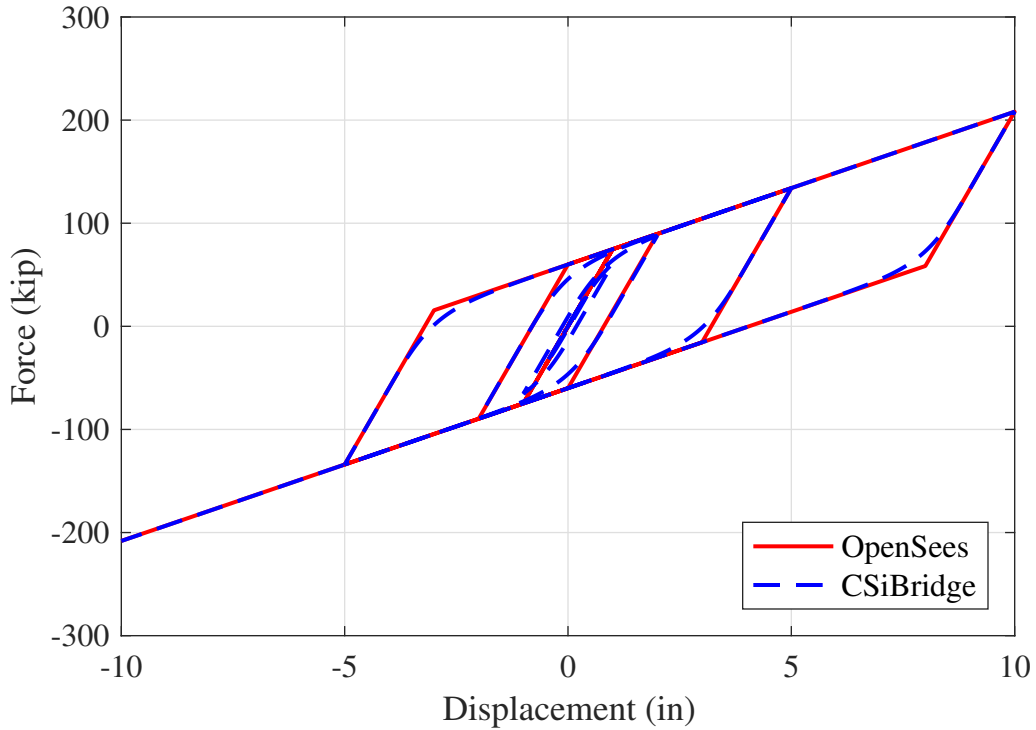
Figure 4.24: Bent isolation bearing cyclic force-displacement resultant response for OSB3

presented previously. Here the isolation bearing elements were extracted and subjected to cyclic displacement demands in both OpenSees and CSiBridge.

To check the coupling surface of the elements, the cyclic (symmetric) displacement demand was separately imposed in the two orthogonal lateral directions, followed by simultaneous displacement demands in both directions. Due to the circular yield surface of the bents, only the response of the analysis containing simultaneous demands in both lateral directions is presented here, i.e., both the displacements and forces are the square root-sum-of-squares (SRSS) of each of the orthogonal lateral responses. The comparison of the OpenSees and CSiBridge results is shown in Figure 4.24. Beyond the sharp transition between elastic and plastic branches in the OpenSees model, the responses are identical.

For the abutment isolation bearings, the properties varied in each of the two lateral directions; therefore, individual responses are presented in addition to the case presented for the bent isolation bearings. The individual orthogonal lateral responses are presented in Figure 4.25. Note, these were obtained from an analysis where simultaneous displacement demands in both directions were imposed, not the case where displacements where imposed separately in each lateral direction. The individual component responses follow the same trends in both software; however, the CSiBridge strengths are higher/lower than OpenSees in the longitudinal/transverse directions, respectively.

The square root-sum-of-squares responses of the two orthogonal lateral components are presented for the abutment isolation bearings in Figure 4.26. Once combined, the responses are nearly identical between the two software. The geometric mean (GM) of the two direc-
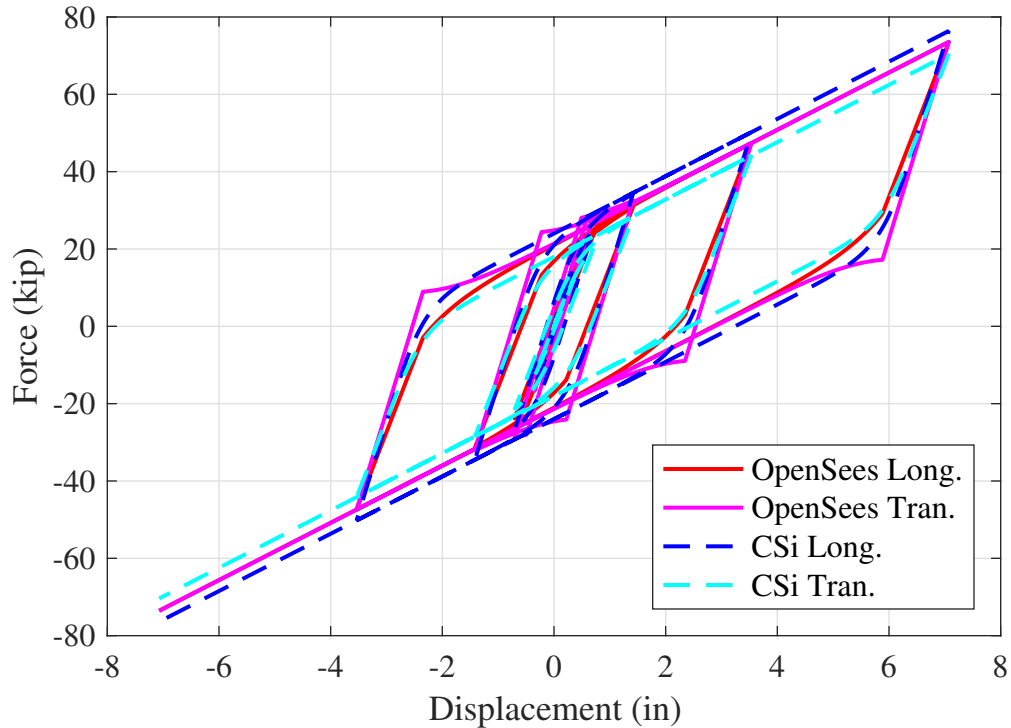
Figure 4.25: Abutment isolator cyclic force-displacement response in each direction for OSB3

tions is also shown for the OpenSees case.

4.3.4 MSBridge

The only modal information reported in [18] was 1.07 and 1.07 sec for the first mode. Each value corresponds to a different type of abutment boundary, referred to as the "Roller with Isolation Bearings" and "EPP-Gap with Isolation Bearings", respectively.

In the EPP-Gap model in [18], a compression-only ElasticPPGap material in OpenSees (although in the report it's labeled as MultiLinear Plastic (Nonlinear) for OSB3) was used for the longitudinal direction with gap of 9 in, stiffness of 2,572 kip/in, and yield force of -1,629 kip. For the transverse direction, a compression-only ElasticPPGap material (again it's listed as MultiLinear Plastic) was used with gap of 1 in, stiffness of 100 kip/in, and yield force of -179.4 kip. The vertical direction had a single-point constraint.

It appears the superstructure was treated as a box girder (equivalent elastic properties). The isolator properties at the bent had yield strength and initial elastic stiffness of 74.8 kip and 74.8 kip/in, respectively. The isolation bearings at the abutments had yield strength and initial stiffness of 37.4 kip and 37.4 kip/in, respectively. All isolators had a post-yield stiffness ratio of 0.1981.
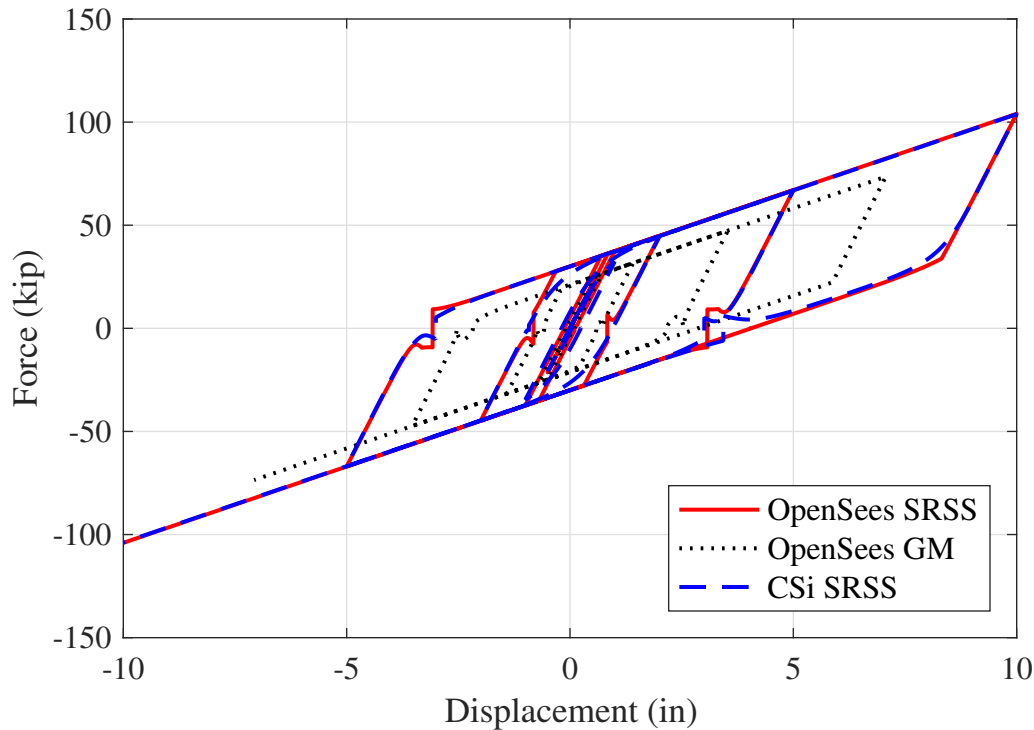
Figure 4.26: Abutment isolator cyclic force-displacement resultant response for OSB3

4.4   Ordinary Standard Bridge 4 (OSB4)

OSB4 is a two-span concrete bridge with a single column bent at the center. Each span is 150 ft long and the clear column height is 16 ft. The precast reinforced concrete circular column is a 5'-6" in diameter. The column section contains 22 bundled #11 longitudinal bars (i.e., 22 bundles or 44 total bars) and #8 at 6" transverse spirals. The precast columns are constructed in two parts with a 9" precast concrete shell (containing the reinforcement) and self-consolidating concrete in the center. There is a 2" clear concrete cover. The precast columns are connected to the pile cap using 4" galvanized pipes (4' extension into the cap) filled with UHPC. A 4x4 pile group is used consisting of 24" CIDH piles.

The hammerhead pier/bent cap is precast and contains similar 4" galvanized pipes with 4' extension that are then filled with UHPC. The precast cap is transversely post tensioned with 270 ksi low relaxation strands to 3500 kip. Four isolation bearings are used, with an arrangement of 2 in the bridge longitudinal direction at each of two locations spaced at 9'-8" distance from the column centerline. The isolation bearings sit in a recessed pocket in the precast bent cap so that a 3" gap is created between the cap and the superstructure. Unlike OSB3, there are only single (2'-6" diameter typical) isolation bearings at each location (a total of two for the bent).

The bearings are then connected to a precast concrete "T-cap". The T-cap is inverted (4' wide at the top and 8' wide at the bottom). The T-cap accepts a coped prestressed wide flange girder on each side, with a moment-resisting connection created by vertical and

horizontal reinforcement. The deck and diaphragm are cast in place.

The 4 precast prestressed girders are spaced at 9'-8" on center. The deck slab is 7.75 in thick. The girders are typical CA wide flange girders with depth 5'-6", bottom flange width 3'-9" and top flange width 4'. There are 50 0.6" diameter strands with 43.9 k/strand jacking force.

There is a standard diaphragm at the abutment that is 4' wide and connected to the PS girders. The diaphragm is seated on a total of two isolation bearings, each 9'-8" from the bridge centerline. The stem wall and backwall, with a 9" gap, are supported by a pile cap at 8x2 pile group of 16" class 140 piles. The backwall to stem wall interface contains a construction joint as does the exterior shear key to stem wall interface.

The specified material properties are $f'_c = 3.6$ ksi for the abutments, slabs, and bent pile cap, $f'_c = 4$ ksi for the bridge structural concrete and inverted T-cap, $f'_c = 4$ ksi for the SCC, $f'_c = 8$ ksi for the PC/PS girders, and $f_y = 60$ ksi. The isolation bearings at the bent and abutments were assumed to have the same properties as those for OSB3.

4.4.1   CSiBridge

The moment of inertia of the column was reduced by using a modifier of 0.5 in both directions. The column is fixed at the base and a body constraint for all degrees of freedom was used at the top end of the column. The gross elastic properties of the column cross section are the same as those shown for OSB2. A rubber isolator element was used to model the link between the upper part and the lower part of the bent cap with a nonlinear properties for the longitudinal and transverse direction of freedom (local U2 and U3). The stiffness, yield force, and hardening ratio of the link used for nonlinear analysis case in both the U2 and U3 directions are 897.6 k/ft, 74.8 k, and 0.198, respectively. The effective stiffness for the linear analysis case is 272.79 k/ft. The stiffness for all analysis cases for vertical direction (local U1) is 144000 k/ft and 2×10^6 k/ft for all the rotational degrees of freedom.

Two rubber isolator links were used at each abutments to link the upper and lower part. The stiffness, yield force, and hardening ratio of each link used for the nonlinear analysis case in the U2 direction are 448.8 k/ft, 37.4 k, and 0.198, respectively. For the U3 direction, the stiffness, yield force, and hardening ratio of each link for the nonlinear analysis case are 569.12 k/ft, 35.57 k, and 0.1562, respectively. The effective stiffness for the linear analysis case for both U2 and U3 is 136.4 k/ft. The stiffness for all analysis cases for vertical direction (local U1) is 72000 k/ft and 1×10^6 k/ft for all the rotational degrees of freedom.

Similar to OSB3, a body constraint for all degrees of freedom was used at both the left and right abutments between the deck end node and the center node on the top transverse array. A multilinear plastic link was used to define the nonlinear properties of the longitudinal and transverse degree of freedoms for the abutment. For the longitudinal direction (local U2), the effective stiffness, yield force, and gap are 24296 k/ft, -1282 k, and -0.75 ft, respectively. For the transverse direction (local U3), the effective stiffness, yield force, and the gap are 1200 k/ft, -179.4 k, and -0.083 ft, respectively.

To more easily quantify the resultant behavior of the abutment elements and nonlinear behaviors, the load-displacement relationship of the abutment in OSB4 is shown in Fig-

ure 4.27. The resultant force in the figure is only for the multilinear plastic link. The displacement is of the center node on the top transverse array. Therefore, this figure is a direct representation of the link properties. The total abutment load-displacement relationship is shown in Figure 4.28. The resultant force in the figure is the summation of the two isolator reactions as well as the link force. As mentioned, the response is therefore the parallel combination of the three elements (two isolators and one abutment spring) in each degree of freedom.
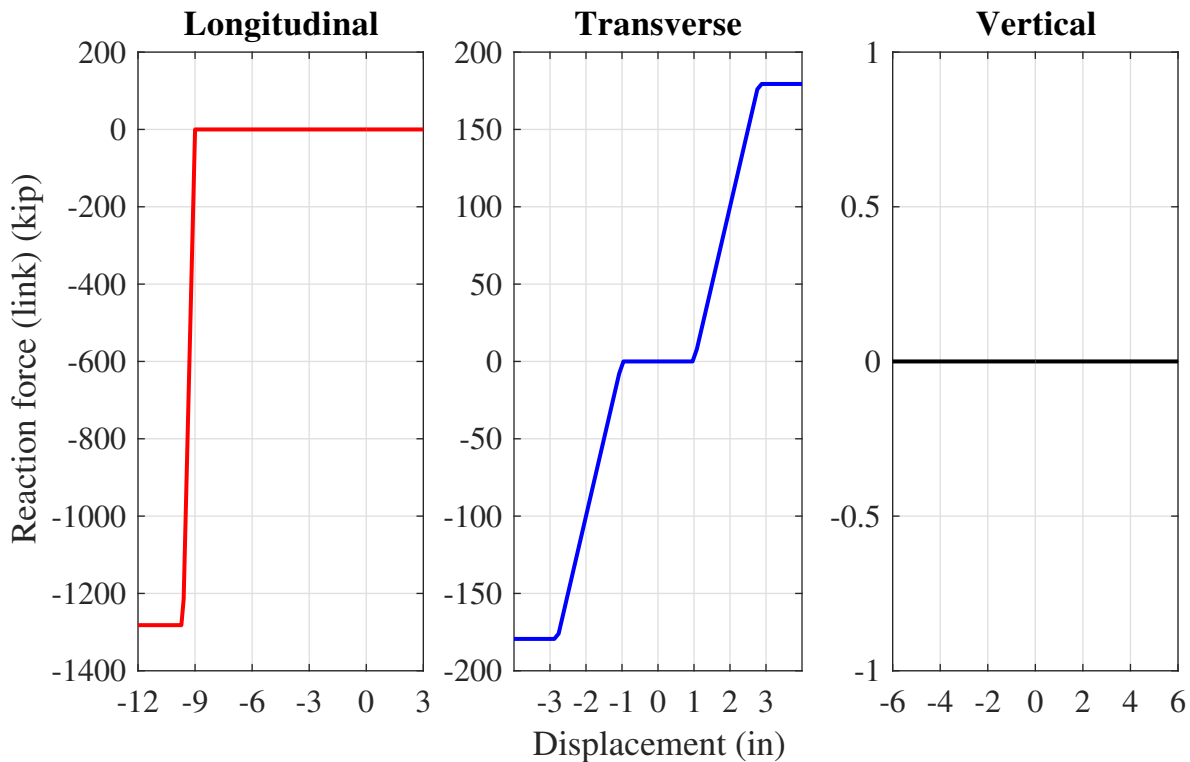
Figure 4.27: Abutment plastic link load-displacement relationship for OSB4 in CSiBridge

An open box girder was used to model the superstructure of the bridge with a depth of 6.33 ft and width of 37.5 ft. The superstructure's material and cross section properties are listed in Table 4.16. The center of mass in the CSiBridge model is located at 17 ft above the column bases.

4.4.2   OpenSees

The OpenSees modeling approach was the same as that for OSB3, with the change to the single column bent model. The forceBeamColumn element was used for a majority of the bent cap, superstructure, and column elements. These column elements used a fiber model consisting of core concrete, cover concrete, and longitudinal reinforcing steel. The section discretization and constitutive models employed were identical to those of OSB2. Two forceBeamColumn elements were used to model each column using the Lobatto integration
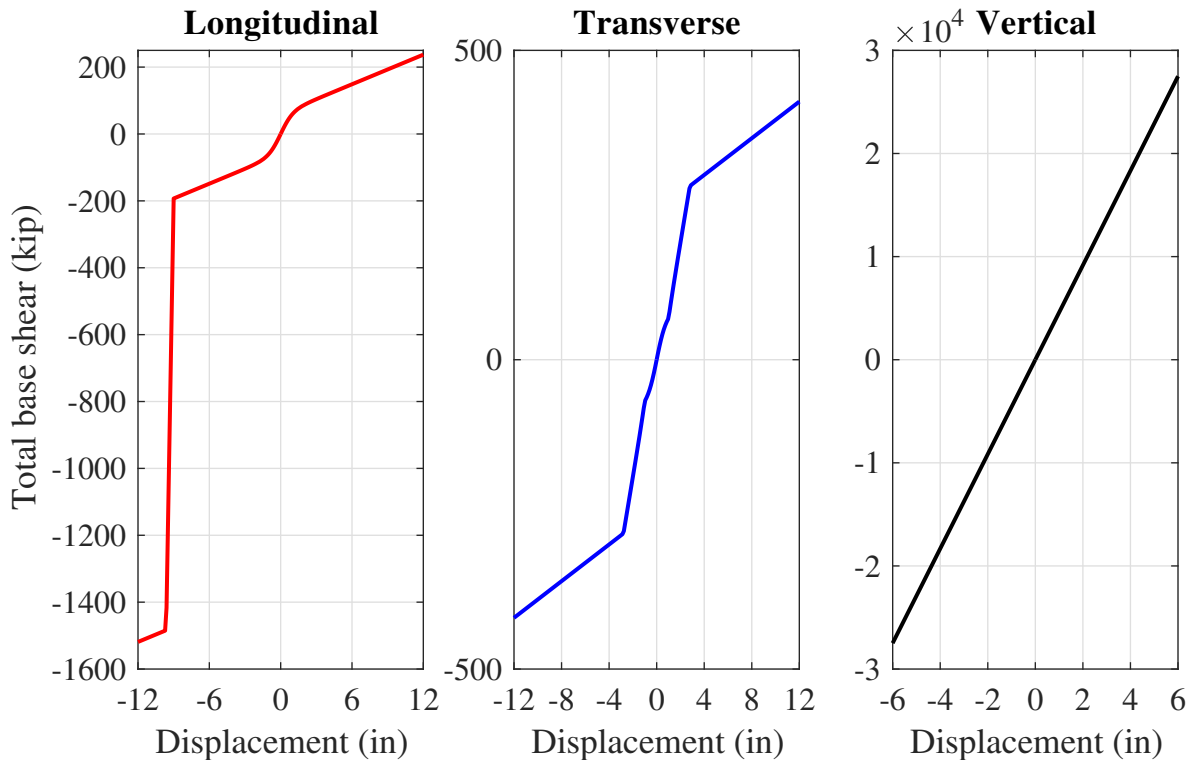
Figure 4.28: Abutment resultant load-displacement relationship for OSB4 in CSiBridge (includes isolators)

Table 4.16: OSB4 superstructure material and section properties

Parameters	Value
Cross section area (ft^2)	58.56
Moment of inertia, I_{22} (ft^4)	353.3
Moment of inertia, I_{33} (ft^4)	6359.8
Torsion constant (ft^4)	1079.643
Youngs modulus (ksi)	3420
Shear modulus (ksi)	1425

101

rule with three integration points. The offset between column top and the deck center of gravity was modeled using an elasticBeamColumn element with stiff properties. The rigid elements were connected to the column elements via zero-length bidirectional sections in OpenSees that have the properties of the bent isolation bearings given previously. The bottom node of the column was fixed.

The bent cap, end diaphragms, bearing cap and superstructure were modeled with the elasticBeamColumn element in OpenSees. The material and geometric properties used for the bent cap and end diaphragms are the same as for OSB3 and are given in Table 4.14 and Table 4.15 respectively. The cross section used for the bearing cap is sufficient to produce rigid behavior of the element. The material and geometric properties used for the superstructure are given in Table 4.16.

To define the nonlinear properties of the longitudinal and transverse degree of freedom at each abutment, compression-only ElasticPPGap materials in OpenSees were used. The longitudinal material used a gap, effective stiffness, and yield force of -0.75 ft, 24296 k/ft and -1282 k respectively. The transverse material used a gap, effective stiffness, and yield force of -0.083 ft, 1200 k/ft and -179.4 k respectively. In the vertical direction, the abutment was fixed. The abutment isolators were modeled with zero-length Elliptical sections (as the two orthogonal lateral directions did not have the same properties) and the properties of the abutment isolation bearings given previously. The model configuration can be seen in Figure 4.29.

Due to the duplication of constitutive models, cross sections, and isolation bearings with the models previously employed for OSB2 and OSB3, no further constitutive, section, or isolation characterization is performed here.

4.4.3   MSBridge

The only modal information reported in [18] was 0.96 and 0.96 sec for the first mode. Each value corresponds to a different type of abutment boundary, referred to as the "Roller with Isolation Bearings" and "EPP-Gap with Isolation Bearings", respectively.

In the EPP-Gap model in [18], a compression-only ElasticPPGap material in OpenSees (although in the report it's labeled as MultiLinear Plastic (Nonlinear) for OSB4) was used for the longitudinal direction with gap of 9 in, stiffness of 2,025 kip/in, and yield force of -1,282 kip. For the transverse direction, a compression-only ElasticPPGap material (again it's listed as MultiLinear Plastic) was used with gap of 1 in, stiffness of 100 kip/in, and yield force of -179.4 kip. The vertical direction had a single-point constraint.

It appears the superstructure was treated as a box girder (equivalent elastic properties), as in CSiBridge. The isolation bearings at the bent had yield strength and initial elastic stiffness of 74.8 kip and 74.8 kip/in, respectively. The isolation bearings at the abutments had yield strength and initial stiffness of 37.4 kip and 37.4 kip/in, respectively. All isolators had a post-yield stiffness ratio of 0.1981.

(a) Perspective

(b) Profile

(c) Longitudinal
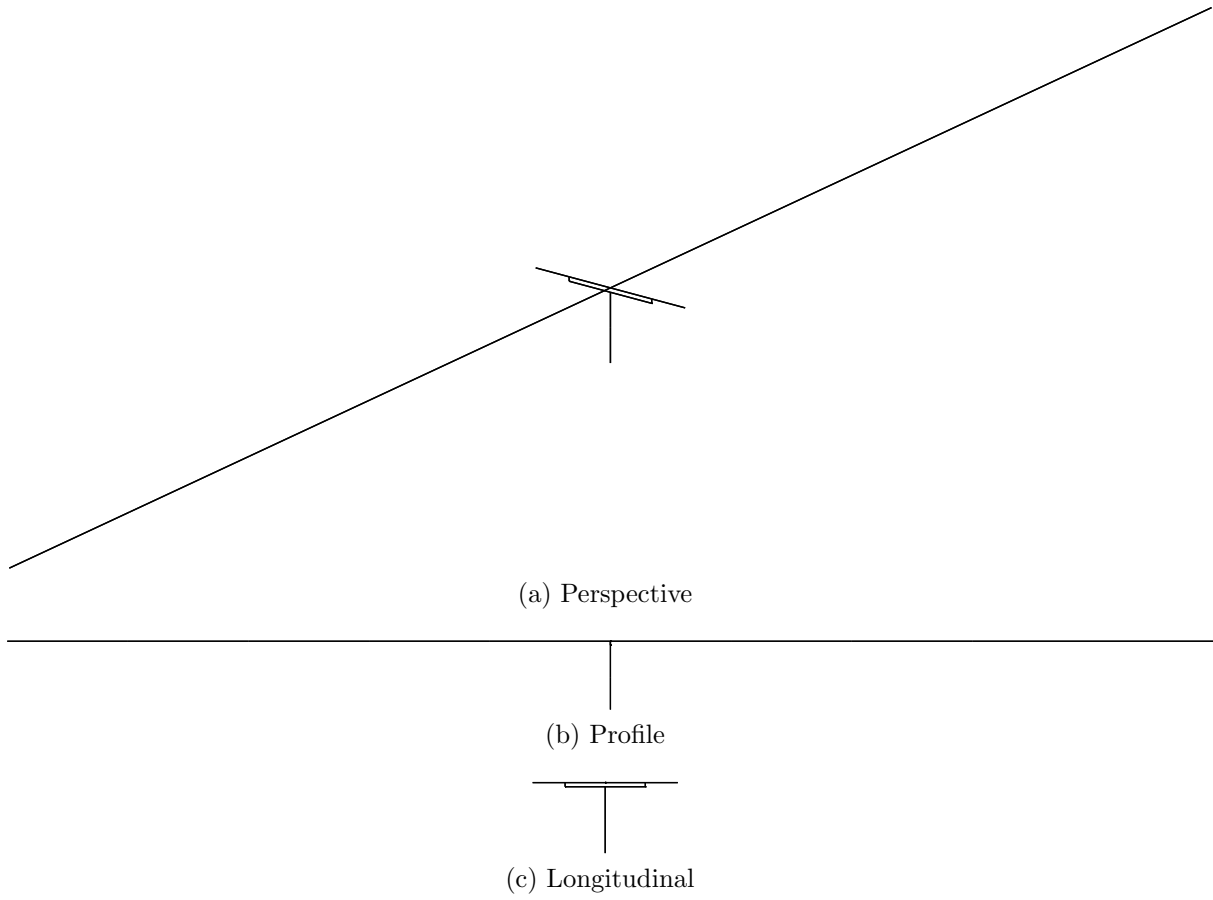
Figure 4.29: OpenSees model of OSB4

4.5　Summary

This chapter presents a summary of the four OSB case studies. The bridge descriptions, geometry, properties, and modeling parameters were presented for both OpenSees and CSiBridge models. The CSiBridge models were utilized directly from Caltrans, with the only modification being to consider the case with the original abutment models, followed by a simpler case containing only roller abutments. The OpenSees models were developed with the specific goal of matching the CSiBridge models with an understanding of the limitations of the underlying material and element models.

The first step of calibration was performed in this chapter – standardizing the stress-strain responses of the column constitutive models: longitudinal reinforcing steel, unconfined cover concrete, and confined core concrete. It was demonstrated that the steel models could be specified to match exactly, whereas both the unconfined and confined concrete models exhibited unanticipated differences. It was not possible to directly match all aspects of the concrete models, specifically the softening, tension softening, and cyclic unloading and reloading rules.

The second phase of calibration was also performed in this chapter – section response of the column cross sections, nonlinear static pushover response of the column hinge elements, and the element responses of the isolation bearings. The differences in the softening behaviors of the concrete models yielded slightly different curvature capacity estimates, as well as peak load and ductility of the column hinges during nonlinear static pushover analysis. The isolation bearings yielded almost identical monotonic and cyclic responses, with only slight differences due to the elastic-to-plastic transitions in the two implementations.

The primary challenges encountered in producing OpenSees models to closely match the CSiBridge counterparts were two-fold. The first related to the differences in the achieved responses of the underlying constitutive models than would have been expected based on the inputs. The second related to some specific modeling choices made for OSB1 and OSB2. The OSB1 hinge at the top of the bent columns was complicated by the choice of rigid offset and rigid zone factor that were not easily reproduced. The OSB2 hinge was inadvertently assigned a plastic hinge length 10% of the expected value, which led to much more brittle (and therefore sensitive to changes in the inputs and constitutive models) behaviors. It was demonstrated standardized response could still be nominally achieved for this case, but the time history results presented in Chapter 5 should be interpreted relative to this modeling choice.

Chapter 5

Benchmark Bridges – Analysis

This chapter contains the nonlinear static and nonlinear time history analysis (NTHA) results for the four Ordinary Standard Bridges (OSBs). The description, geometry, and materials for each bridge were described previously in Chapter 4. The results in this chapter are based on the models in CSiBridge and OpenSees introduced in the previous chapter. Specifically, the CSiBridge models were taken without change from Caltrans, while the OpenSees models were developed with the specific objective of matching as closely as possible the behaviors and responses. Two variants of each OSB model are included in the analysis results presented here. The first entailed modifying the abutments in both the OpenSees and CSiBridge models to be simple rollers, as is denoted as the "roller" abutment herein. The second entailed developing OpenSees models to mimic the assumed abutment boundary conditions already modeled in CSiBridge and is denoted as the "original" abutment herein.

Several types of analyses were performed in parallel on the bridge models in each software implementation. Modal analysis was performed first to ascertain differences in the basic mass and stiffness properties of the models. Bridge pushover analysis was then conducted in both the longitudinal and transverse bridge directions (independently) to study the nonlinear static responses. The same roller abutment boundary models were once again utilized. Finally, time history analysis was performed on a small selection of ground motions identified in previous studies on the OSB bridges. Based on the consistent elastic, modal, and nonlinear static responses between the two software implementations, the time history analyses are included to demonstrate that the results are close for some ground motion scenarios, but necessarily different based on the unloading and reloading rules. Time history results are illustrated for both the original abutments, as well as the simplified roller abutments.

5.1 Modal Analysis

Modal analysis was performed to determine the first six modes for each bridge. The eigenvalue analysis results are summarized in the following tables. Each mode shape is shown graphically in Appendix A for roller abutments and Appendix B for the original abutments. Throughout this section, the vertical mode shapes are listed as either asymmetric or sym-

metric relative to whether the sense of the vertical deformation on either side of the bent are opposite or the same, respectively. The modes listed as in-plane bending describe the in plane (horizontal plane) bending of the superstructure. This in-plane bending is often accompanied by a transverse displacement of the bent.

5.1.1   OSB1

Results from the modal analysis of OSB1 are shown in Table 5.1 and Table 5.2 for the CSiBridge and OpenSees implementations, respectively.

Table 5.1: Modal periods and frequencies obtained from CSiBridge model of OSB1

		Roller Abutment			Original Abutment	
Mode	Period	Freq-uency	Mode Shape	Period	Freq-uency	Mode Shape
-	sec	Hz	-	sec	Hz	-
1	6.033	0.166	Torsion	0.614	1.629	Transverse
2	1.012	0.988	Longitudinal	0.609	1.643	Vertical (asym.)
3	0.915	1.092	Transverse	0.403	2.484	Vertical (sym.)
4	0.567	1.762	Vertical (asym.)	0.352	2.840	Torsion
5	0.405	2.463	Vertical (sym.)	0.283	3.528	Longitudinal
6	0.203	4.907	In-plane bending	0.157	6.354	Vertical (higher mode, asym.)

Table 5.2: Modal periods and frequencies obtained from OpenSees model of OSB1

		Roller Abutment			Original Abutment	
Mode	Period	Freq-uency	Mode Shape	Period	Freq-uency	Mode Shape
-	sec	Hz	-	sec	Hz	-
1	5.934	0.189	Torsion	0.591	1.829	Transverse
2	1.002	1.040	Longitudinal	0.563	1.902	Vertical (asym.)
3	0.863	1.396	Transverse	0.390	2.549	Vertical (sym.)
4	0.533	1.986	Vertical (asym.)	0.343	2.859	Torsion
5	0.390	2.551	Vertical (sym.)	0.282	3.598	Longitudinal
6	0.204	4.946	In-plane Bending	0.149	6.855	Vertical (higher mode, asym.

The modes match exactly between both the roller and original abutment models. The periods are also very close, with the OpenSees slightly stiffer, as evidenced in the nonlinear static responses presented previously. The vertical eigenvalues are not identical in this case due to the different discretization of superstructure mass and use of non-prismatic members

in CSiBridge. The frame action in the transverse direction is sensitive to the modeling assumptions of the hinge.

5.1.2 OSB2

Results from the modal analysis of OSB2 are shown in Table 5.3 and Table 5.4 for the CSiBridge and OpenSees implementations, respectively. The different boundary conditions specified for the two ends of the superstructure have a definitive impact on the mode shapes in the case of the original abutment models (consistent in both CSiBridge and OpenSees). Notice for these mode shape (original abutment), although the vertical deformation of the superstructure is listed as symmetric or asymmetric, the effect is less pronounced on the side with the additional constraints (left abutment).

Table 5.3: Modal periods and frequencies obtained from CSiBridge model of OSB2

	Roller Abutment			Original Abutment		
Mode	Period	Freq-uency	Mode Shape	Period	Freq-uency	Mode Shape
-	sec	Hz	-	sec	Hz	-
1	5.09	0.1964	Torsion	0.600	1.668	Long. + vertical (asym.)
2	0.686	1.457	Vertical (asym.)	0.398	2.511	Long. + vertical (sym.)
3	0.629	1.587	Transverse	0.319	3.138	Vertical (sym.)
4	0.427	2.339	Vertical (sym.)	0.276	3.626	Transverse
5	0.391	2.553	Longitudinal	0.149	6.696	Vertical (higher mode, asym.)
6	0.212	4.709	In-plane bending	0.115	8.728	Vertical (higher mode, sym.)

The OpenSees stiffness values are slightly lower for OSB2, hence the periods are slightly higher than those reported from CSiBridge. This phenomenon is particularly evident in the transverse direction. However, both the mode shapes and the eigenvalues show excellent agreement. It is also worth mentioning that, unlike OSB1, OSB2 has gapping behavior in both the longitudinal and transverse directions according to the original abutment model for the bridge. The difference in the linear properties utilized for initial elastic eigenvalue analysis are therefore contributors to the reported periods.

5.1.3 OSB3

Results from the modal analysis of OSB3 are shown in Table 5.5 and Table 5.6 for the CSiBridge and OpenSees implementations, respectively.

Table 5.4: Modal periods and frequencies obtained from OpenSees model of OSB2

	Roller Abutment			Original Abutment		
Mode	Period	Freq-uency	Mode Shape	Period	Freq-uency	Mode Shape
-	sec	Hz	-	sec	Hz	-
1	6.66	0.158	Torsion	0.613	2.011	Long. + vertical (asym.)
2	0.698	1.492	Vertical (asym.)	0.420	2.912	Long. + vertical (sym.)
3	0.685	1.562	Transverse	0.321	3.389	Vertical (sym.)
4	0.428	2.340	Vertical (sym.)	0.311	4.600	Transverse
5	0.418	2.525	Longitudinal	0.150	7.907	Vertical (higher mode, asym.)
6	0.252	4.171	In-plane bending	0.116	9.226	Vertical (higher mode, sym.)

Table 5.5: Modal periods and frequencies obtained from CSiBridge model of OSB3

	Roller Abutment			Original Abutment		
Mode	Period	Freq-uency	Mode Shape	Period	Freq-uency	Mode Shape
-	sec	Hz	-	sec	Hz	-
1	4.193	0.238	Torsion	1.234	0.811	Transverse
2	2.931	0.341	Transverse	0.746	1.341	Torsion
3	2.926	0.341	Longitudinal	0.572	1.749	Vertical (asym.)
4	0.604	1.653	Vertical (asym.)	0.395	2.530	Vertical (sym.)
5	0.413	2.417	Vertical (sym.)	0.289	3.462	Longitudinal
6	0.216	4.618	In-plane bending	0.233	4.298	In-plane bending

Table 5.6: Modal periods and frequencies obtained from OpenSees model of OSB3

	Roller Abutment			Original Abutment		
Mode	Period	Freq-uency	Mode Shape	Period	Freq-uency	Mode Shape
-	sec	Hz	-	sec	Hz	-
1	4.679	0.214	Torsion	1.194	0.838	Longitudinal
2	1.681	0.595	Transverse	1.122	0.891	Transverse
3	1.668	0.600	Longitudinal	0.842	1.188	Torsion
4	0.580	1.724	Vertical (asym.)	0.537	1.862	Vertical (asym.)
5	0.405	2.469	Vertical (sym.)	0.382	2.618	Vertical (sym.)
6	0.223	4.129	In-plane bending	0.225	4.444	In-plane bending

The roller abutment mode shapes coincide directly between CSiBridge and OpenSees. However, the eigenvalues are not the same for the torsion, longitudinal, and transverse modes. The reason for this (and later observations of differences in the NTHA responses) is not immediately obvious given the exact agreement of the bent isolator hysteresis. The predicted longitudinal and transverse periods are near 3 sec for the CSiBridge roller abutment models, which may be due to the difference in the assumed linear vs nonlinear behavior of the elements used to represent the isolators. This may be surmised from the effective linear stiffness for linear analysis cases that is approximately one quarter the nonlinear stiffness of the bearings at the bents.

The original abutment models appear to not match up, but it is due to the shifting of the longitudinal mode, the order of the other modes remains the same between CSiBridge and OpenSees. The changes in the eigenvalues between CSiBridge and OpenSees are also an amalgamation of the changes in the linear vs nonlinear properties (for both the original abutment links as well as the isolation bearings). While the periods listed for the primary modes (longitudinal and transverse) are different by 10-100%, it is interesting to note that that NTHA responses of OSB3 track identically in CSiBridge and OpenSees until nonlinearity develops in the abutment and isolator links.

5.1.4   OSB4

Results from the modal analysis of OSB4 are shown in Table 5.7 and Table 5.8 for the CSiBridge and OpenSees implementations, respectively.

Table 5.7: Modal periods and frequencies obtained from CSiBridge model of OSB4

Mode	Roller Abutment			Original Abutment		
	Period	Freq-uency	Mode Shape	Period	Freq-uency	Mode Shape
-	sec	Hz	-	sec	Hz	-
1	5.094	0.196	Torsion	1.163	0.860	Transverse
2	2.681	0.373	Transverse	0.692	1.444	Torsion
3	2.675	0.374	Longitudinal	0.527	1.899	Vertical (asym.)
4	0.557	1.792	Vertical (asym.)	0.372	2.686	Vertical (sym.)
5	0.389	2.567	Vertical (sym.)	0.296	3.375	Longitudinal
6	0.266	3.751	In-plane bending	0.280	3.566	In-plane bending

Similar to OSB3, the roller abutment mode shapes are the same between the two software. However, the eigenvalues are substantially different, with the CSiBridge periods at approximately 2.7 sec for the roller abutment longitudinal and transverse modes. Similarly, there is a similarity in the original abutment modes; however, they are shifted because of the longitudinal mode (1st for OpenSees, 5th for CSiBridge). This is likely due to the discrepancy in the linear vs nonlinear analysis properties assigned in CSiBridge (whereas the eigenvalues in OpenSees are defined entirely by the input constitutive models and elements).

Table 5.8: Modal periods and frequencies obtained from OpenSees model of OSB4

Mode	Roller Abutment			Original Abutment		
	Period	Freq-uency	Mode Shape	Period	Freq-uency	Mode Shape
-	sec	Hz	-	sec	Hz	-
1	6.139	0.163	Torsion	1.083	0.923	Longitudinal
2	1.548	0.646	Transverse	1.027	0.974	Transverse
3	1.515	0.661	Longitudinal	0.786	1.272	Torsion
4	0.538	1.859	Vertical (asym.)	0.491	2.037	Vertical (asym.)
5	0.369	2.682	Vertical (sym.)	0.345	2.899	Vertical (sym.)
6	0.284	3.342	In-plane bending	0.280	3.571	In-plane bending

5.2 Bent Pushovers

The generation of similar results between the two software implementations is extended in this section to nonlinear static responses. To isolate the effect of the bent and column models in the nonlinear static response, the roller abutment boundary case was adopted again in this section. The models of OSB1 through OSB4 are used unchanged other than the roller abutment.

Two independent pushover analyses were performed. Both utilize a single monitoring point in the center of the bent at the level of the superstructure mass. Due to all of the OSB bridges having only a single bent and roller abutment boundaries, only a single point load was applied at the monitoring point for the longitudinal pushover analysis. For the transverse pushover analysis, a point load of the same magnitude was applied at the monitoring point as well as at each end of the spans (at the location of the roller abutment).

The important nonlinear static responses studied in this section are related to the frame hinges. Therefore, only results for OSB1 and OSB2 are presented and compared here. The two base isolated bridges have nonlinear static responses governed by the nonlinear isolation bearing responses. The responses of the OpenSees and CSiBridge bearing elements were compared previously in Chapter 4.

5.2.1 CSiBridge

In this section, a pushover analysis of OSB1 and OSB2 was carried out in both the longitudinal and transverse directions. A 100 kip reference load was applied independently in both directions (for each pushover, respectively) at the center node of the bridge at the level of the superstructure. Nonlinear analysis with displacement control was adopted (in 500 steps).

Figure 5.1 shows the pushover analysis results for OSB1 in the longitudinal and transverse directions. Since this bridge has two columns, the monitored displacement versus the base shear of each column was plotted for the transverse direction. The 1st column mentioned in Figure 5.1 is located in the direction of the monitored displacement (i.e., is in compression)

while the 2nd column is located in the opposite direction (i.e., is in tension). For the longitudinal direction, the monitored displacement versus the base shear of one column was plotted since their response is identical.
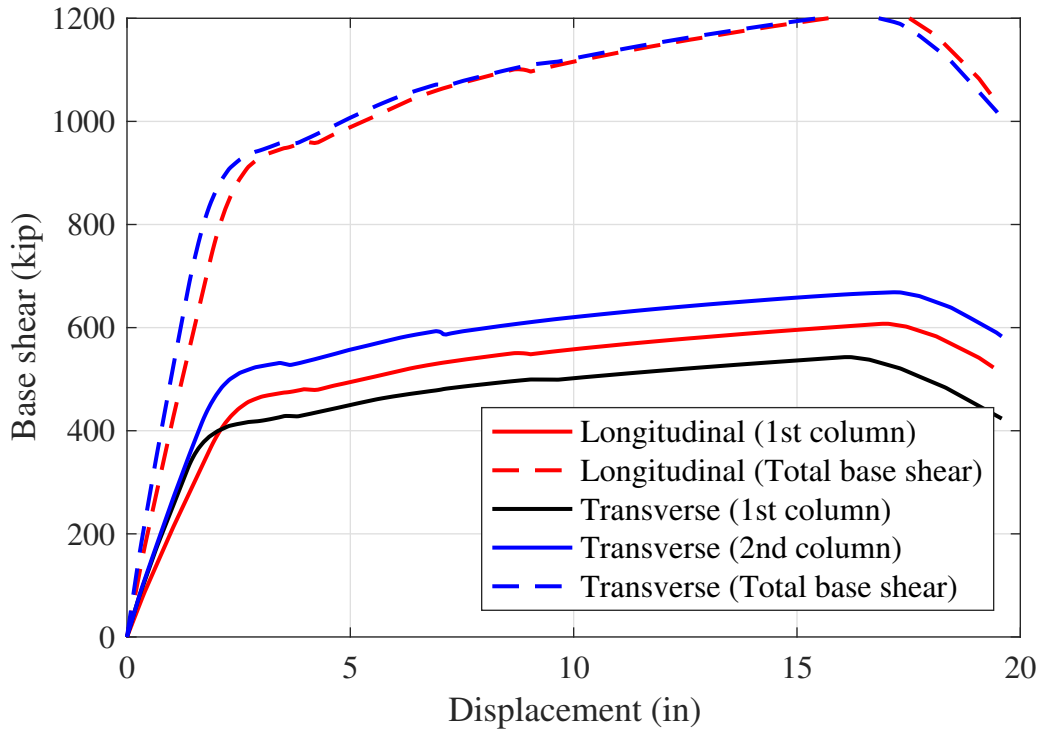
Figure 5.1: OSB1 bent load-displacement pushover in CSiBridge

5.2.2 OpenSees

In this section, a pushover analysis of OSB1 and OSB2 was performed in the longitudinal and transverse directions independently. A reference load of 100 kip was applied to the bridge structures and displacement control was used to increment the load over 100 steps. In the longitudinal pushover, the load was applied only to the center node of the bridge at the deck height (i.e., the center of the bent) in the longitudinal direction. For the transverse pushover, the load was applied at the center node of the bridge at deck height and at each end of the bridge at deck height in the transverse direction.

Figure 5.3 shows the pushover results for OSB1 in the longitudinal and transverse directions. Figure 5.4 shows the pushover results for OSB2 in the longitudinal and transverse directions.

The total pushover curves (summation of the base shears for each column in the case of OSB1) are shown together on the same plot for comparison purposes between the results obtained from CSiBridge and OpenSees. The longitudinal and transverse pushovers from OSB1 are shown in Figure 5.5, and the longitudinal and transverse pushovers from OSB2 are shown in Figure 5.6.

Figure 5.2: OSB2 bent load-displacement pushover in CSiBridge

Figure 5.3: OSB1 bent load-displacement pushover in OpenSees

112

Figure 5.4: OSB2 bent load-displacement pushover in OpenSees

Figure 5.5: OSB1 bent load-displacement pushover comparison
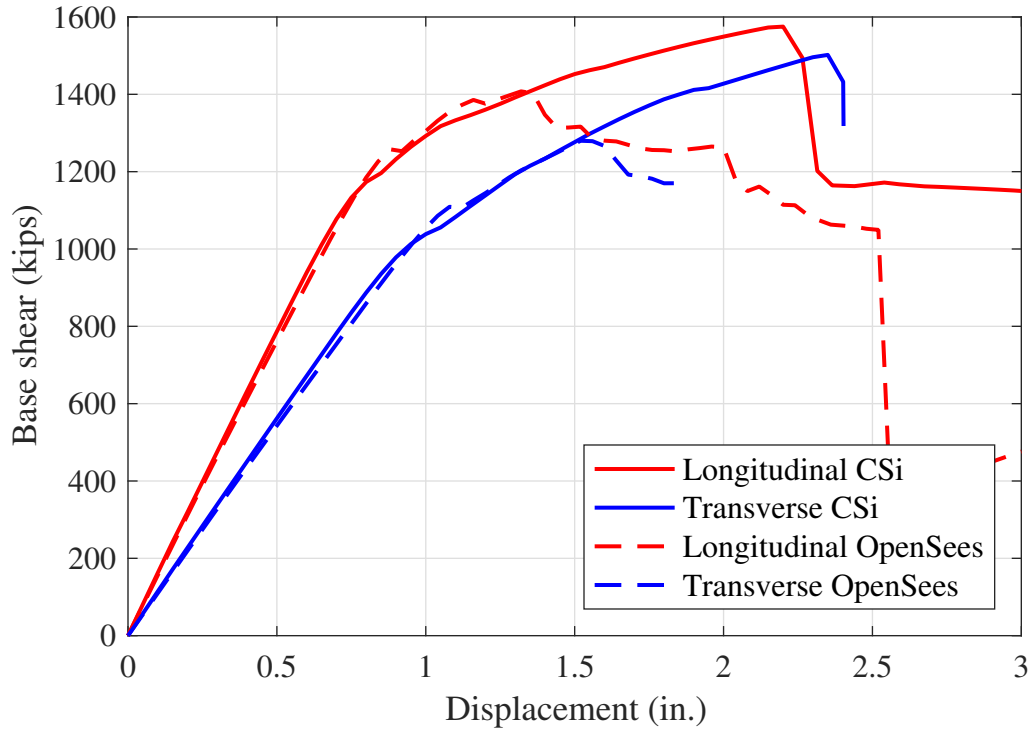
Figure 5.6: OSB2 bent load-displacement pushover comparison

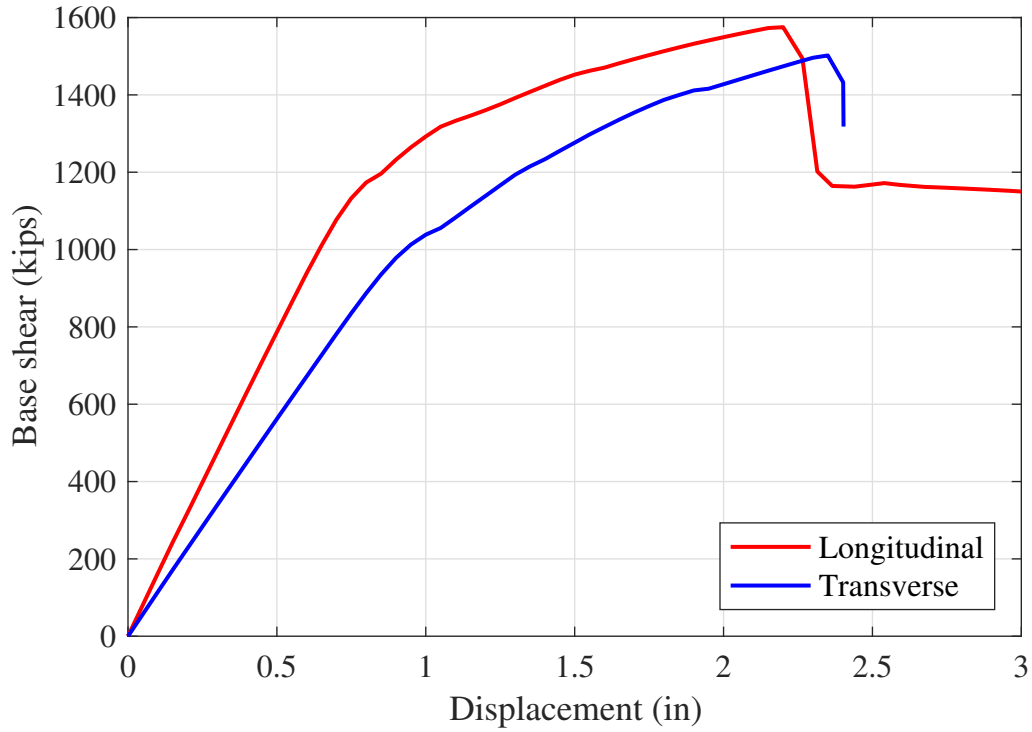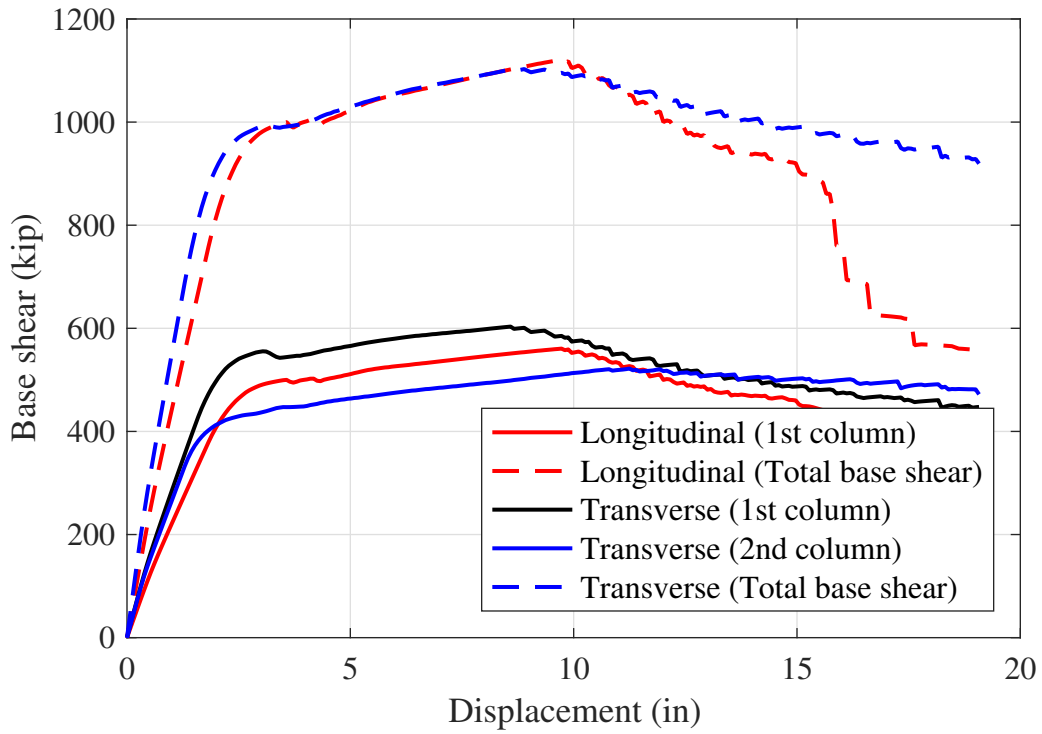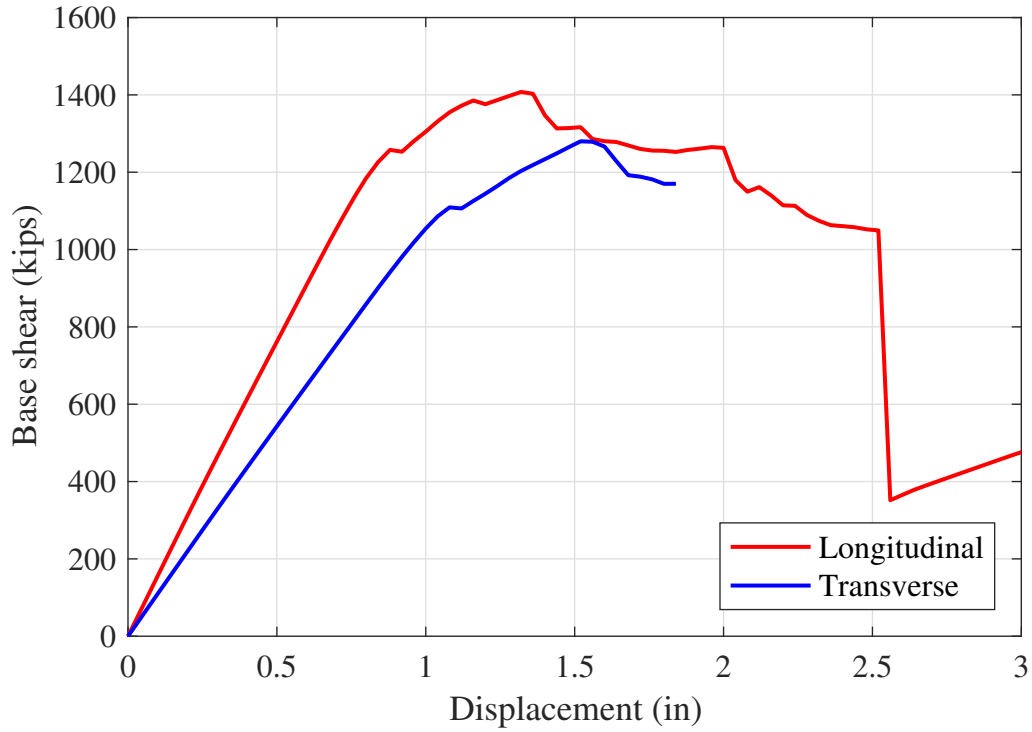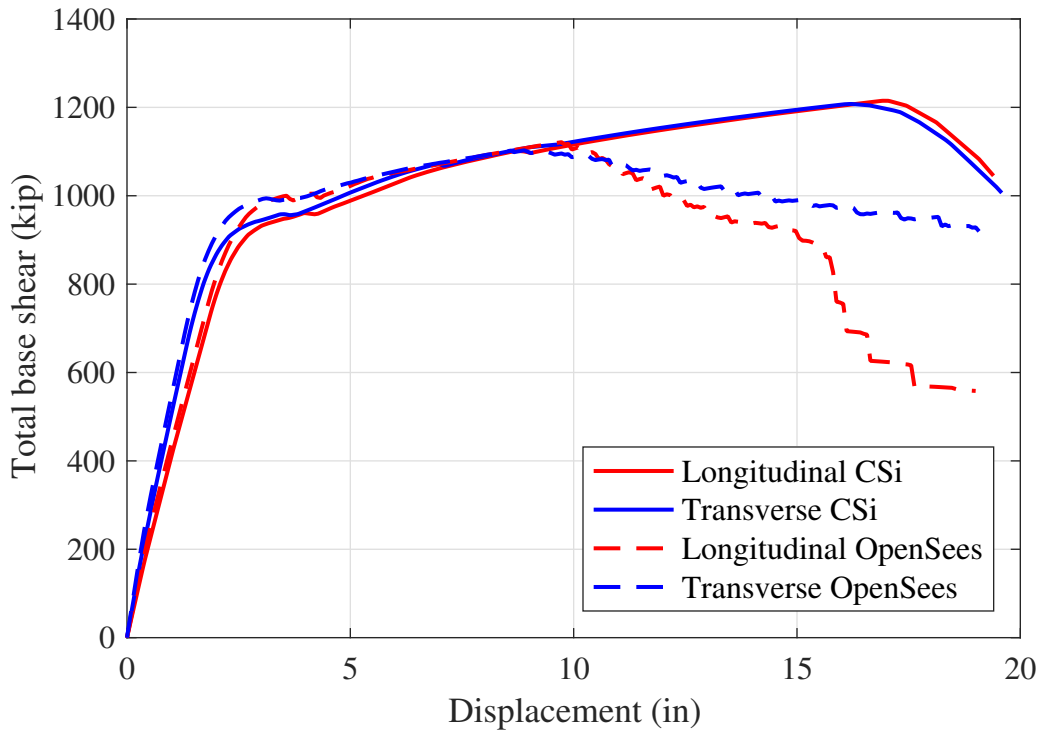Several observations can be drawn from the pushover comparison plots. For OSB1, although the sectional responses and hinge pushovers exhibited nearly identical initial stiffness and yield points, the pushover curves show stiffer behavior and a larger yield force in the OpenSees models. These nominal differences are likely due to the combined effects of the complex choice of hinge parameters in CSiBridge (rigid offset plus rigid zone factor) that were not easily duplicated in OpenSees, plus the use of the non-prismatic superstructure, whereas the OpenSees model was assumed prismatic. These two items created a slightly different boundary condition at the top of the bent columns between the two software.

The other obvious difference for OSB1 is the extended ductility of the CSiBridge model, which causes a nearly 20% difference in the estimated peak base shear. The only way to recover this ductile behavior is to remove the limitation on the crushing strain of the confined concrete in compression. If the OpenSees constitutive model is allowed to continue along the compressive backbone without dropping to zero stress, the exact same peak base shear and displacement at peak base shear can be recovered. This is due to the ultimate failure mode triggered by the steel reaching the softening branch. However, this corresponds to a strain in the concrete in excess of -0.03. Note this is also in conflict with the moment-curvature results presented in the previous chapter (it appears the moment-curvature is based on the theoretical constitutive models, not the actual ones used in the frame hinges).

OSB2 was a simpler model of both the superstructure and the hinges, and therefore easier to replicate. The difficulty with OSB2 was more in the modeling choice made (short hinge length) that led to brittle results, abundantly obvious when comparing the displacement

capacity of the bridges in Figure 5.5 and Figure 5.6. The effect of the ultimate concrete strain limit in OpenSees is also evident for OSB2, as with OSB1, although the change in ductility is not nearly as pronounced given the short hinge length.

5.3 Nonlinear Time History Analysis

NTHA was performed using a small set of recorded ground motion accelerations. The ground motions utilized, including pertinent ground motion characteristics, are shown in Table 5.9. The strong motion duration (SMD) was computed based on the standard Arias 5-95 bounds. The naming scheme and numbering matches that of the ground motion records in [18]. Two lateral orthogonal components of excitation were applied to the bridges along the longitudinal and transverse bridge axes; therefore, only the input motions with two components were utilized from the previous study (this eliminates the set of single component synthetic motions). The component listed as 000 was applied in the transverse bridge direction, while the component listed as 090 was applied in the longitudinal bridge direction. The vertical ground acceleration input was not included in the current analysis.

Table 5.9: Recorded ground motion acceleration time history properties

Tag	Name	Pulse	dt	Component 000				Component 090			
				SMD	PGA	PGV	PGD	SMD	PGA	PGV	PGD
#	-	(Y/N)	s	s	g	cm/s	cm	s	g	cm/s	cm
1	ROCKS1N1	N	0.005	25.5	0.700	89.4	54.9	-	-	-	-
2	ROCKS1N2	N	0.005	19.6	0.381	83.4	56.9	-	-	-	-
3	ROCKS1N3	N	0.005	21.4	0.317	76.0	41.8	-	-	-	-
4	ROCKS1N4	N	0.005	19.6	0.337	91.3	112	-	-	-	-
5	ROCKS1N5	N	0.005	21.8	0.526	73.3	64.5	-	-	-	-
6	ROCKS1N6	N	0.005	42.0	0.422	65.0	95.3	-	-	-	-
7	ROCKS1N7	N	0.005	22.6	0.356	89.1	105	-	-	-	-
8	ROCKS1P1	Y	0.005	25.5	0.709	113	115	-	-	-	-
9	ROCKS1P2	Y	0.005	18.4	0.441	105	130	-	-	-	-
10	ROCKS1P3	Y	0.005	21.7	0.477	115	103	-	-	-	-
11	ROCKS1P4	Y	0.005	19.5	0.319	103	181	-	-	-	-
12	ROCKS1P5	Y	0.005	21.2	0.672	136	155	-	-	-	-
13	ROCKS1P6	Y	0.005	24.0	0.412	62.1	95.5	-	-	-	-
14	ROCKS1P7	Y	0.005	21.1	0.396	140	136	-	-	-	-
22	ROCKN1N1	N	0.005	15.0	0.399	59.2	25.7	13.2	0.576	77.9	44.8
23	ROCKN1P1	N	0.005	13.8	1.42	64.2	173	13.8	1.42	64.2	173
24	SANDN1N1	N	0.005	37.0	0.784	86.3	33.3	36.3	0.812	67.9	30.7
25	CLAYN1N1	N	0.005	29.1	0.788	104	57.7	30.4	0.706	108	95.9

The ground acceleration records and linear response spectra (5% damping) for both components of the four ground motions (ROCKN1N1, ROCKN1P1, SANDN1N1, and CLAYN1N1)

are shown in Figures 5.7 through 5.14. All spectra were obtained using 5% equivalent viscous damping.
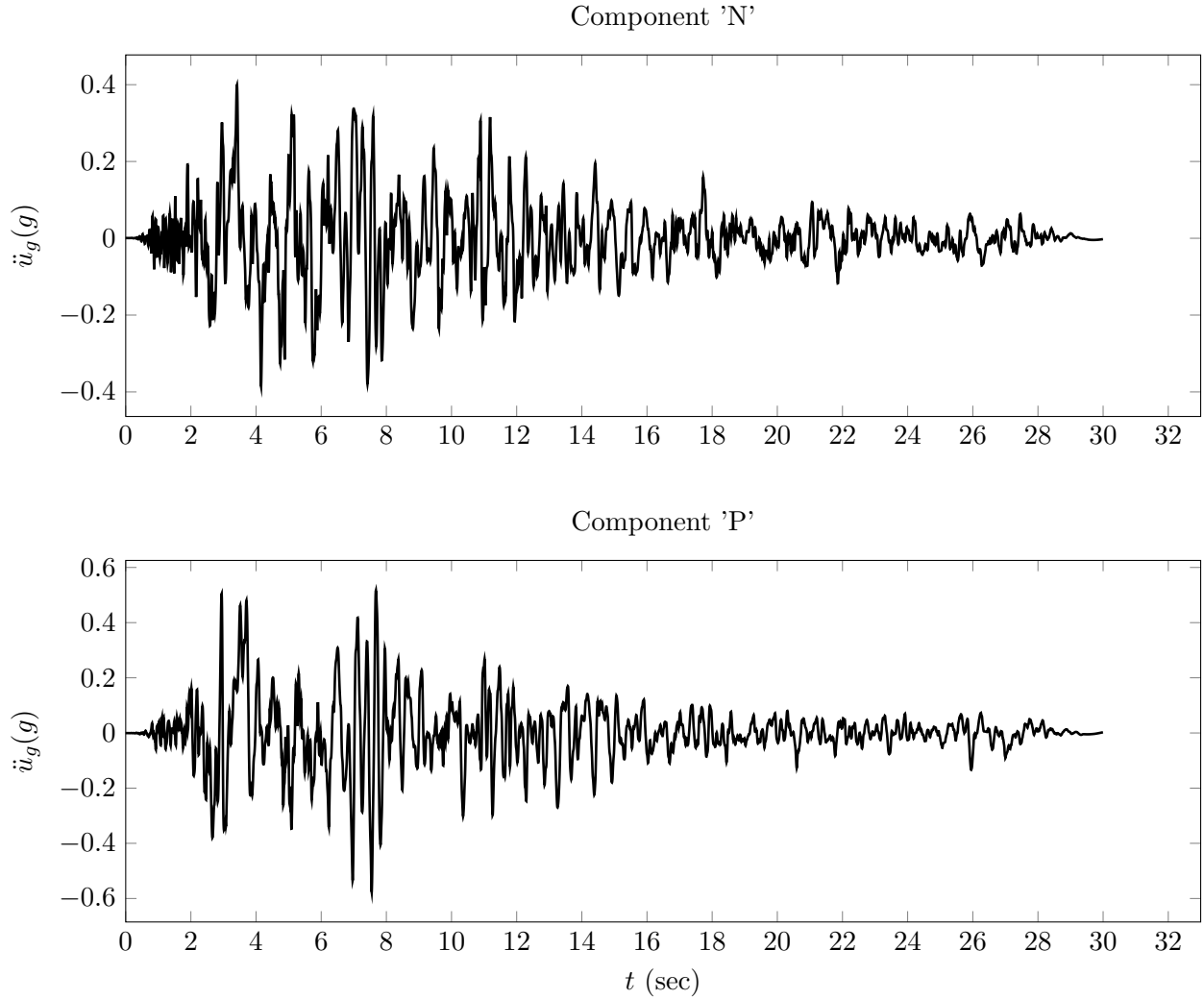
Figure 5.7: Ground acceleration records for ROCKN1N1 ground motion

As shown in previous sections, the modal characteristics and initial elastic stiffness of the OpenSees models match the CSiBridge response very closely for the case of the roller abutment. The nonlinear strengths and post-yielding behaviors differ slightly due to the constitutive models and the limitations on the lumped plasticity formulation used in the CSiBridge elements. However, while the modal and nonlinear static results are very similar, the NTHA results will differ because of differences between the OpenSees and CSiBridge models in capturing softening of the nonlinear systems during the ground motion excitation and other implementation differences in the numerical time integration scheme. In addition, the ground motions that cause highly nonlinear behavior (large displacement demands on the bents) tend to deviate between the two software due to the ultimate concrete compressive strain impact on the peak shear/moment capacity (for OSB1 and OSB2).
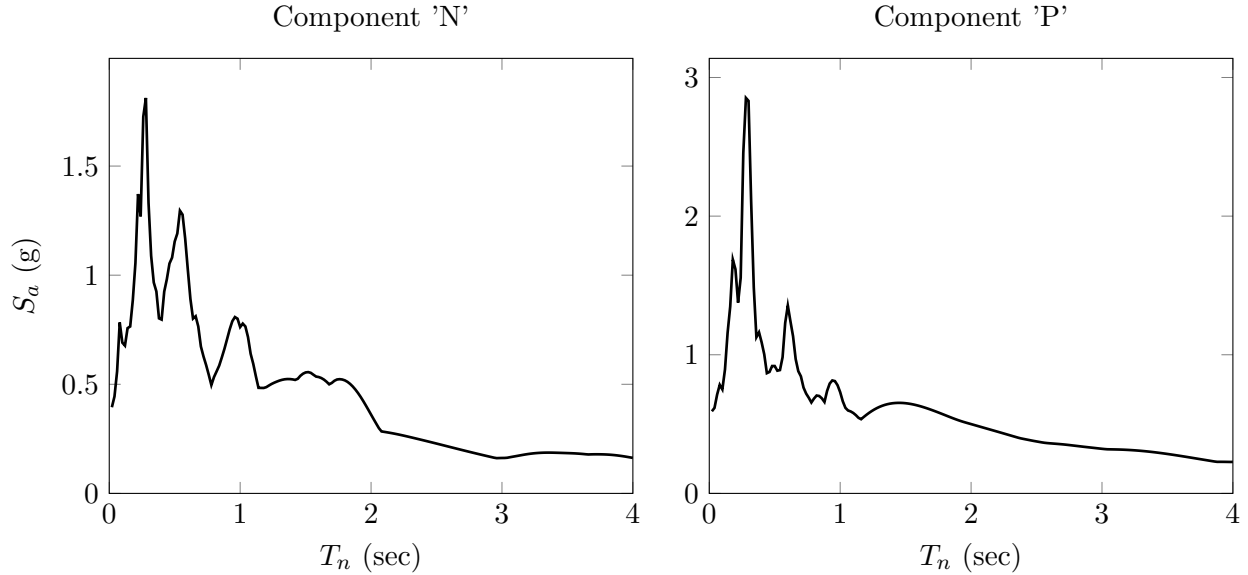
Figure 5.8: Response spectra for ROCKN1N1 ground motion with 5% damping

5.3.1 Original Abutment Model

In the CSiBridge analysis, a damping ratio of 0.05 was used in the analysis which was defined at periods of 1.2 and 0.7 second for OSB1, 0.889 and 0.692 second for OSB2, 1.233 and 0.746 second for OSB3, and 1.162 and 0.691 second for OSB4. For the time integration scheme, the Hilber-Hughes-Taylor method was employed with $\gamma = 0.5$, $\beta = 0.25$, $\alpha = 0$. The mass proportional coefficients are 0.3307, 0.3974, 0.3175, and 0.3391 for OSB1, OSB2, OSB3, and OSB4, respectively. The stiffness proportional coefficients are 7.036e-3, 6.193e-3, 7.397e-3, and 6.897e-3 for OSB1, OSB2, OSB3, and OSB4, respectively. The same values were used directly in the OpenSees analysis. The stiffness-proportional values were used with the initial stiffness in OpenSees.

For all of the bridge responses presented in this section, it should be remembered that the original abutment models were employed. While the nonlinear static backbone response and the abutment links as well as the boundary conditions were matched between the CSiBridge and OpenSees models, the nonlinear response discrepancies that arise have a component from the nonlinearity in the columns, but also the nonlinearity at the abutments. Understanding the nonlinear contributions from the columns alone (or bent isolators alone in the case of OSB3 and OSB4) is best accomplished viewing the time history results for the roller abutment model in the next section.

OSB1

The displacement time history responses of OSB1 at the center of mass of the bent for the CLAYN1N1, ROCKN1N1, and SANDN1N1 ground motions are shown in Figures 5.15, 5.16, and 5.17, respectively. The displacement time histories are shown independently for
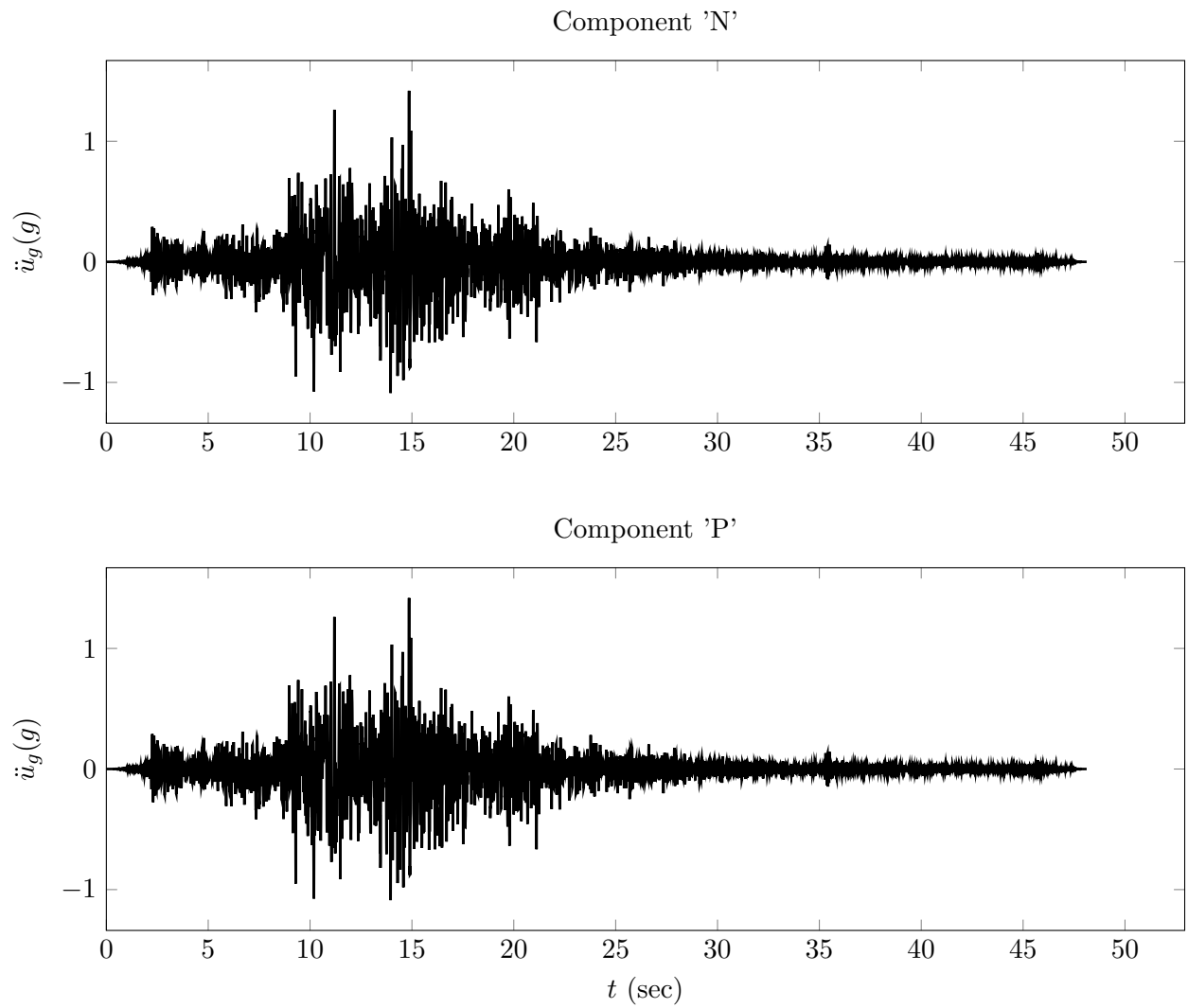
Component 'N'

Component 'P'

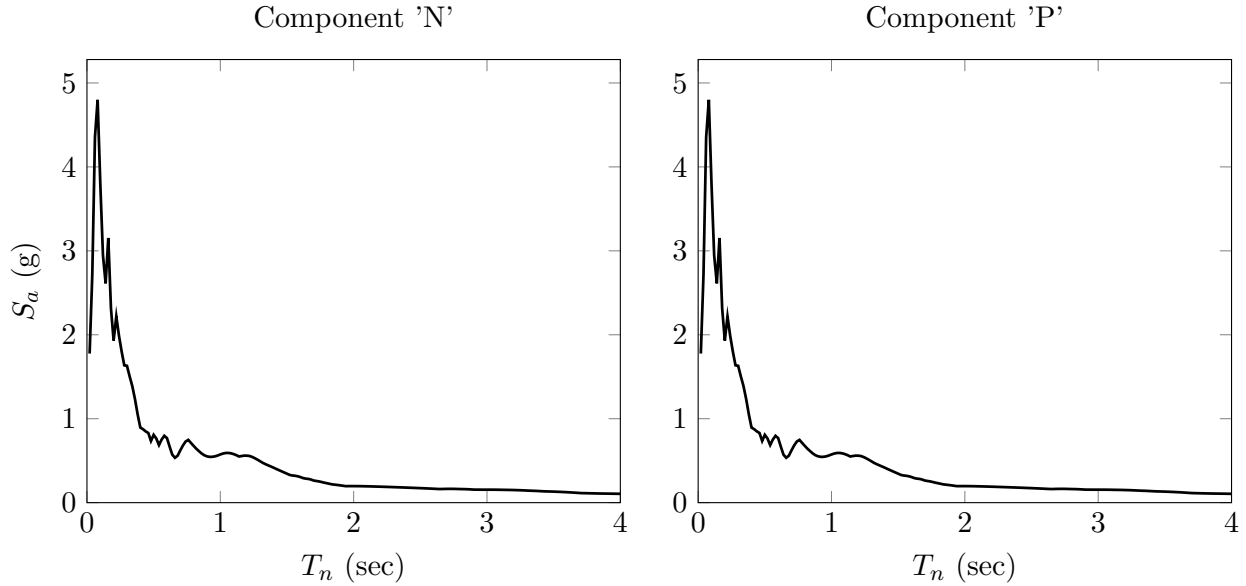Figure 5.9: Ground acceleration records for ROCKN1P1 ground motion

Figure 5.10: Response spectra for ROCKN1P1 ground motion with 5% damping

the bridge longitudinal (labeled Long.) and transverse (labeled Tran.) directions.

The phasing and agreement between the transverse response peaks for CLAY are nearly identical. The longitudinal responses begin similarly at small amplitudes but rapidly diverge after the peak response at approximately 15 sec. The contribution of the abutment model and abutment (longitudinal) hysteresis is primarily the cause in this case. The OSB1 original abutment is elastic in the transverse and vertical directions; therefore, the only difference arises in the longitudinal springs, and the mild differences observed in the stiffness and strength from the nonlinear static cases. The substantial period elongation seen in the CSiBridge longitudinal response does not follow from the expected component/material behaviors at 5 in displacement.

The displacements of OSB1 under the ROCK ground motion are smaller than CLAY. However, there is similar agreement in the transverse direction and lack of phasing/period elongation in the longitudinal direction. The frequency content of the response is higher in ROCK for the CSiBridge longitudinal response. Similar conclusions can be drawn from the responses under the SAND ground motion. The longitudinal amplitude and phasing agreement is lost rapidly after the initial peak at approximately 13 sec.

The moment-curvature responses at the top of the two bent columns for the CLAYN1N1, ROCKN1N1, and SANDN1N1 ground motions are shown in Figures 5.18, 5.19, and 5.20, respectively. As with the pushover analysis results presented previously, the two columns are labeled "1st col." and "2nd col.". The moment-curvature responses are shown independently for the moment and curvature in the longitudinal (labeled Long.) and transverse (labeled Tran.) directions. The moment in the longitudinal direction implies bending is about the bridge transverse axis. The curvature was obtained from the CSiBridge hinge rotations (using a plastic hinge length of 2.8 ft). The sign of the moment and curvature were calibrated to be
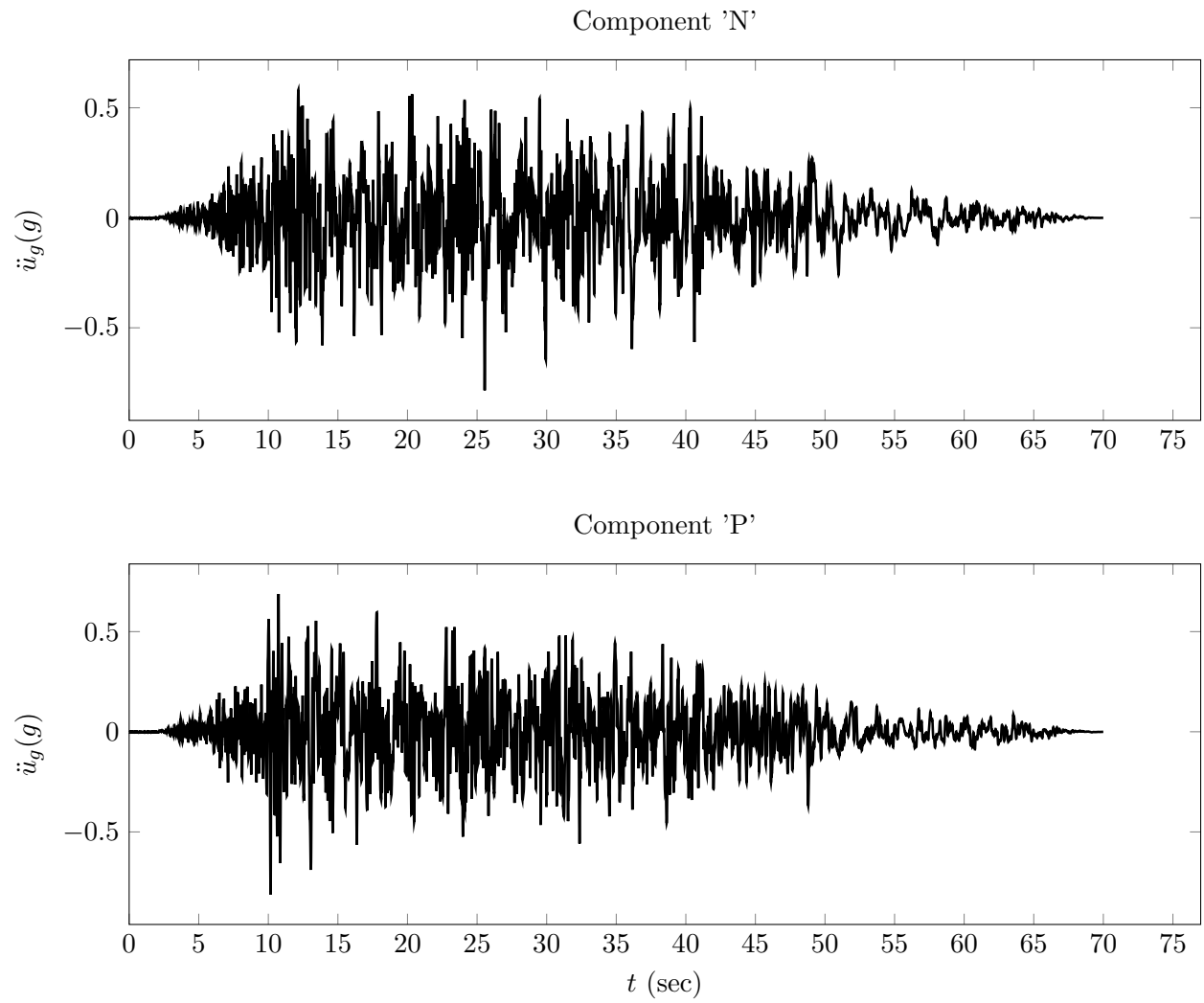
Component 'N'

Component 'P'

Figure 5.11: Ground acceleration records for SANDN1N1 ground motion

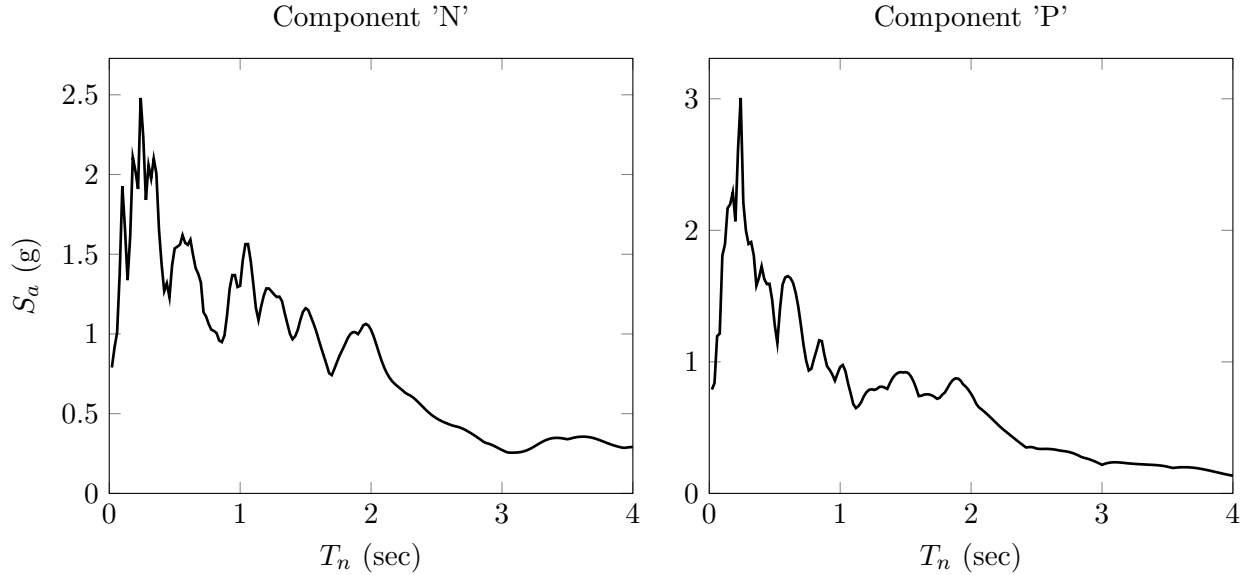Component 'N'   Component 'P'

Figure 5.12: Response spectra for SANDN1N1 ground motion with 5% damping

the same as the displacement, i.e., the peak positive displacement has a corresponding peak positive curvature, etc. In addition, for each figure, the HE is listed. The HE was obtained as the integral of the moment-curvature history and therefore has units of kip.

As would be expected based on the transverse displacement responses, the moment-curvature and HE show close agreement between CSiBridge and OpenSees for CLAY. The longitudinal direction also shows good agreement in the peak curvature; however, there is substantial energy dissipation that occurs in the longitudinal direction in CSiBridge beyond the peak that is different from the prediction in OpenSees. In addition, the CSiBridge HE predictions are approximately equal in the longitudinal and transverse directions, which does not agree with the OpenSees results. As consistent with the cyclic constitutive model results presented earlier, there is substantially higher energy dissipation in the concrete constitutive models that is reflected directly here.

The curvature demands are particularly small in the case of the ROCK ground motion, as evidenced by the magnitude of the displacements (consistent in both software results). The only nonlinear response that occurs is in the transverse direction. The HE and curvature demands are nearly identical between CSiBridge and OpenSees, as would be expected based on the standardization activities performed.

The moment-curvature and HE response trends of OSB1 under the SAND ground motion are similar to those of the CLAY ground motion. The transverse displacements are nearly identical between OpenSees and CSiBridge, yet the CSiBridge model shows enhanced energy dissipation capacity. Similarly, the longitudinal displacements show substantial period elongation and corresponding increases in energy dissipation not realized in the OpenSees results. The contribution of the original abutment model to this energy dissipation is more easily understood when comparing the roller abutment model responses in the next section.
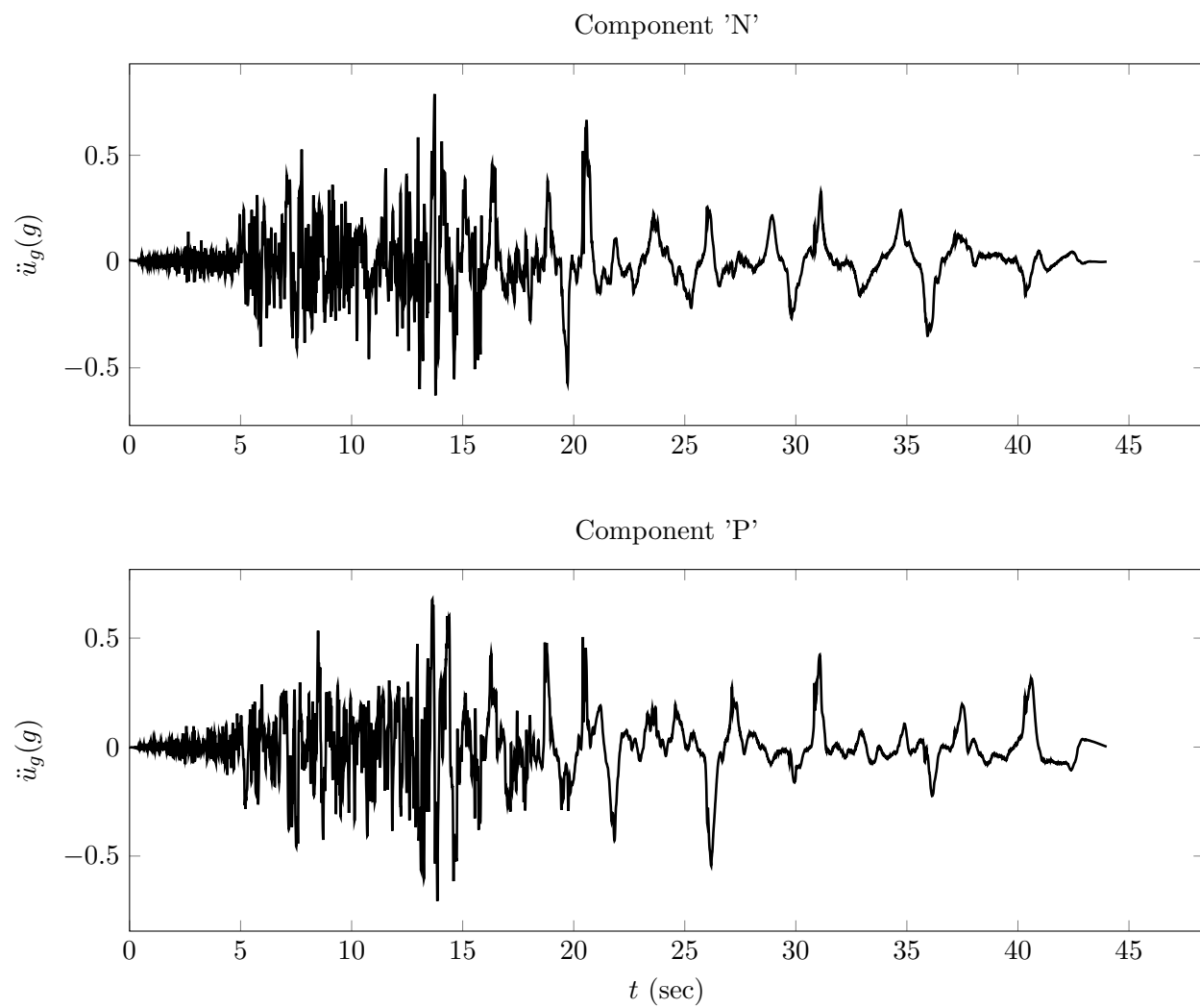
Component 'N'

Component 'P'

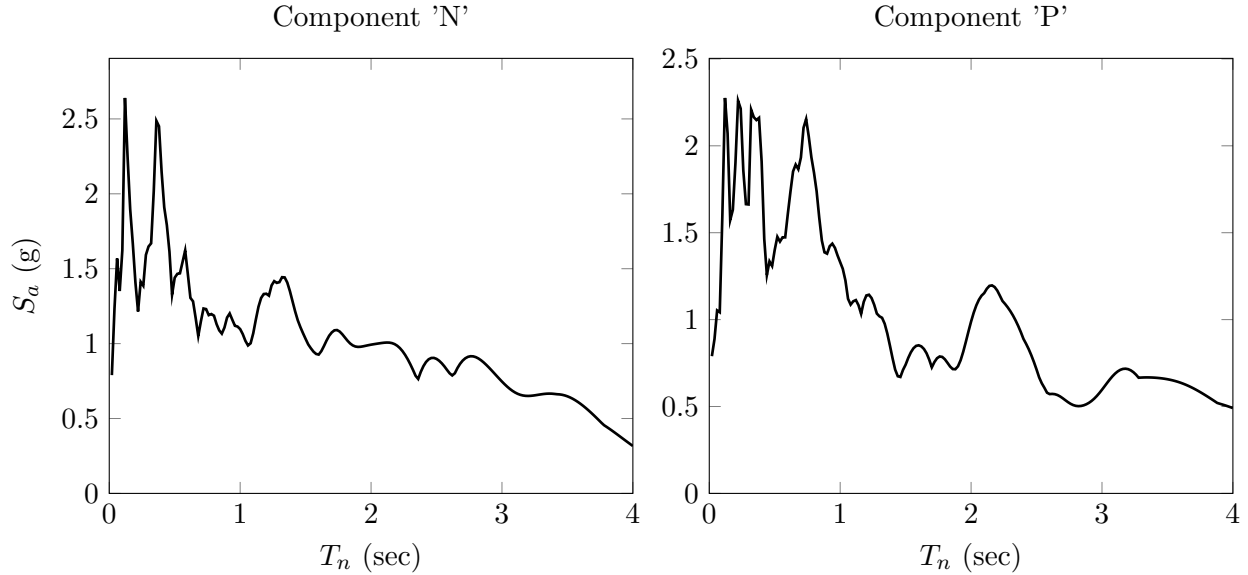Figure 5.13: Ground acceleration records for CLAYN1N1 ground motion

Figure 5.14: Response spectra for CLAYN1N1 ground motion with 5% damping

OSB2

The displacement time history responses of OSB2 at the center of mass of the bent for the CLAYN1N1, ROCKN1N1, and SANDN1N1 ground motions are shown in Figures 5.21, 5.22, and 5.23, respectively. The displacement time histories are shown independently for the bridge longitudinal (labeled Long.) and transverse (labeled Tran.) directions. As mentioned several times for OSB2, the inadvertent modeling choice of hinge length made the stiffness higher than would be expected. In addition, the bridge model exhibits brittle behavior at displacement demands that are small (2 to 3 in). Therefore, as may be expected, the frequency content of the OSB2 time history results for all the ground motions was higher, particularly in the transverse direction due to the boundary conditions in the original abutment model.

Both models show an initial gravity displacement in the longitudinal direction (for all ground motions utilizing the original abutment model). Based on the observations of the roller abutment models in the next section, this initial offset appears to be due to the non-symmetric boundary conditions at the abutments in OSB2.

The overall trends observed in the OSB2 time history responses were consistent with the observations made from OSB1. Specifically, the transverse responses show acceptable agreement between CSiBridge and OpenSees, and the longitudinal responses match until the first substantial inelastic displacement peak, beyond which the CSiBridge results show significant period elongation. However, for the case of the CLAY motion, the transverse responses are not identical. The magnitude of the peak displacements are 50% different (OpenSees larger) and also occur at a different time during the ground motion history. While the low frequency portion of the transverse displacement response matches, the high frequency content differs substantially. It is not immediately clear whether the change in frequency content (as observed in the longitudinal CSiBridge responses as well) is due to
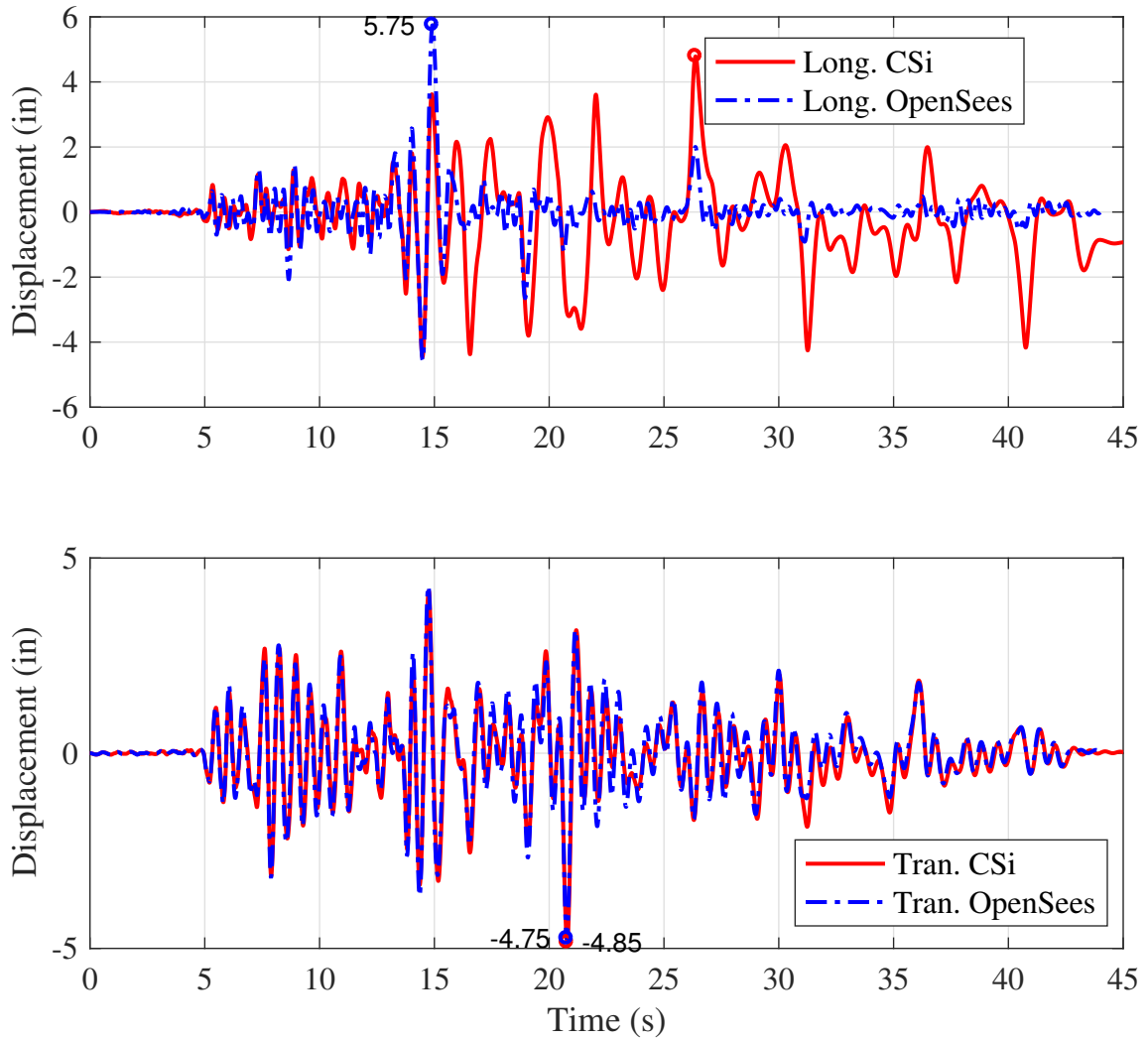
Figure 5.15: OSB1 (original abutment) center of mass displacement time histories for motion CLAYN1N1
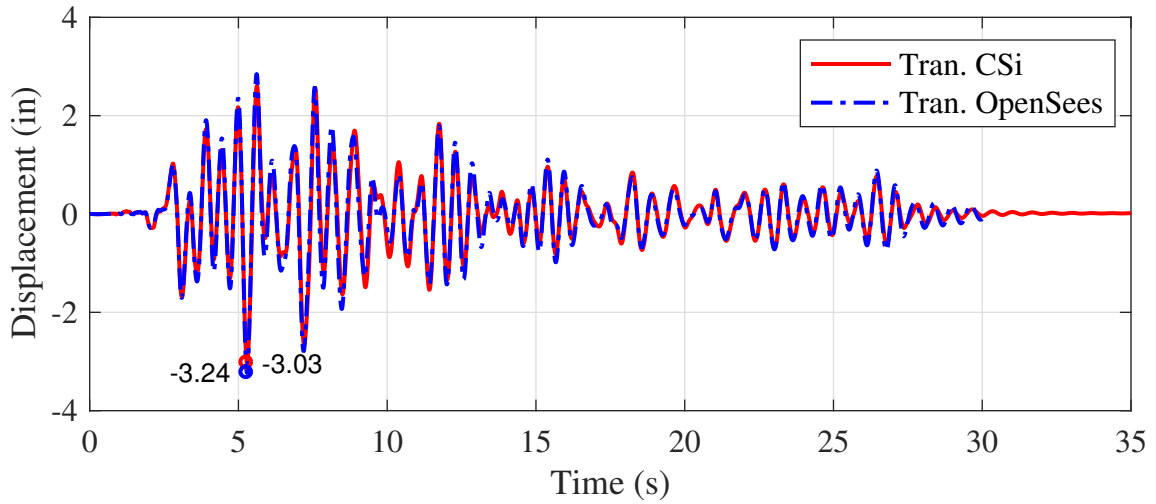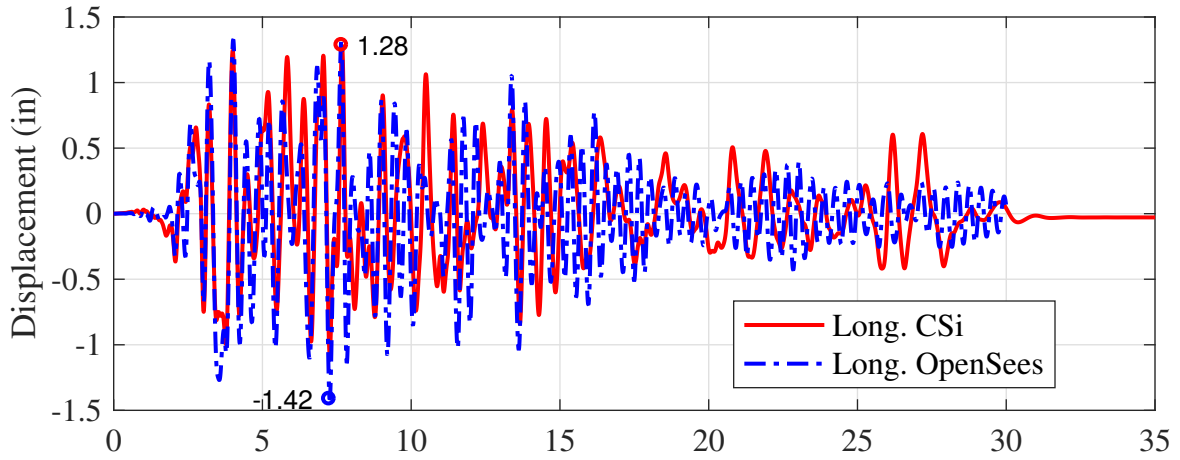
Figure 5.16: OSB1 (original abutment) center of mass displacement time histories for motion ROCKN1N1
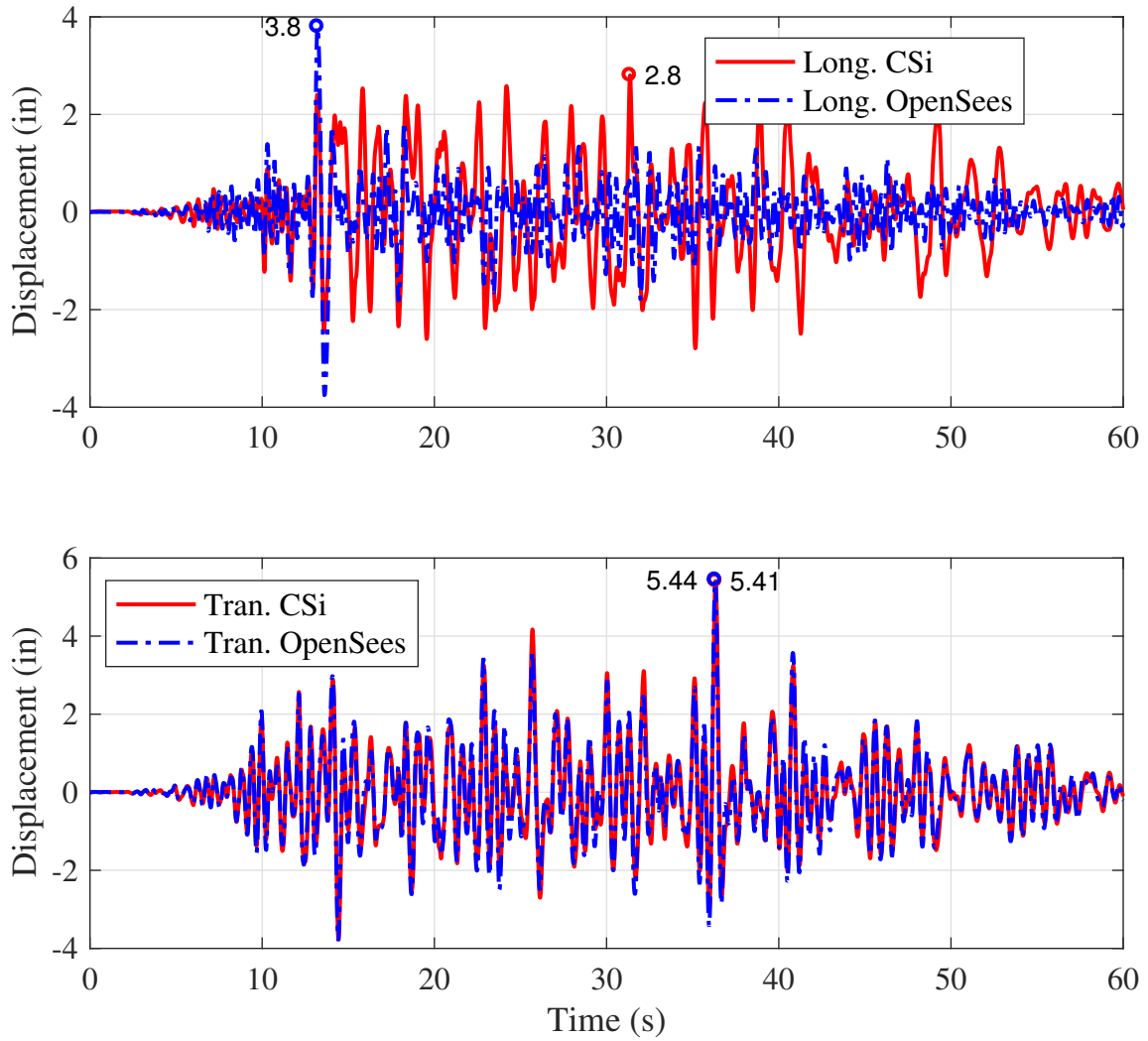
Figure 5.17: OSB1 (original abutment) center of mass displacement time histories for motion SANDN1N1
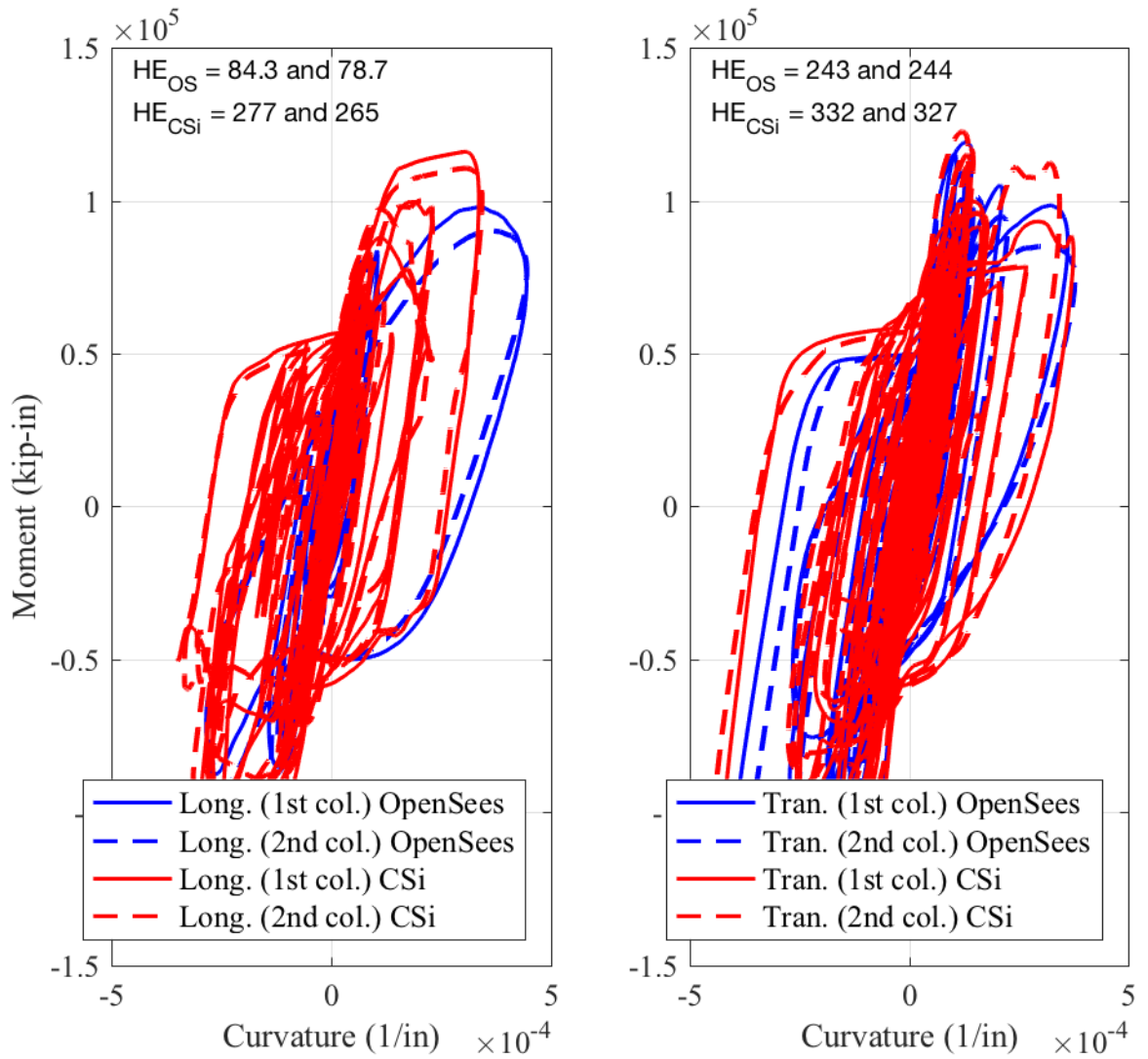
Figure 5.18: OSB1 (original abutment) column top moment-curvature responses for motion CLAYN1N1
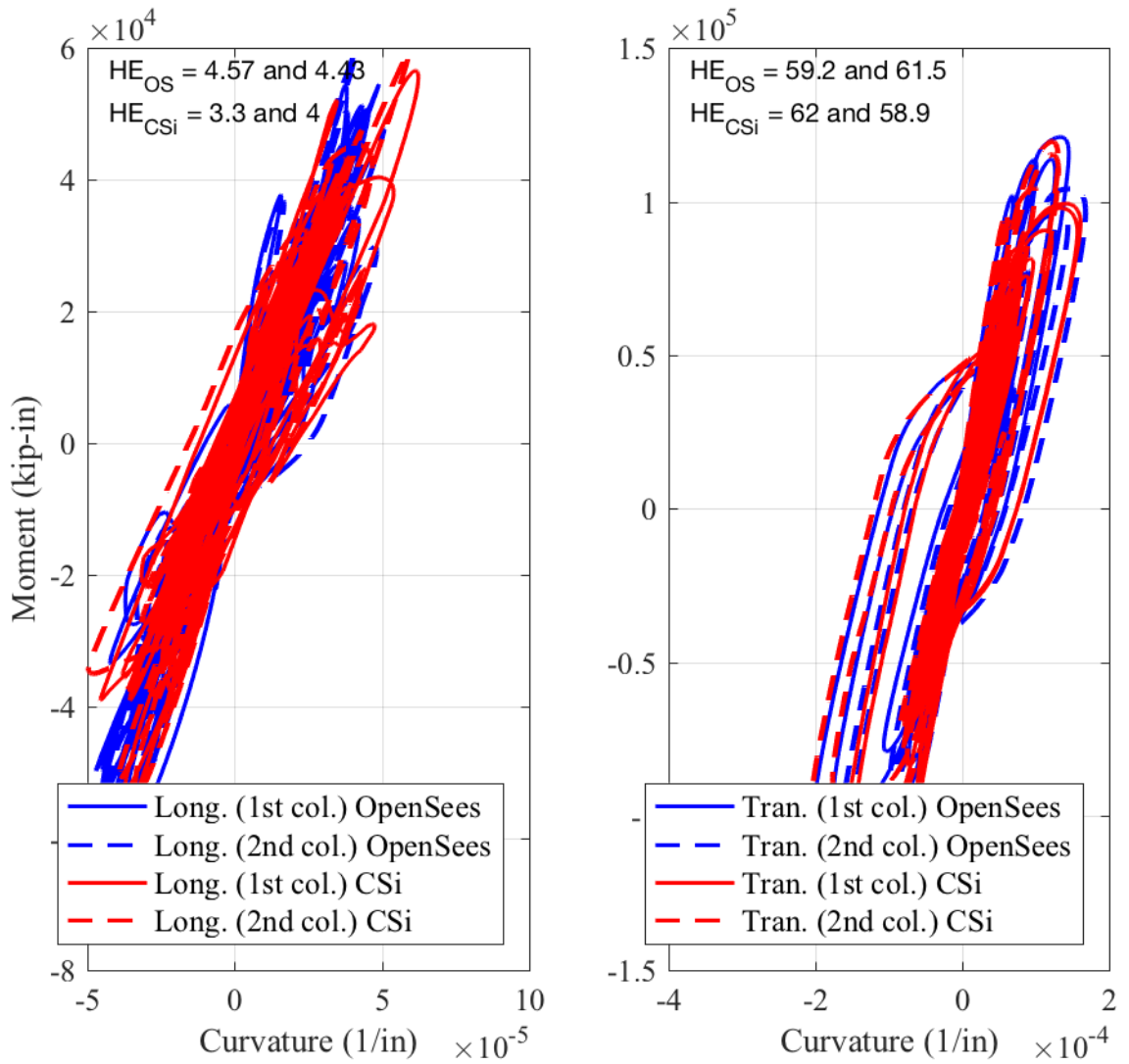
Figure 5.19: OSB1 (original abutment) column top moment-curvature responses for motion
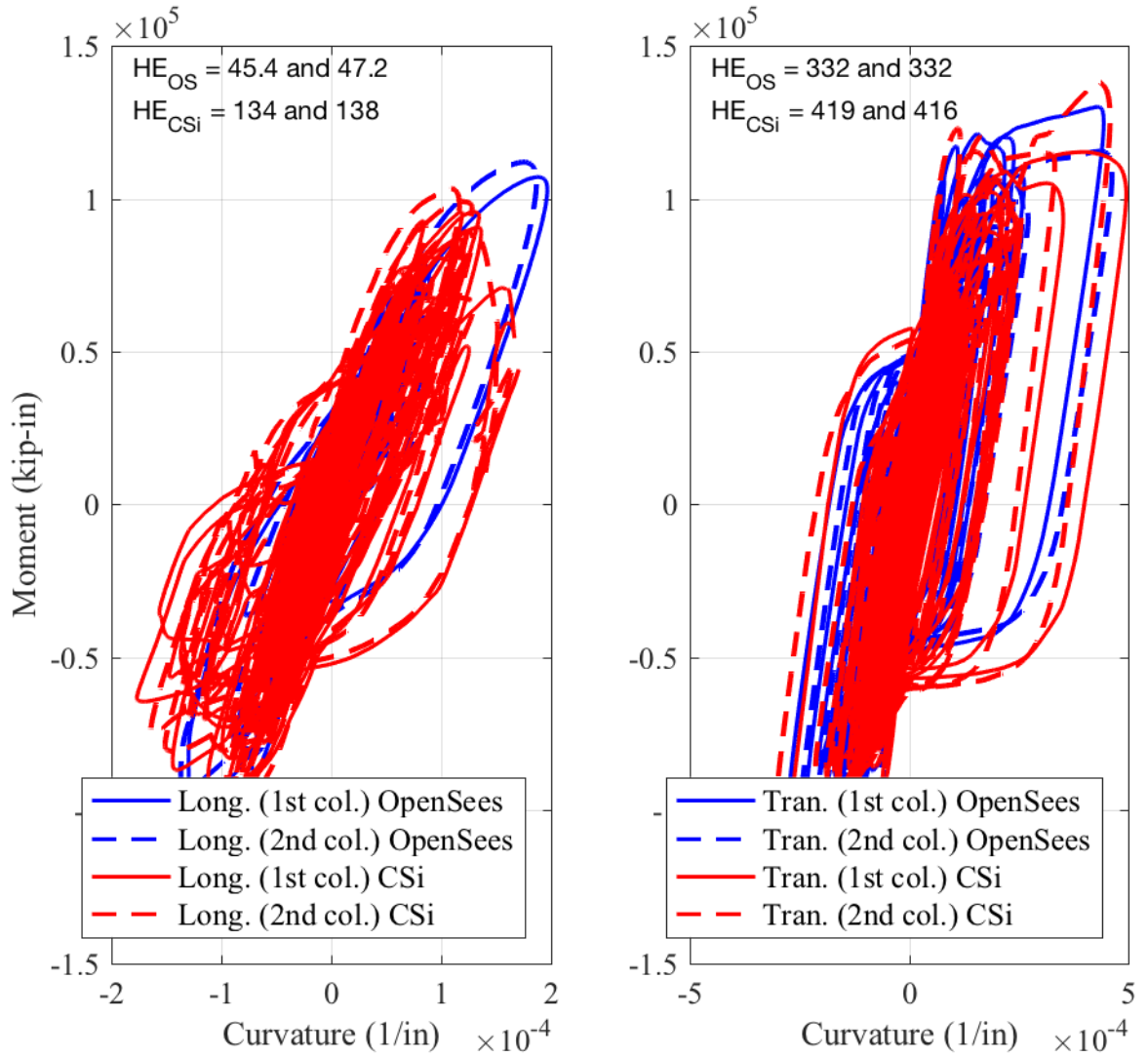ROCKN1N1

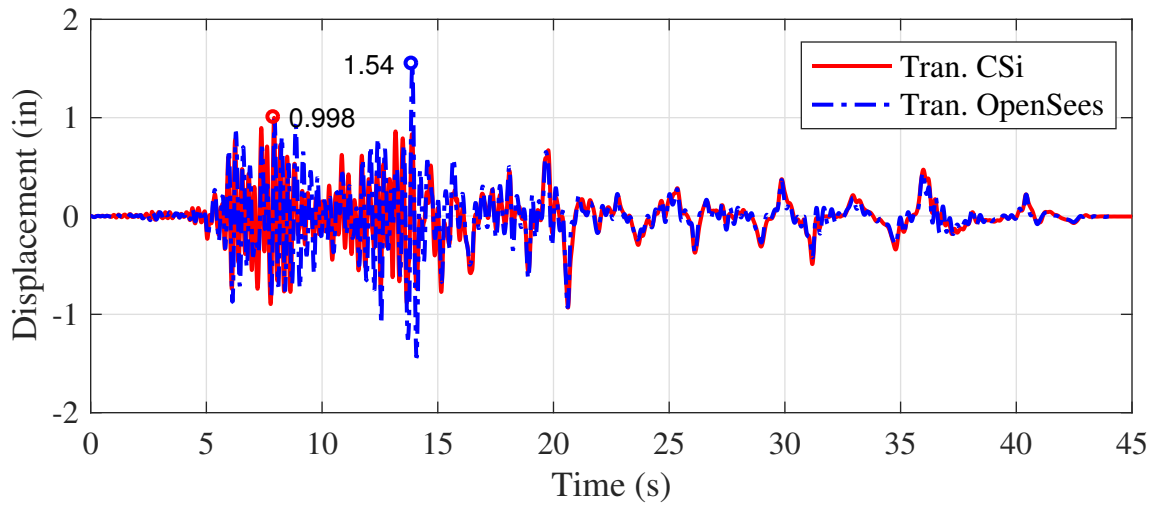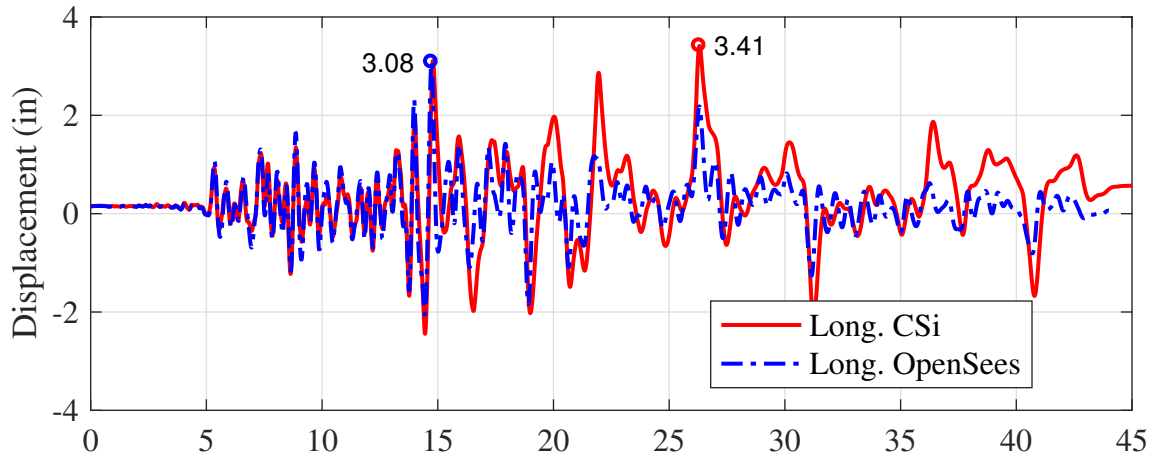Figure 5.20: OSB1 (original abutment) column top moment-curvature responses for motion SANDN1N1

Figure 5.21: OSB2 (original abutment) center of mass displacement time histories for motion CLAYN1N1

the change in the concrete constitutive models, or whether other changes are made to the integrator during time history analysis.
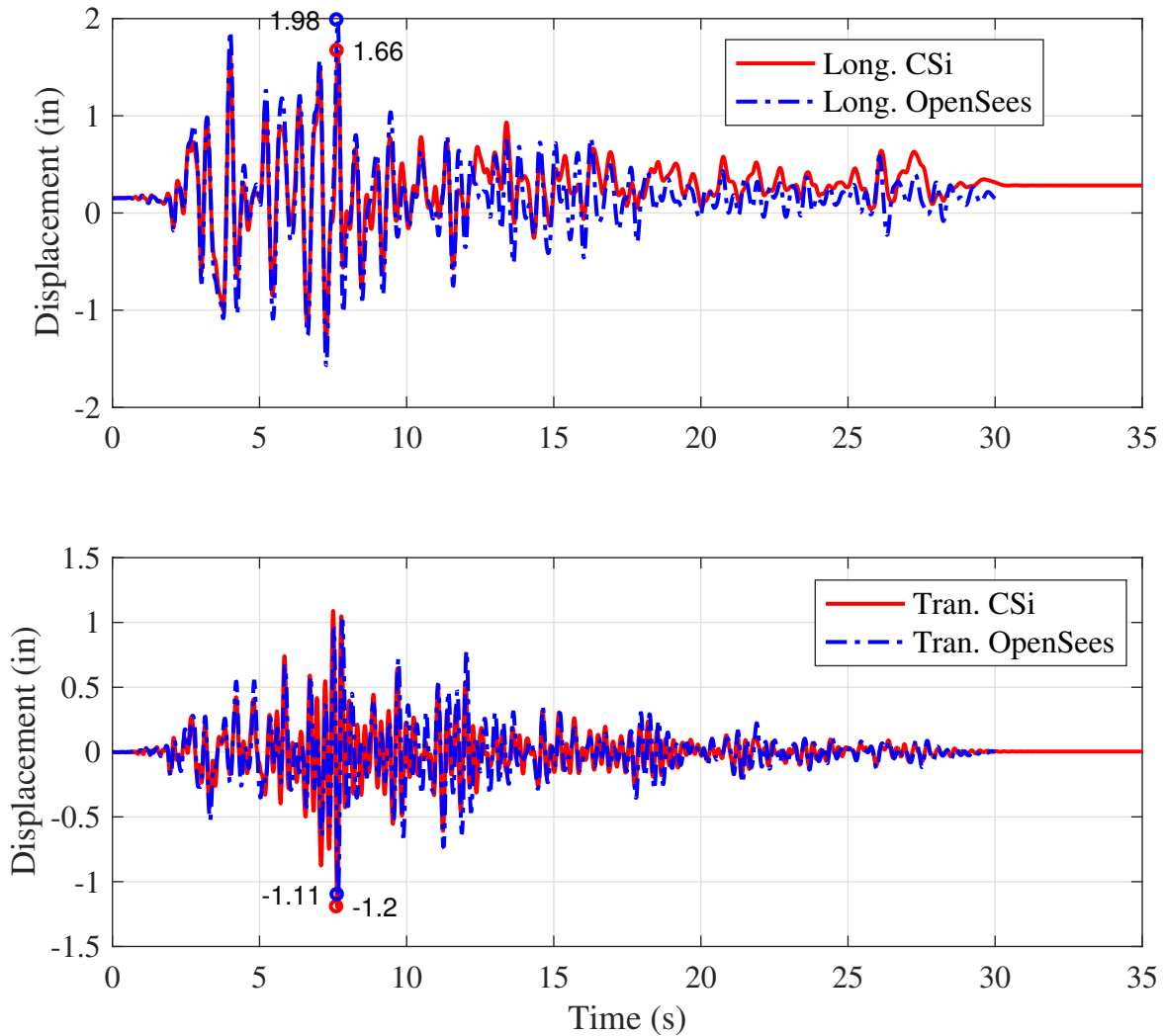
Figure 5.22: OSB2 (original abutment) center of mass displacement time histories for motion ROCKN1N1

The peak displacement demands are smaller for the ROCK ground motion, particularly in the transverse direction. Therefore, the agreement between the CSiBridge and OpenSees results remain consistent for most of the time history in both the transverse and longitudinal directions (as response is primarily elastic). The phasing and magnitude of the response following the peak longitudinal displacement in the SAND ground motion differ, as observed with the CLAY motion.

It was not possible to obtain the moment-rotation (and therefore moment-curvature) for the hinge at the bottom of the column from the OSB2 CSiBridge outputs. Therefore, the moment-curvature responses at the top of the column for the CLAYN1N1, ROCKN1N1, and
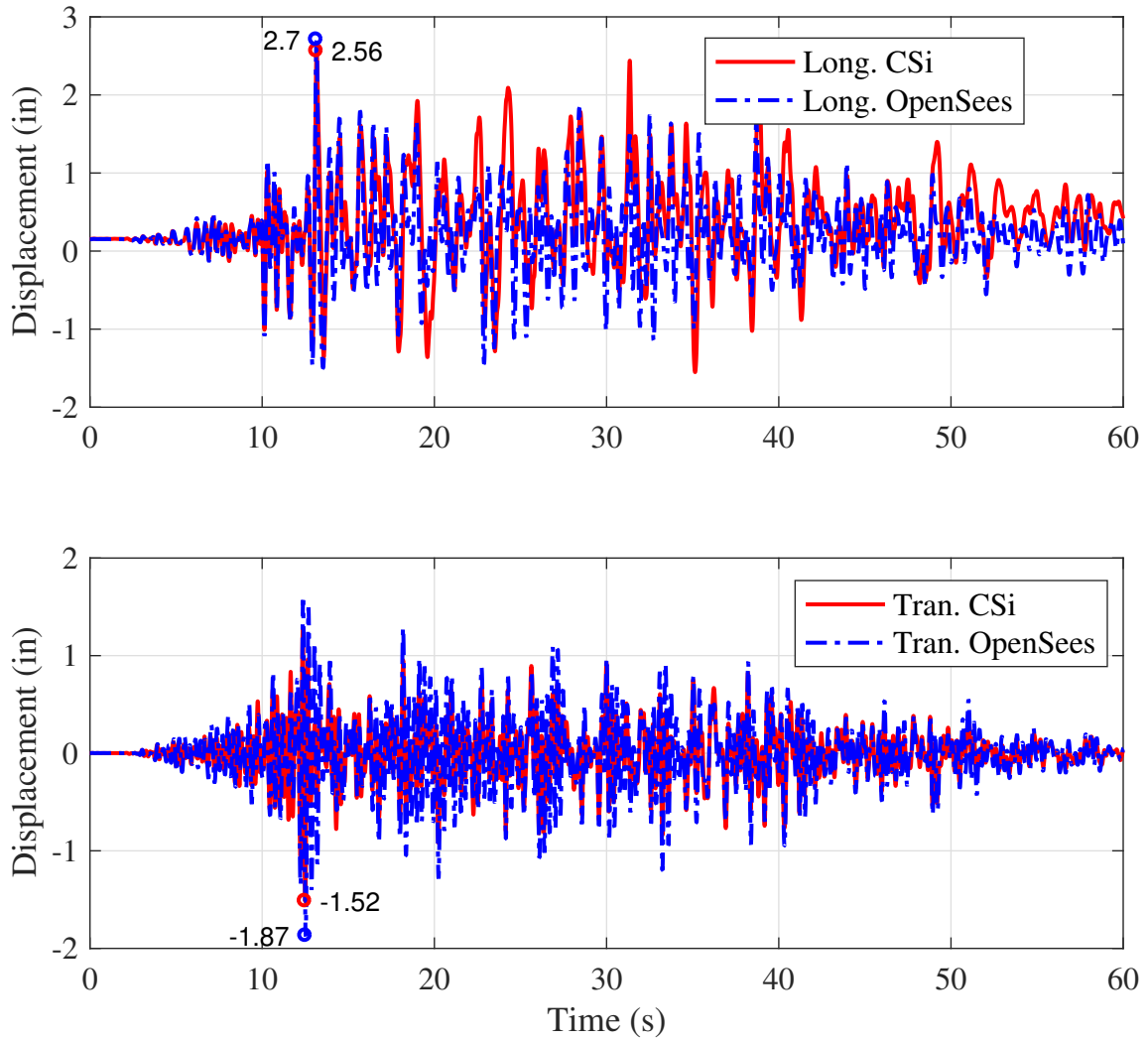
Figure 5.23: OSB2 (original abutment) center of mass displacement time histories for motion SANDN1N1

SANDN1N1 ground motions are shown in Figures 5.24, 5.25, and 5.26, respectively. The moment-curvature responses are shown independently for the moment and curvature in the longitudinal (labeled Long.) and transverse (labeled Tran.) directions. The moment in the longitudinal direction implies bending is about the bridge transverse axis. The curvature in the CSiBridge responses were obtained from the hinge rotations and the plastic hinge length of 3.36 in. The sign of the moment and curvature were calibrated to be the same as the displacement, i.e., the peak positive displacement has a corresponding peak positive curvature, etc. In addition, for each figure, the HE is listed.
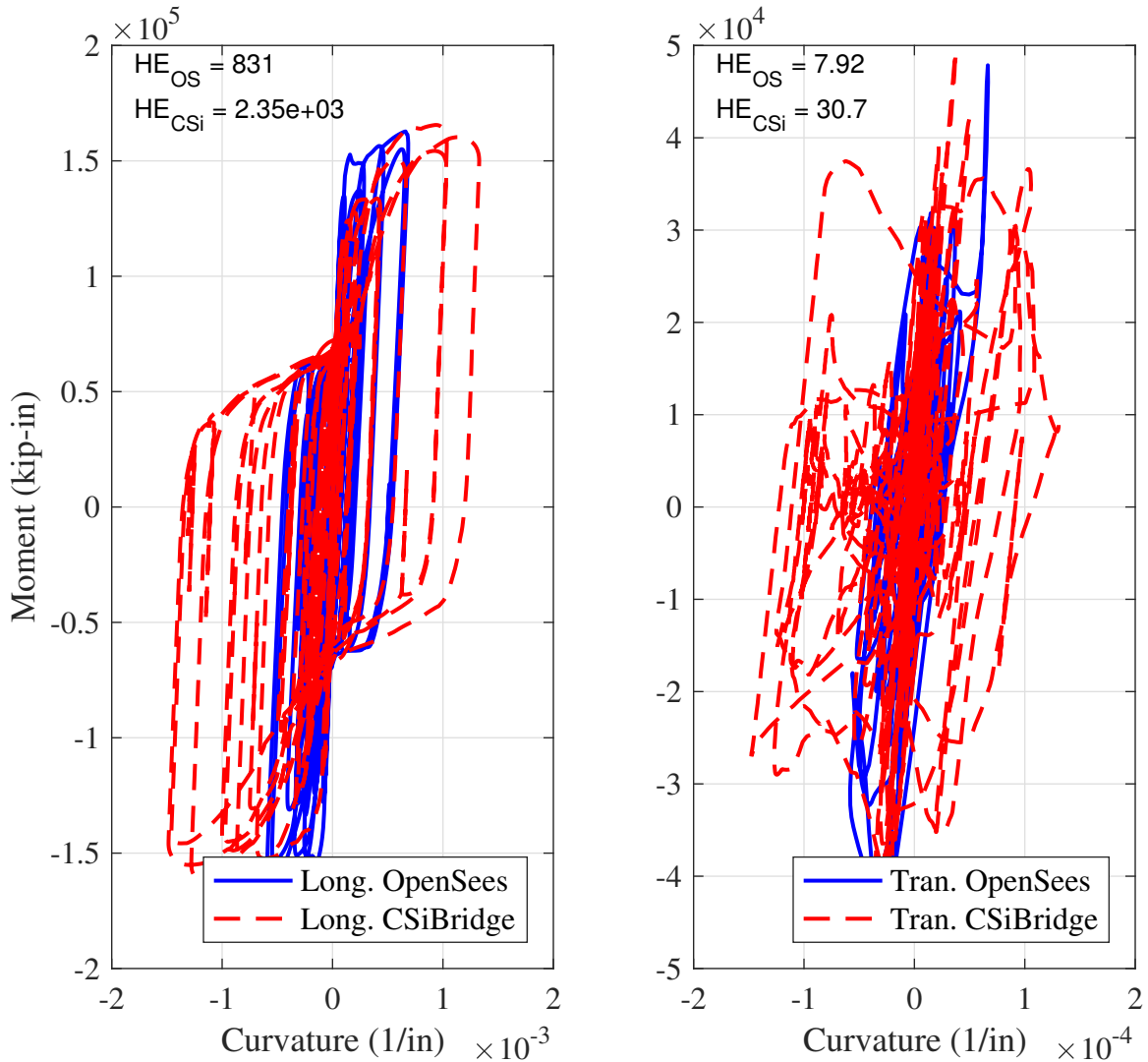

Figure 5.24: OSB2 (original abutment) column top moment-curvature responses for motion CLAYN1N1

Both the shape and energy dissipated are similar between CSiBridge and OpenSees for the longitudinal response to the CLAY motion up to the peak around 14 sec. However, the

additional displacement peaks in the CSiBridge response (including the maximum predicted longitudinal displacement around 26 sec) lead to a substantially larger HE. In addition, it is noticeable that the reloading stiffness softens in the CSiBridge response at smaller curvature demands than the OpenSees response. The transverse displacements, and hence curvatures, particularly at the top of the column, remain mostly in the elastic range. The peak displacement achieved in CSiBridge was 1.0 in, which is close to the first yield. Rotational inertia may contribute to slightly larger transverse curvature demands at the top of the column in CSiBridge than OpenSees. However, the increased CSiBridge curvature demands may also be a byproduct of the general difficultly performing numerical simulation on the OSB2 bridge (because of the hinge length).
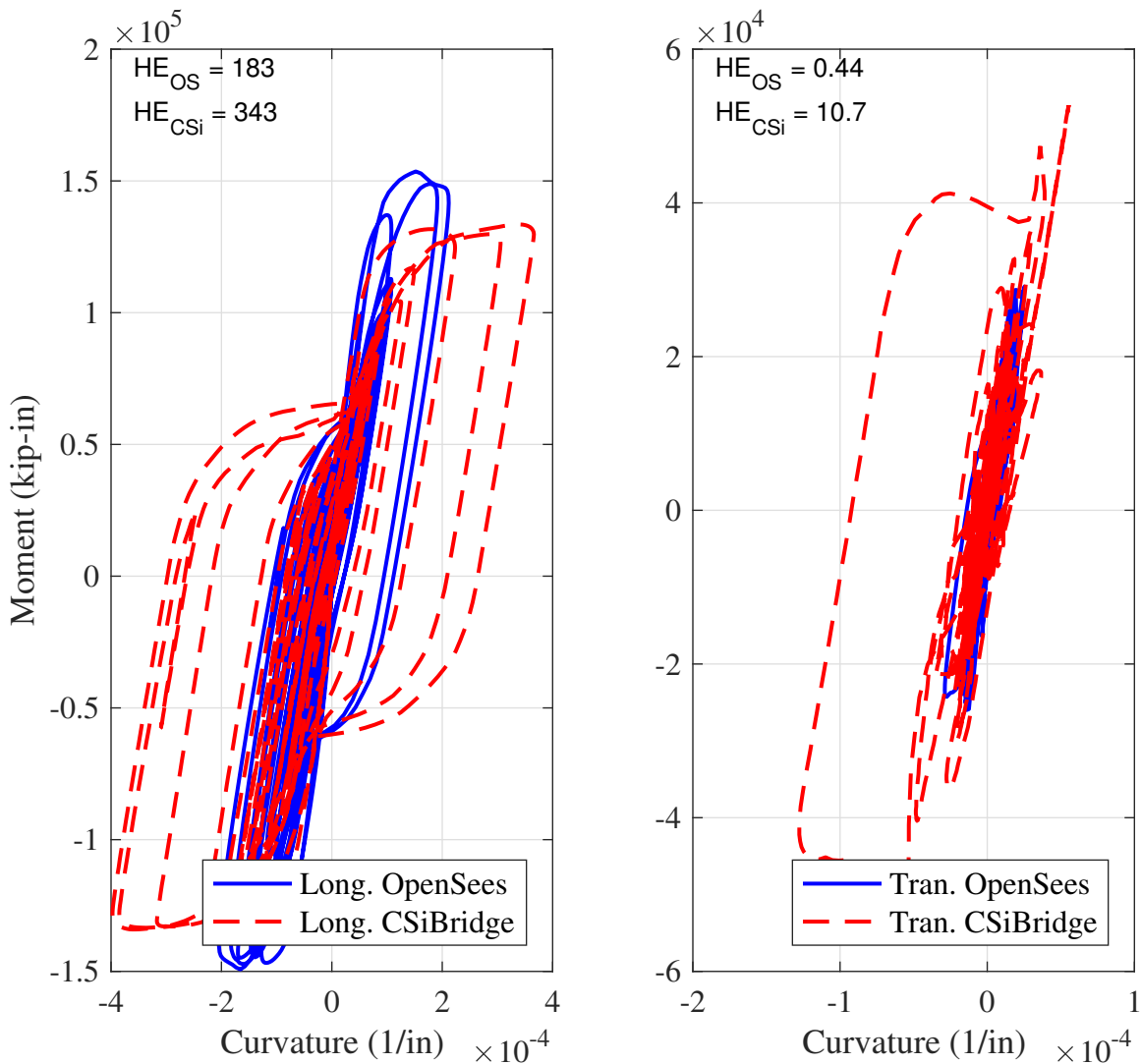

Figure 5.25: OSB2 (original abutment) column top moment-curvature responses for motion ROCKN1N1

The displacement demands for the ROCK ground motion are smaller than CLAY (both directions). Therefore, the HE values reported are smaller. The good agreement in the responses shown in Figure 5.22 result in relatively close agreement between the models. However, it should be noted that the CSiBridge model shows larger curvature demand even though the displacements are smaller. Therefore, the CSiBridge model shows larger HE. The transverse hysteresis is approximately elastic for both models, except the single curvature excursion in CSiBridge at the maximum displacement (approximately 8 sec). The SAND ground motion shows a larger curvature demand in CSiBridge than OpenSees although the displacements maxima are similar. The substantial number of large amplitude displacement peaks in the CSiBridge response can be seen by the larger HE demand.
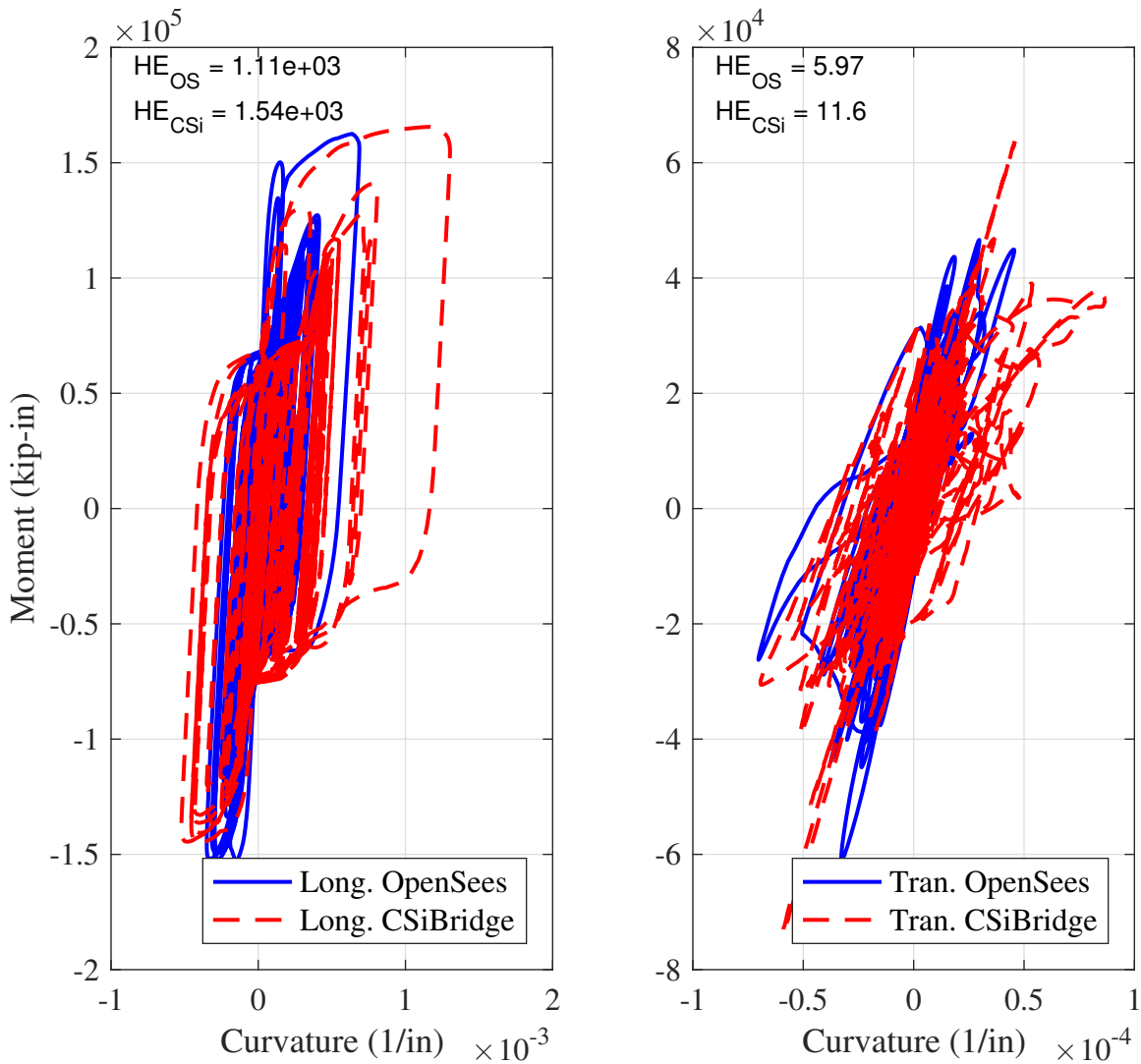

Figure 5.26: OSB2 (original abutment) column top moment-curvature responses for motion SANDN1N1

OSB3

The displacement time history responses of OSB3 at the center of mass of the bent for the CLAYN1N1, ROCKN1N1, and SANDN1N1 ground motions are shown in Figures 5.27, 5.28, and 5.29, respectively. The displacement time histories are shown independently for the bridge longitudinal (labeled Long.) and transverse (labeled Tran.) directions. An important distinction between the responses for OSB3 relative to those previously presented for OSB1 and OSB2 is the magnitude of the displacement demands. The significance has to do with the nonlinear contributions of the abutment links in the responses presented in this section (original abutment model). While the nonlinear contributions and unloading/reloading rules had only a minor impact on OSB1 (peak displacement was 5.75 in for CLAY motion), here the displacements are on the order of 10 to 20 in.
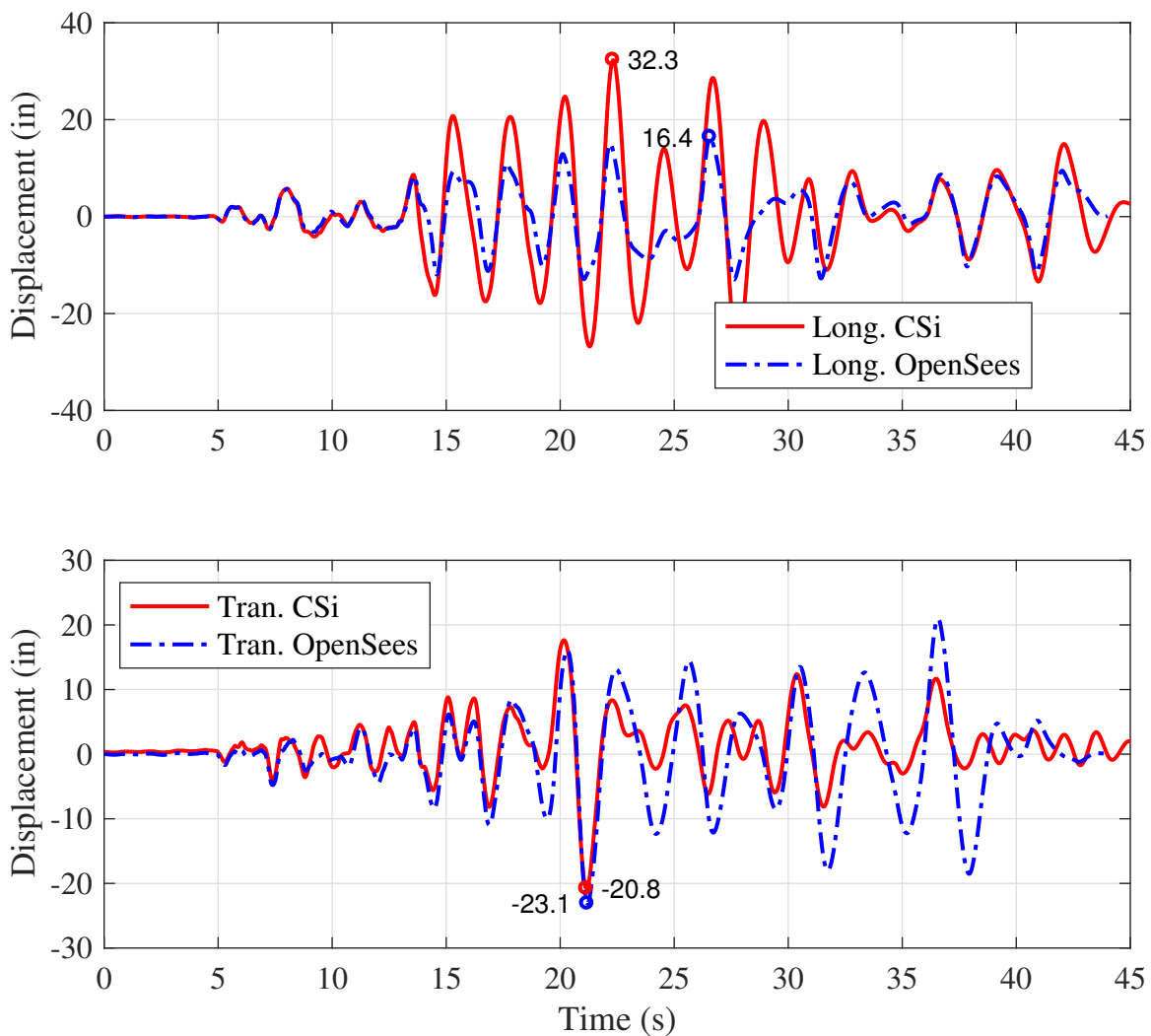

Figure 5.27: OSB3 (original abutment) center of mass displacement time histories for motion CLAYN1N1

The initial phasing and magnitude of both the longitudinal and transverse responses for CLAY show good agreement. However, beyond 15 sec and a displacement of approximately 10 in for each direction, the magnitudes differ substantially. In the longitudinal case, the peak displacement demand reported by CSiBridge is double that of OpenSees. Once the displacement amplitudes drop below 10 in, the longitudinal phasing and amplitudes again match, indicating there was no period elongation coming from the abutment models. However, the transverse responses do not exhibit this return of phasing. Due to the standardization of the isolator responses performed in the previous chapter, the differences observed are likely due to the abutments, which is confirmed in the next section.
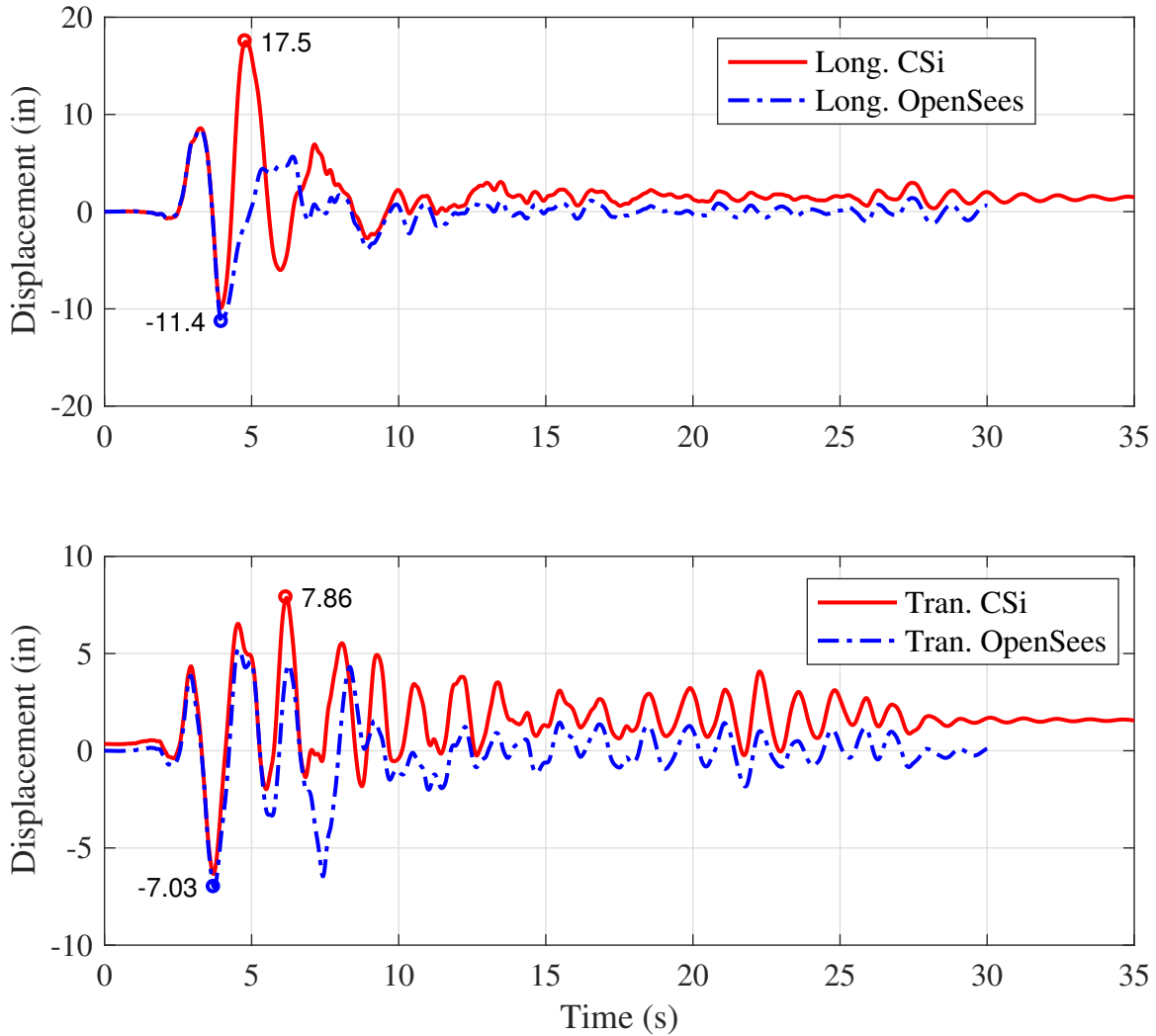

Figure 5.28: OSB3 (original abutment) center of mass displacement time histories for motion ROCKN1N1

The peak displacement demands are smaller for the ROCK and SAND ground motions than the CLAY ground motion. As a consequence, it appears the phasing is similar for both

the longitudinal and transverse responses between CSiBridge and OpenSees. The only case where a substantial difference occurs is again in the peak displacement demand in the longitudinal direction. The CSiBridge shows additional peaks with magnitudes approximately 50% greater than the peak reported in OpenSees. The CSiBridge model shows a gravity load transverse displacement for the original abutment case (more obvious in ROCK and SAND due to the displacement scale). The same gravity offset is present in the roller abutment results for OSB3. The isolator time histories confirm the displacement is occurring in the isolation layer.
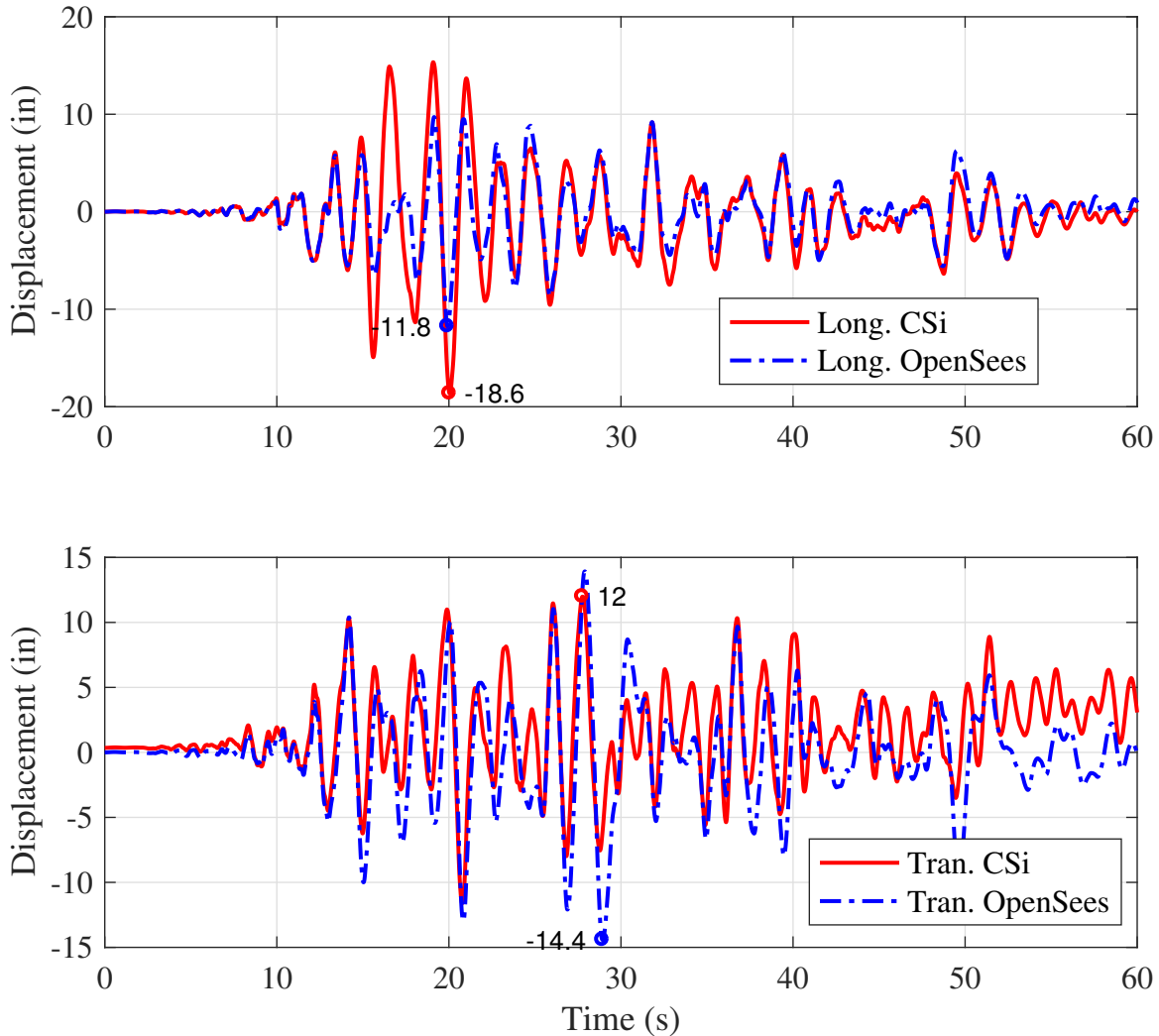

Figure 5.29: OSB3 (original abutment) center of mass displacement time histories for motion SANDN1N1

The column moment-curvature responses are not shown for OSB3, as the response is essentially linear for all the ground motions. However, the nonlinear response is concentrated in the isolation bearings. Some sample hysteresis plots are shown for the bent isolators for

the CLAYN1N1, ROCKN1N1, and SANDN1N1 ground motions in Figures 5.30, 5.31, and 5.32, respectively. The longitudinal and transverse directions are shown independently. In addition, there are isolators at the top of each bent column in OSB3, so the same naming scheme is adopted from OSB1, i.e., 1st column and 2nd column. The HE dissipated in the bent isolators is reported in the figures, and was obtained as the integral of the force-deformation history and therefore has units of kip-in.
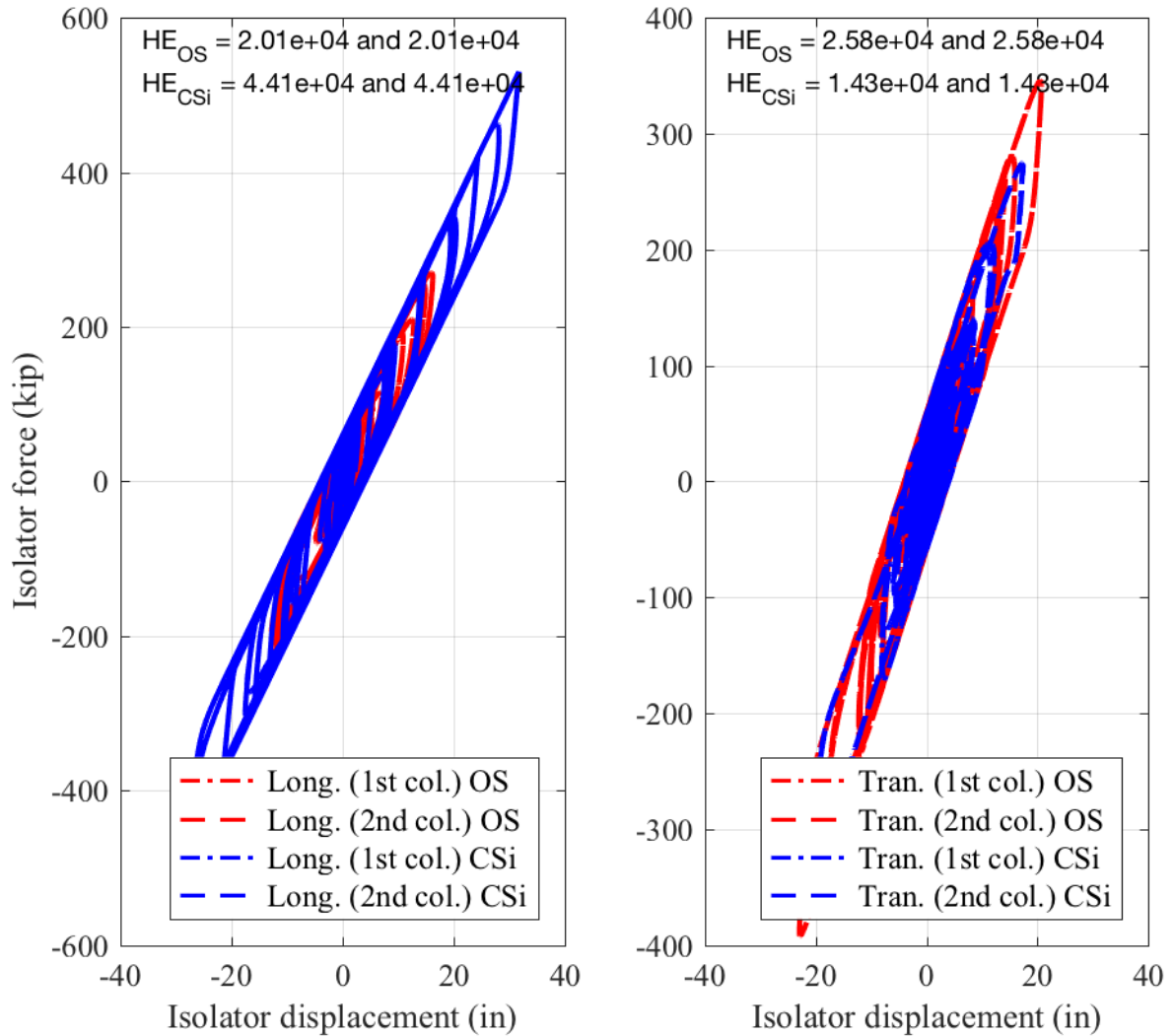

Figure 5.30: OSB3 (original abutment) bent isolator hysteresis for motion CLAYN1N1

As would be expected from the displacement time histories, a majority of the deformations are accommodated in the isolation layer. Nothing of particular notice is evident in the hysteresis plots, other than the OpenSees and CSiBridge results follow the same hysteresis

rules, which was established in Chapter 4. In addition, there is no substantial torsional deformation of the bridge (both bent isolators exhibit the same loops). The longitudinal CLAY deformations are higher in CSiBridge, and therefore the energy dissipation is substantially higher. The converse is true in the transverse direction.
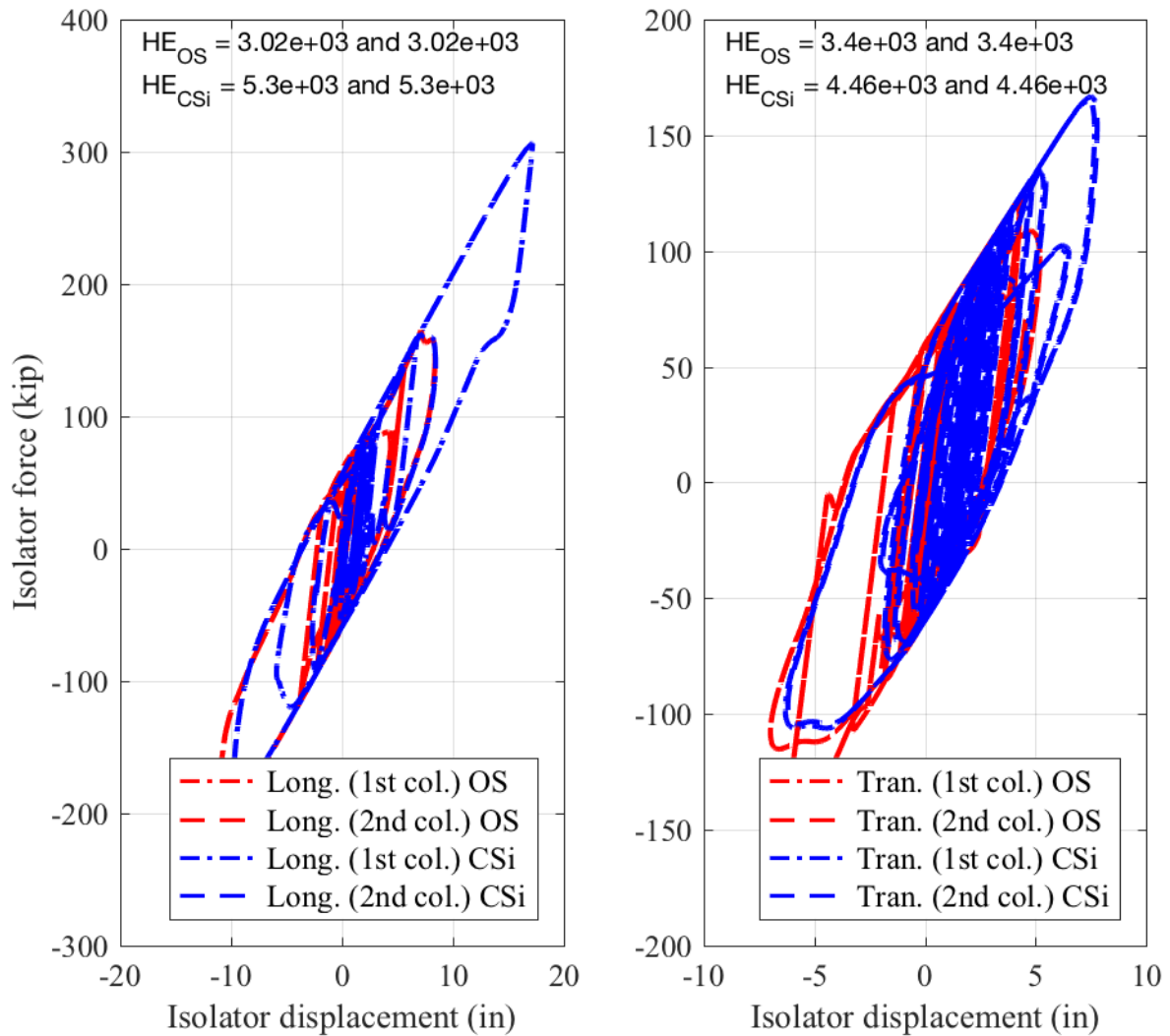
Figure 5.31: OSB3 (original abutment) bent isolator hysteresis for motion ROCKN1N1

The first large negative excursion in the ROCK longitudinal response shows close agreement between OpenSees and CSiBridge; however, the subsequent positive excursion in the CSiBridge prediction only yields a larger energy dissipation. The differences in the transverse direction responses are smaller, with the CSiBridge solution oscillating around a permanent deformation beyond the maximum displacement. The HE quantities are similar in the trans-

verse component of response to the ROCK motion.
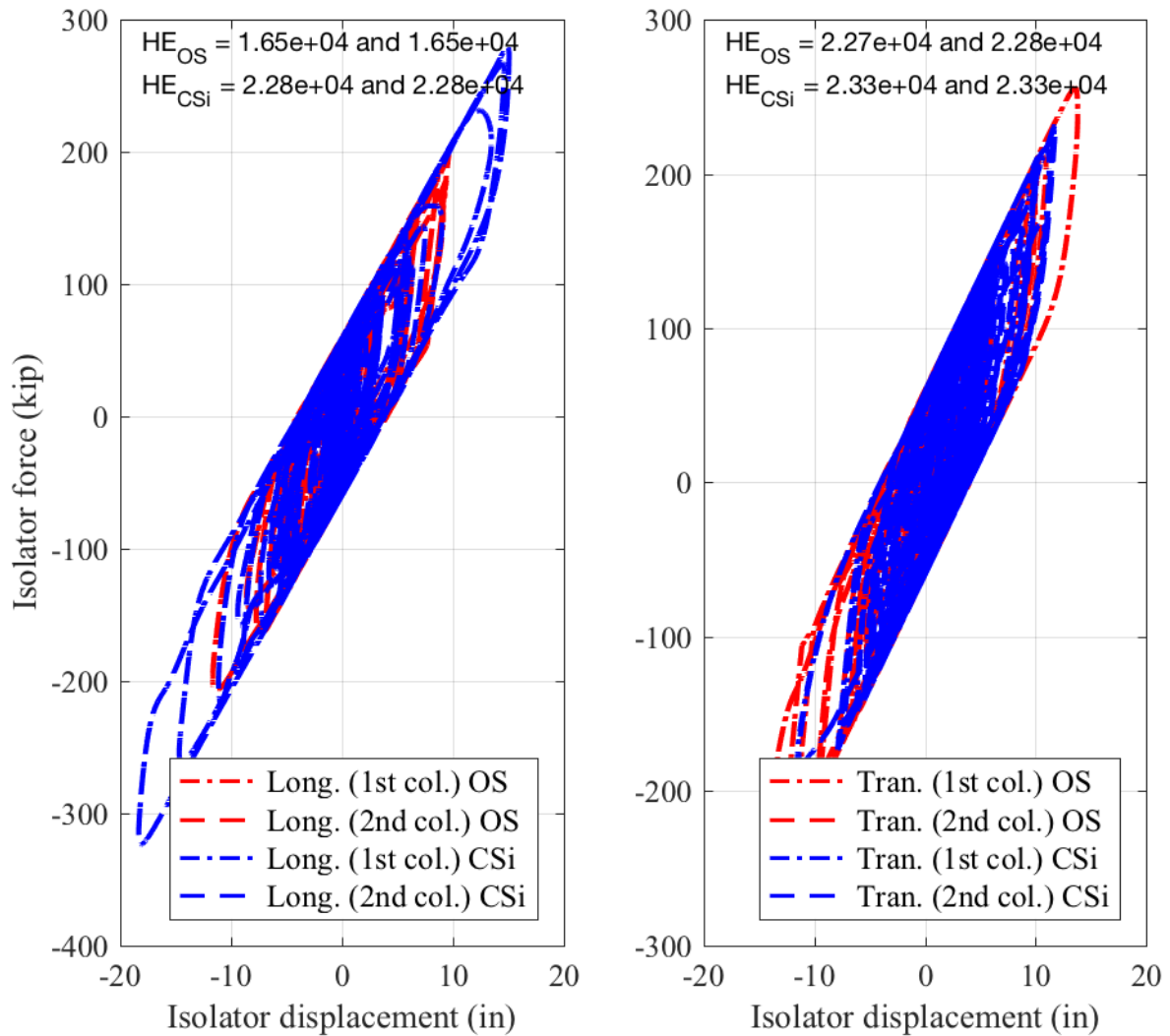
Figure 5.32: OSB3 (original abutment) bent isolator hysteresis for motion SANDN1N1

The three successive cycles at large displacement amplitude in the longitudinal response of the CSiBridge model to the SAND ground motion leads to a larger HE. The energy dissipated is coincidentally similar in the transverse direction for SAND, i.e., not due to close matching of the displacement time histories.

OSB4

The displacement time history responses of OSB4 at the center of mass of the bent for the CLAYN1N1, ROCKN1N1, and SANDN1N1 ground motions are shown in Figures 5.33,

5.34, and 5.35, respectively. The displacement time histories are shown independently for the bridge longitudinal (labeled Long.) and transverse (labeled Tran.) directions. As with OSB3, there is an initial gravity offset in the transverse direction that occurs in the isolation layer for OSB4 in the CSiBridge model.
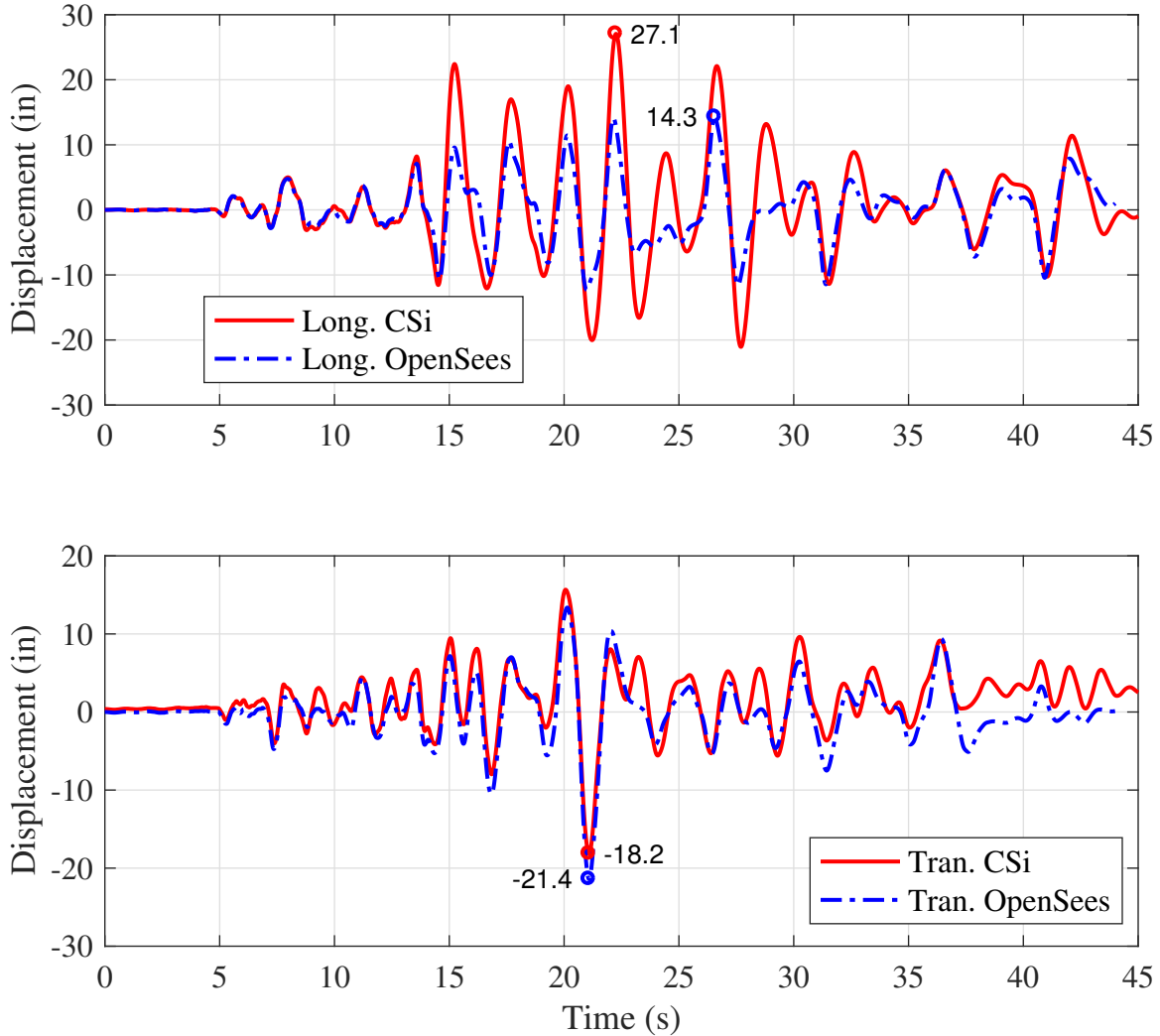
Figure 5.33: OSB4 (original abutment) center of mass displacement time histories for motion CLAYN1N1

The trends in the responses for the OSB4 bridge are very similar to those previously presented for OSB3 (since the isolation system and center of mass were the same between the two bridges). The transverse abutment properties were also identical between the two bridges (the longitudinal stiffness at the abutment differs somewhat). The period of large displacement amplitudes is slightly smaller in OSB4 compared to OSB3. The difference in the peak longitudinal displacement demands for CLAY, ROCK, and SAND motions were 90%, 42%, and 65% (CSiBridge larger than OpenSees).

143

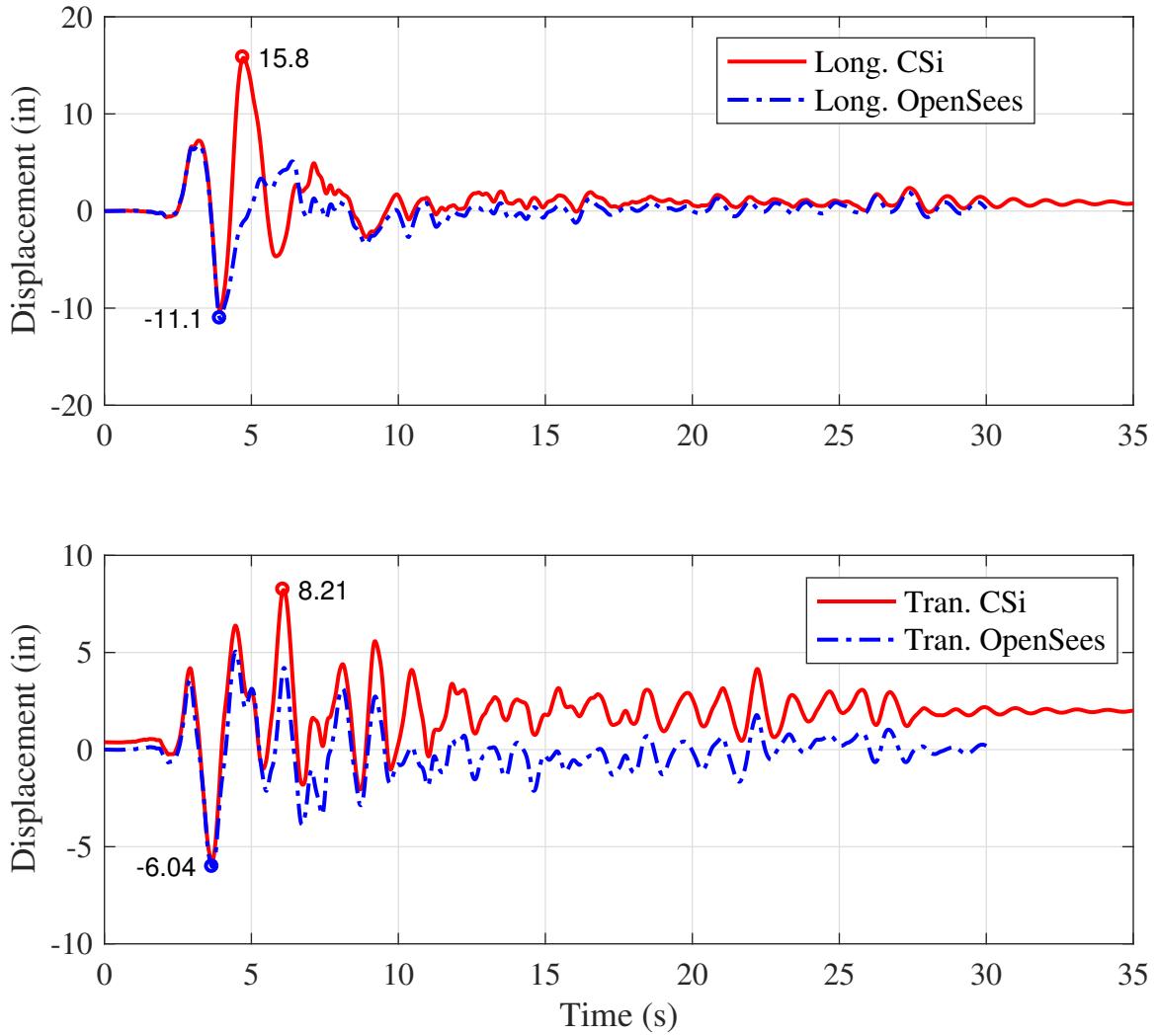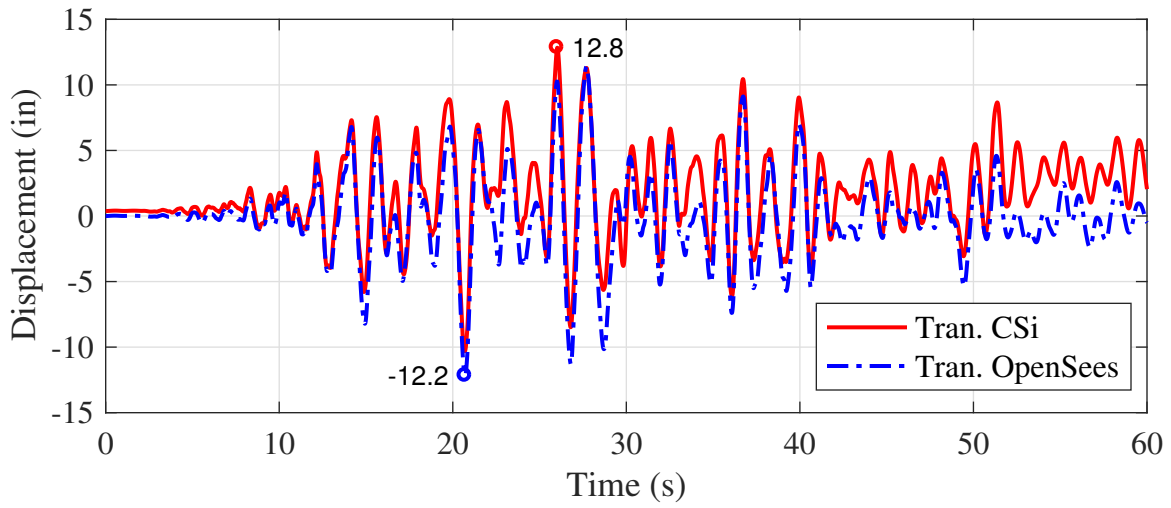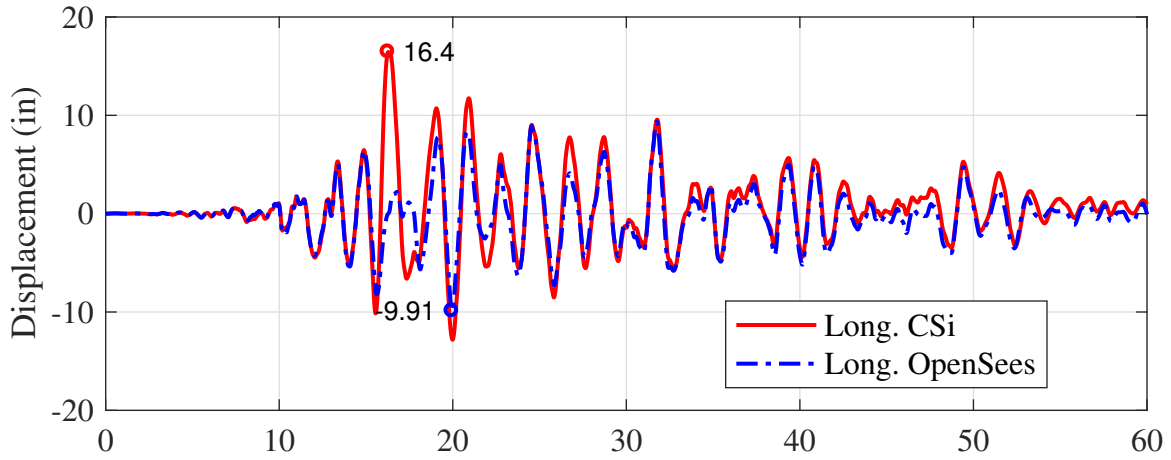Figure 5.34: OSB4 (original abutment) center of mass displacement time histories for motion ROCKN1N1

Figure 5.35: OSB4 (original abutment) center of mass displacement time histories for motion SANDN1N1

The column moment-curvature responses are not shown for OSB4, as the response is essentially linear for all the ground motions. However, the nonlinear response is concentrated in the isolation bearings. Hysteresis plots are shown for the bent isolators for the CLAYN1N1, ROCKN1N1, and SANDN1N1 ground motions in Figures 5.36, 5.37, and 5.38, respectively. The longitudinal and transverse directions are shown independently. The HE dissipated in the bent isolators is reported in the figures, and was obtained as the integral of the force-deformation history, and therefore has units of kip-in. While there is only a single column in the OSB4 bent, there are two isolation bearings on the hammerhead pier, the response of which are labeled 1st bearing and 2nd bearing, consistent with the notation for ordering of columns in OSB1 and OSB3.
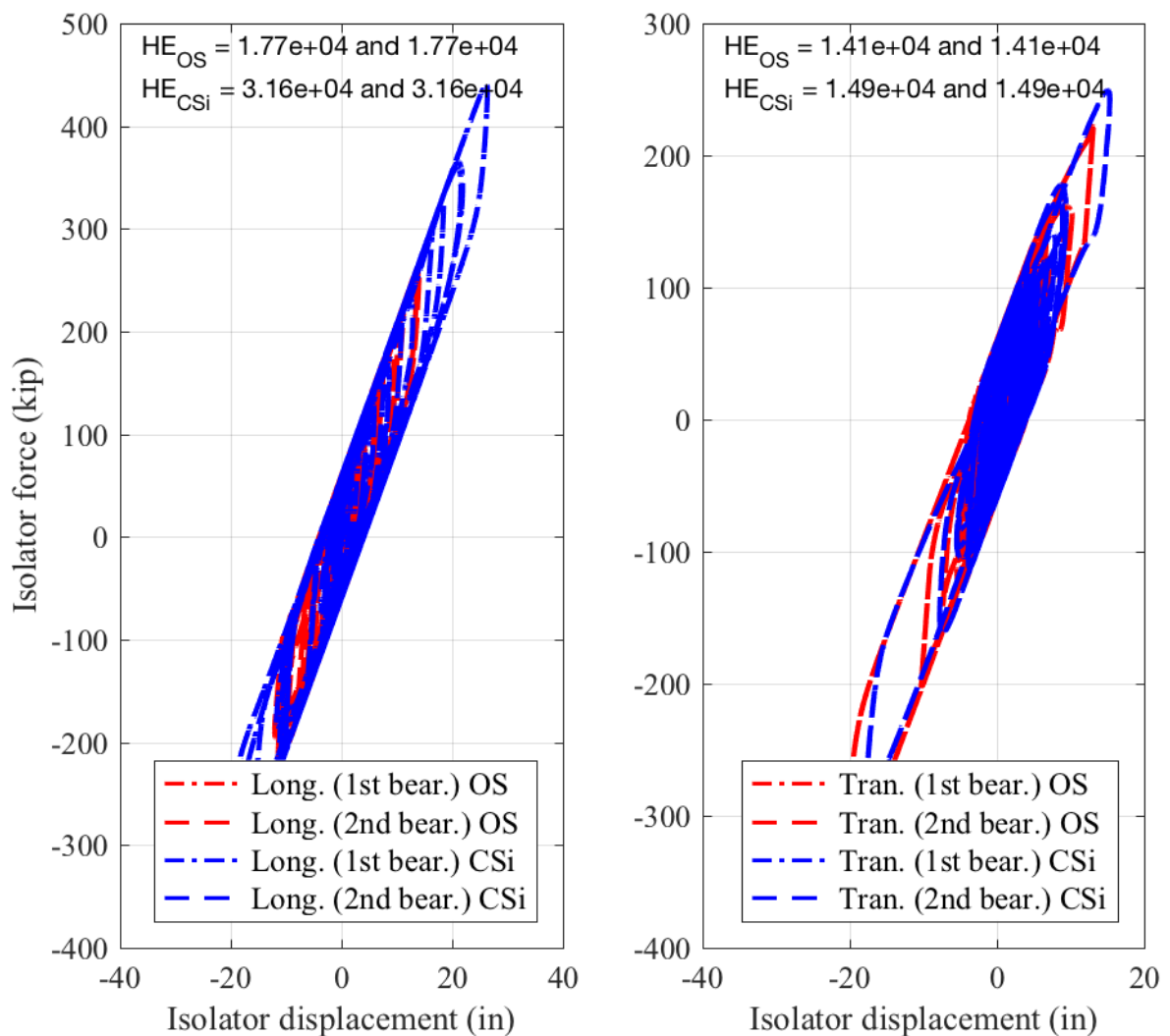
Figure 5.36: OSB4 (original abutment) bent isolator hysteresis for motion CLAYN1N1

Similar observations can be drawn from the hysteresis plots for OSB4 as for OSB3. The best agreement in energy dissipation occurred with the transverse response under the CLAY and SAND ground motions. However, this was not due to exact matching of the displacement time histories, but rather with the oscillation around the permanent offset developed after the peak displacement excursion in the CSiBridge model.

Figure 5.37: OSB4 (original abutment) bent isolator hysteresis for motion ROCKN1N1

5.3.2 Roller Abutment Model

In the CSiBridge analysis, a damping ratio of 0.05 was used in the analysis, as well as the same exact Rayleigh damping model used for the original abutment case. Again, the same
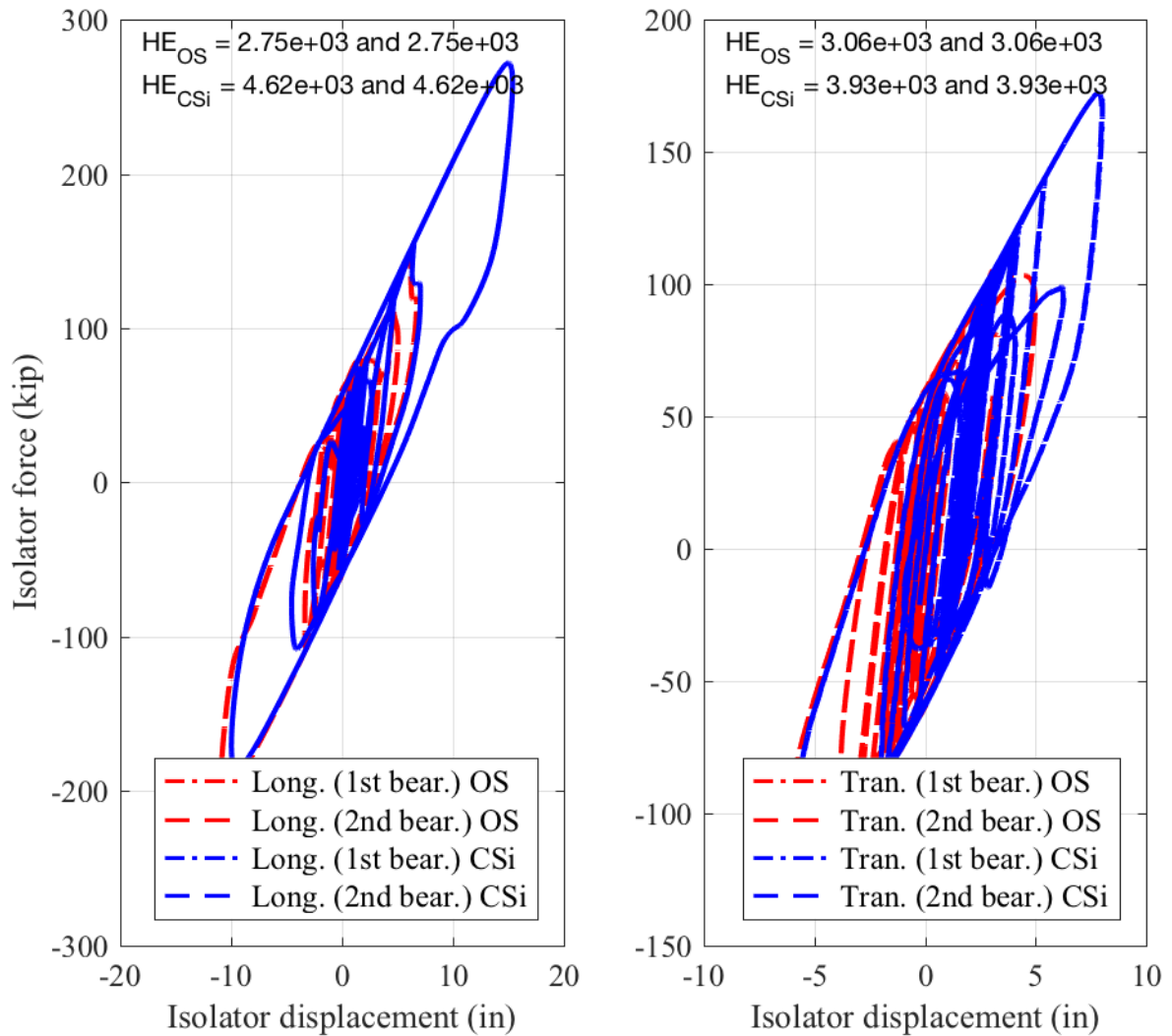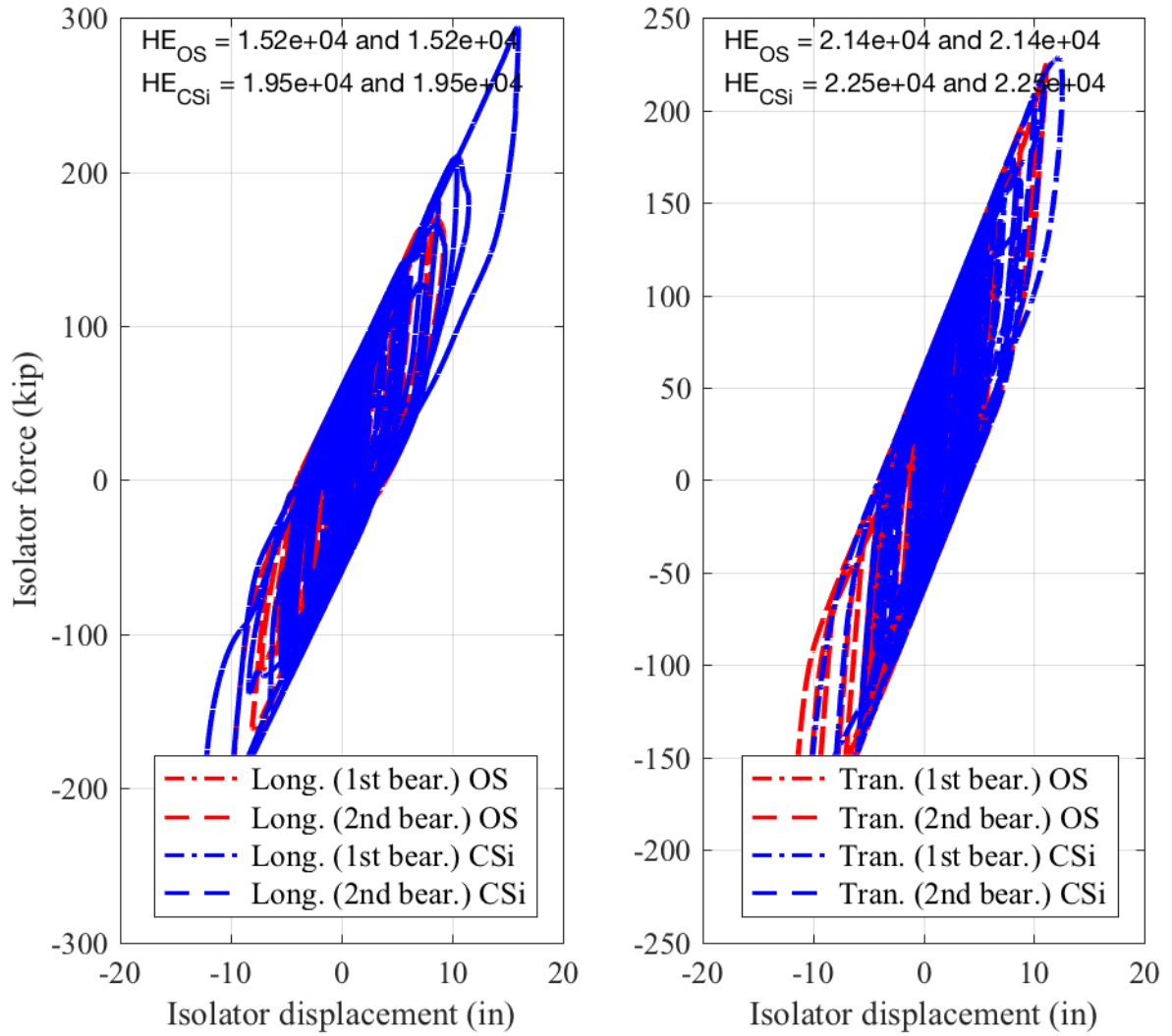
Figure 5.38: OSB4 (original abutment) bent isolator hysteresis for motion SANDN1N1

values were used directly in the OpenSees analysis. The use of the roller abutment models are more effective in identifying differences in response due to the nonlinearity at the bents (OSB1 and OSB2) and bent isolators (OSB3 and OSB4). Therefore, as may be expected based on the component-level calibrations performed, the responses here show a higher level of agreement between CSiBridge and OpenSees than those in the original abutment model section.

OSB1

The displacement time history responses of OSB1 at the center of mass of the bent for the CLAYN1N1, ROCKN1N1, and SANDN1N1 ground motions are shown in Figures 5.39, 5.40, and 5.41, respectively. The displacement time histories are shown independently for the bridge longitudinal (labeled Long.) and transverse (labeled Tran.) directions.

The CLAY longitudinal and transverse displacements show excellent agreement throughout the time history of response, particularly the phasing. The peak displacement magnitudes differ by 17% (CSiBridge values larger relative to OpenSees) and 21% for the longitudinal and transverse directions, respectively. The differences observed in the larger inelastic peak displacement demands are due to the differences observed in the concrete constitutive models, particularly evident in the moment-curvature plots presented below. The changes in the inelastic peaks also end in a larger residual displacement in both the longitudinal and transverse directions for CSiBridge.

The ROCK ground motion responses show similar agreement; however, the peak longitudinal displacement demand occurs early in the time history (approximately 4 sec, which roughly coincides with the transverse peak as well). Therefore, both the longitudinal and transverse histories exhibit an offset proportional to the differences in the displacement peaks at that time instant. The peak displacement magnitudes differ by 14% (CSiBridge values larger relative to OpenSees) and 13% for the longitudinal and transverse directions, respectively. The residual displacement in the CSiBridge responses are larger than OpenSees.

The slight discrepancy in the peak displacement excursions for the SAND motion caused the peak longitudinal displacement in OpenSees to occur at a different time instant. However, the overall differences were small, 16% (CSiBridge values larger relative to OpenSees) and 5% for the longitudinal and transverse directions, respectively. For all three ground motions used to excited OSB1, the CSiBridge maximum and residual displacements were larger in both components. However, this result is not consistent for all ground motions and bridges; therefore, it should not be extrapolated that CSiBridge results are always conservative.

The moment-curvature responses at the top of the two bent columns for the CLAYN1N1, ROCKN1N1, and SANDN1N1 ground motions are shown in Figures 5.42, 5.43, and 5.44, respectively. As with the pushover analysis results presented previously, the two columns are labeled "1st col." and "2nd col.". The moment-curvature responses are shown independently for the moment and curvature in the longitudinal (labeled Long.) and transverse (labeled Tran.) directions. The moment in the longitudinal direction implies bending is about the bridge transverse axis. The sign of the moment and curvature were calibrated to be the same as the displacement, i.e., the peak positive displacement has a corresponding peak positive
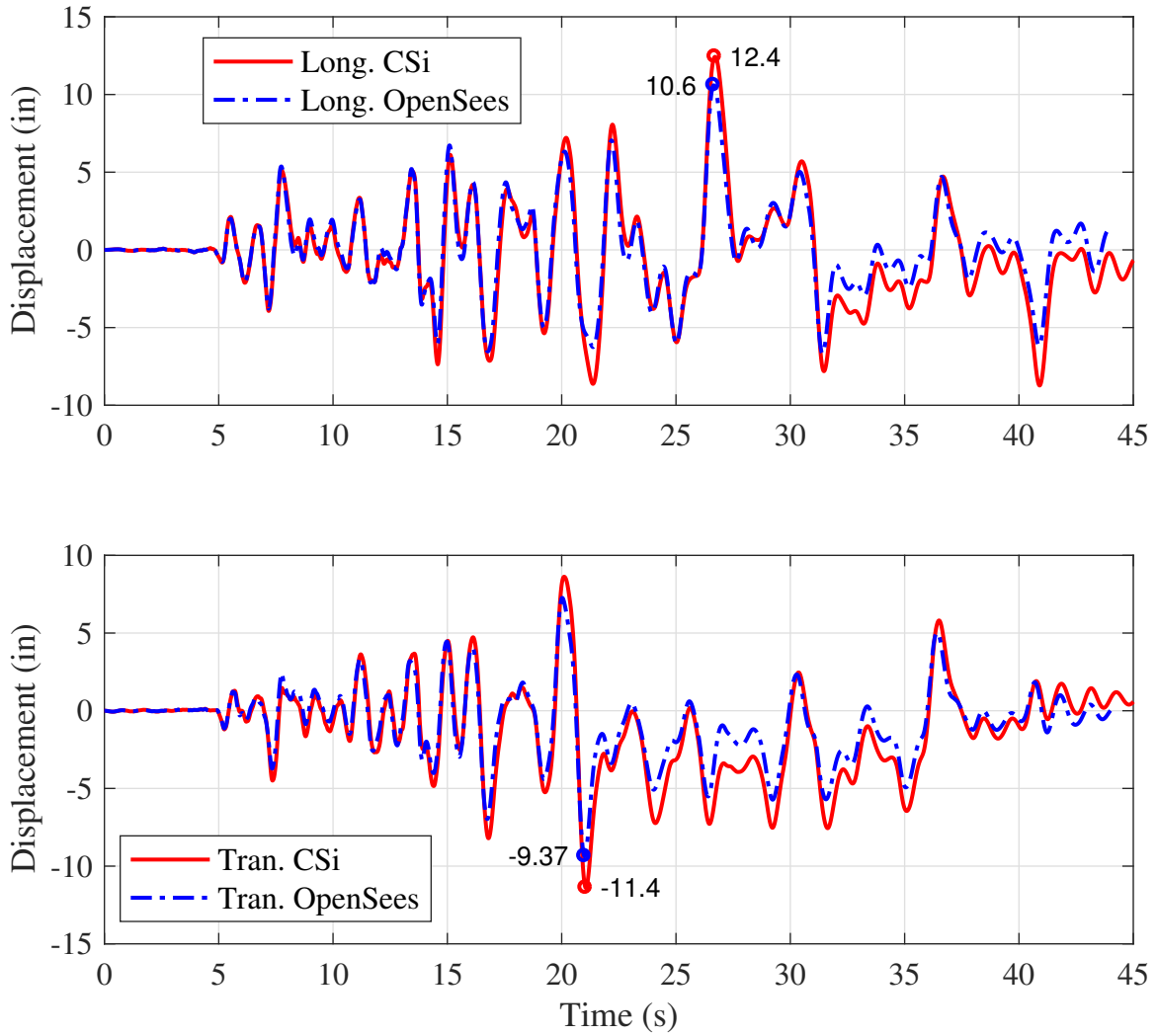
Figure 5.39: OSB1 (roller abutment) center of mass displacement time histories for motion CLAYN1N1
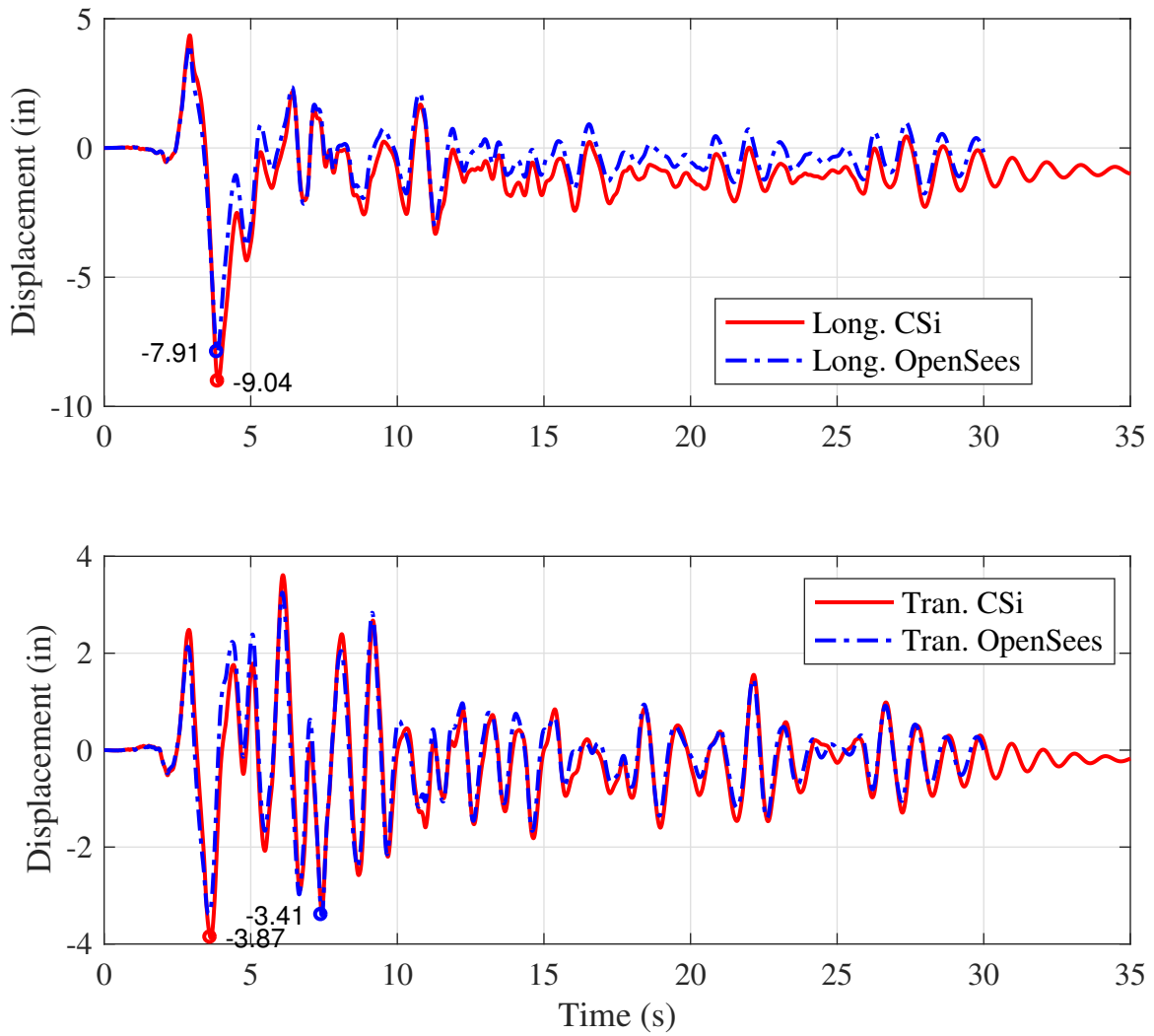
Figure 5.40: OSB1 (roller abutment) center of mass displacement time histories for motion ROCKN1N1
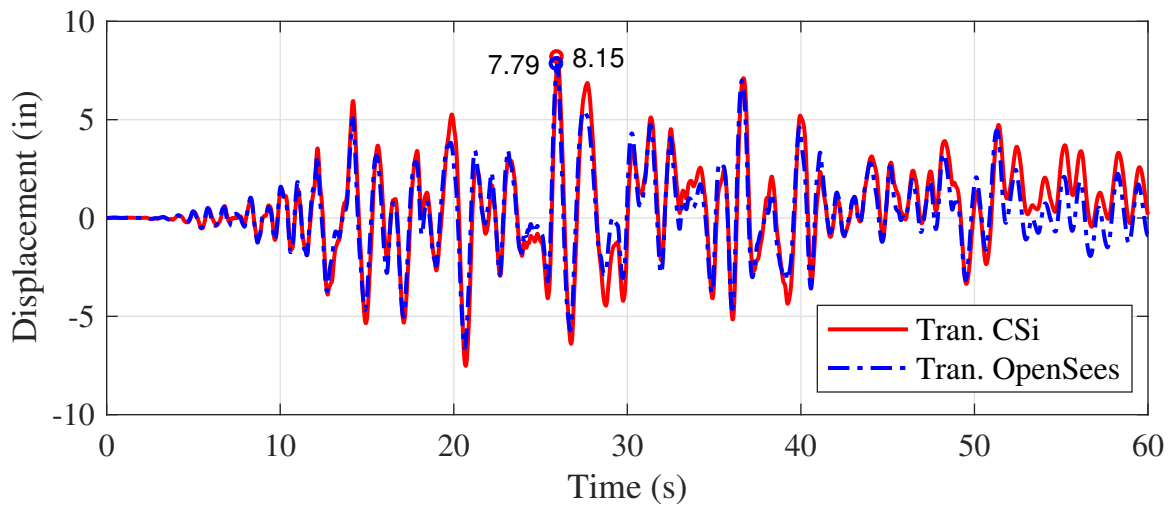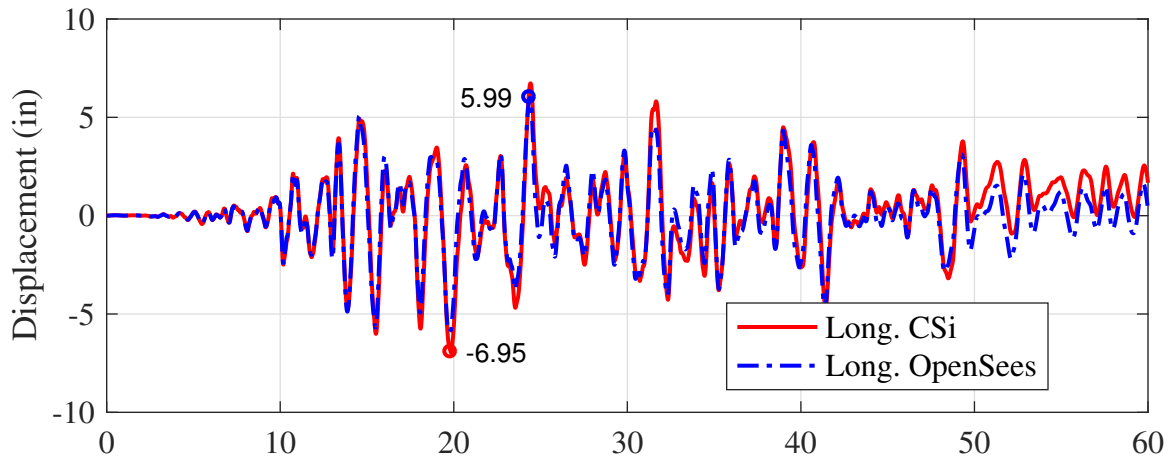
Figure 5.41: OSB1 (roller abutment) center of mass displacement time histories for motion SANDN1N1

curvature, etc. In addition, for each figure, the HE is listed. The HE was obtained as the integral of the moment-curvature history and therefore has units of kip.
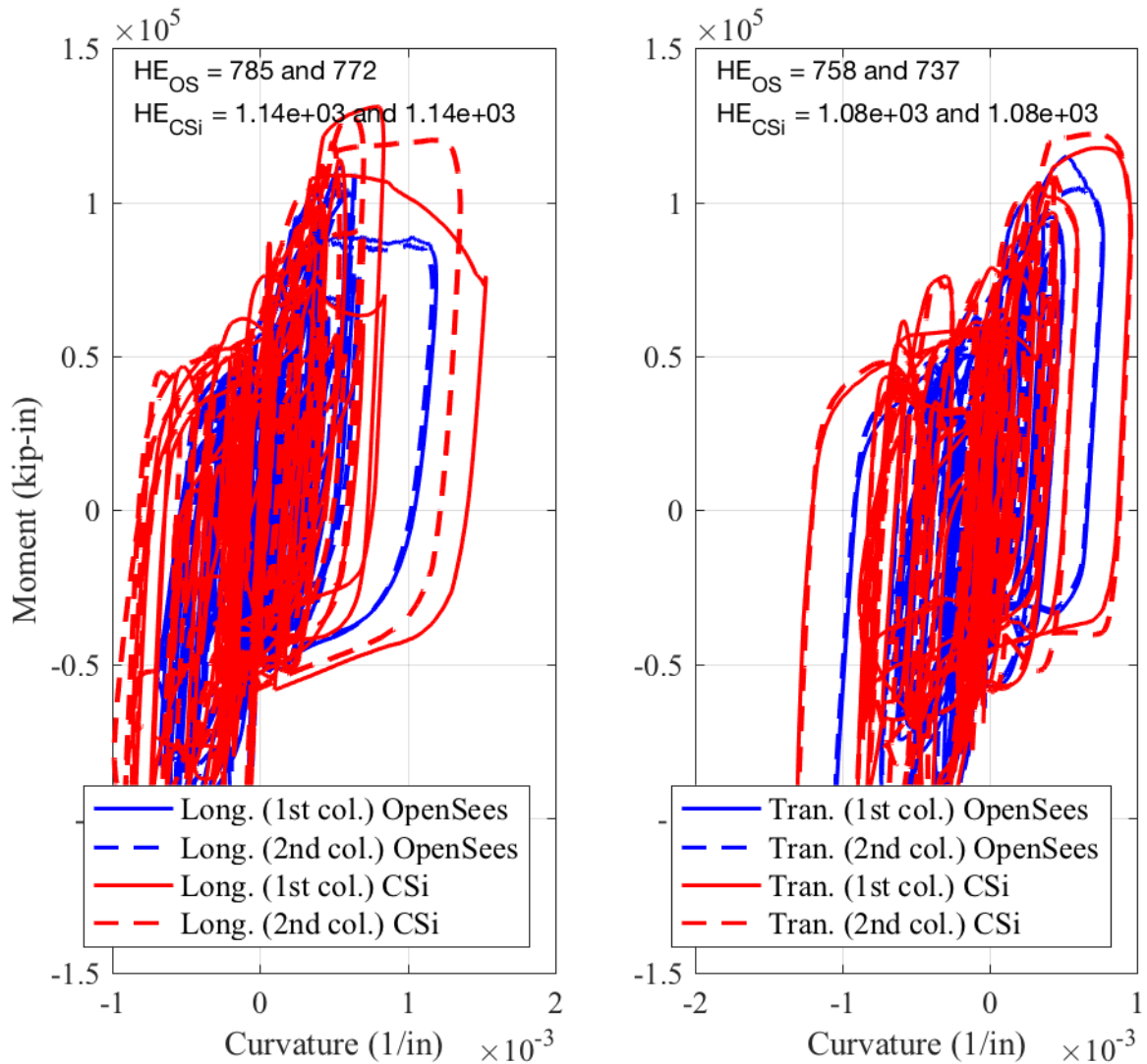
Figure 5.42: OSB1 (roller abutment) column top moment-curvature responses for motion CLAYN1N1

The CLAY hysteretic plots demonstrate that as the plastic curvature increases, there is a clear difference in the OpenSees response. The OpenSees response softens according to the concrete constitutive and sectional results presented in the previous chapter. However, the CSiBridge results show continued ductility and approximately 40% increase in energy dissipation.

The displacement demands are smaller in the ROCK ground motion compared to the
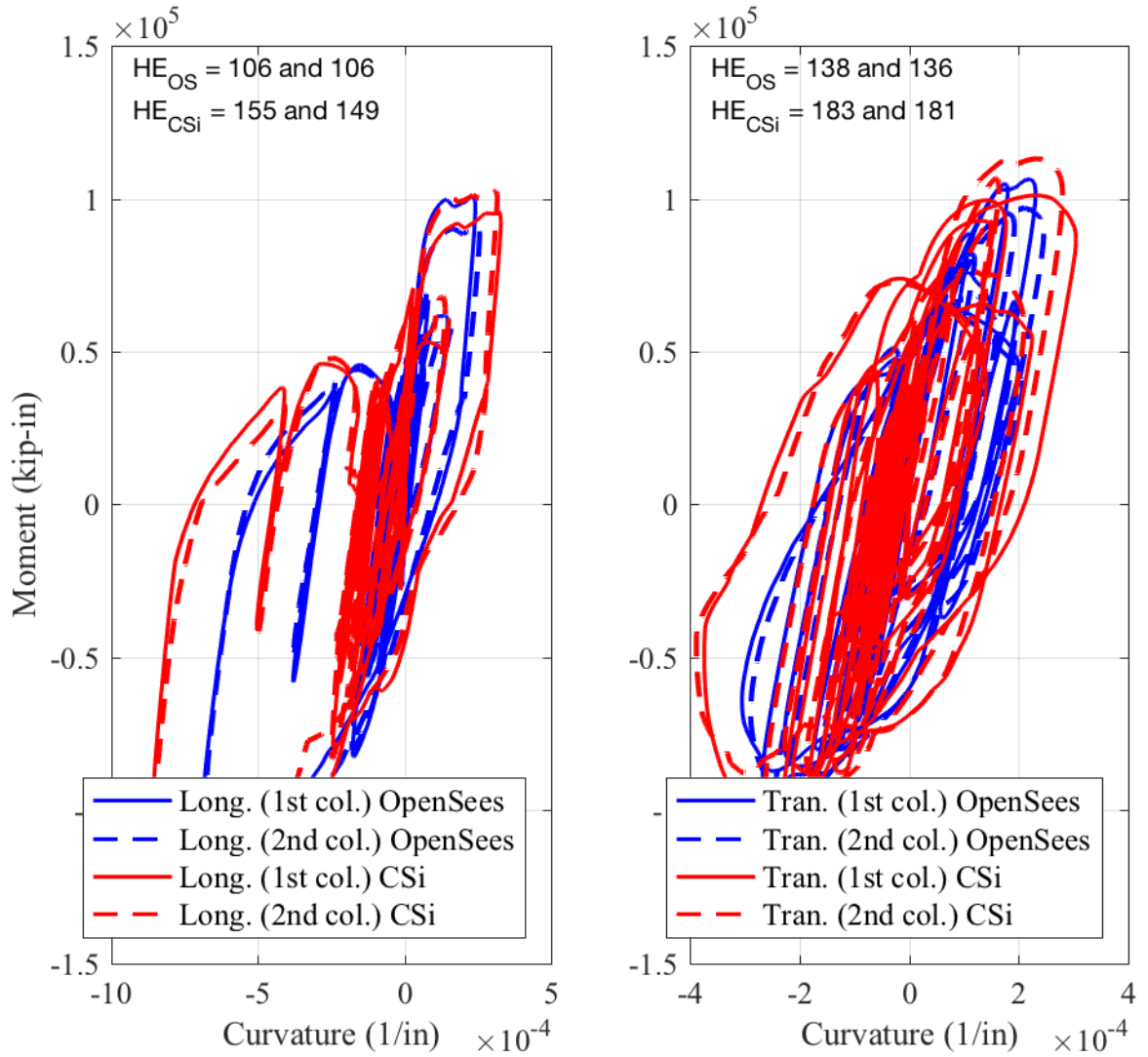
Figure 5.43: OSB1 (roller abutment) column top moment-curvature responses for motion ROCKN1N1

CLAY motion. The curvature demands are similarly smaller, particularly in the transverse direction. The differences in the energy dissipated are 40-50% although the trends show close agreement. The SAND ground motion induces more inelastic cycles than the ROCK motion, and there is a resulting increase in the HE, although the peak displacement demands are similar between the two motions.
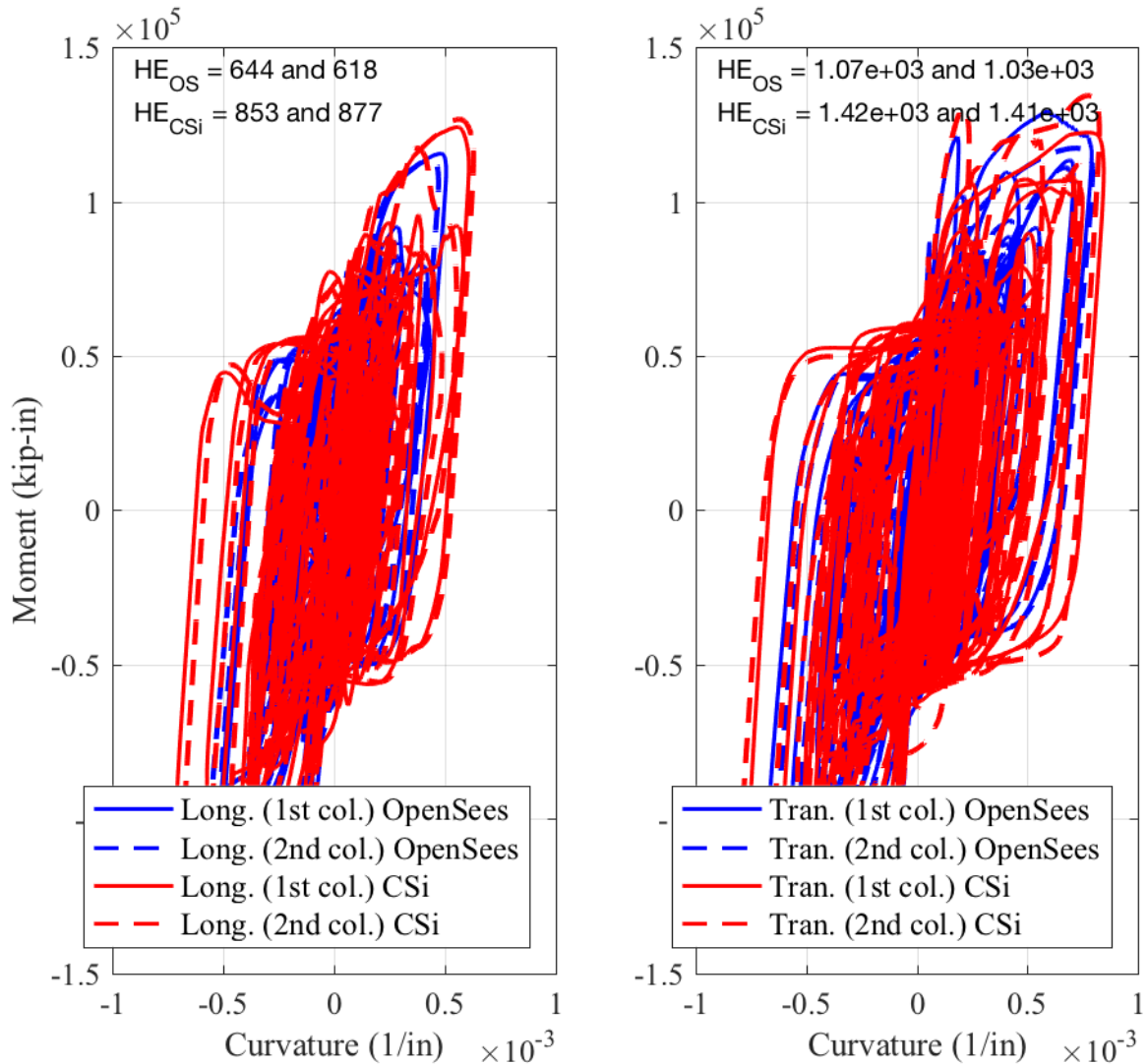

Figure 5.44: OSB1 (roller abutment) column top moment-curvature responses for motion SANDN1N1

OSB2

The displacement time history responses of OSB2 at the center of mass of the bent for the CLAYN1N1, ROCKN1N1, and SANDN1N1 ground motions are shown in Figures 5.45, 5.46, and 5.47, respectively. The displacement time histories are shown independently for the bridge longitudinal (labeled Long.) and transverse (labeled Tran.) directions. As mentioned previously, the model responses for OSB2 should not be overly scrutinized due to the inadvertent modeling choice for the hinges. This manifested itself clearly in the curvature demands shown for the original abutment case, but was particularly evident in the NTHA for all ground motions and the roller abutment case. All records failed to converge and reported curvature demands several orders of magnitude larger than possible given the displacements. The ROCKN1N1 is the only ground motion (not coincidentally the ground motion with the smallest displacement maxima for the original abutment case) that converged for the full time history.

The CLAY ground motion terminated at approximately 12 sec for the CSiBridge analysis. Prior to the convergence issues, the phasing and displacement peaks were very similar between the two software. The discrepancy grew rapidly for post-yielding (beyond 1 to 1.5 in) displacement peaks. The ROCK ground motion converged for the full time history; however, the responses diverged rapidly after the peak displacement demands that occurred at approximately 4 sec and 7 sec in the longitudinal and transverse directions, respectively. Similar conclusions can be drawn from the SAND responses; however, the CSiBridge analysis terminated at approximately 19 sec.

The moment-curvature responses at the top of the column for the CLAYN1N1, ROCKN1N1, and SANDN1N1 ground motions are shown in Figures 5.48, 5.49, and 5.50, respectively. As with the original abutment responses, the curvature demands from the bottom hinge could not reliably be obtained from CSiBridge. In fact, the time steps preceding the end of the analysis correspond to the onset of non-physical curvatures (values greater than 1). The moment-curvature responses are shown independently for the moment and curvature in the longitudinal (labeled Long.) and transverse (labeled Tran.) directions. The moment in the longitudinal direction implies bending is about the bridge transverse axis. The sign of the moment and curvature were calibrated to be the same as the displacement, i.e., the peak positive displacement has a corresponding peak positive curvature, etc. In addition, for each figure, the HE is listed.

The CLAY and SAND HE values are not comparable due to the different early termination of the CSiBridge analyses. For the initial cycles, the agreement is good in both longitudinal and transverse directions. However, as with the original abutment case, the curvature demands in CSiBridge are larger than OpenSees at a given displacement demand. This is particularly apparent looking at the hysteresis in the longitudinal direction for SAND. The ROCK HE are more comparable due to the consistent time history of responses; however, the CSiBridge models show higher HE although the peak displacements are nearly identical between the two software.

Figure 5.45: OSB2 (roller abutment) center of mass displacement time histories for motion CLAYN1N1

Figure 5.46: OSB2 (roller abutment) center of mass displacement time histories for motion ROCKN1N1
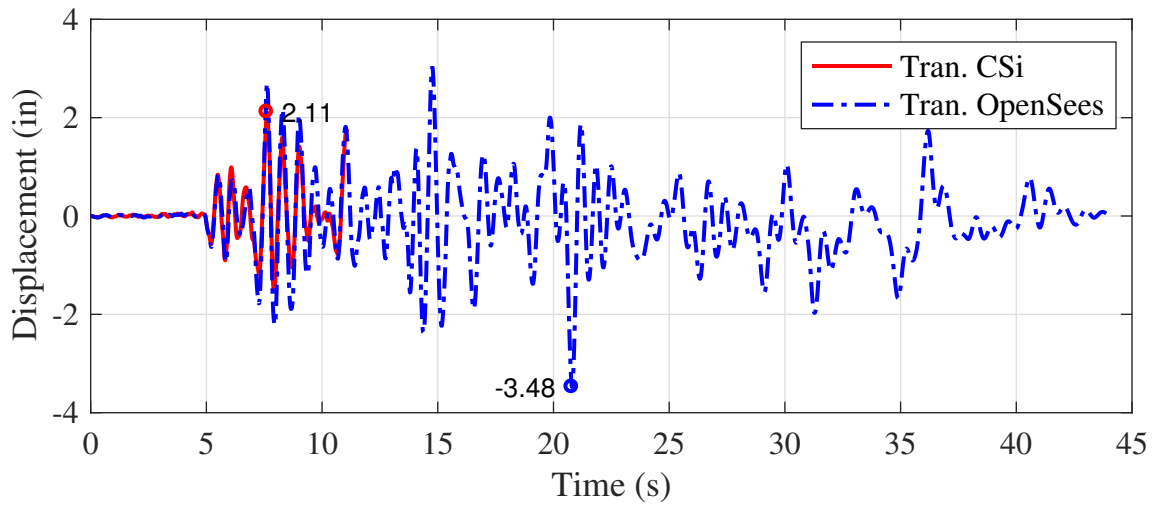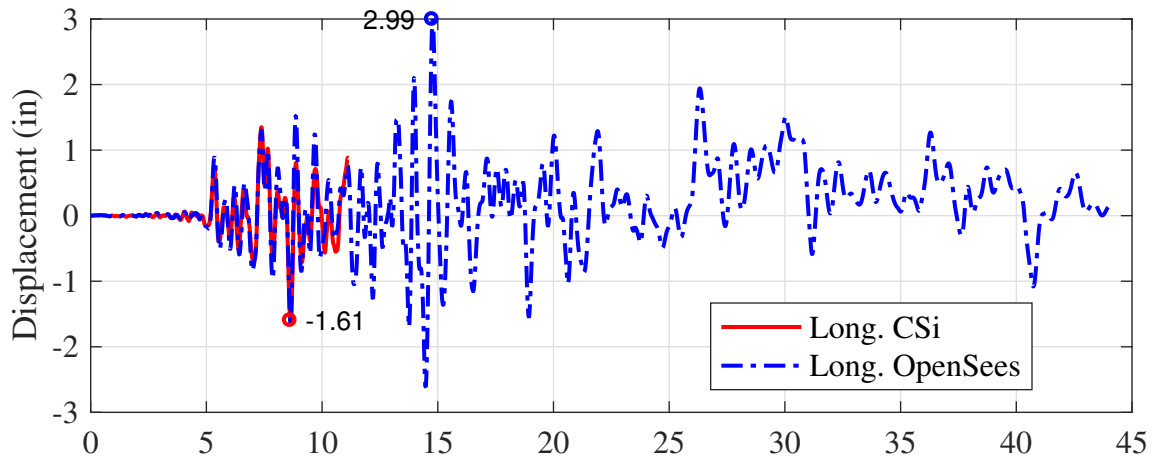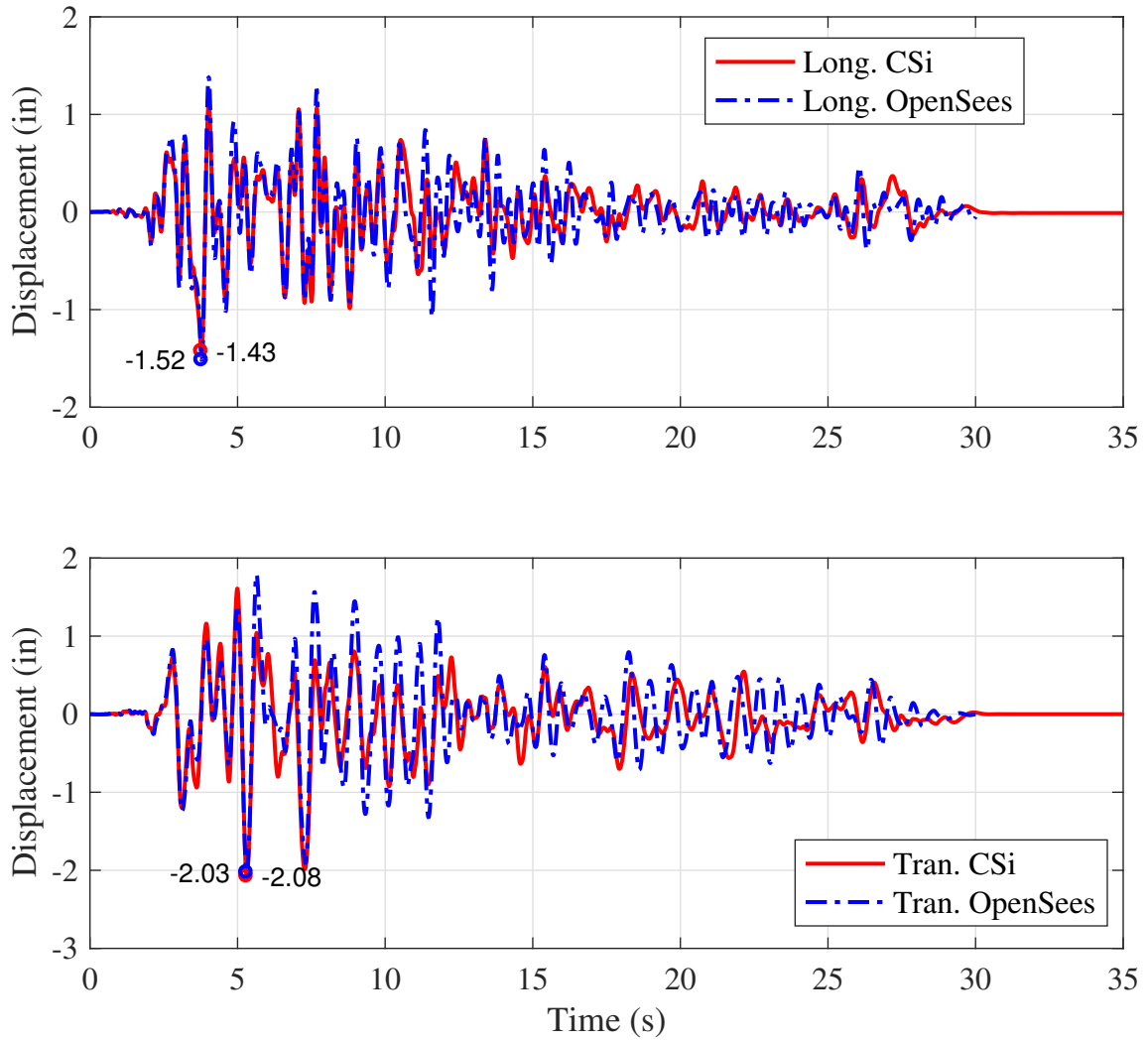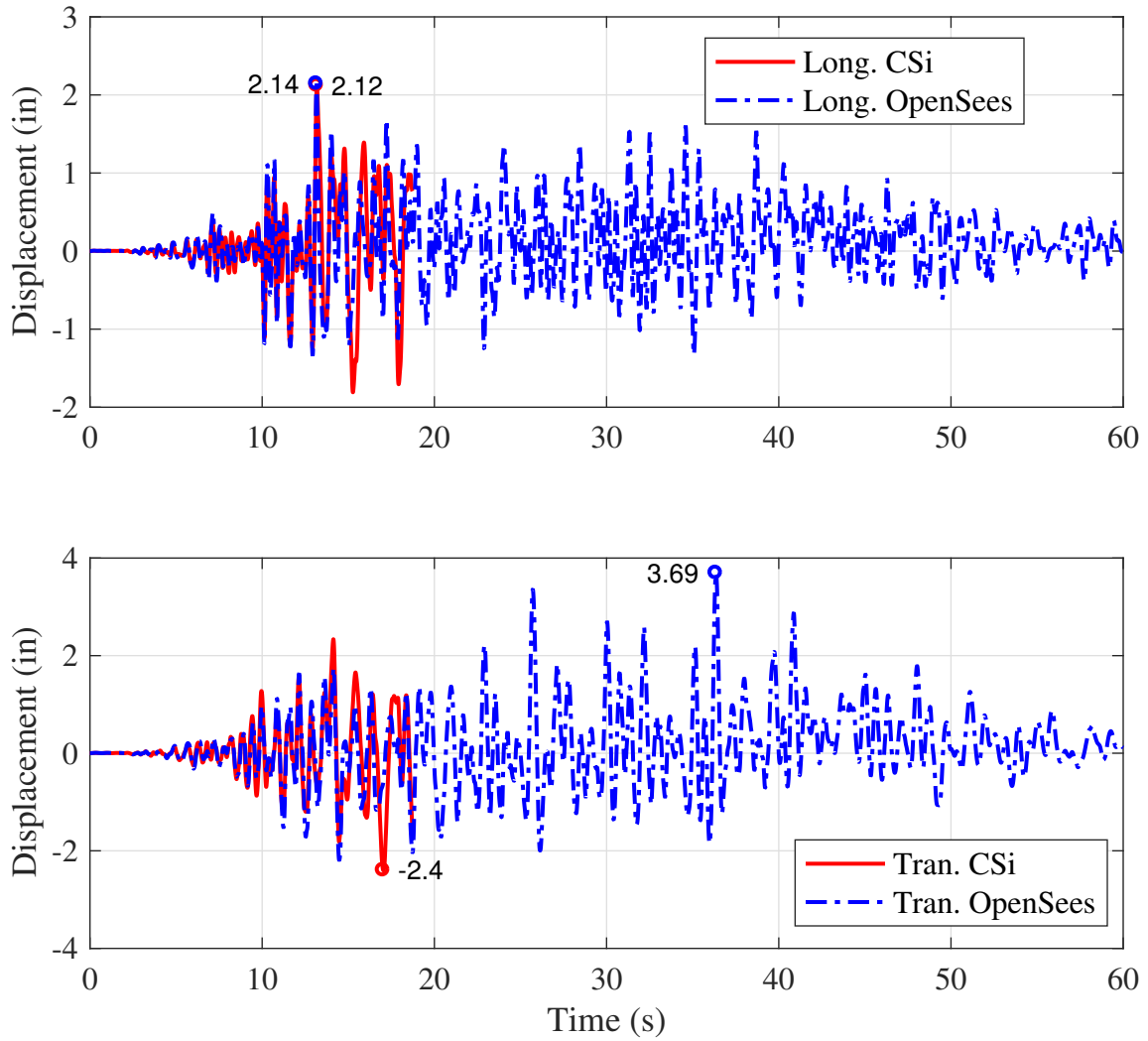
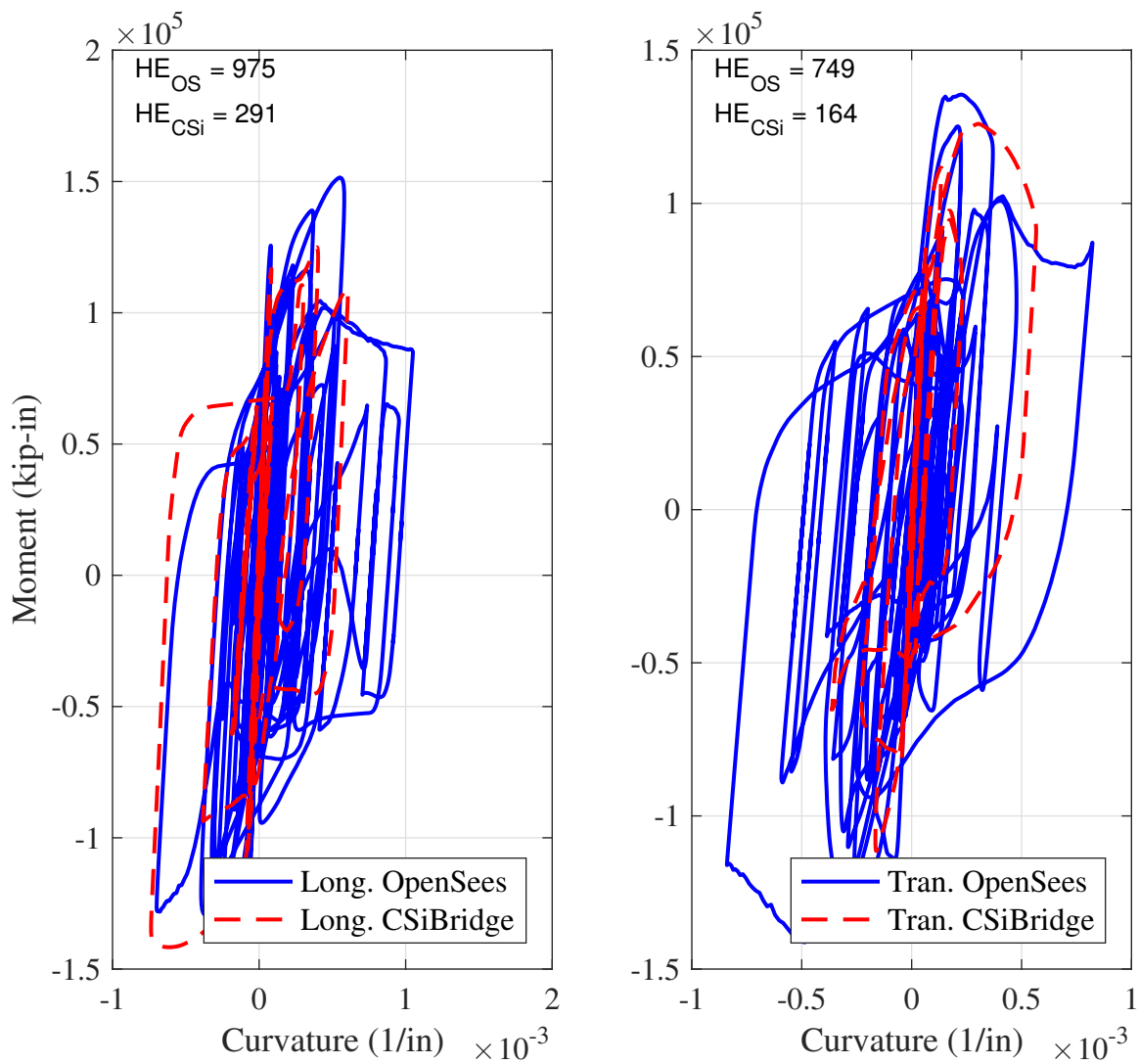Figure 5.47: OSB2 (roller abutment) center of mass displacement time histories for motion SANDN1N1

Figure 5.48: OSB2 (roller abutment) column base moment-curvature responses for motion CLAYN1N1
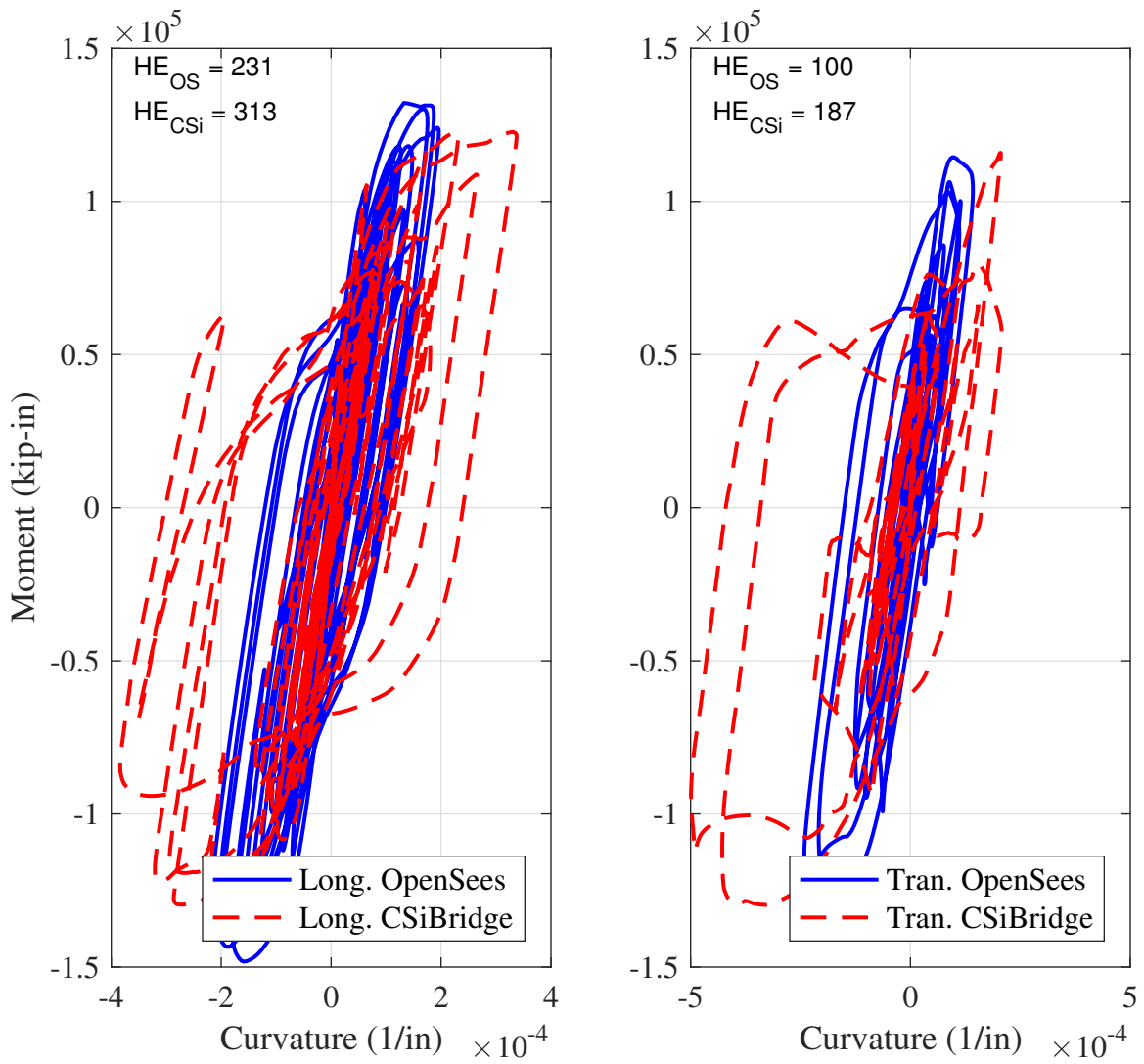
Figure 5.49: OSB2 (roller abutment) column base moment-curvature responses for motion ROCKN1N1
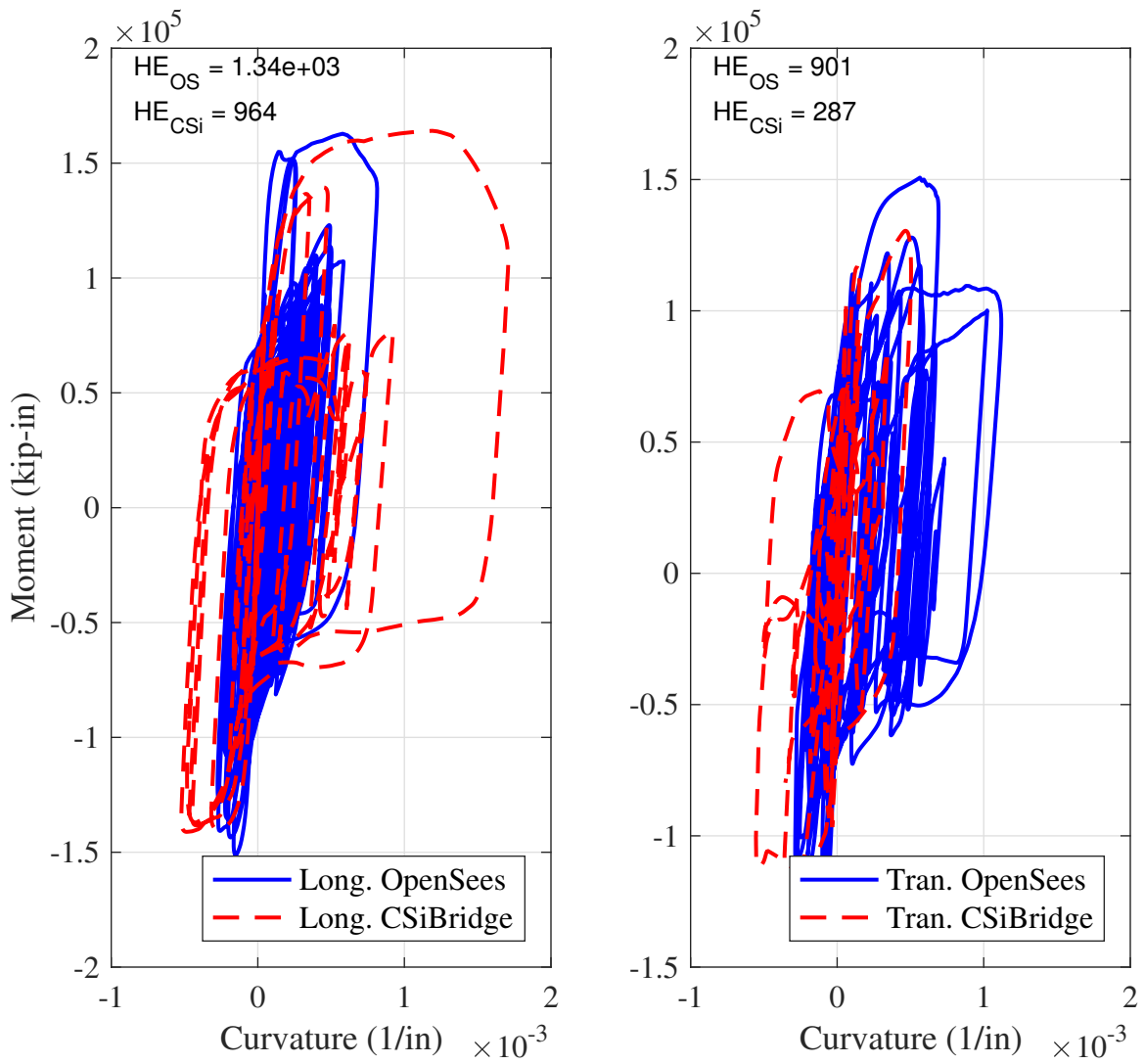
Figure 5.50: OSB2 (roller abutment) column base moment-curvature responses for motion SANDN1N1

OSB3

The displacement time history responses of OSB3 at the center of mass of the bent for the CLAYN1N1, ROCKN1N1, and SANDN1N1 ground motions are shown in Figures 5.51, 5.52, and 5.53, respectively. The displacement time histories are shown independently for the bridge longitudinal (labeled Long.) and transverse (labeled Tran.) directions. The same CSiBridge gravity load offset in the transverse direction was observed as the original abutment case.
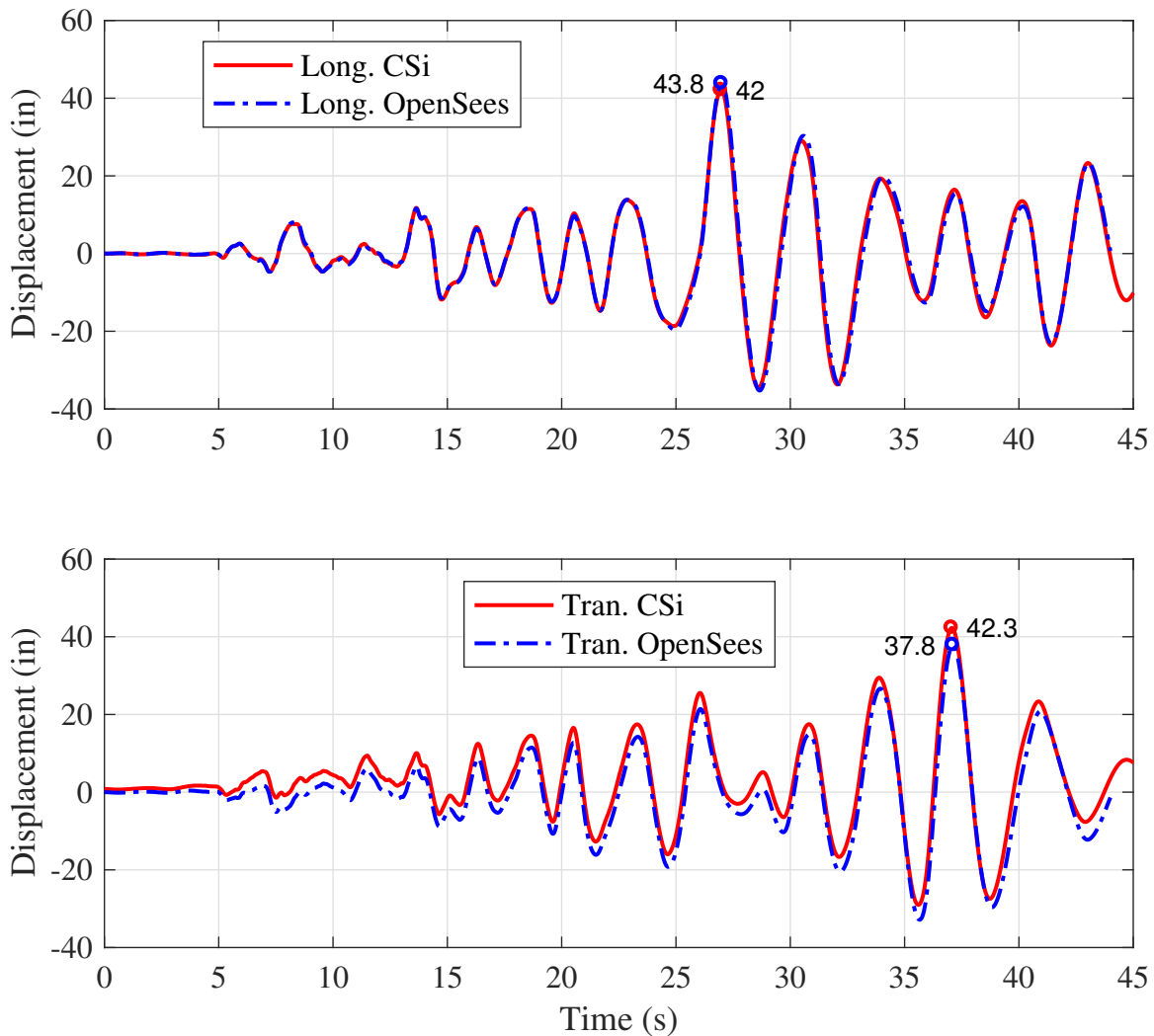
Figure 5.51: OSB3 (roller abutment) center of mass displacement time histories for motion CLAYN1N1

The displacement responses for the CLAY ground motion track directly between the two software, as would be expected. It is not exactly clear why the peak displacement magnitude is not the same, given the bearing responses were previously calibrated. The OpenSees predicted peak is 1.8 in larger than CSiBridge in the longitudinal direction. The

transverse responses are also similar; however, are offset by the initial gravity displacement in CSiBridge. By the time instant at peak response, the peak displacement demand in CSiBridge was 4.5 in.
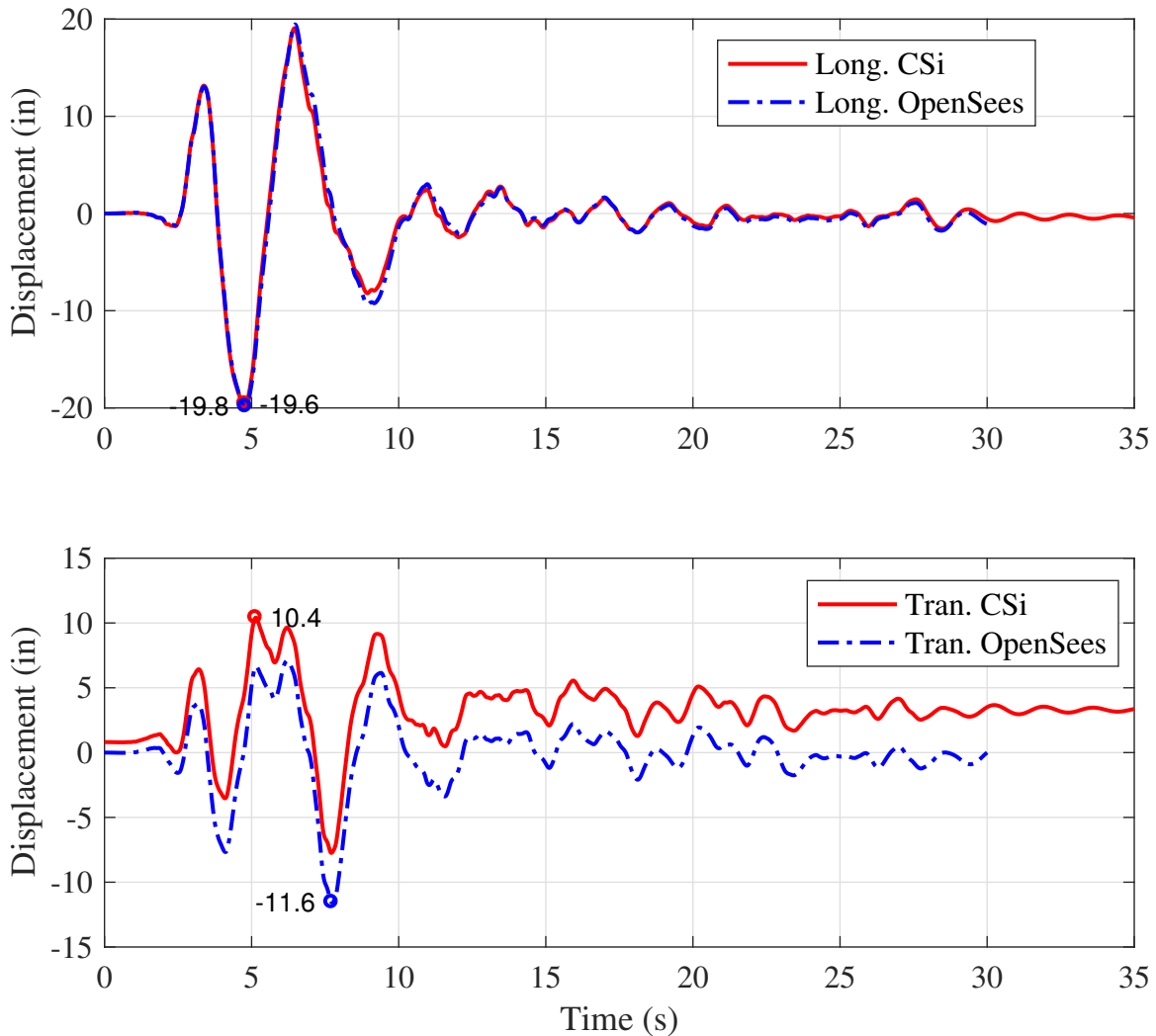
Figure 5.52: OSB3 (roller abutment) center of mass displacement time histories for motion ROCKN1N1

The ROCK and SAND responses show similar trends to the CLAY motion. The peak displacement demands are smaller than the CLAY motion, and the difference between the two software predictions is 0.2 in and 0.7 in for longitudinal response under ROCK and SAND, respectively. The transverse responses are offset by the initial gravity load displacement in CSiBridge. The consequence are differences of 1.2 in and 1.1 in for ROCK and SAND, respectively. In addition, there is a shift in the time that the peaks occur.
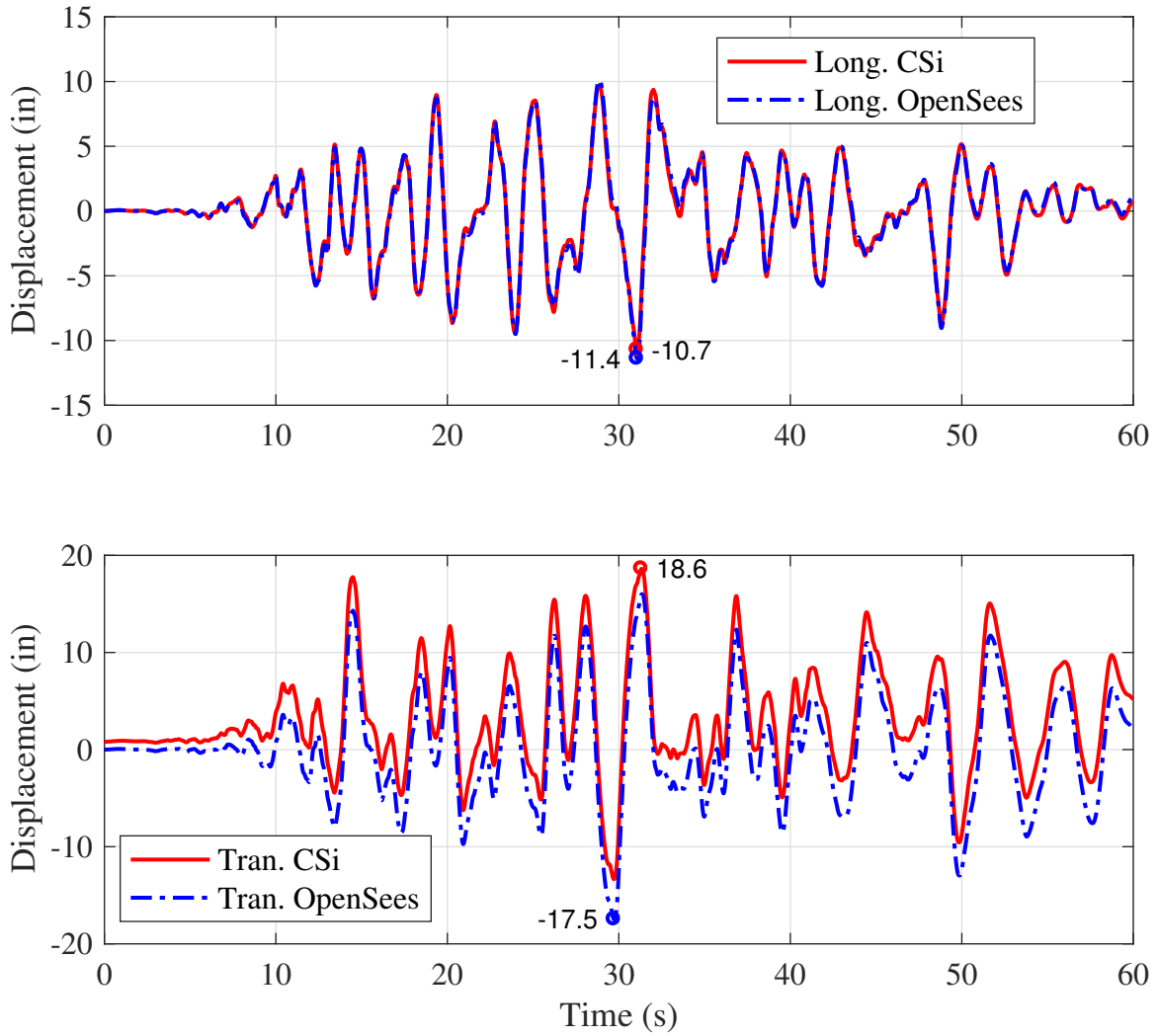
Figure 5.53: OSB3 (roller abutment) center of mass displacement time histories for motion SANDN1N1

OSB4

The displacement time history responses of OSB4 at the center of mass of the bent for the CLAYN1N1, ROCKN1N1, and SANDN1N1 ground motions are shown in Figures 5.54, 5.55, and 5.56, respectively. The displacement time histories are shown independently for the bridge longitudinal (labeled Long.) and transverse (labeled Tran.) directions. The magnitudes, times at peak displacement excursion, and trends are very similar to OSB3.
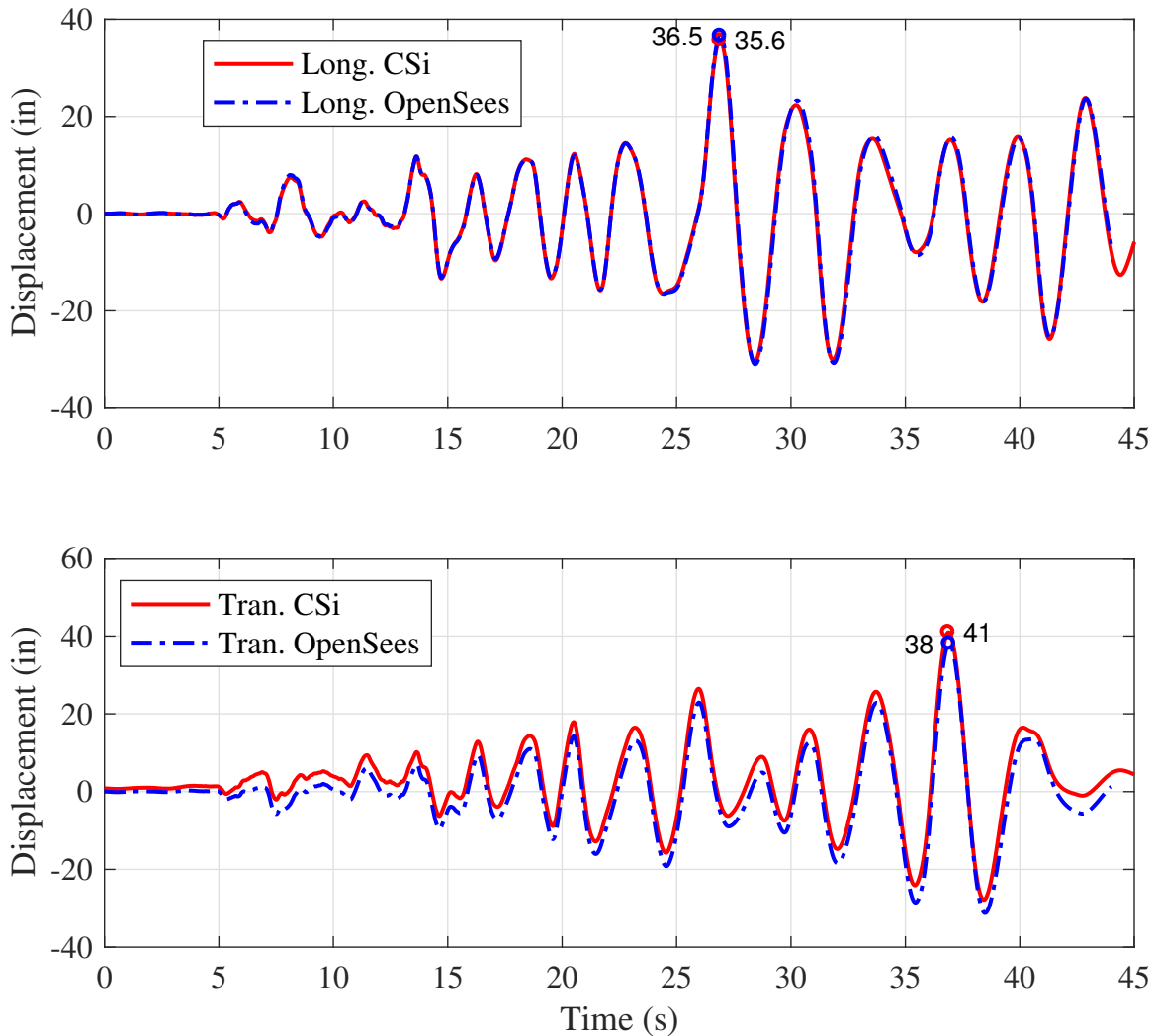
Figure 5.54: OSB4 (roller abutment) center of mass displacement time histories for motion CLAYN1N1

The peak CLAY longitudinal displacement demands differ by 0.9 in (OpenSees larger), whereas the transverse differ by 3 in (CSiBridge larger). The same gravity load offset in the transverse direction is seen in the isolation layer of the OSB4 roller abutment bridges. The longitudinal maximum displacements are 0.1 in and 0.2 in different between OpenSees and CSiBridge for the ROCK and SAND motions, respectively. However, while the phasing is the

same for the transverse responses, the time at peak displacement, the residual displacement, and the magnitude of the peak displacement is different for the ROCK and SAND ground motions. The CSiBridge response to the ROCK motion shows approximately 4 in of residual displacement, which is approximately 40% of the maximum displacement. The magnitudes of the peak transverse responses in the SAND motion are 3.2 in different (CSiBridge larger).
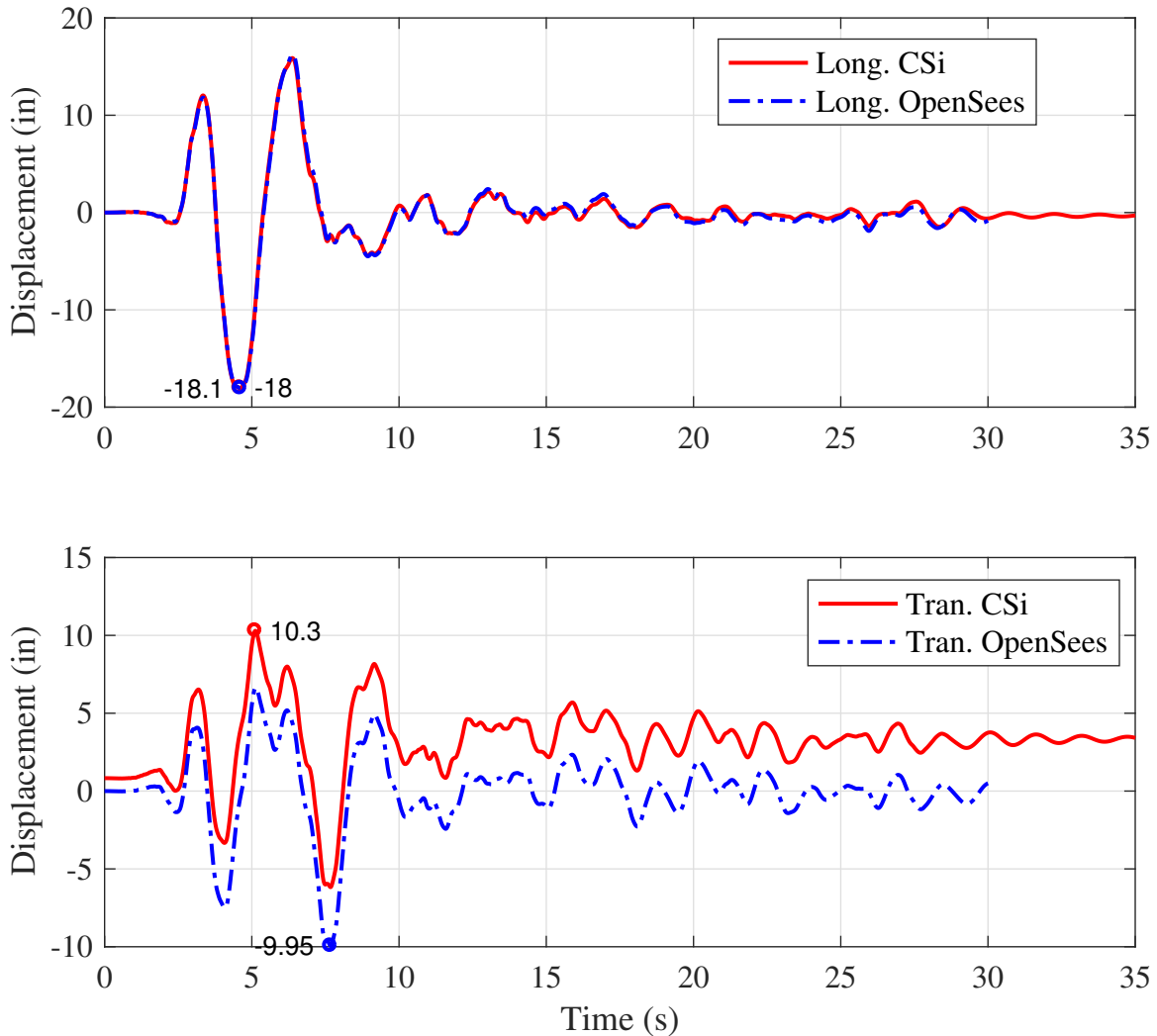
Figure 5.55: OSB4 (roller abutment) center of mass displacement time histories for motion ROCKN1N1

5.3.3 Damping Study

A common problem encountered in standardizing nonlinear dynamic responses is the contribution from damping, and the corresponding dependence of the results on the parameters and behavior of the damping model selected. In this study, Rayleigh damping was used

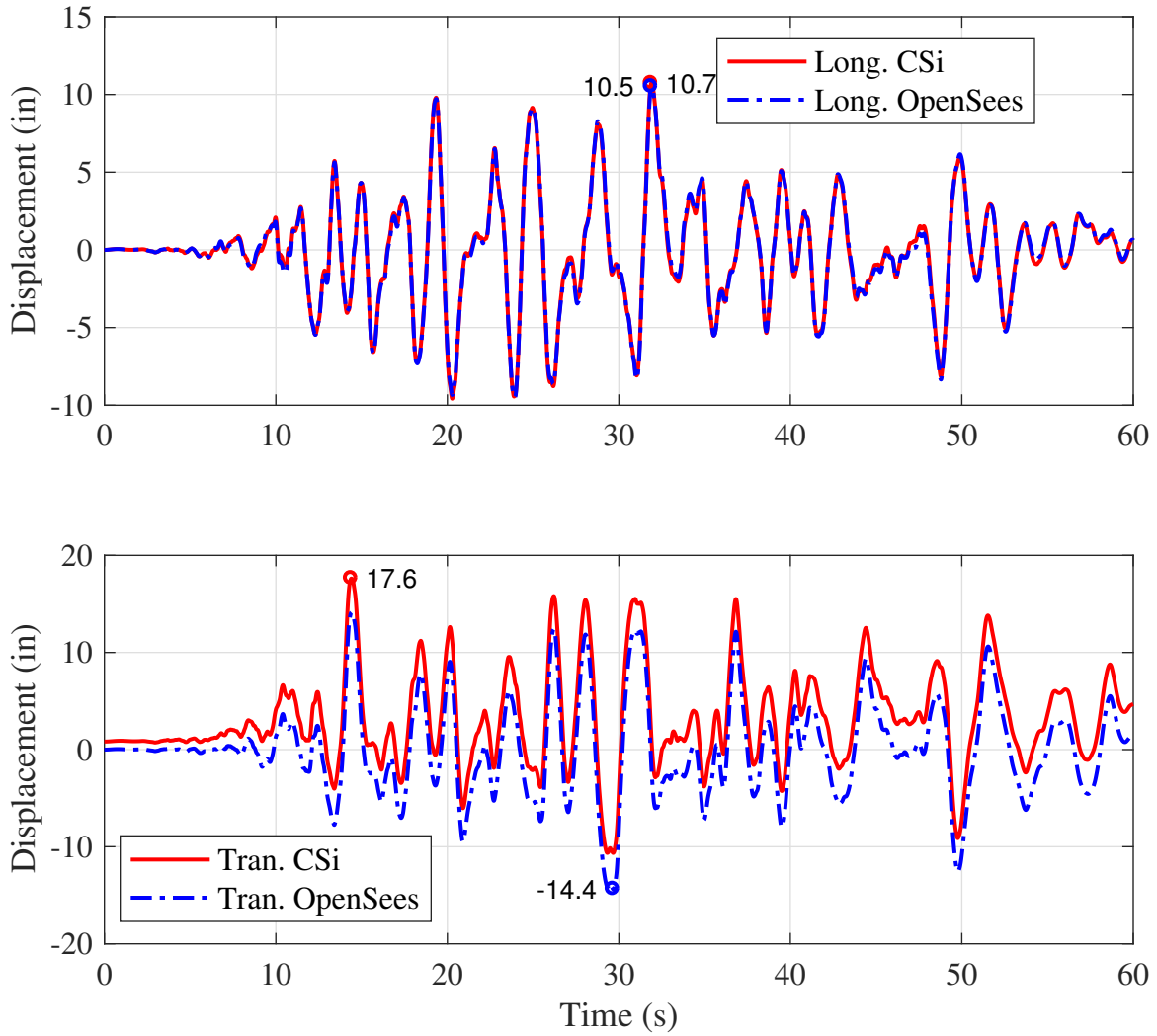Figure 5.56: OSB4 (roller abutment) center of mass displacement time histories for motion SANDN1N1

for both the OpenSees and CSiBridge analyses, using exactly the same mass and stiffness-proportional coefficients. In all the OpenSees analyses, the stiffness proportional factor was employed using the initial stiffness. Therefore, an additional case study is added here where the stiffness proportional term is used with the last committed (tangent) stiffness.

The displacement time history responses of OSB1 at the center of mass of the bent for the ROCKN1N1 ground motion and roller abutment are shown in Figure 5.57. The displacement time histories are shown independently for the bridge longitudinal (labeled Long.) and transverse (labeled Tran.) directions. The ROCK motion and roller abutment model were selected, because there is a significant difference in the peak displacement demand. The difference between the two stiffness-proportional approaches is not typically this large. While clearly an important modeling choice, it is clear from studying the time history responses that the CSiBridge responses are more similar to the damping based on the initial stiffness. The use of the degraded tangent stiffness leads to larger displacements at all inelastic cycles with a corresponding increase in period elongation.

To further isolate the changes in the nonlinearities of materials and elements on the responses, OSB1 with the original abutment model was studied in both software without the consideration of damping. The displacement time history responses of OSB1 at the center of mass of the bent for the CLAYN1N1 ground motion are shown in Figure 5.58. The displacement time histories are shown independently for the bridge longitudinal (labeled Long.) and transverse (labeled Tran.) directions.

Several important observations can be made from comparing the responses in the figure and similar time history plots for the other ground motion cases (not presented here). The OpenSees peak displacement demand increased from 5.75 in to 7.74 in and 4.75 in to 6.63 in for the longitudinal and transverse directions, respectively. The transverse direction occurred at any earlier time, but otherwise the changes in phasing were small. On the other hand, the CSiBridge peak displacement demand increased from 4.78 in to 21.5 in and 4.85 in to 12.6 in for the longitudinal and transverse directions, respectively. No only was the increase in displacement excessive, but the overall phasing of the response and location/number of peaks was significantly different.

While the transverse response in Figure 5.15 matches almost exactly, the differences in the transverse response in Figure 5.58 are more than 100%. Due to the elastic abutment boundary for the transverse direction in the original abutment models, this difference is arising entirely due to the loss of the damping term in the equation of motion. The chaotic response seen in the longitudinal direction (also observed with the original damping model) likely has a large contribution from the longitudinal abutment hysteresis, as previously mentioned.

5.4   Summary

This chapter presented the results of nonlinear static and nonlinear dynamic analyses using the OSB1 through OSB4 bridge models in CSiBridge and OpenSees. The OpenSees bridge models were developed to reproduce, as closely as possible, the response in CSiBridge, and not as representative bridge models that would be typically built using the suite of elements,
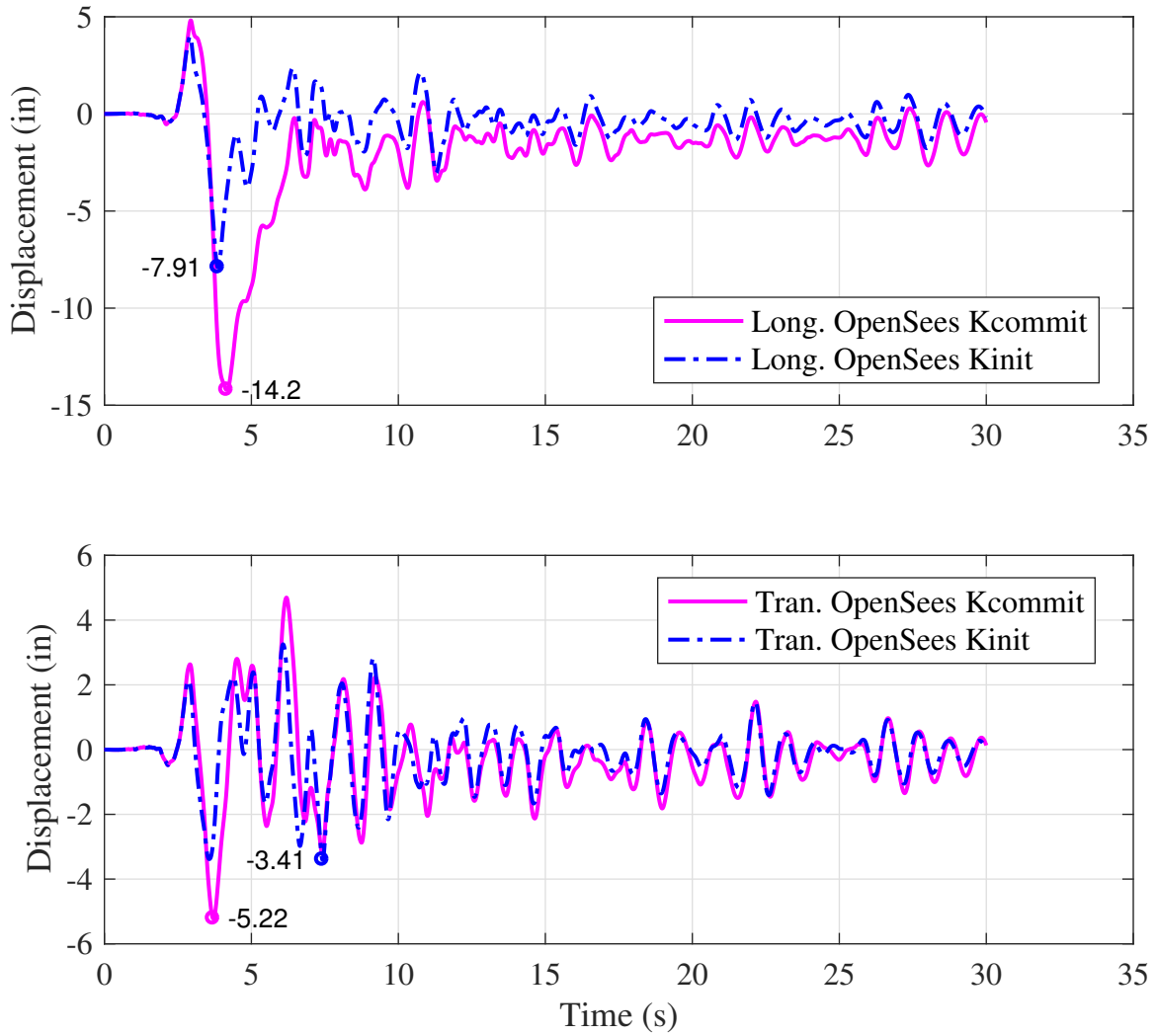
Figure 5.57: OSB1 (roller abutment with damping using last committed stiffness) center of mass displacement time histories for motion ROCKN1N1
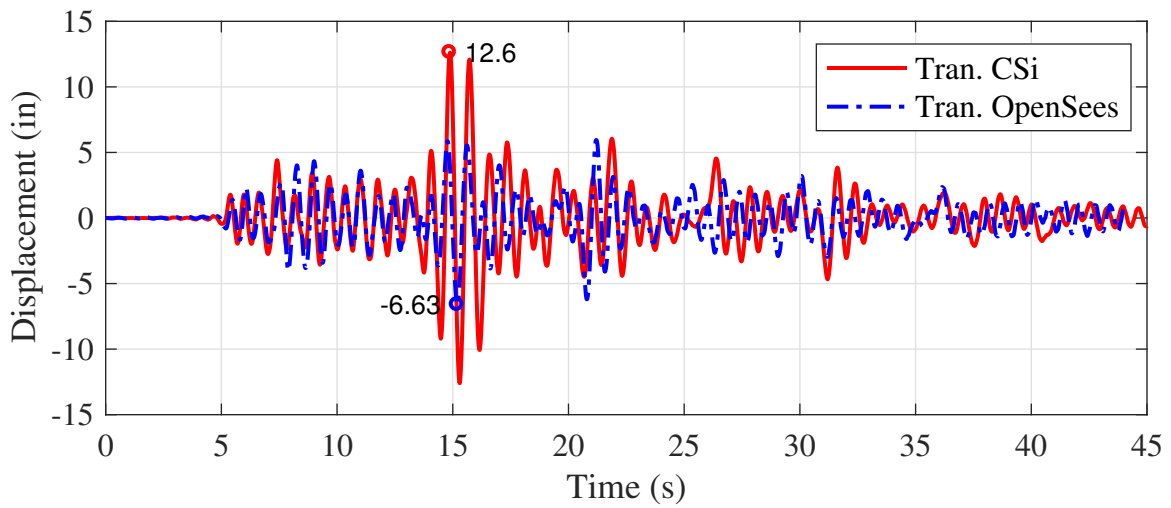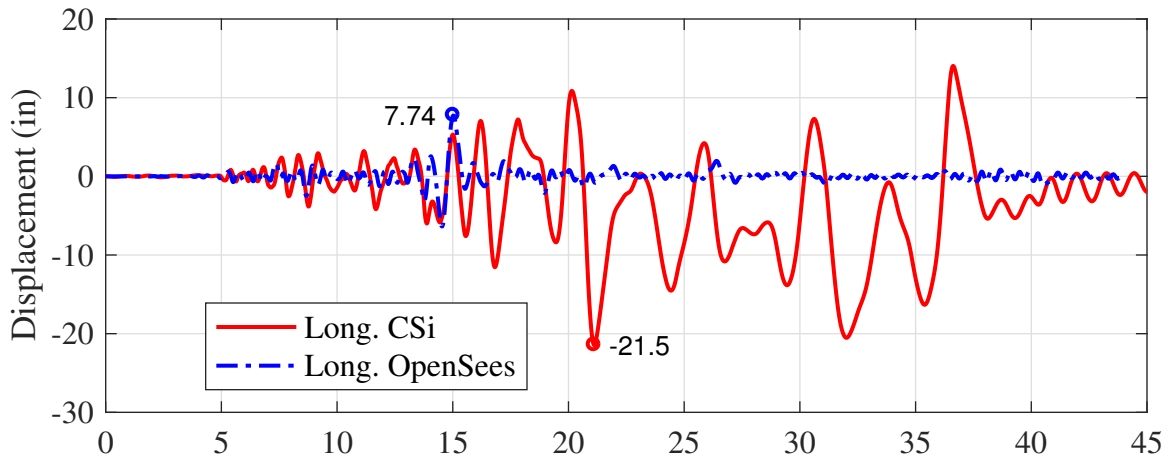
Figure 5.58: OSB1 (original abutment without damping) center of mass displacement time histories for motion CLAYN1N1

sections, and materials available in OpenSees. While it was possible to obtain similar backbone responses of the individual constitutive models, the behaviors of the frame hinges was not necessarily identical, leading to discrepancies in the nonlinear static pushover results, particularly at high ductility levels.

Due to the close agreement of the nonlinear static responses, particularly the initial stiffness and nominal yield forces in the columns, the modal analysis results (both mode shapes as well as the eigenvalues themselves) were themselves close when comparing the two software. However, as anticipated by the differences in the constitutive models under cyclic loads, and the differences in the section and hinge behaviors as the nonlinearity became more extreme, the NTHA results did not exhibit agreement except for the initial elastic cycles.

The study was broken into many individual calibration sub-studies to identify the source of the differences observed in the NTHA results. It can therefore be stated that the steel constitutive models, isolation bearing elements, and abutment links (when included) were identical for static and dynamic analysis between the two softwares. It was not possible to isolate the confined constitutive models directly, but it can also be concluded that the cyclic response of the concrete constitutive models were not in agreement. However, due to the differences in the nonlinear static section (moment curvature) responses and frame hinge responses, there are also some discrepancies arising from implementation of the formulation alone that were not observed in Chapter 3 for the simple cantilever cases. These concrete constitutive model differences led to the observed discrepancies in the nonlinear pushover response of OSB1 and OSB2, as well as the differences observed in the NTHA results for the roller abutment case.

The other significant source of nonlinearity in the models is at the abutments. These boundaries drive a significant portion of the observed nonlinear response history maxima and energy dissipation. This effect was separated out by studying the bridge models with the original abutments separate from the roller abutments. It was also known that the nonlinear backbone responses were common between the OpenSees and CSiBridge models were the same for the abutments. Therefore, the (sometimes large) differences observed in the nonlinear time history responses for the original abutment models were due entirely to the cyclic behavior of the abutment models.

Finally, to remove the possible effect of damping model discrepancies, the damping was set to zero, with large differences observed between the two models. While the same transient integrators were used, it is not clear how the time-stepping strategy in CSiBridge proceeds with enforcing equilibrium and the unbalance obtained at each iteration and time increment.

Chapter 6

Sensitivity Analysis

Sensitivity analysis is an important tool for nonlinear analysis because it allows for the quantification of uncertainty due to either random material properties or modeling assumptions. This can shed light on the parameters and components of a bridge model that have the most significant effect on the simulated response.

There are a variety of approaches to computing response sensitivity for nonlinear finite element models including the finite difference method, complex perturbation method, adjoint structure method, and the direct differentiation. The most basic approach is the finite difference method where, after computing the deterministic, or mean, response, the analysis is repeated for perturbed values of each uncertain parameter. The sensitivity is then obtained by differencing the perturbed and mean responses. Although the finite difference approach is easy to implement, it requires running the full time history analysis for each parameter in the model. This imposes a heavy time and computation burden. In addition, the finite difference approximations are subject to round off errors. The complex perturbation method is more accurate than the finite difference method; however, it relies on complex algebra to compute the response sensitivity and it also requires re-analysis for each parameter of the finite element model.

The direct differentiation method computes response sensitivity directly from the finite element response and it is based on the analytic differentiation of the discretized equations that govern the finite element response as well as the constitutive response of each element in the model. Unlike the finite difference method, the direct differentiation method computes the sensitivity for all parameter during the analysis for the deterministic, or mean, response. This is accomplished by assembly of "sensitivity" load vectors and forward and backward substitutions with the factorized dynamic tangent stiffness matrix at each time step. This makes the response sensitivity on the same order of accuracy as the deterministic response, i.e., it is not subject to round off errors. The adjoint structure method also computes analytical response sensitivity; however, it is not applicable to path-dependent problems such as those encountered in NTHA of bridges.

The focus herein will be on the direct differentiation method (DDM), which has been implemented in the OpenSees framework for the element and constitutive models used for the four OSB models. The finite difference method (FDM) can be used as a means of verifying

that the DDM is giving mathematically correct results for the OSB models [12, 26]. Some minor changes to the OSB models were made, compared to those in Chapter 4, in order to accommodate the DDM implementations available in OpenSees and to utilize the distributed plasticity frame element formulations in OpenSees that are not available in CSiBridge. The same boundary conditions from the CSiBridge models were used for the column bases and abutments.

6.1   OpenSees Bridge Models

To consider common bridge properties for DDM sensitivity analysis, changes were made to the OpenSees model relative to those described in Chapter 4. The following modeling approach, which represents a standard approach for bridge modeling in OpenSees, was used for sensitivity analysis. This standard approach represents the modeling choices a user of OpenSees would likely make after attending an OpenSees workshop or similar session.

- Column members for all OSBs were modeled using the forceBeamColumn element with five Gauss-Lobatto integration points.

- The RCCircSection fiber section was used at each integration point of the force-based elements in the columns.

- Concrete01 and Steel01 uniaxial material models were used for the stress-strain response of each fiber in the column cross-sections. This differs from Chapter 4 where Concrete02 and Steel02 were used. DDM sensitivity is not currently implemented for the Concrete02 and Steel02 models in OpenSees.

- Abutment gaps were modeled using zeroLength elements with the EPPGapMaterial one-dimensional force-deformation relationship.

- Isolators for OSB3 and OSB4 were modeled using zeroLength elements with the Elliptical and Bidirectional two-dimensional force-deformation relationship for the abutments and bent, respectively.

All other model and bridge details, e.g., the superstructure elements and bridge mass, are the same as those previously described in Chapter 4. The original abutment models are used throughout this chapter, no roller abutment models are considered. Comparisons between the "sensitivity" and "matched CSiBridge" models for the pushover and nonlinear time history response of each OSB are made throughout the remainder of this chapter, along with response sensitivity analyses.

6.2   Parameters Considered

The model parameters considered for sensitivity analysis of each OSB are summarized in Table 6.1. Each column parameter maps to all objects in the bridge model that contain that

parameter, e.g., the column diameter parameter represents the diameter of both columns in the two-column bents (OSB1 and OSB3) and the column longitudinal reinforcing steel strength represents the strength of all reinforcing bars in the column(s). In addition, the bent and abutment isolator parameters map to all isolators at the bent and abutments, respectively. Parameters of the superstructure (elastic and shear modulus) are considered in order to assess their effect on the seismic response of each OSB. The superstructure stiffness can be a source of modeling uncertainty in the seismic analysis of bridges. An assumed coefficient of variation (COV) is listed in Table 6.1 in order to reflect uncertainty, either aleatoric or epistemic, of the nominal values of each parameter.

Table 6.1: Nominal values of modeling parameters considered for nonlinear static and time history response sensitivity analysis of the OSB models.

Parameter		COV	OSB1	OSB2	OSB3	OSB4
Column diameter (in)	d_{col}	0.02	66.00	66.00	66.00	66.00
Cover concrete strength (ksi)	$f'_{c,cover}$	0.15	-4.00	-4.00	-3.60	-4.00
Core concrete strength (ksi)	$f'_{c,core}$	0.15	-5.56	-5.56	-5.05	-5.56
Steel yield strength (ksi)	f_y	0.1	60.00	60.00	60.00	60.00
Bent isolator stiffness (kip/in)	$k_{iso,bent}$	0.1	–	–	74.80	74.80
Bent isolator strength (kip)	$F_{y,iso,bent}$	0.1	–	–	74.80	74.80
Abutment isolator stiffness (kip/in)	$k_{iso,abut}$	0.1	–	–	41.67	41.67
Abutment isolator strength (kip)	$F_{y,iso,abut}$	0.1	–	–	36.00	36.00
Longitudinal abutment stiffness (kip/in)	$k_{gap,l}$	0.15	2591.67	1466.37	2572.08	2023.33
Longitudinal abutment strength (kip)	$F_{y,gap,l}$	0.15	-1555.00	-1031.00	1629.00	1282.00
Transverse abutment stiffness (kip/in)	$k_{gap,t}$	0.15	315.00	100.00	100.00	100.00
Transverse abutment strength (kip)	$F_{y,gap,t}$	0.15	–	179.40	179.40	179.40
Superstructure elastic modulus (ksi)	E_{ss}	0.2	3420.00	3420.00	3420.00	3420.00
Superstructure shear modulus (ksi)	G_{ss}	0.2	1425.00	1425.00	1425.00	1425.00

6.3 Response Sensitivity Analysis of OSB1

Sensitivity analysis of the nonlinear static and dynamic time history response of OSB1 are presented here with respect to the applicable parameters listed in Table 6.1. A schematic and node numbers of the OSB1 OpenSees model are shown in Figure 6.1. The global X direction is transverse while Y is longitudinal.
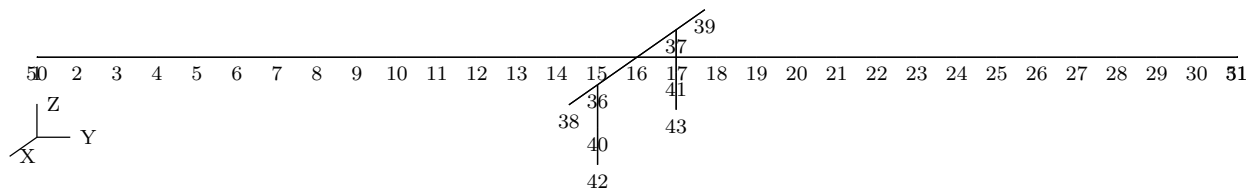

Figure 6.1: Node numbers for OpenSees model of OSB1.

6.3.1 Pushover Analysis

Pushover analysis of OSB1 in the transverse and longitudinal directions is shown in Figure 6.2 for the "matched to CSiBridge" and "sensitivity" OpenSees models. The pushover response is computed via a displacement-controlled analysis. Due to the differences in element and constitutive models between the "matched to CSiBridge" and "sensitivity" models, the initial stiffness differs; however, the yield and ultimate base shear match fairly well up to a maximum displacement of 5 inches in both the transverse and longitudinal directions. Due to the integration point being at the center of the rigid hinge region, the yield force is overestimated in the lumped plasticity responses.
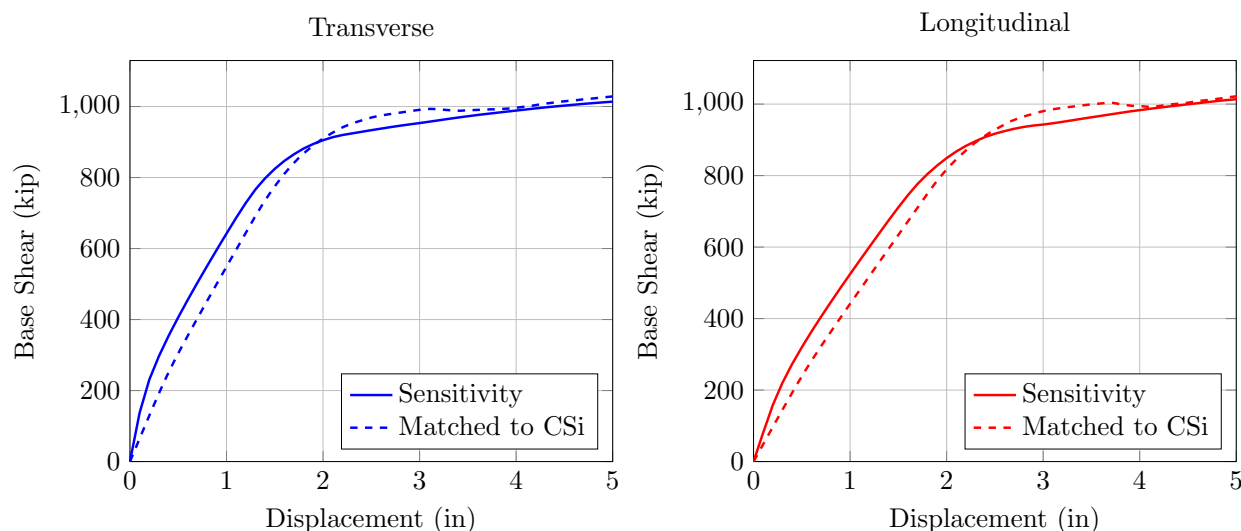
Figure 6.2: Comparison of lateral load-displacement response of OSB1 with original abutments for OpenSees models matched to CSiBridge and used for sensitivity.

The sensitivity of the load factor, λ, with respect to the yield stress of the longitudinal reinforcing steel in the columns is computed via the DDM, as shown in Figure 6.3. Note that the load factor is a scaling of the total lateral load applied to the bridge deck in the pushover analysis. As a result, the base shear of the column bents is some portion of the total lateral load with the remaining lateral load going to the abutments.

The sensitivity, $d\lambda/df_y$, is scaled by one standard deviation of f_y. In addition to putting the sensitivity in units of force, the plotted values represent the change in lateral load for a one standard deviation increase in f_y. To the point of just over 1 inch displacement in both the transverse and longitudinal directions, the sensitivity to the steel yield strength is zero. This indicates that all longitudinal reinforcement bars are in the elastic range up to this displacement. The sensitivity increases rapidly as the columns form a plastic hinge, then stabilizes at about 60 kip. This indicates that at a displacement of 5 inch, OSB1 would be able to resist an additional 60 kip of lateral load if f_y of its columns' longitudinal reinforcing steel is increased by one standard deviation.
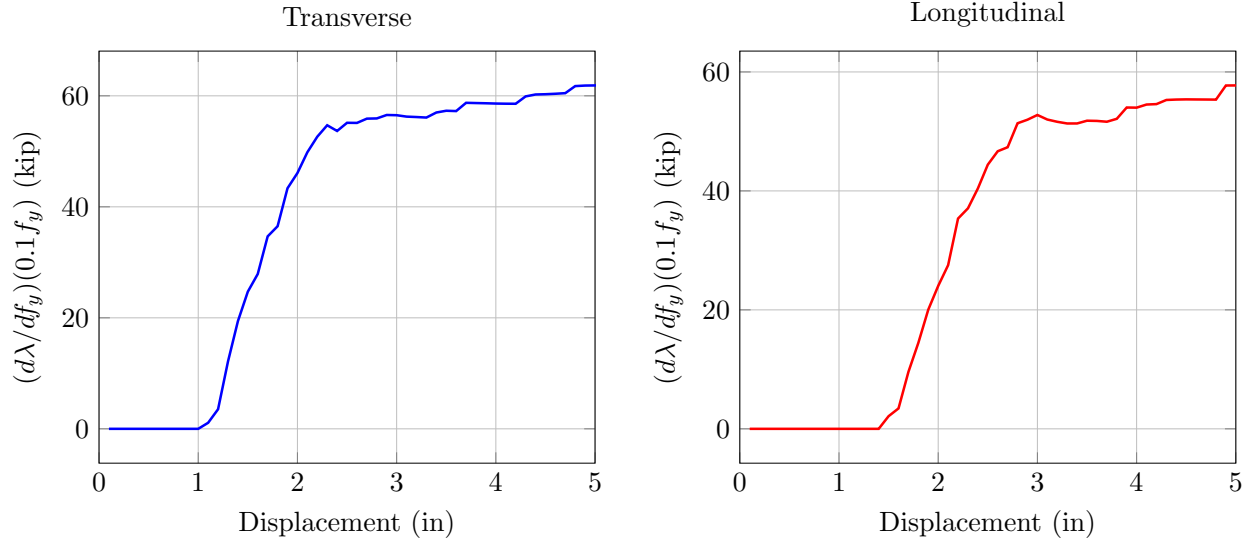
Figure 6.3: Sensitivity of OSB1 lateral load-displacement response with respect to one standard deviation increase in yield strength of the column longitudinal reinforcing steel.

The sensitivity of the load factor with respect to the elastic modulus of the bridge superstructure, $d\lambda/dE_{ss}$, is shown in Figure 6.4. In the transverse direction, the sensitivity increases linearly after the columns start to yield at about 1 inch displacement. This is due to the modeling assumption that the transverse abutment response is linear-elastic, which leads to all of the lateral load applied to the deck going to the transverse abutment springs. In the longitudinal direction, where the abutment springs are EPP-gap, the sensitivity of the load factor to the superstructure stiffness reduces after the longitudinal abutments reach their yield strength at a little over 0.5 inch displacement. There is a second reduction in the sensitivity after the columns start to yield at about 1.5 inch displacement. This indicates that the superstructure stiffness becomes less important after yielding of the abutments and columns, i.e., as a mechanism starts to form.

Similar plots of the load-displacement response sensitivity can be made for the remaining parameters listed in Table 6.1 for OSB1. Rather than show each of these plots, the peak sensitivity (assuming a one standard deviation in each parameter) is listed in Table 6.2 along with the corresponding lateral displacement at which the peak sensitivity occurs. Among the column section parameters, the compressive strength of the cover and core regions have relatively less influence, compared to the reinforcing steel strength, on the lateral load-displacement response. In addition, the peak sensitivity for the concrete compressive strength is realized early in the pushover curve when the concrete reaches its peak strength and begins to crush. These findings are consistent with reinforced concrete mechanics.

Turning to the abutment parameters for OSB1, Table 6.2 shows that the stiffness and strength of the longitudinal abutment model (EPP Gap), compared to the RC column properties, have a much larger influence on the lateral load displacement response as the abutment reaches its peak resisting force at 0.60–0.70 inch longitudinal displacement. A one standard
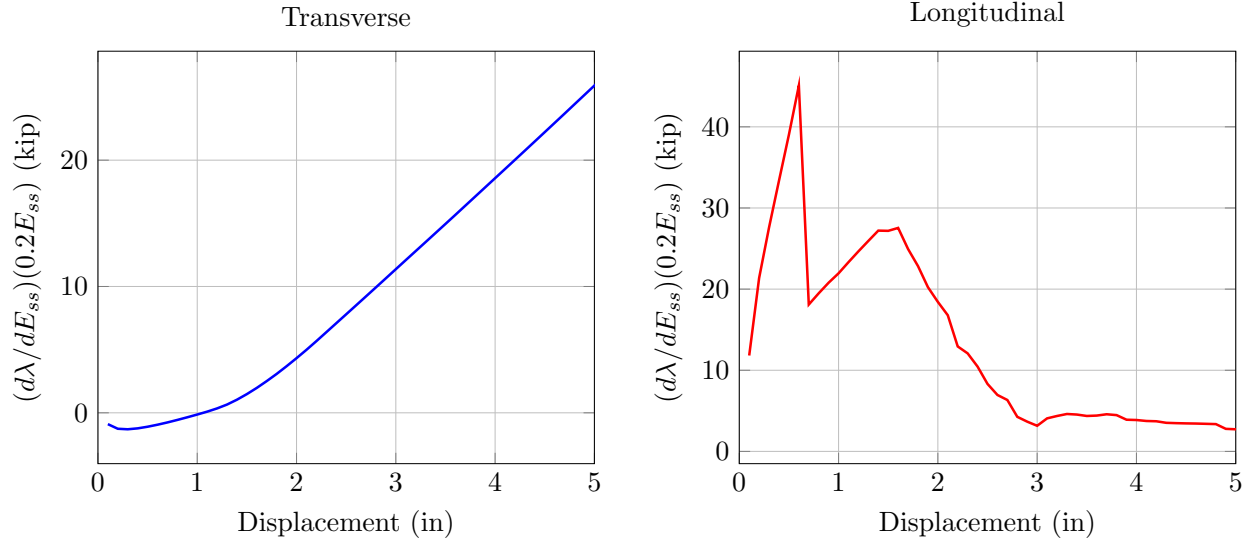
Figure 6.4: Sensitivity of OSB1 lateral load-displacement response with respect to one standard deviation increase in elastic modulus of the bridge superstructure.

Table 6.2: Maximum load factor sensitivity for one standard deviation increase in each parameter for pushover analysis of OSB1 and corresponding lateral displacement where the maximum occurs.

Parameter	Transverse		Longitudinal	
	$\Delta\lambda$ (kip)	u (in)	$\Delta\lambda$ (kip)	u (in)
d_{col}	32.5	1.20	27.6	2.10
$f'_{c,cover}$	8.0	1.20	6.3	1.60
$f'_{c,core}$	22.0	1.20	18.6	3.00
f_y	61.9	5.00	57.7	5.10
$k_{gap,l}$	0.0	–	188.9	0.60
$F_{y,gap,l}$	0.0	–	233.4	4.90
$k_{gap,t}$	431.4	5.10	0.0	–
E_{ss}	26.6	5.10	45.1	0.60
G_{ss}	0.0	–	0.0	–

deviation increase in the stiffness and strength of the longitudinal abutment model leads to increases of 189 kip and 233 kip, respectively, in the lateral load that OSB1 can resist. This finding confirms the importance of abutment models on determining the resistance of bridge structures to lateral loads. It is noted that the stiffness of the transverse abutment model has the largest influence on the response of OSB1; however, this is a direct result of the modeling assumption that the transverse abutment is linear-elastic.

6.3.2 Nonlinear Time History Analysis

Nonlinear time history response for the deck displacement of OSB1 is shown in Figure 6.5. The dynamic response is computed with average acceleration Newmark time integration using a time step of 0.005 sec.
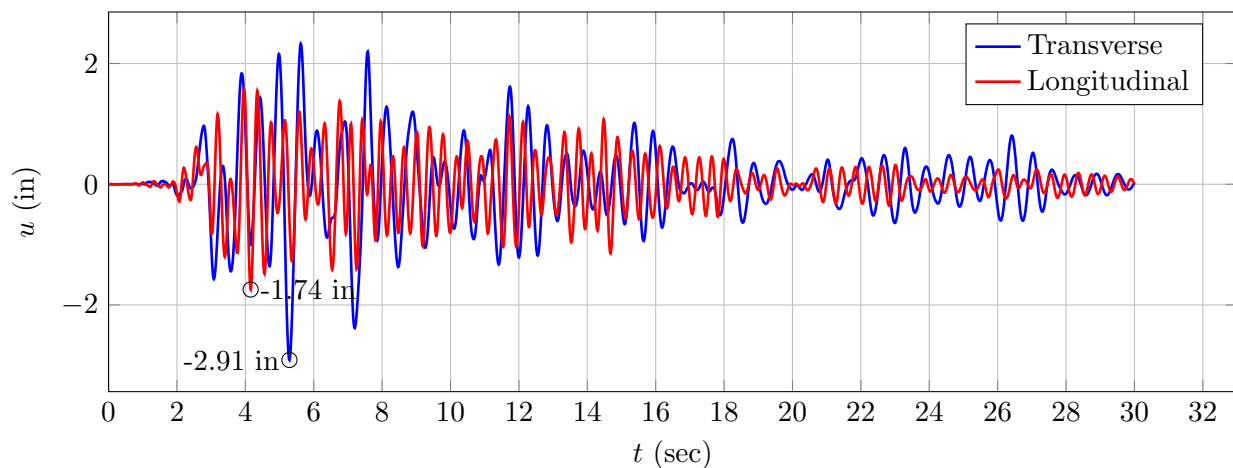
Figure 6.5: Nonlinear time history response of OSB1 for the ROCKN1N1 ground motion.

Peak values of deck displacement in the transverse and longitudinal directions are indicated in Figure 6.5 and agree well with the "matched to CSiBridge" results. Comparisons of the response time history for the "matched to CSiBridge" and "sensitivity" models are made in Figure 6.6.

The DDM time history of sensitivity of the deck displacement with respect to the yield strength of the column longitudinal reinforcing steel is shown in Figure 6.7. The computed sensitivity, du/df_y, is scaled by one standard deviation of the nominal value of f_y. This scaling puts the values on the vertical axis of Figure 6.7 in to units of length and these values thus represent the change in displacement for a one standard deviation increase in f_y.

As seen in Figure 6.7, the deck displacement is relatively insensitive to changes in the steel yield strength with peak value of 0.12 inch and 0.08 inch in the transverse and longitudinal directions, respectively. It is noted that the first yield of a longitudinal steel reinforcing bar is just after 3.0 seconds in to the ground motion, as this is the time where the sensitivity becomes non-zero. In addition, the peak values of displacement sensitivity are not coincident in time with the peak values of the displacement response.
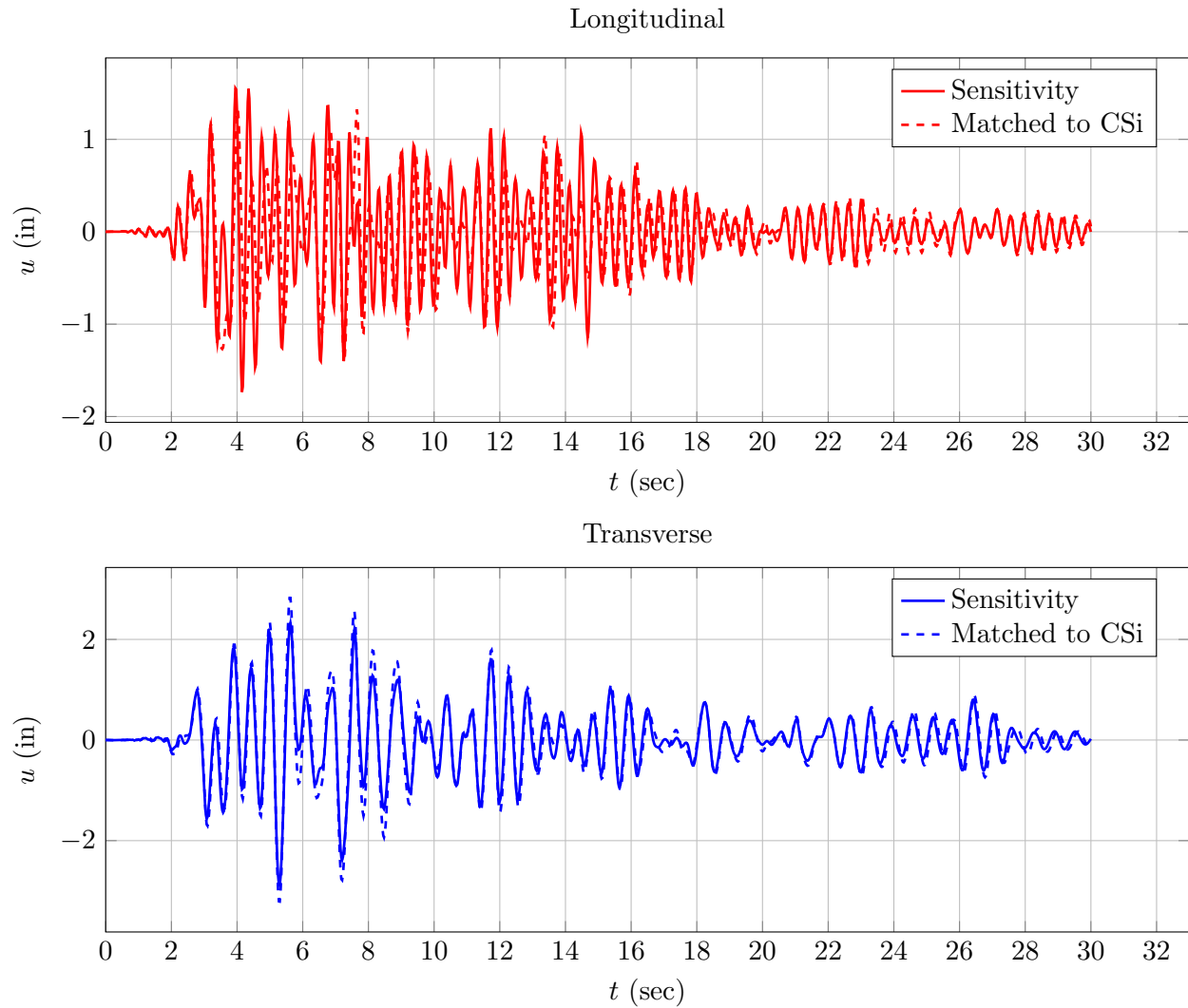
179

Figure 6.6: Comparison of nonlinear time history response of OSB1 for the ROCKN1N1 ground motion with original abutments for OpenSees models matched to CSiBridge and used for sensitivity.
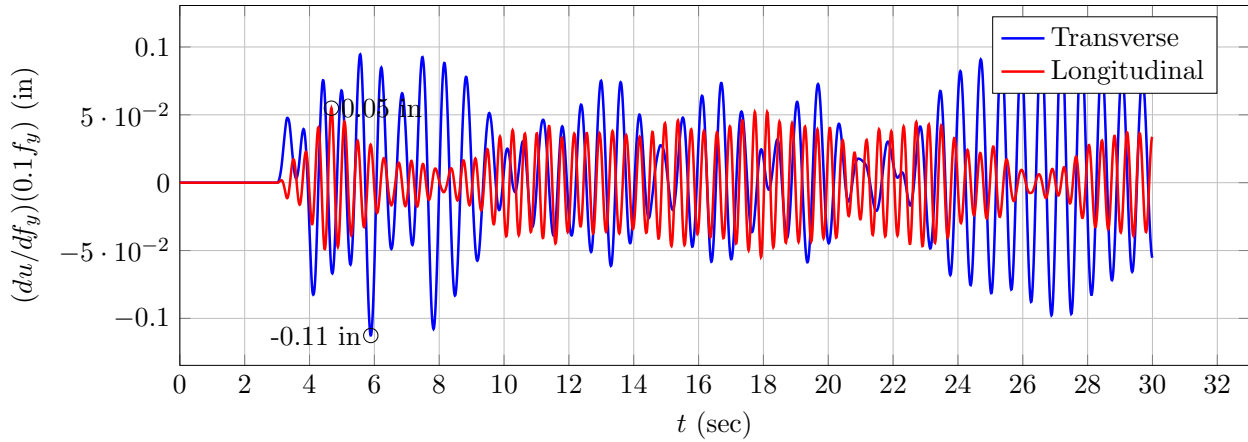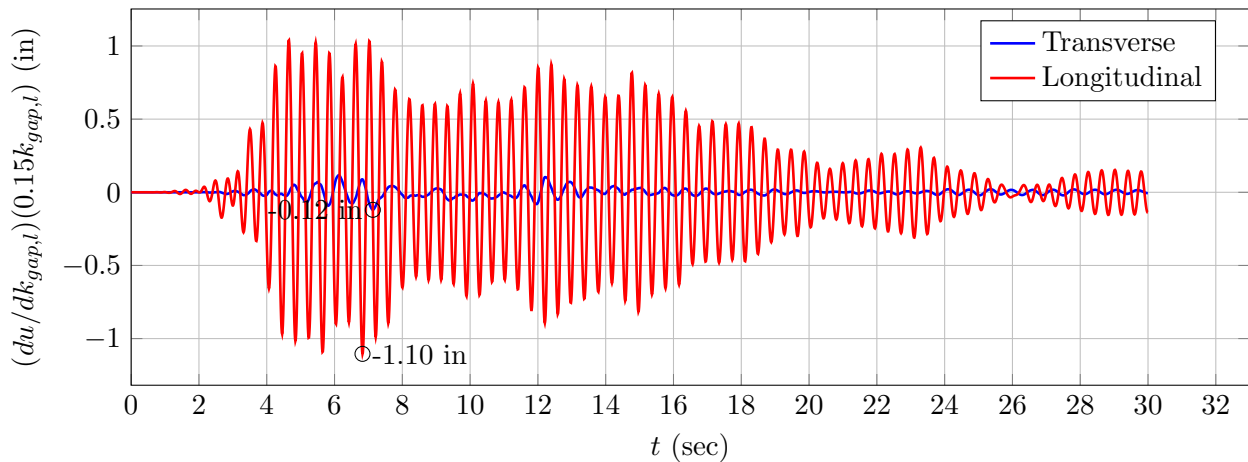
Figure 6.7: Sensitivity of nonlinear time history response with respect to one standard deviation increase in column reinforcing steel strength for OSB1 for the ROCKN1N1 ground motion.

The sensitivity of the deck displacement to the stiffness of the longitudinal abutment, which was also found to have a large influence on the pushover response of OSB1, is shown in Figure 6.8. In the transverse direction, the sensitivity to the longitudinal abutment stiffness is small, but non-zero due to bidirectional earthquake excitation.

Figure 6.8: Sensitivity of nonlinear time history response with respect to one standard deviation increase in longitudinal abutment stiffness for OSB1 for the ROCKN1N1 ground motion.

Similar plots of the deck displacement sensitivity with respect to the parameters listed in Table 6.1 for OSB1 can be made. In lieu of showing all plots, Table 6.3 lists the maximum displacement sensitivity and the coincident time where it occurs for each parameter. The RC column properties have very little influence on the displacement while the abutment parameters play a more significant role. Similar sensitivities are tabulated in Tables 6.4

181

through 6.6 for the other three ground motions considered in this study.

Table 6.3: Maximum displacement sensitivity for one standard deviation increase in each parameter for nonlinear time history analysis of OSB1 and corresponding time where the maximum occurs for the ROCKN1N1 ground motion.

Parameter	Transverse		Longitudinal	
	Δu (in)	t (sec)	Δu (in)	t (sec)
d_{col}	-0.13	8.95	0.07	7.01
$f'_{c,cover}$	-0.02	8.93	-0.01	7.19
$f'_{c,core}$	-0.08	8.95	-0.03	12.19
f_y	-0.11	5.89	0.05	4.67
$k_{gap,l}$	-0.12	7.13	-1.10	6.83
$F_{y,gap,l}$	0.07	7.13	0.66	6.83
$k_{gap,t}$	-0.66	7.72	0.04	5.27
E_{ss}	-0.04	7.50	-0.25	5.22
G_{ss}	0.0	–	0.0	–

Table 6.4: Maximum displacement sensitivity for one standard deviation increase in each parameter for nonlinear time history analysis of OSB1 and corresponding time where the maximum occurs for the ROCKN1P1 ground motion.

Parameter	Transverse		Longitudinal	
	Δu (in)	t (sec)	Δu (in)	t (sec)
d_{col}	0.13	12.93	0.06	16.27
$f'_{c,cover}$	-0.03	10.15	0.01	16.27
$f'_{c,core}$	-0.09	10.15	0.03	16.25
f_y	-0.13	11.40	-0.05	11.55
$k_{gap,l}$	-0.04	13.46	0.86	16.28
$F_{y,gap,l}$	0.02	13.46	-0.52	16.28
$k_{gap,t}$	0.60	12.95	-0.02	10.85
E_{ss}	0.03	14.66	0.20	16.27
G_{ss}	0.0	–	0.0	–

Table 6.5: Maximum displacement sensitivity for one standard deviation increase in each parameter for NTHA of OSB1 and corresponding time where the maximum occurs for the SANDN1N1 ground motion.

Parameter	Transverse		Longitudinal	
	Δu (in)	t (sec)	Δu (in)	t (sec)
d_{col}	0.12	14.55	0.09	34.73
$f'_{c,cover}$	0.03	9.80	-0.02	34.51
$f'_{c,core}$	0.09	14.54	-0.06	34.53
f_y	0.16	26.30	0.07	33.20
$k_{gap,l}$	-0.20	13.67	-1.67	32.97
$F_{y,gap,l}$	0.12	13.67	1.00	32.97
$k_{gap,t}$	-1.01	36.52	-0.10	32.97
E_{ss}	0.06	35.60	0.29	35.13
G_{ss}	0.0	–	0.0	–

Table 6.6: Maximum displacement sensitivity for one standard deviation increase in each parameter for NTHA of OSB1 and corresponding time where the maximum occurs for the CLAYN1N1 ground motion.

Parameter	Transverse		Longitudinal	
	Δu (in)	t (sec)	Δu (in)	t (sec)
d_{col}	-0.12	11.04	0.08	9.89
$f'_{c,cover}$	0.03	7.04	0.02	9.88
$f'_{c,core}$	0.10	7.04	0.05	12.62
f_y	0.18	15.34	0.07	15.45
$k_{gap,l}$	-0.27	15.48	1.71	15.03
$F_{y,gap,l}$	0.16	15.48	-1.03	15.03
$k_{gap,t}$	1.14	15.33	0.11	16.18
E_{ss}	0.04	14.53	0.24	15.02
G_{ss}	0.0	–	0.0	–

6.4 Response Sensitivity Analysis of OSB2

Sensitivity analysis of the nonlinear static and dynamic time history response of OSB2 are presented here with respect to the applicable parameters listed in Table 6.1. A schematic and node numbers of the OSB2 OpenSees model are shown in Figure 6.9. The global X direction is transverse while Y is longitudinal.
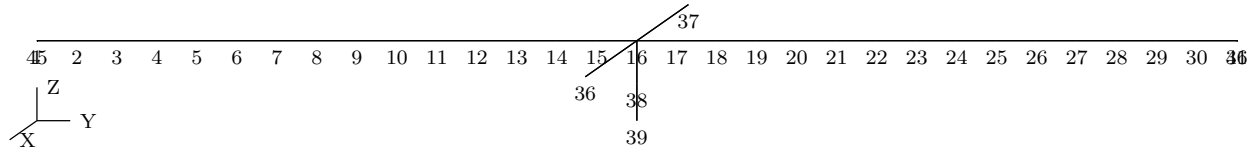
Figure 6.9: Node numbers for OpenSees model of OSB2.

6.4.1 Pushover Analysis

Pushover analysis of OSB2 in the transverse and longitudinal directions is shown in Figure 6.10 for the "matched to CSiBridge" and "sensitivity" OpenSees models. The pushover response is computed via a displacement-controlled analysis. Due to the differences in element and constitutive models between the "matched to CSiBridge" and "sensitivity" models, the initial stiffness differs slightly. In both the transverse and longitudinal directions, the post-yield load-displacement behavior differs considerably at low lateral displacements (less than 2 in) because the "sensitivity" model uses indefinite strain hardening and has a more accurate representation of the spread of plasticity along the column height. The "matched to CSiBridge" model uses the concrete and steel stress-strain responses as described in Chapter 4, plus had the inadvertent modeling choice that led to a very small plastic hinge length of 3.36 in that drastically reduced ductility (the results are slightly different to Figure 5.4 due to the use of the original abutment model in this chapter).

The sensitivity of the load factor, λ, with respect to the yield stress of the longitudinal reinforcing steel in the columns is computed via the DDM, as shown in Figure 6.11. The load factor is the multiplier applied to the entire lateral load on the bridge, not the base shear of the column. The sensitivity, $d\lambda/df_y$, is scaled by one standard deviation of f_y. In addition to putting the sensitivity in units of force, the plotted values represent the change in base shear for a one standard deviation increase in f_y. As was the case for OSB1, the steel yield strength has the largest influence on the lateral load-displacement response compared to the other RC column section properties listed in Table 6.7.

The maximum sensitivities of the load factor with respect the one standard deviation changes in all parameters defined for OSB2 are shown in Table 6.7. The stiffness and strength of the longitudinal abutment have a significant influence on the longitudinal pushover. The flexural and shear stiffnesses of the bridge superstructure appear to have a large effect on the load-displacement response; however, this is due to the boundary conditions of the abutments being set equal to those used in the CSiBridge model of OSB2, in which the abutments were
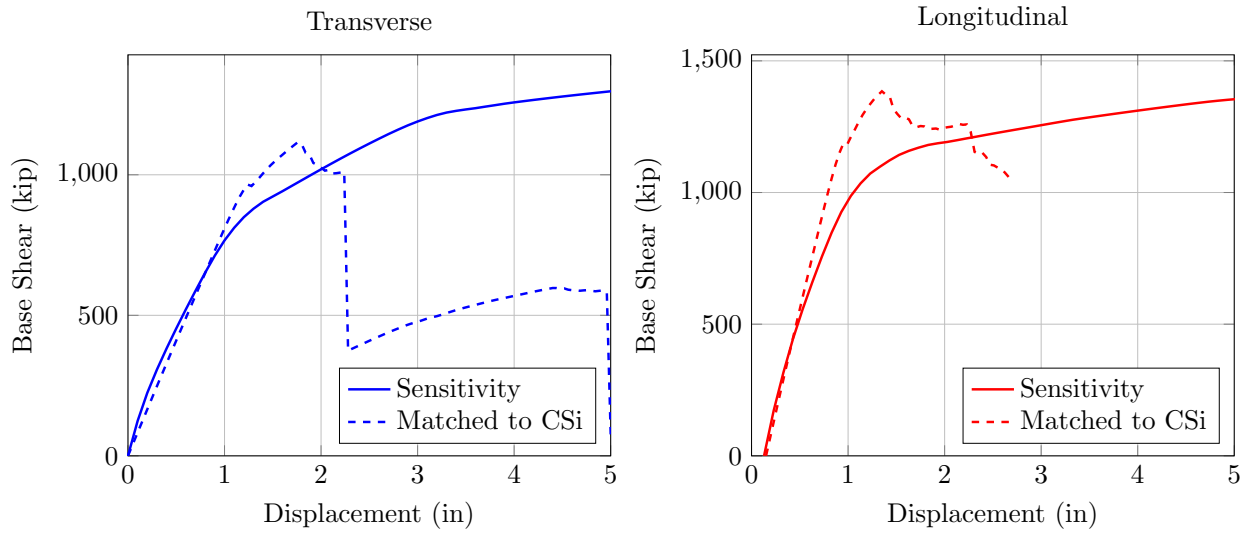
Figure 6.10: Comparison of lateral load-displacement response of OSB2 with original abutments for OpenSees models matched to CSiBridge and used for sensitivity.
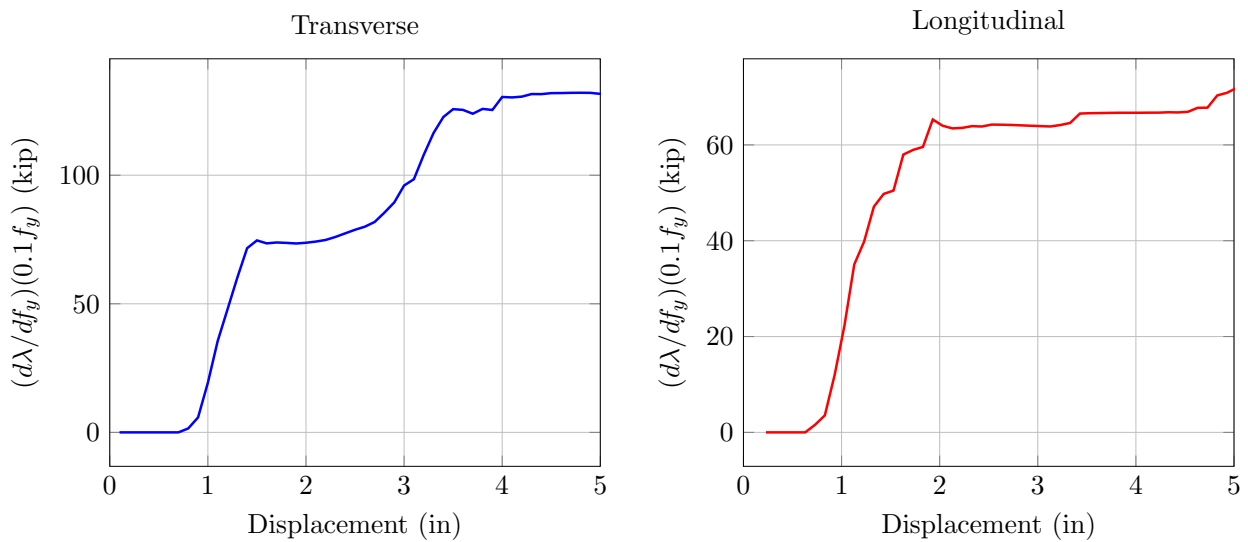
Figure 6.11: Sensitivity of OSB2 lateral load-displacement response with respect to one standard deviation increase in yield strength of the column longitudinal reinforcing steel.

over-restrained. In essence, the superstructure acts like a fixed-fixed elastic beam under transverse loading.

Table 6.7: Maximum load factor sensitivity for one standard deviation increase in each parameter for pushover analysis of OSB2 and corresponding lateral displacement where the maximum occurs.

Parameter	Transverse		Longitudinal	
	$\Delta\lambda$ (kip)	u (in)	$\Delta\lambda$ (kip)	u (in)
d_{col}	56.5	5.10	32.2	4.53
$f'_{c,cover}$	11.2	0.90	8.0	0.83
$f'_{c,core}$	49.4	4.90	26.3	1.93
f_y	132.1	4.80	71.9	5.03
$k_{gap,l}$	0.0	–	138.6	2.73
$F_{y,gap,l}$	0.0	–	154.7	4.93
E_{ss}	2416.4	5.10	52.5	0.33
G_{ss}	102.6	2.50	0.0	–

6.4.2 Nonlinear Time History Analysis

Nonlinear time history response for the deck displacement of OSB2 is shown in Figure 6.12. The dynamic response is computed with average acceleration Newmark time integration using a time step of 0.005 sec.
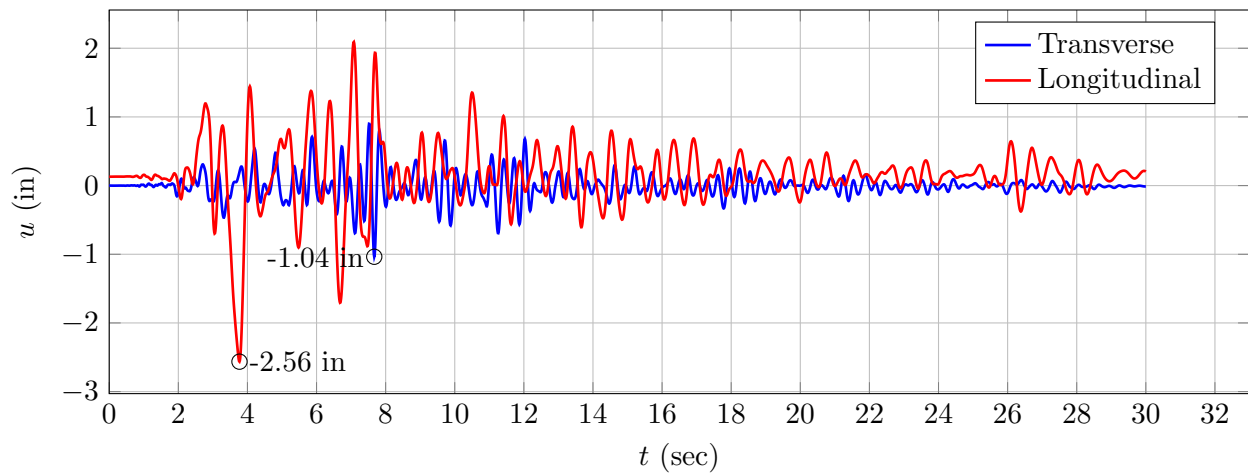
Figure 6.12: Nonlinear time history response of OSB2 for the ROCKN1N1 ground motion.

Peak values of deck displacement in the transverse and longitudinal directions are indicated in Figure 6.12 and agree well with the "matched to CSiBridge" results summarized in Table 6.1. Comparisons of the response time history for the "matched to CSiBridge" and

"sensitivity" models are made in Figure 6.13. Unlike OSB1, there are noticeable differences between the "matched" and "sensitivity" OpenSees models. This is a direct result of the differences in the lateral load-displacement response (Figure 6.10) at the displacement levels encountered in the time history response for earthquake loading.

Longitudinal

Transverse
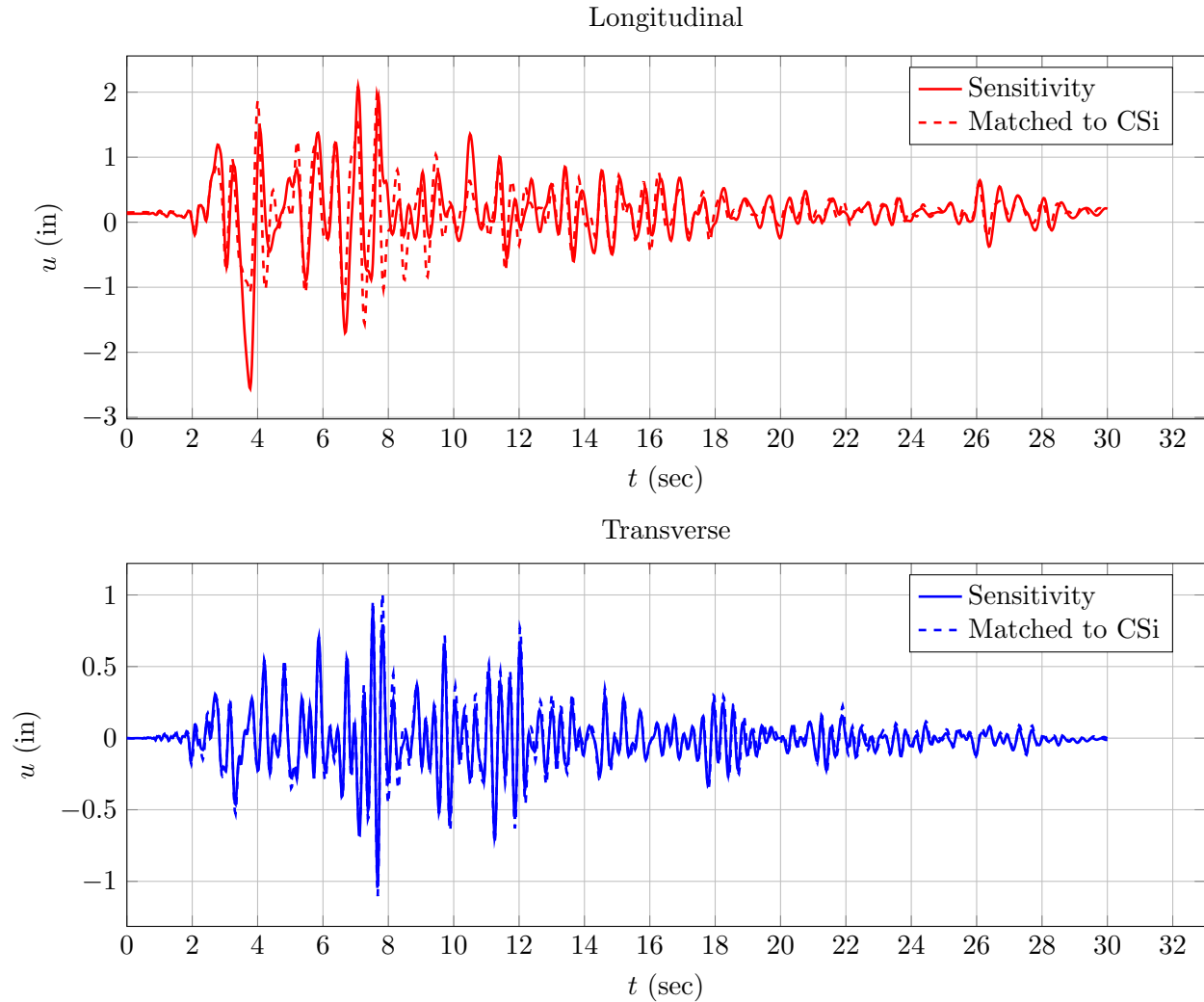
Figure 6.13: Comparison of nonlinear time history response of OSB2 for the ROCKN1N1 ground motion with original abutments for OpenSees models matched to CSiBridge and used for sensitivity.

The DDM time history of sensitivity of the deck displacement with respect to the yield strength of the column longitudinal reinforcing steel is shown in Figure 6.14. The computed sensitivity, du/df_y, is scaled by one standard deviation of the nominal value of f_y. This scaling puts the values on the vertical axis in to units of length and these values thus represent the change in displacement for a one standard deviation increase in f_y.

Similar plots of the deck displacement sensitivity with respect to the parameters listed in
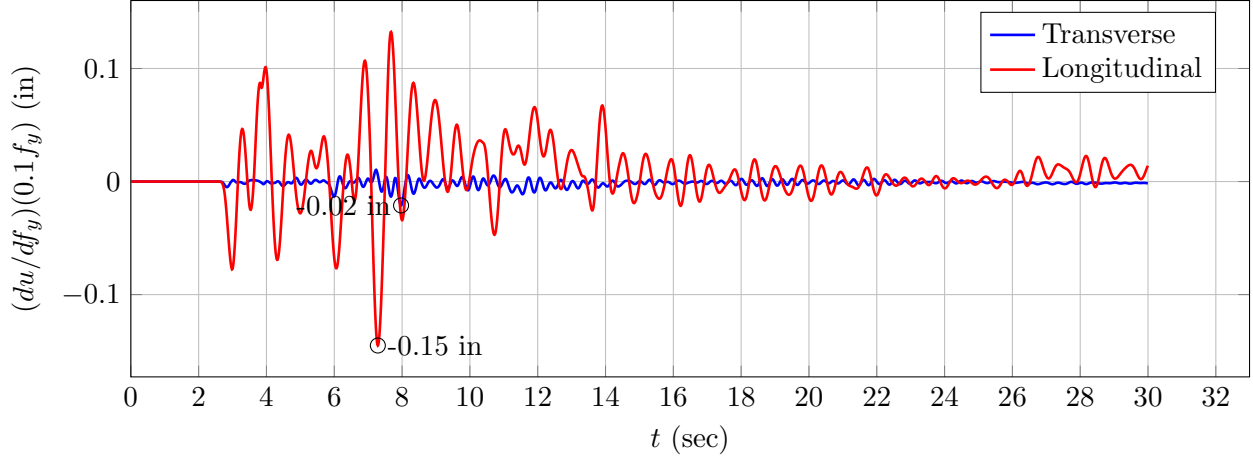
Figure 6.14: Sensitivity of nonlinear time history response with respect to one standard deviation increase in column longitudinal steel yield strength for OSB2 for the ROCKN1N1 ground motion.

Table 6.1 for OSB2 can be made. In lieu of showing all plots, Table 6.8 through 6.11 lists the maximum displacement sensitivity and the coincident time where it occurs for each parameter considering the four ground motions of this study. None of the parameters have a significant influence on the transverse displacement history. For the longitudinal displacement history, the RC column steel yield strength has the largest influence followed by the stiffness of the longitudinal abutment gap and the concrete compressive strength of the RC column core. Like in the static pushover analyses, the superstructure stiffness has a significant effect on the deck displacement due to the boundary conditions at the abutments.

Table 6.8: Maximum displacement sensitivity for one standard deviation increase in each parameter for NTHA of OSB2 and corresponding time where the maximum occurs for the ROCKN1N1 ground motion.

Parameter	Transverse		Longitudinal	
	Δu (in)	t (sec)	Δu (in)	t (sec)
d_{col}	-0.03	12.10	-0.09	2.92
$f'_{c,cover}$	0.0	–	-0.02	2.91
$f'_{c,core}$	0.02	12.24	-0.07	5.97
f_y	-0.02	7.97	-0.15	7.29
$k_{gap,l}$	0.0	–	0.09	3.91
$F_{y,gap,l}$	0.0	–	0.0	–
E_{ss}	-0.32	7.92	0.63	8.20
G_{ss}	-0.06	7.91	0.0	–

188

Table 6.9: Maximum displacement sensitivity for one standard deviation increase in each parameter for NTHA of OSB2 and corresponding time where the maximum occurs for the ROCKN1P1 ground motion.

Parameter	Transverse		Longitudinal	
	Δu (in)	t (sec)	Δu (in)	t (sec)
d_{col}	0.04	10.79	0.10	13.91
$f'_{c,cover}$	0.01	10.79	-0.02	10.12
$f'_{c,core}$	0.03	10.79	0.07	13.93
f_y	0.04	10.86	-0.17	11.38
$k_{gap,l}$	0.0	–	-0.01	11.34
$F_{y,gap,l}$	0.0	–	0.0	–
E_{ss}	0.55	10.81	0.49	12.33
G_{ss}	0.09	10.80	0.02	10.54

Table 6.10: Maximum displacement sensitivity for one standard deviation increase in each parameter for NTHA of OSB2 and corresponding time where the maximum occurs for the SANDN1N1 ground motion.

Parameter	Transverse		Longitudinal	
	Δu (in)	t (sec)	Δu (in)	t (sec)
d_{col}	0.05	12.60	0.16	36.22
$f'_{c,cover}$	0.01	12.59	0.03	11.77
$f'_{c,core}$	0.04	12.61	0.15	11.80
f_y	0.05	12.64	0.28	36.27
$k_{gap,l}$	0.0	–	-0.08	31.55
$F_{y,gap,l}$	0.0	–	-0.15	13.46
E_{ss}	0.67	12.62	-0.62	25.86
G_{ss}	0.12	12.94	0.02	24.58

Table 6.11: Maximum displacement sensitivity for one standard deviation increase in each parameter for NTHA of OSB2 and corresponding time where the maximum occurs for the CLAYN1N1 ground motion.

Parameter	Transverse		Longitudinal	
	Δu (in)	t (sec)	Δu (in)	t (sec)
d_{col}	-0.04	12.78	-0.26	26.45
$f'_{c,cover}$	-0.01	12.78	0.03	7.16
$f'_{c,core}$	-0.03	6.66	-0.15	26.45
f_y	-0.05	13.99	-0.66	26.45
$k_{gap,l}$	0.0	–	-0.10	26.43
$F_{y,gap,l}$	-0.02	15.44	-0.67	26.46
E_{ss}	0.64	14.17	0.69	7.14
G_{ss}	0.09	14.14	0.02	13.53

6.5 Response Sensitivity Analysis of OSB3

Sensitivity analysis of the nonlinear dynamic time history response of OSB3 is presented here with respect to the applicable parameters listed in Table 6.1. A schematic and node numbers of the OSB3 OpenSees model are shown in Figure 6.15. The global X direction is transverse while Y is longitudinal. Since the bridge deck rests on isolators at the bent and both abutments, only dynamic time history response is reported.
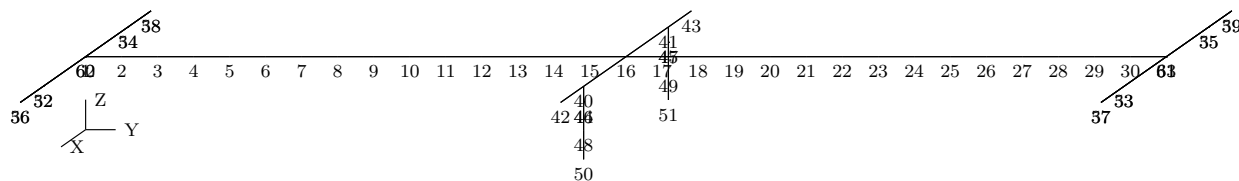
Figure 6.15: Node numbers for OpenSees model of OSB3.

Nonlinear time history response for the deck displacement of OSB3 is shown in Figure 6.16. The dynamic response is computed with average acceleration Newmark time integration using a time step of 0.005 sec.

Peak values of deck displacement in the transverse and longitudinal directions are indicated in Figure 6.16 and are compared with the "matched to CSiBridge" results summarized in Table 6.1. Comparisons of the response time history for the "matched to CSiBridge" and "sensitivity" models are made in Figure 6.17 where it is seen that the response is identical. This is due to the use of the same isolator models in the "matched" and "sensitivity" bridge models and the RC columns of the bent remaining in the elastic range of response. The displacement and force orbits and hysteresis of the bent and abutment isolators are shown in Figures 6.18 and 6.19, respectively.
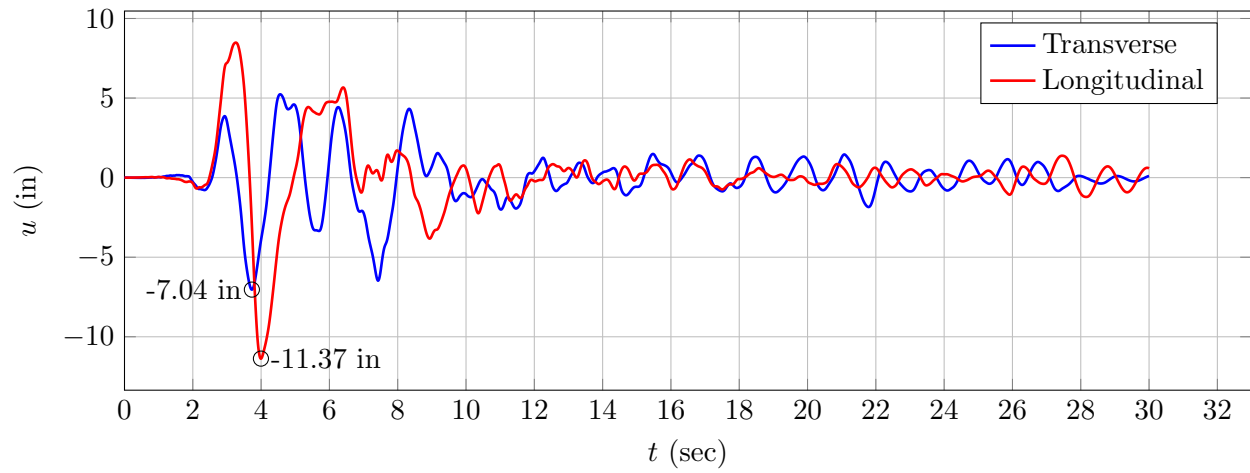
Figure 6.16: Nonlinear time history response of OSB3 for the ROCKN1N1 ground motion.
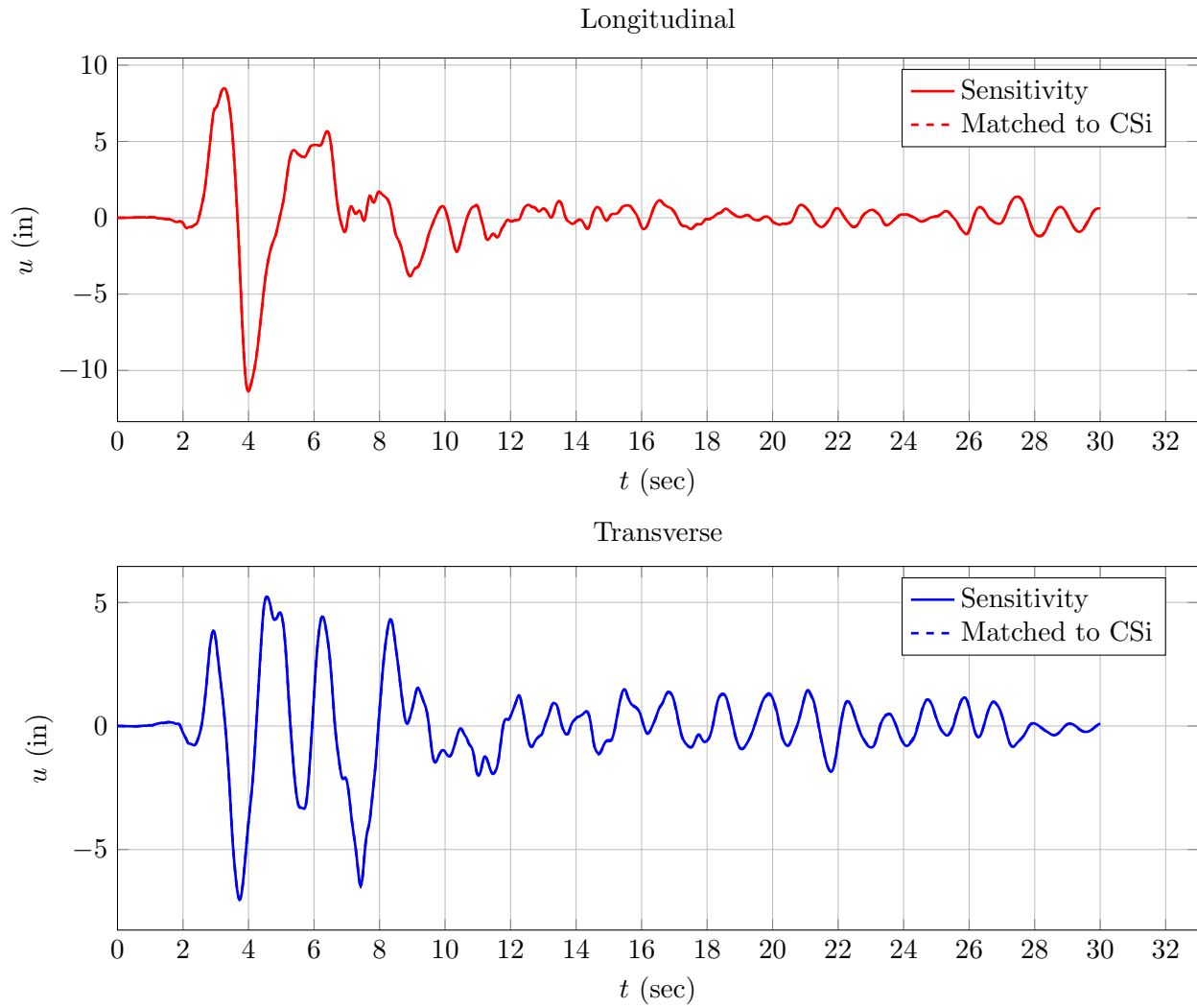
Figure 6.17: Comparison of nonlinear time history response of OSB3 for the ROCKN1N1 ground motion with original abutments for OpenSees models matched to CSiBridge and used for sensitivity.
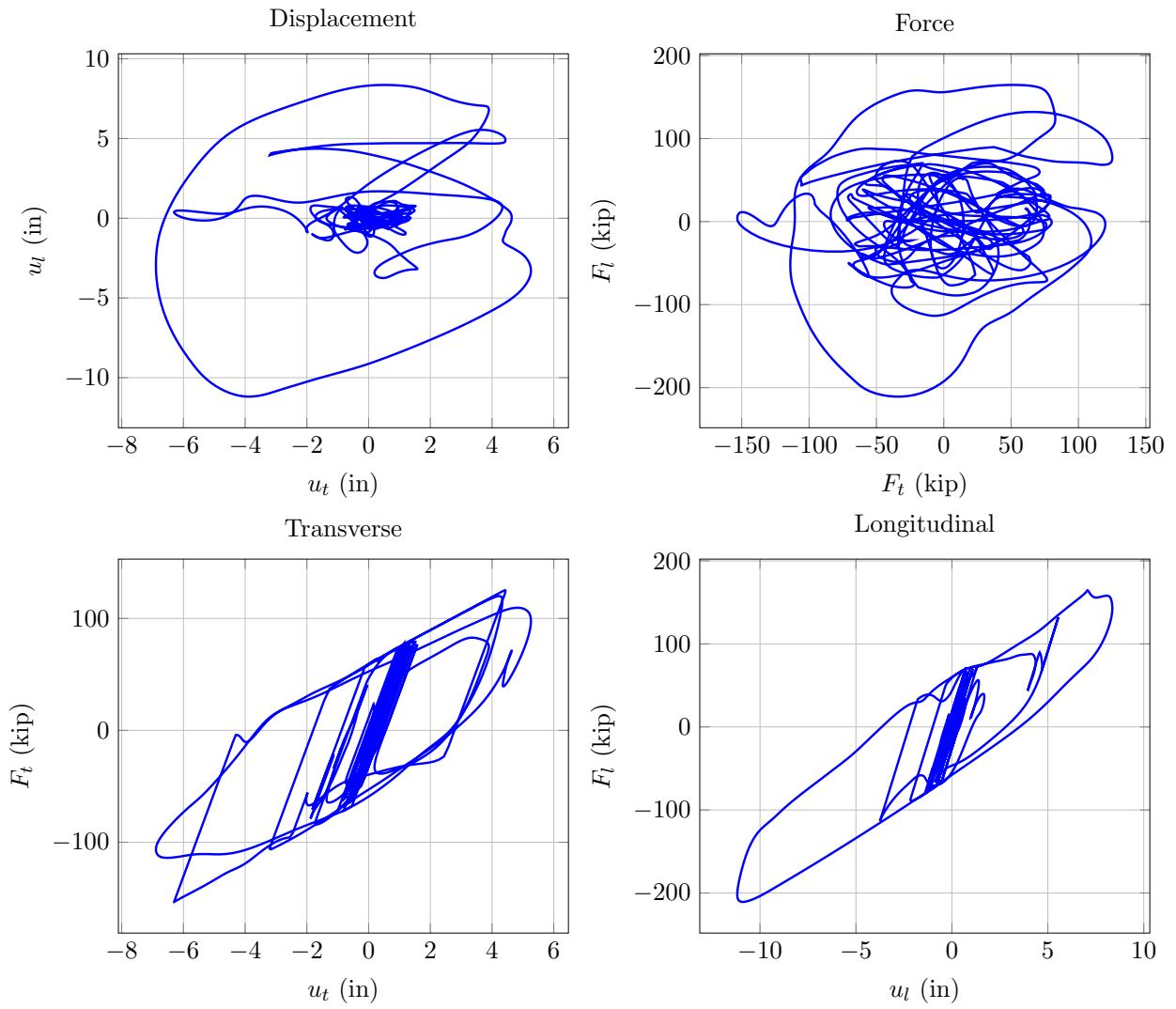
Figure 6.18: Displacement and force orbits and hysteresis of bent isolator of OSB3 for the ROCKN1N1 ground motion.
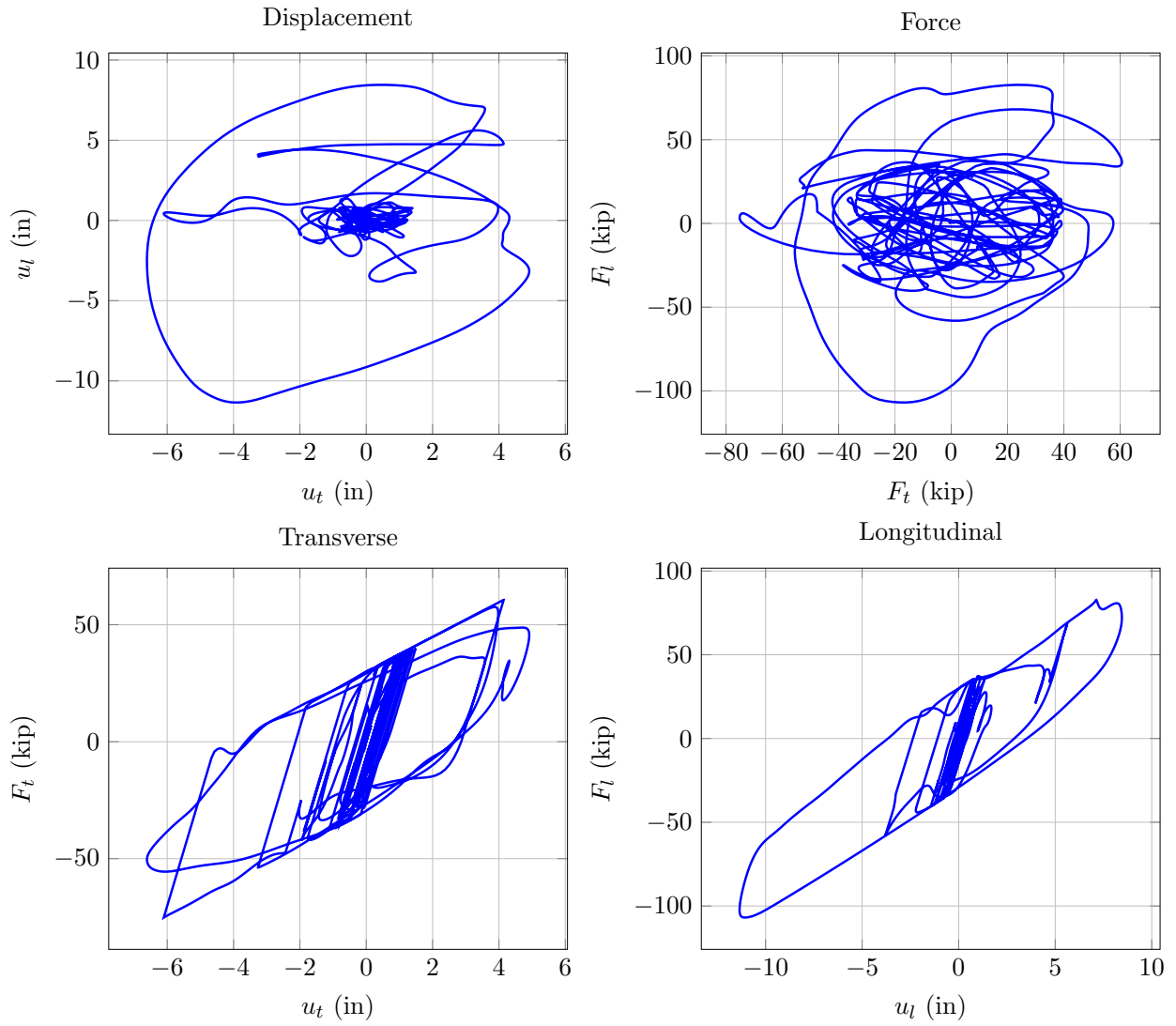
Figure 6.19: Displacement and force orbits and hysteresis of abutment isolator of OSB3 for the ROCKN1N1 ground motion.

The DDM time history of sensitivity of the deck displacement with respect to the yield force of the bent and abutment isolators is shown in Figure 6.20 and 6.21, respectively. The computed sensitivities are scaled by one standard deviation of the nominal parameter values. This scaling puts the values on the vertical axis in to units of length and these values thus represent the change in displacement for a one standard deviation increase in isolator strengths.
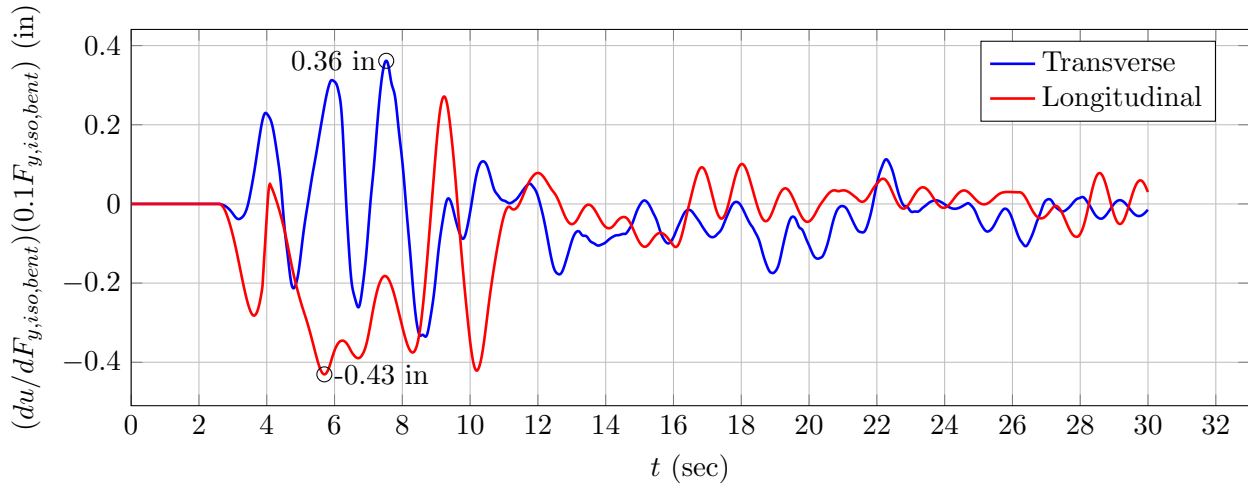
Figure 6.20: Sensitivity of nonlinear time history response with respect to one standard deviation increase in bent isolator strength for OSB3 for the ROCKN1N1 ground motion.
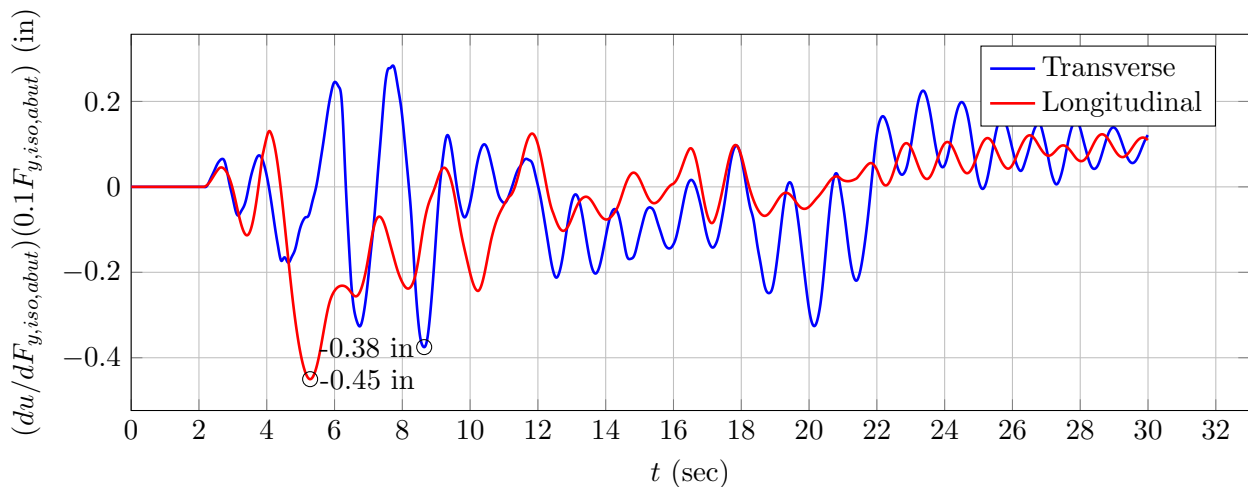
Figure 6.21: Sensitivity of nonlinear time history response with respect to one standard deviation increase in abutment isolator strength for OSB3 for the ROCKN1N1 ground motion.

Similar plots of the deck displacement sensitivity with respect to the parameters listed in Table 6.1 for OSB3 can be made. In lieu of showing all plots, Tables 6.12 through 6.15

195

list the maximum displacement sensitivity and the coincident time where it occurs for each parameter. As expected for an isolated bridge deck, the RC column properties do not have any appreciable influence on the deck displacement. In addition, the stiffness and strength of the abutment and bent isolators as well as the stiffness and strength of the abutment gap models have a very low influence on the deck displacement. Due to the isolator bearings between the superstructure and the bent and abutments, the stiffness of the superstructure has very little effect on the deck displacement.

Table 6.12: Maximum displacement sensitivity for one standard deviation increase in each parameter for NTHA of OSB3 and corresponding time where the maximum occurs for the ROCKN1N1 ground motion.

Parameter	Transverse		Longitudinal	
	Δu (in)	t (sec)	Δu (in)	t (sec)
d_{col}	0.0	–	0.0	–
$f'_{c,cover}$	0.0	–	0.0	–
$f'_{c,core}$	0.0	–	0.0	–
f_y	0.0	–	0.0	–
$k_{iso,bent}$	0.37	24.36	-0.32	5.07
$F_{y,iso,bent}$	0.36	7.53	-0.43	5.70
$k_{iso,abut}$	0.22	24.30	0.25	29.64
$F_{y,iso,abut}$	-0.38	8.64	-0.45	5.28
$k_{gap,l}$	-0.14	4.92	-0.18	4.55
$F_{y,gap,l}$	-0.24	4.93	-0.47	4.25
$k_{gap,t}$	0.18	3.79	0.12	9.25
$F_{y,gap,t}$	-0.84	6.91	0.50	4.79
E_{ss}	0.07	3.79	-0.03	6.34
G_{ss}	0.0	–	0.0	–

Table 6.13: Maximum displacement sensitivity for one standard deviation increase in each parameter for NTHA of OSB3 and corresponding time where the maximum occurs for the ROCKN1P1 ground motion.

Parameter	Transverse		Longitudinal	
	Δu (in)	t (sec)	Δu (in)	t (sec)
d_{col}	0.0	–	0.0	–
$f'_{c,cover}$	0.0	–	0.0	–
$f'_{c,core}$	0.0	–	0.0	–
f_y	0.0	–	0.0	–
$k_{iso,bent}$	0.26	25.65	-0.19	8.35
$F_{y,iso,bent}$	-0.14	10.71	-0.22	11.05
$k_{iso,abut}$	-0.25	25.07	-0.22	8.35
$F_{y,iso,abut}$	0.18	22.58	-0.25	13.88
$k_{gap,l}$	0.0	–	0.0	–
$F_{y,gap,l}$	0.0	–	0.0	–
$k_{gap,t}$	-0.14	11.85	-0.11	12.14
$F_{y,gap,t}$	-0.58	11.54	0.25	14.07
E_{ss}	-0.08	11.81	-0.03	12.12
G_{ss}	0.0	–	0.0	–

Table 6.14: Maximum displacement sensitivity for one standard deviation increase in each parameter for NTHA of OSB3 and corresponding time where the maximum occurs for the SANDN1N1 ground motion.

Parameter	Transverse		Longitudinal	
	Δu (in)	t (sec)	Δu (in)	t (sec)
d_{col}	0.03	21.66	-0.02	21.15
$f'_{c,cover}$	0.02	21.66	-0.01	21.16
$f'_{c,core}$	0.03	21.66	-0.02	21.16
f_y	0.0	–	0.0	–
$k_{iso,bent}$	1.97	21.65	-1.38	21.16
$F_{y,iso,bent}$	-0.84	21.83	-0.73	32.32
$k_{iso,abut}$	0.27	21.54	0.20	27.89
$F_{y,iso,abut}$	0.92	21.52	-0.76	21.16
$k_{gap,l}$	-0.20	34.08	-0.34	32.44
$F_{y,gap,l}$	-1.93	21.65	-1.55	22.00
$k_{gap,t}$	-0.22	21.60	-0.23	32.53
$F_{y,gap,t}$	-0.78	20.55	-0.41	21.20
E_{ss}	-0.14	21.57	-0.08	13.77
G_{ss}	0.0	–	0.0	–

Table 6.15: Maximum displacement sensitivity for one standard deviation increase in each parameter for NTHA of OSB3 and corresponding time where the maximum occurs for the CLAYN1N1 ground motion.

Parameter	Transverse		Longitudinal	
	Δu (in)	t (sec)	Δu (in)	t (sec)
d_{col}	0.01	21.57	0.02	15.93
$f'_{c,cover}$	0.0	–	0.0	–
$f'_{c,core}$	0.0	–	0.01	15.90
f_y	0.0	–	0.0	–
$k_{iso,bent}$	0.57	21.57	0.75	15.91
$F_{y,iso,bent}$	-0.87	33.03	-0.86	26.70
$k_{iso,abut}$	0.26	21.58	-0.22	26.71
$F_{y,iso,abut}$	-1.02	32.91	0.71	40.56
$k_{gap,l}$	-0.36	23.14	0.33	22.59
$F_{y,gap,l}$	3.27	27.73	2.54	26.73
$k_{gap,t}$	-0.21	12.69	0.21	14.42
$F_{y,gap,t}$	-1.01	21.62	-0.82	16.41
E_{ss}	0.11	21.54	-0.05	17.53
G_{ss}	0.0	–	0.0	–

6.6 Response Sensitivity Analysis of OSB4

Sensitivity analysis of the nonlinear dynamic time history response of OSB4 is presented here with respect to the applicable parameters listed in Table 6.1. A schematic and node numbers of the OSB4 OpenSees model are shown in Figure 6.22. The global X direction is transverse while Y is longitudinal. Since the bridge deck rests on isolators at the bent and both abutments, only dynamic time history response is reported.
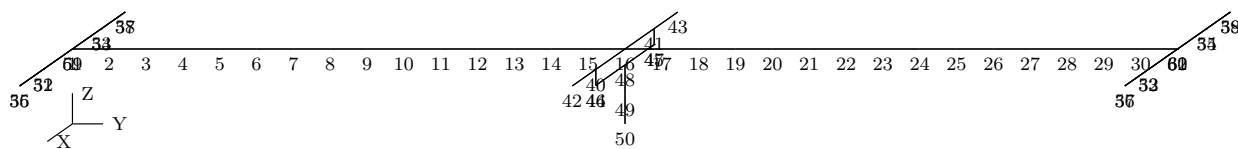
Figure 6.22: Node numbers for OpenSees model of OSB4.

Nonlinear time history response for the deck displacement of OSB4 is shown in Figure 6.23. The dynamic response is computed with average acceleration Newmark time integration using a time step of 0.005 sec.

Peak values of deck displacement in the transverse and longitudinal directions are indicated in Figure 6.23 and are compared with the "matched to CSiBridge" results summarized in Table 6.1. Comparisons of the response time history for the "matched to CSiBridge" and "sensitivity" models are made in Figure 6.24 where it is seen that the response is identical.
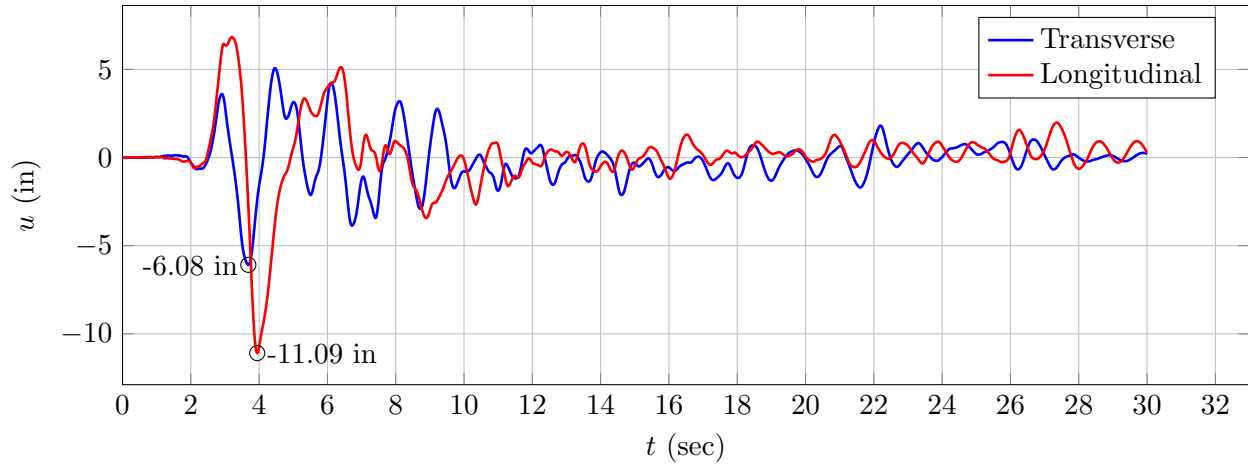
Figure 6.23: Nonlinear time history response of OSB4 for the ROCKN1N1 ground motion.

This is due to the use of the same isolator models in the "matched" and "sensitivity" bridge models and the RC columns of the bent remaining in the elastic range of response. The displacement and force orbits and hysteresis of the bent and abutment isolators are shown in Figures 6.25 and 6.26, respectively.
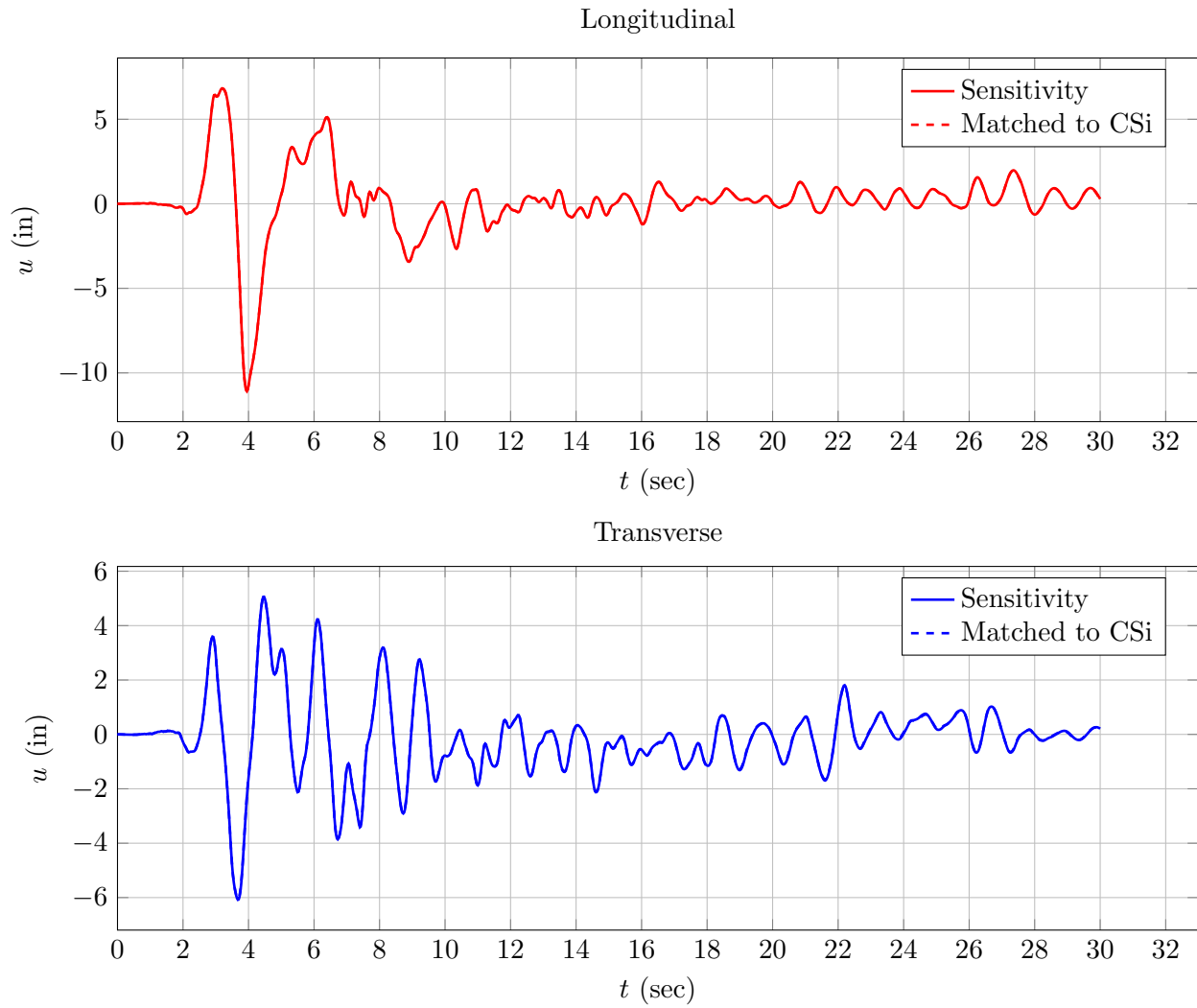
Figure 6.24: Comparison of nonlinear time history response of OSB4 for the ROCKN1N1 ground motion with original abutments for OpenSees models matched to CSiBridge and used for sensitivity.
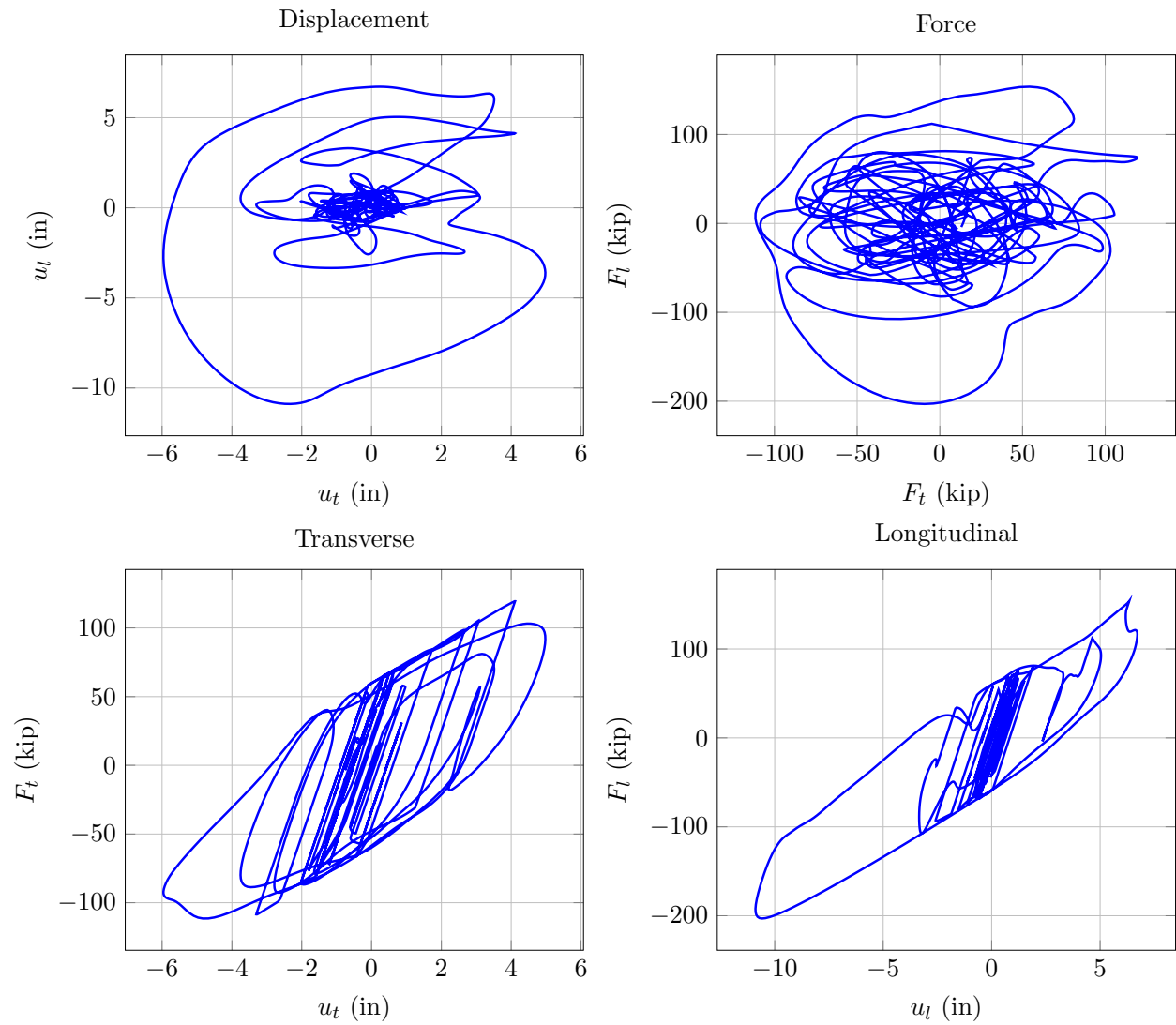
Figure 6.25: Displacement and force orbits and hysteresis of bent isolator of OSB4 for the ROCKN1N1 ground motion.
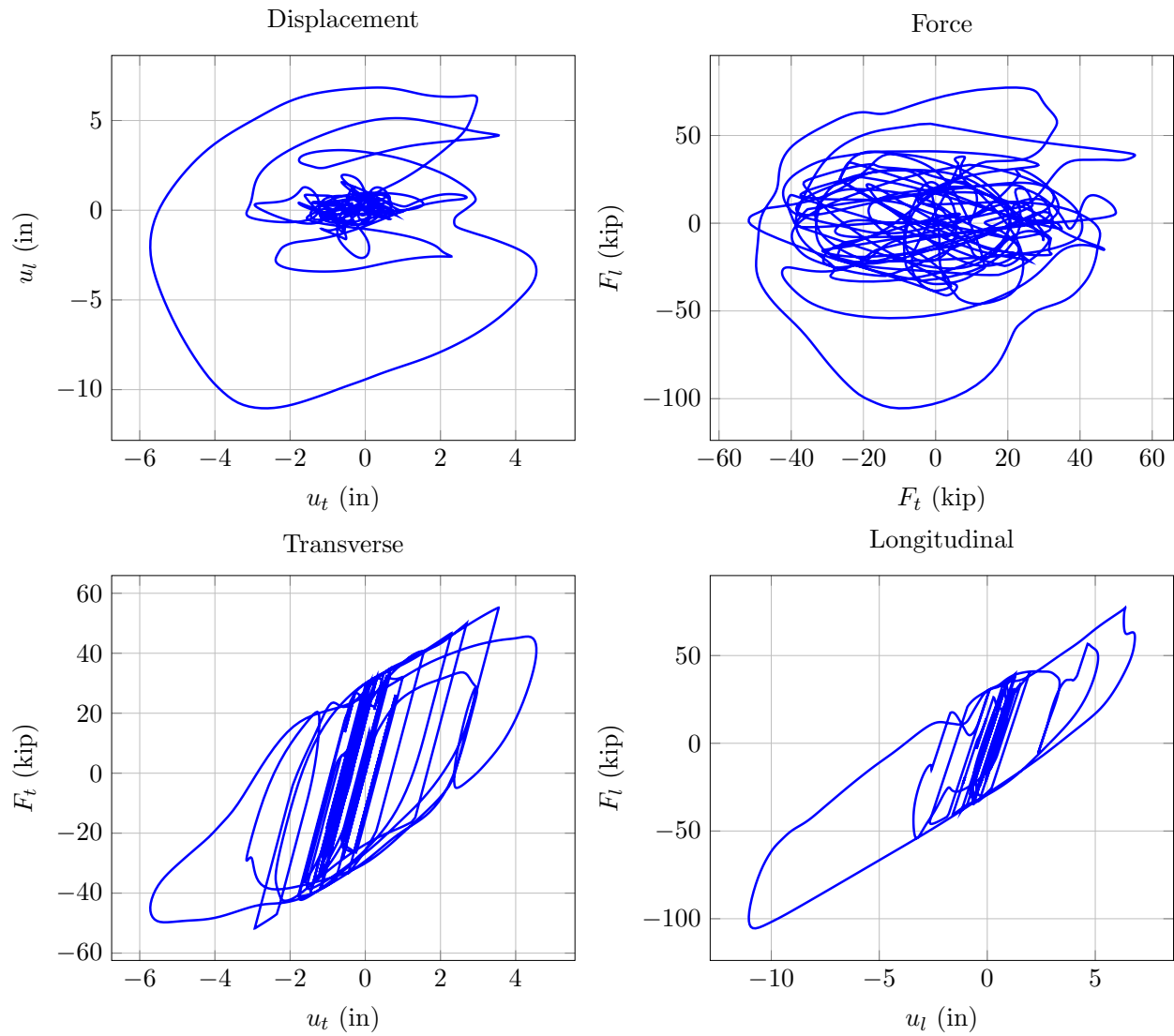
Figure 6.26: Displacement and force orbits and hysteresis of abutment isolator of OSB4 for the ROCKN1N1 ground motion.

The DDM time history of sensitivity of the deck displacement with respect to the yield force of the bent and abutment isolators is shown in Figure 6.27 and 6.28, respectively. The computed sensitivities are scaled by one standard deviation of the nominal parameter values. This scaling puts the values on the vertical axis in to units of length and these values thus represent the change in displacement for a one standard deviation increase in isolator strengths.
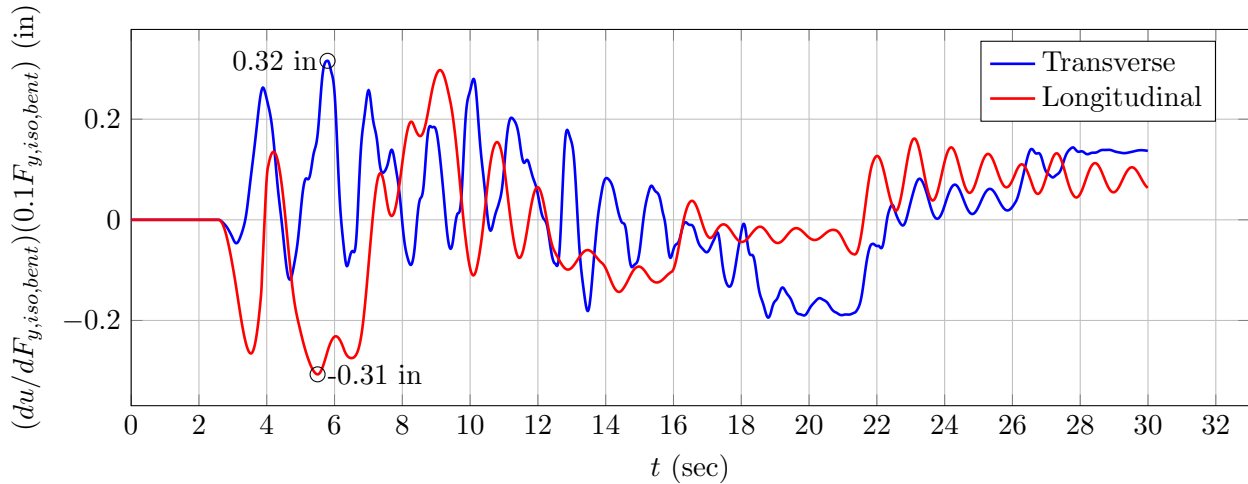
Figure 6.27: Sensitivity of nonlinear time history response with respect to one standard deviation increase in bent isolator strength for OSB4 for the ROCKN1N1 ground motion.
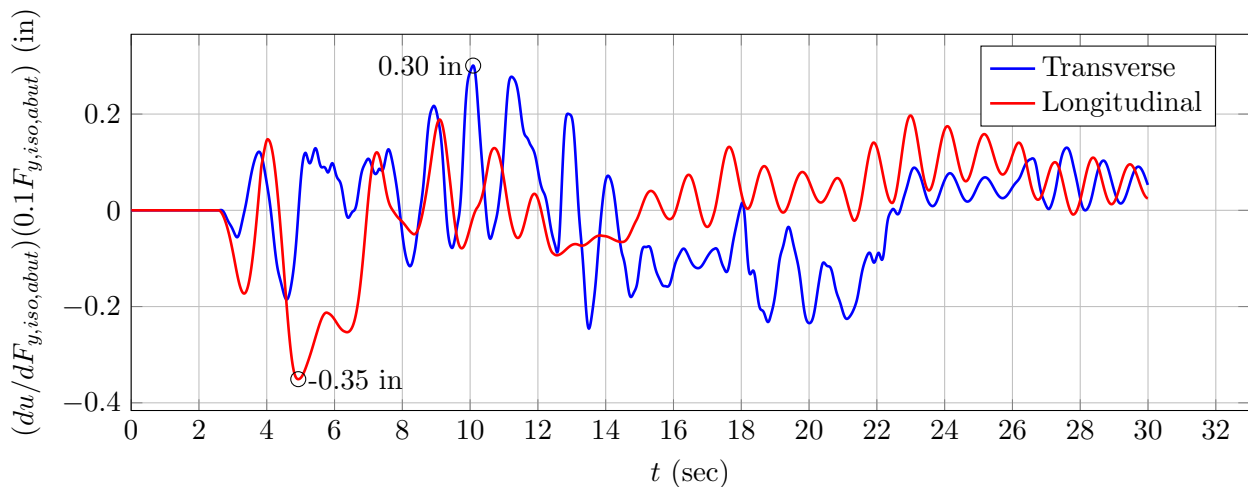
Figure 6.28: Sensitivity of nonlinear time history response with respect to one standard deviation increase in abutment isolator strength for OSB4 for the ROCKN1N1 ground motion.

Similar plots of the deck displacement sensitivity with respect to the parameters listed in Table 6.1 for OSB4 can be made. In lieu of showing all plots, Tables 6.16 through 6.19

203

list the maximum displacement sensitivity and the coincident time where it occurs for each parameter. As expected for an isolated bridge deck, the RC column properties do not have any appreciable influence on the deck displacement. In addition, the stiffness and strength of the abutment and bent isolators as well as the stiffness and strength of the abutment gap models have a very low influence on the deck displacement. The stiffness of the superstructure also has relatively little effect on the deck displacement.

Table 6.16: Maximum displacement sensitivity for one standard deviation increase in each parameter for NTHA of OSB4 and corresponding time where the maximum occurs for the ROCKN1N1 ground motion.

Parameter	Transverse		Longitudinal	
	Δu (in)	t (sec)	Δu (in)	t (sec)
d_{col}	0.0	–	0.0	–
$f'_{c,cover}$	0.0	–	0.0	–
$f'_{c,core}$	0.01	11.15	0.01	3.84
f_y	0.0	–	0.0	–
$k_{iso,bent}$	0.30	11.14	-0.28	4.74
$F_{y,iso,bent}$	0.32	5.79	-0.31	5.50
$k_{iso,abut}$	0.18	19.00	0.32	29.36
$F_{y,iso,abut}$	0.30	10.09	-0.35	4.93
$k_{gap,l}$	-0.10	5.20	-0.11	4.46
$F_{y,gap,l}$	-0.46	5.21	-0.49	4.26
$k_{gap,t}$	0.44	9.12	-0.21	9.46
$F_{y,gap,t}$	-0.78	4.84	0.40	4.74
E_{ss}	0.19	7.85	-0.18	8.97
G_{ss}	0.01	8.81	0.01	6.92

Table 6.17: Maximum displacement sensitivity for one standard deviation increase in each parameter for NTHA of OSB4 and corresponding time where the maximum occurs for the ROCKN1P1 ground motion.

Parameter	Transverse		Longitudinal	
	Δu (in)	t (sec)	Δu (in)	t (sec)
d_{col}	0.0	–	-0.01	11.96
$f'_{c,cover}$	0.0	–	0.0	–
$f'_{c,core}$	0.0	–	-0.01	11.96
f_y	0.0	–	0.0	–
$k_{iso,bent}$	-0.15	12.62	-0.33	11.97
$F_{y,iso,bent}$	0.31	12.55	-0.23	10.97
$k_{iso,abut}$	0.18	24.20	0.29	24.38
$F_{y,iso,abut}$	0.19	18.84	-0.30	12.09
$k_{gap,l}$	0.0	–	0.0	–
$F_{y,gap,l}$	0.0	–	0.0	–
$k_{gap,t}$	0.18	12.88	-0.16	14.26
$F_{y,gap,t}$	-0.56	12.89	0.31	14.24
E_{ss}	0.13	14.45	-0.07	11.96
G_{ss}	0.0	–	-0.02	11.92

Table 6.18: Maximum displacement sensitivity for one standard deviation increase in each parameter for NTHA of OSB4 and corresponding time where the maximum occurs for the SANDN1N1 ground motion.

Parameter	Transverse		Longitudinal	
	Δu (in)	t (sec)	Δu (in)	t (sec)
d_{col}	0.02	26.95	-0.01	33.60
$f'_{c,cover}$	0.0	–	0.0	–
$f'_{c,core}$	0.02	46.09	-0.02	33.61
f_y	0.0	–	0.0	–
$k_{iso,bent}$	0.48	26.95	-0.43	33.60
$F_{y,iso,bent}$	0.68	28.88	-0.53	23.09
$k_{iso,abut}$	0.30	66.72	0.28	32.42
$F_{y,iso,abut}$	0.79	28.86	-0.56	23.00
$k_{gap,l}$	-0.07	32.40	-0.13	32.34
$F_{y,gap,l}$	0.25	20.86	-0.42	20.39
$k_{gap,t}$	-0.51	32.67	-0.40	32.63
$F_{y,gap,t}$	-1.01	20.21	-0.51	21.01
E_{ss}	0.42	20.54	-0.28	20.44
G_{ss}	0.03	26.94	-0.03	33.52

Table 6.19: Maximum displacement sensitivity for one standard deviation increase in each parameter for NTHA of OSB4 and corresponding time where the maximum occurs for the CLAYN1N1 ground motion.

	Transverse		Longitudinal	
Parameter	Δu (in)	t (sec)	Δu (in)	t (sec)
d_{col}	0.02	16.07	0.03	15.63
$f'_{c,cover}$	0.0	–	0.01	15.63
$f'_{c,core}$	0.03	16.07	0.04	15.62
f_y	0.0	–	0.0	–
$k_{iso,bent}$	-0.61	23.03	0.88	15.64
$F_{y,iso,bent}$	-0.60	20.31	0.83	41.20
$k_{iso,abut}$	-0.22	22.98	0.33	41.14
$F_{y,iso,abut}$	-0.51	42.20	1.01	41.13
$k_{gap,l}$	-0.15	19.45	0.25	26.89
$F_{y,gap,l}$	1.37	23.05	2.54	26.75
$k_{gap,t}$	-0.34	30.18	-0.26	34.33
$F_{y,gap,t}$	-1.03	15.34	-0.63	16.41
E_{ss}	-0.27	20.52	0.24	21.95
G_{ss}	0.05	21.26	0.03	15.63

6.7 Summary

While there is significant uncertainty in the response of each OSB based on the element formulations and constitutive models used for the columns, abutments, and isolators, sensitivity analysis based on the direct differentiation method can show which parameters within a given model have the greatest influence on the bridge response. Based on the foregoing sensitivity analyses, it is clear that modeling decisions on abutment response play a significant role in nonlinear static and dynamic analyses. As expected, the stiffness and strength of isolators in bridges with isolated superstructures (OSB3 and OSB4) play a key role. Simply constraining the ends of the superstructure from translation and rotation, as was done for OSB2, can lead to overestimates of the importance of the deck stiffness on nonlinear response.

Chapter 7

Modeling Recommendations

Based on the analyses conducted in Chapter 3 through Chapter 6, several recommendations can be made on best modeling practices. The recommendations can be divided into two main parts. The first part relates to the choices of models themselves, i.e., element formulation, constitutive models, boundary conditions, etc. The second part relates to the parameters of the models selected. Specifically, in Chapters 3, 4, 5, the effect of element and constitutive model choice was studied relative to nonlinear response. Whereas in Chapter 6, a "best" model was attempted based on the bridge drawings, not necessarily to satisfy some previous calibration studies. This model was then held constant while sensitivity analysis was performed on the parameters specific to the materials and elements employed.

In summary, it was demonstrated that although there are many important aspects to NTHA, the primary driver is the boundary conditions at the abutments. The column models and constitutive model choices are important, as are the properties of the remaining elastic elements, time integration scheme, damping, etc.; however, the choice of boundary condition, specifically the properties of the nonlinear springs and/or single-point constraints at deck ends drive the elastic and inelastic analysis responses. The order of magnitude of the model error associated with the choices of the abutment parameters suggests that future work should be focused on better experimental and analytical study at these locations, rather than solely on columns. The results should not be extrapolated beyond the types of bridges considered in the present study without further validation, meaning ordinary standard bridges with no skew, either one- or two-column bents, and limited span lengths. Clearly the response sensitivity to the boundary condition parameters is minimized as the number and length of spans increases.

7.1 Benchmark Columns

The bridge analyst should select a modeling approach for nonlinear response of columns. Two common choices are lumped and distributed plasticity. It was demonstrated that both CSiBridge and OpenSees can be used to correctly implement a lumped plasticity approach for 2D and 3D analysis of simple steel and concrete cross sections, relative to the exact so-

lution based on Euler-Bernoulli assumptions. However, once a reinforced concrete section is used and column in double curvature is analyzed, the CSiBridge results begin to diverge from the reference solution. OpenSees can be used to correctly implement the distributed plasticity approach, again relative to the reference solution. In both the lumped and distributed plasticity cases, the explicit consideration of the cross section with associated uniaxial constitutive models should be used to account for axial-moment interaction, as well as excitation about an arbitrary axis for the cross section. The location of the integration point should be at the location of peak moment (i.e., base of cantilever column) otherwise the yield and ultimate loads will be over predicted. The consequence is that preserving the yield force will necessarily lead to a different stiffness, because of the series arrangement of the elements in the lumped approach.

Another item of considerable interest to analysts is how one may modify the behavior of the lumped plasticity models to more closely approximate those of the distributed plasticity ones. This is a problem common to bridge modelers and building modelers. The latter typically modify the elastic properties of the element joining the hinges, whereas the former typically modify the hinge region as well as the elastic element joining the hinges. The results demonstrate that introducing a rigid element (rigid here can be approximated as 3–10 times the original elastic stiffness) equal in length to the plastic hinge length is a good way of approximately correcting the initial elastic stiffness. The yield force is again preserved if the integration point for the hinge remains at the location of peak moment (not in the middle of the hinge region). A consequence of the rigid hinge region is that the post-yielding stiffness is only approximately correct, and consequently also any softening that occurs at larger displacement demands.

For cross sections that change properties (i.e., crack) during loading, the use of a modifier on the elastic properties of the element between the hinges will lead to an underestimate of the initial elastic stiffness, overestimate of the post-cracking stiffness, and variable post-yield hardening and softening stiffnesses. While not quantified directly in this report, the unloading stiffness will similarly be modified in such an approach, which will lead to perhaps unanticipated changes relative to the hysteretic rule choices made at the constitutive model level.

7.2   Benchmark Bridges

Given the ability of both CSiBridge and OpenSees to solve benchmark column problems using lumped plasticity, the response of four OSBs were studied under different analysis cases: modal analysis, nonlinear static pushover, and NTHA. Careful attention was given to ensure that model basics were common in the two implementations: geometry (nodal and element), mass distribution, properties of the elastic elements, properties (not necessarily parameters) of the nonlinear elements, loads (gravity and lateral load patterns, ground motions, etc. where appropriate), and boundary conditions.

It was demonstrated that the two software implementations could be used to generate nominally similar responses for OSB1 and OSB2 if the criteria shown in Table 7.1 were met

(all of the items checked in a given column are necessary in order to standardize the particular response). The last row of the table indicates the level of match attained. It is important to note that it was not possible to exactly match the concrete constitutive softening and cyclic behaviors (see Chapter 4), so the results presented in this report do not match exactly for OSB1 and OSB2, even for the roller abutment case.

Table 7.1: Criteria for matching OSB1 and OSB2 responses between CSiBridge and OpenSees implementations

Inputs	General		Roller abutment			Original abutment		
	Section[1]	Hinge[2]	Modal	Pushover	NTHA	Modal	Pushover	NTHA
Column steel constitutive model backbone	✓	✓	✓	✓	✓	✓	✓	✓
Column steel constitutive model softening		✓		✓	✓		✓	✓
Column steel constitutive model cyclic					✓			✓
Column concrete constitutive model backbone	✓	✓	✓	✓	✓	✓	✓	✓
Column concrete constitutive model softening	✓	✓		✓	✓		✓	✓
Column concrete constitutive model cyclic					✓			✓
Abutment spring model backbone						✓	✓	✓
Abutment spring model cyclic						✓	✓	✓
Overall level of match achieved	High	Med.	High[3]	Med.	High	High[3]	High	Low

[1] Section indicates moment-curvature analysis (monotonically increasing curvature demand)

[2] Hinge indicates hinge pushover analysis (monotonically increasing displacement demand)

[3] OSB3 and OSB4 do not match the isolation modes, potentially due to the different linear properties assigned to the isolator elements

The criteria necessary to standardize the particular responses for OSB3 and OSB4 were not dependent on the column constitutive models and elements. Therefore, the table is not repeated here. However, for the OSB3 and OSB4 time history responses using the roller abutment model, even standardization of the bent isolator hysteresis was not sufficient to match the magnitudes of the peak displacement demands exactly.

Based on the experiences of attempting to standardize responses using complete bridge models, the following modeling suggestions and best practices can be stated:

- It is necessary to have transparency for the user to understand resulting stress-strain responses from constitutive model parameter choices.

- Similar transparency is required for hysteretic rules that govern the cyclic stress-strain response.

- Rigid offsets should be added to the model explicitly through geometric transformations or through the use of approximately rigid elements, not by modifying the properties of a plastic hinge.

- The same hinge modeling guidelines as stated in the previous section should be applied to the bridge models.

- The methods of correcting the hinge responses have merit for modal and pushover analysis; however, the beamWithHinges element or a similar implementation should be used for NTHA if the user wishes to retain the notion of a fixed hinge length.

- The ultimate confined concrete strain is an important parameter. Concrete04 in OpenSees assumes the strength drops to zero beyond this value, so increasing the ultimate strain based on experimentally-based evidence (or use of Concrete02 or other strategies with residual strength) may be appropriate.

- While many studies have been conducted on calibrating longitudinal spring properties for the abutments (often series or parallel combinations of springs), it is clear the backbone behaviors alone are not sufficient for NTHA.

- The ad hoc approaches to the transverse abutment spring properties (including shear keys) or single-point constraints need to be investigated, particularly in reference to the previous point and coupled 3D NTHA.

Standard advice would also dictate that any software package should be used with caution as it is not always clear, even with documentation, what is the exact behavior of each element and constitutive model.

7.3   Parameter Sensitivity

With the confidence that the nonlinear static and dynamic time history analysis of an OSB can be replicated between CSiBridge and OpenSees, a further question is the importance of modeling assumptions and parameter values on the response within one of these softwares. With the DDM sensitivity capabilities of OpenSees, sensitivity analyses of the four OSBs showed that the abutment models have the greatest influence on the lateral load-displacement response as well as on the NTHA for four ground motions. The most influential parameter,

i.e., the parameter that leads to the largest change in transverse and longitudinal response for a one standard deviation increase in the parameter value, is listed in Table 7.2 and Table 7.3, respectively. The meaning of each parameter is listed in Table 6.1.

Table 7.2: Parameter with most significant effect on transverse response of each OSB due to one standard deviation increase in its value.

	Pushover	ROCKN1N1	ROCKN1P1	SANDN1N1	CLAYN1N1
OSB1	$k_{gap,t}$	$k_{gap,t}$	$k_{gap,t}$	$k_{gap,t}$	$k_{gap,t}$
OSB2	E_{ss}	E_{ss}	E_{ss}	E_{ss}	E_{ss}
OSB3	–	$F_{y,gap,t}$	$F_{y,gap,t}$	$k_{iso,bent}$	$F_{y,gap,l}$
OSB4	–	$F_{y,gap,t}$	$F_{y,gap,t}$	$F_{y,gap,t}$	$F_{y,gap,l}$

Table 7.3: Parameter with most significant effect on longitudinal response of each OSB due to one standard deviation increase in its value.

	Pushover	ROCKN1N1	ROCKN1P1	SANDN1N1	CLAYN1N1
OSB1	$F_{y,gap,l}$	$k_{gap,l}$	$k_{gap,l}$	$k_{gap,l}$	$k_{gap,l}$
OSB2	$F_{y,gap,l}$	E_{ss}	E_{ss}	E_{ss}	E_{ss}
OSB3	–	$F_{y,gap,t}$	$F_{y,gap,t}$	$F_{y,gap,l}$	$F_{y,gap,l}$
OSB4	–	$F_{y,gap,l}$	$F_{y,gap,t}$	$F_{y,iso,abut}$	$F_{y,gap,l}$

Although not captured in Tables 7.2 and 7.3, column reinforcing details also play a significant role in the nonlinear response (for OSB1 and OSB2 in this study); however, not to the extent that is warranted based on state of the art finite element models. For bridges where the superstructure is isolated from the bent and abutments, the isolator models have a large influence on the NTHA. In addition, sensitivity analysis revealed that the stiffness of the bridge superstructure can have a large influence on the response depending on the boundary conditions at the abutments. This was particularly evident for OSB2, where the abutments were constrained from translation and rotation in order to keep the same boundary conditions from previous analyses of this bridge, leading to dominance of E_{ss} on the response of OSB2. This result further emphasizes the importance of modeling decisions for the bridge boundary conditions.

7.4 Additional Considerations

There are other important modeling choices that need to be made for seismic bridge response modeling. These were not necessarily studied in this report from either a standardization (between CSiBridge and OpenSees) or sensitivity context. However, based on some observations from modal analysis on the OSB models, some other influential parameters affecting either the frequencies or modes (or both) were:

- Torsional restraint at the column bases in the two-column bent frames. If the pipe pin exhibits torsional resistance (about the axis of the column), the global torsional modes will shift substantially.

- Whether additional mass is lumped at abutments to account for abutment structures or embankment.

- Torsion of the bent cap in the two-column bents. This is currently accounted for by using a rigid elastic material for the bent caps.

- Center of mass (vertical location thereof) of the models. This is important for the dynamic properties, but also has a substantial impact on strength and stiffness, primarily if there are rigid offsets considered (or not as the case may be) for the bent cap.

- Cracked elastic properties for the superstructure, diaphragm, and bent caps. These are more important for the elastic response, and less so for dynamic, but may impact the yield strength as they serve as boundary conditions for the columns.

- Properties assigned to the isolators (OSB3 and OSB4). These were taken from previous studies and not used perhaps in the way in which a typical bridge structure would be designed for seismic isolation. Similarly there were series of more than one bearing at several locations that were not explicitly accounted for in the model.

- Whether or not rotational inertia is assigned to the superstructure elements. Currently the OpenSees models do not have this additional inertia, which has a small impact on the behaviors of OSB2 and OSB4.

Appendix A

Mode Shapes (Roller Abutments)

The first six mode shapes for each OSB with simple roller abutments are presented for both the CSiBridge and OpenSees models.
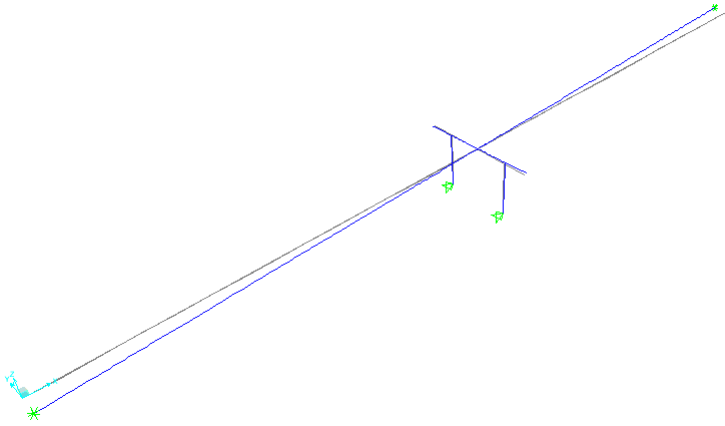
Figure A.1: Mode shape 1 for CSiBridge model of OSB 1 with roller abutments.

(a) Perspective

(b) Profile
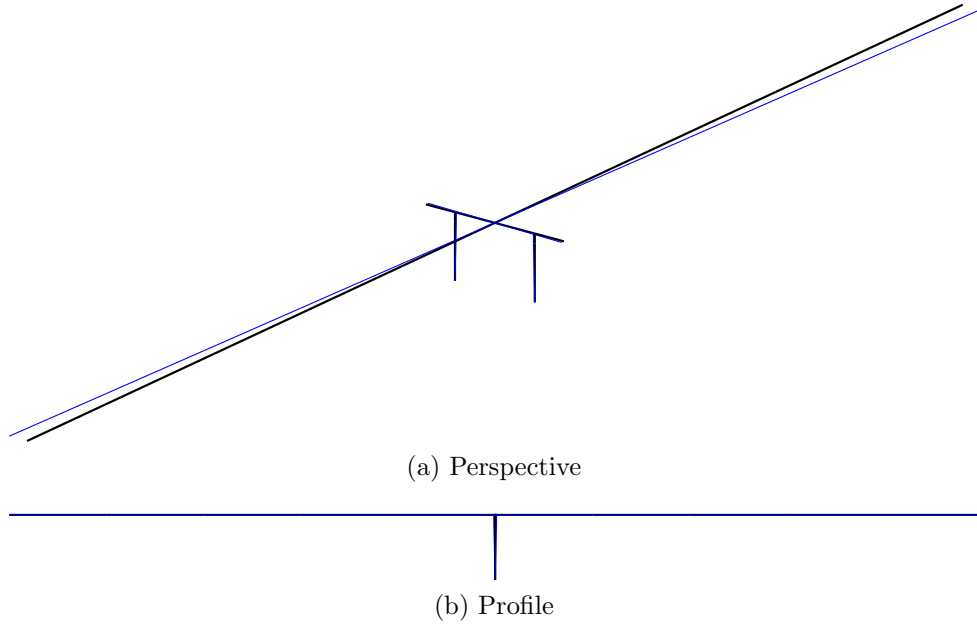
Figure A.2: Mode shape 1 for OpenSees model of OSB 1 with roller abutments.
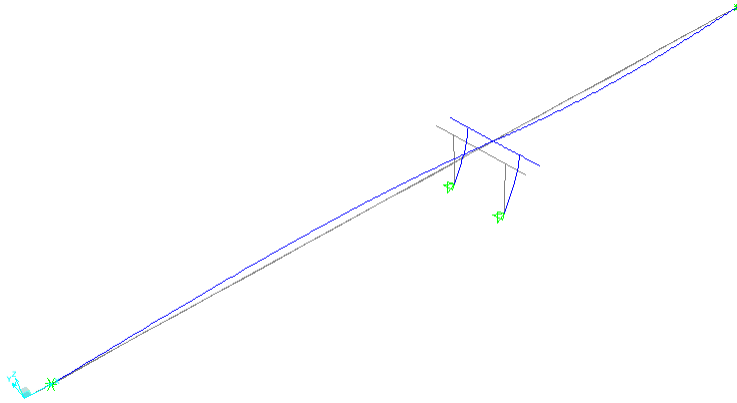
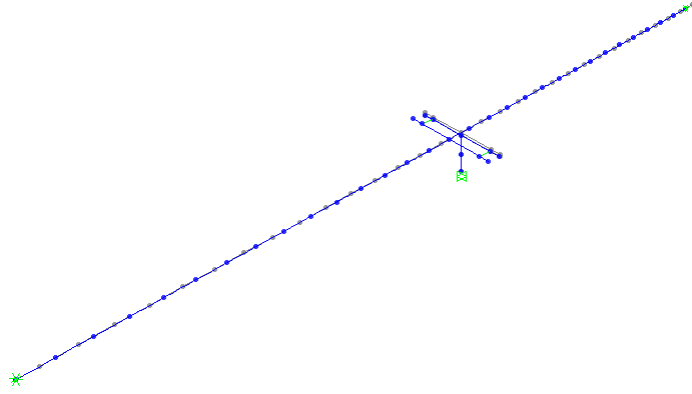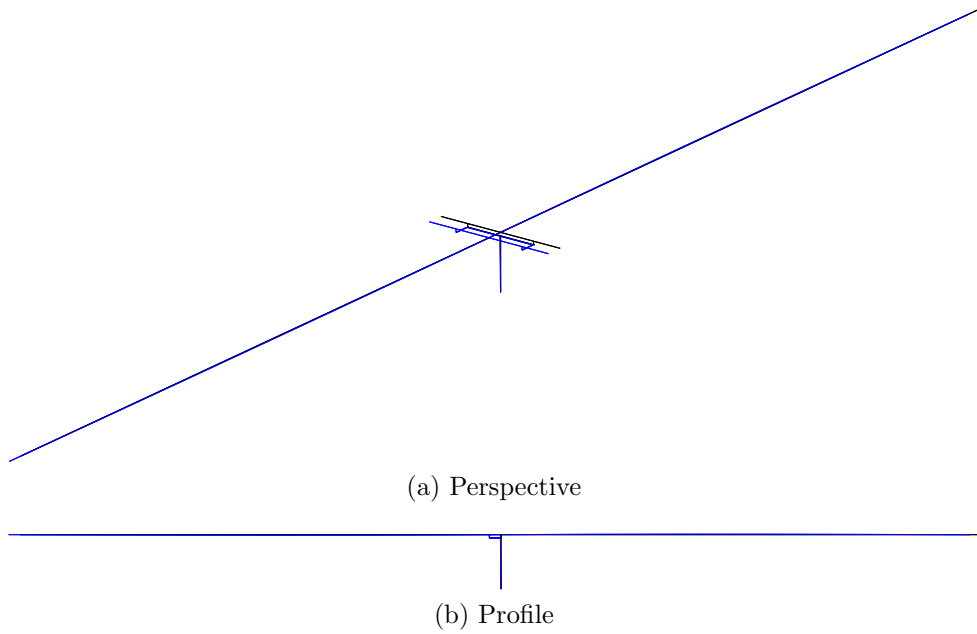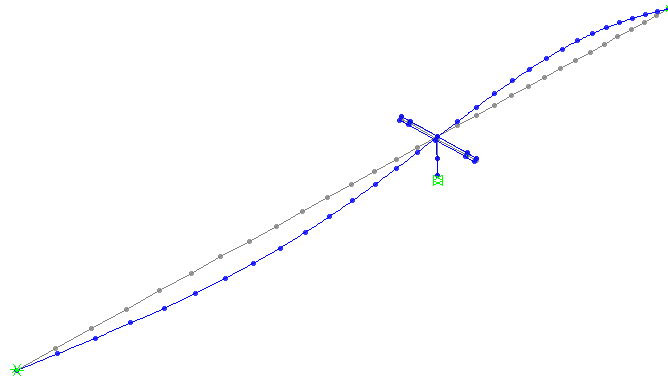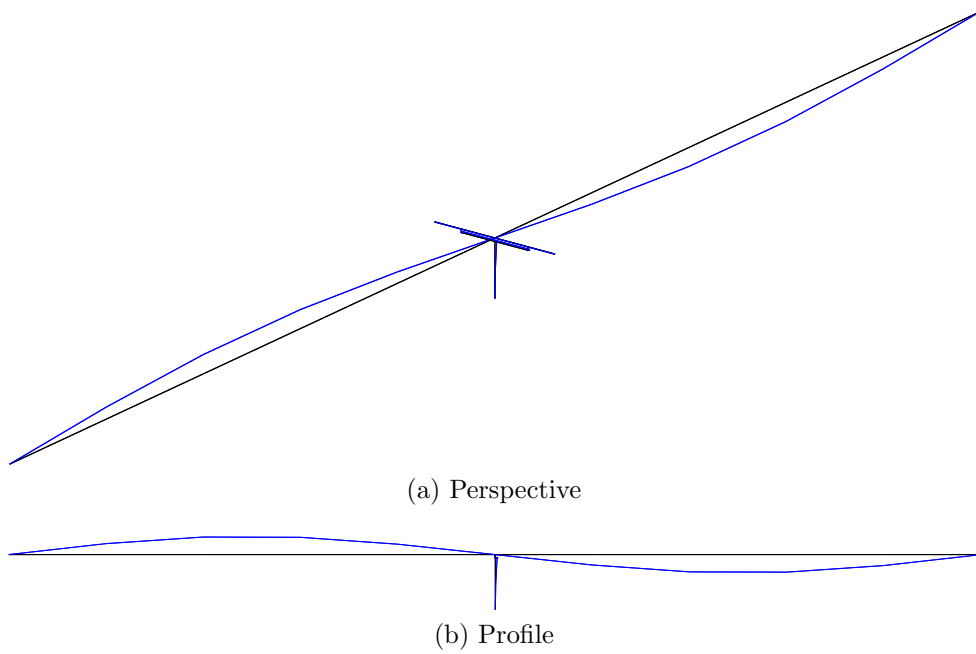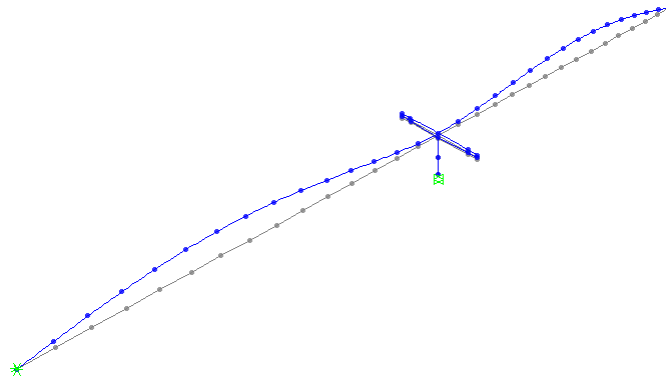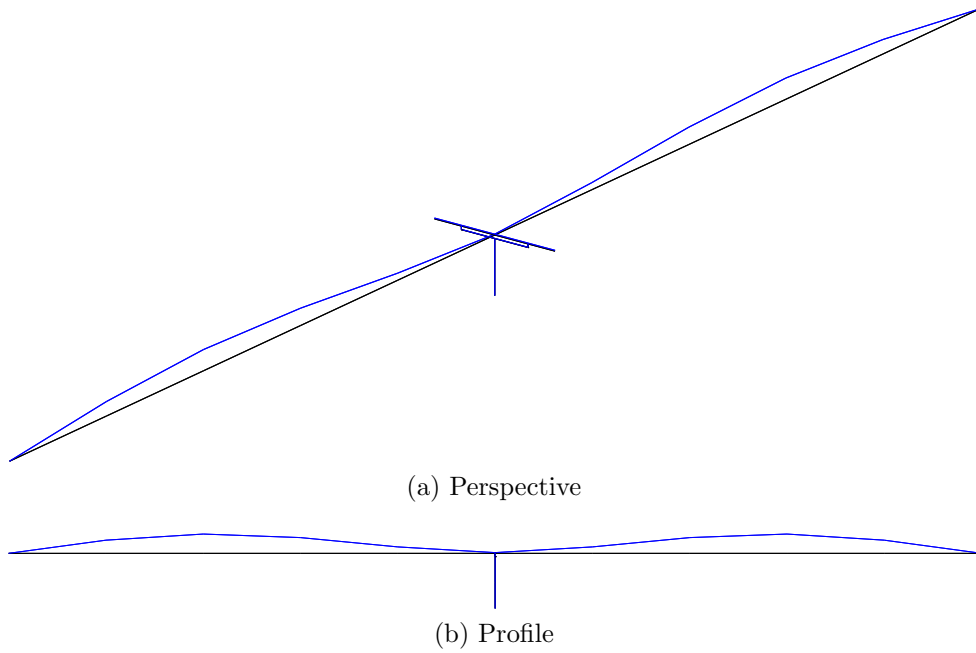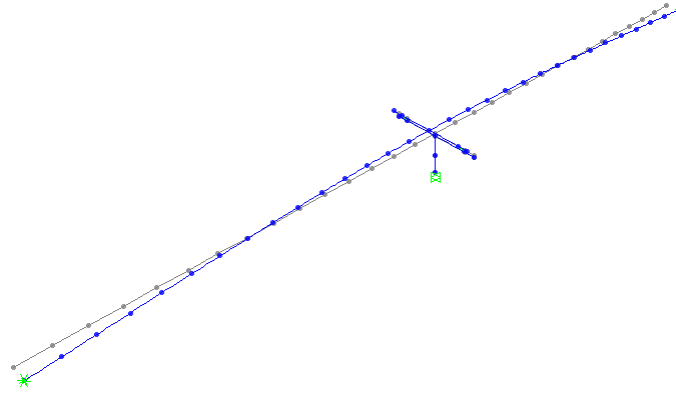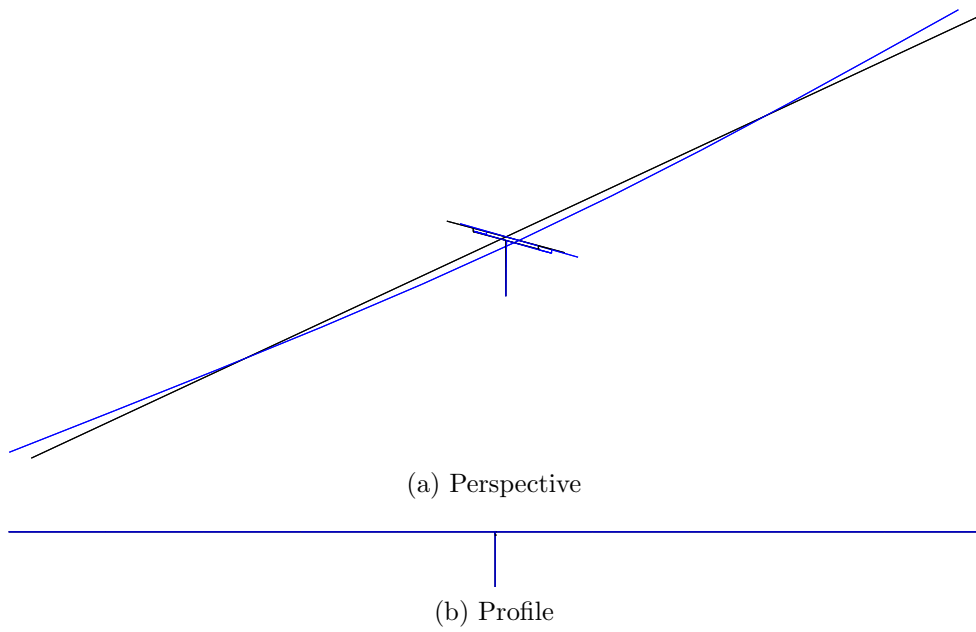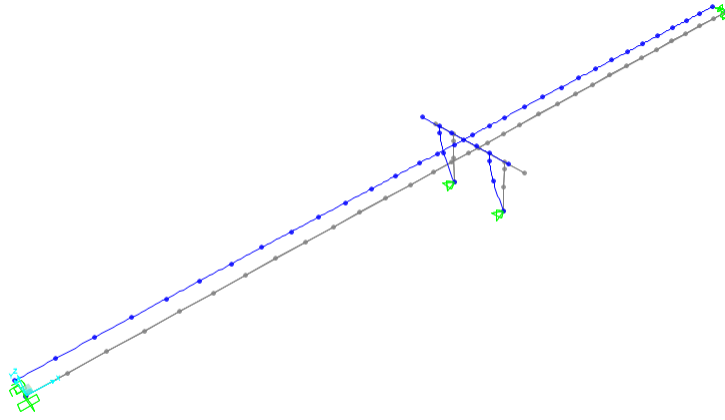Figure A.3: Mode shape 2 for CSiBridge model of OSB 1 with roller abutments.

(a) Perspective

(b) Profile
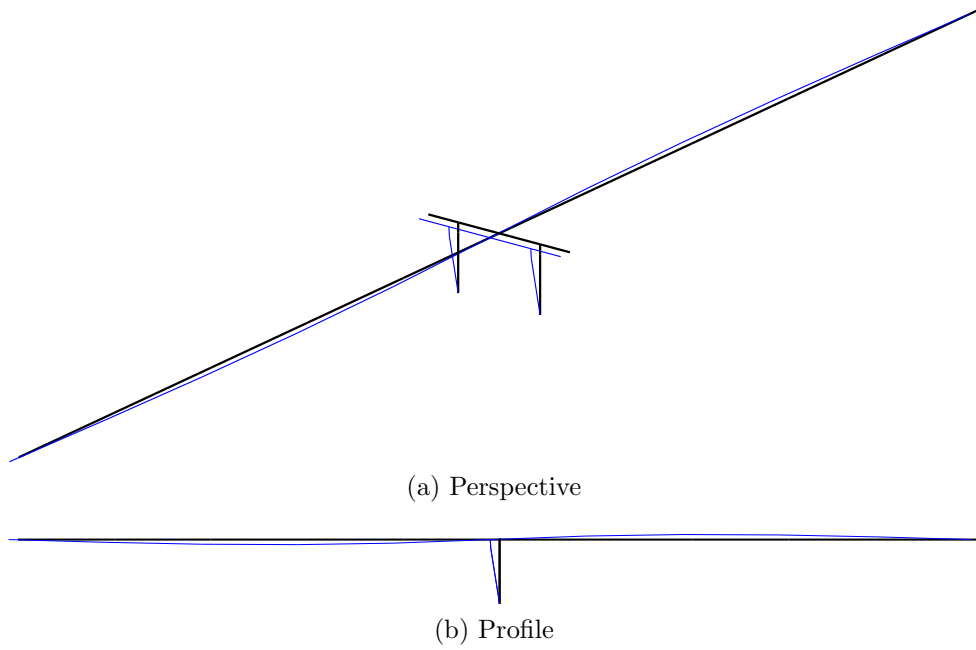
Figure A.4: Mode shape 2 for OpenSees model of OSB 1 with roller abutments.
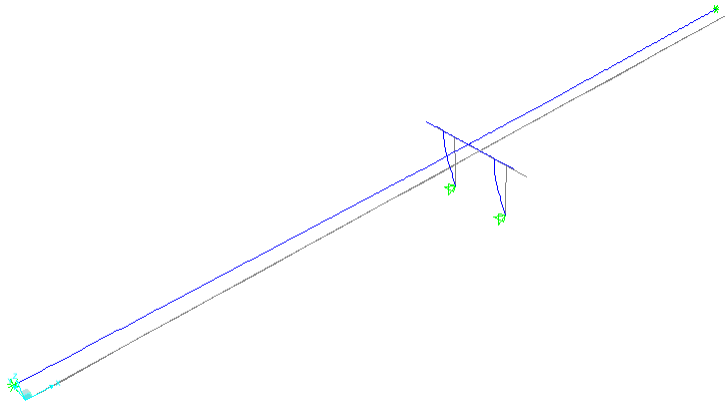
Figure A.5: Mode shape 3 for CSiBridge model of OSB 1 with roller abutments.

(a) Perspective

(b) Profile
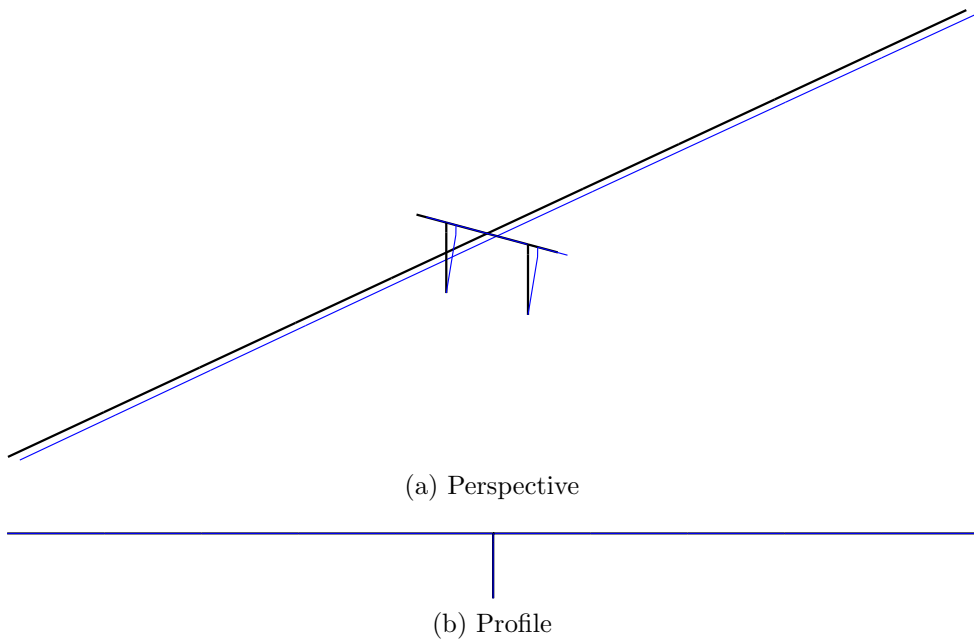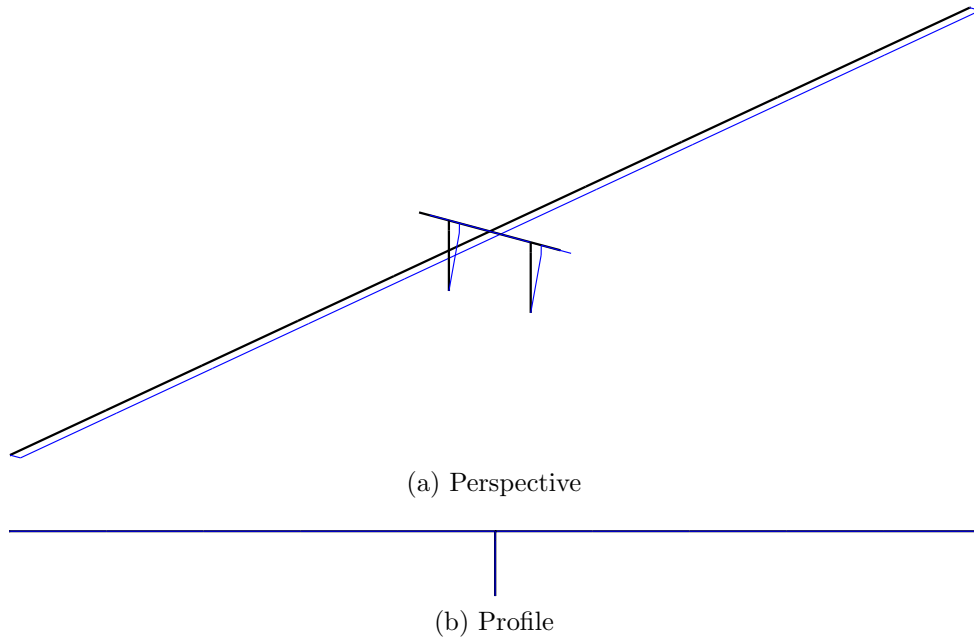
Figure A.6: Mode shape 3 for OpenSees model of OSB 1 with roller abutments.
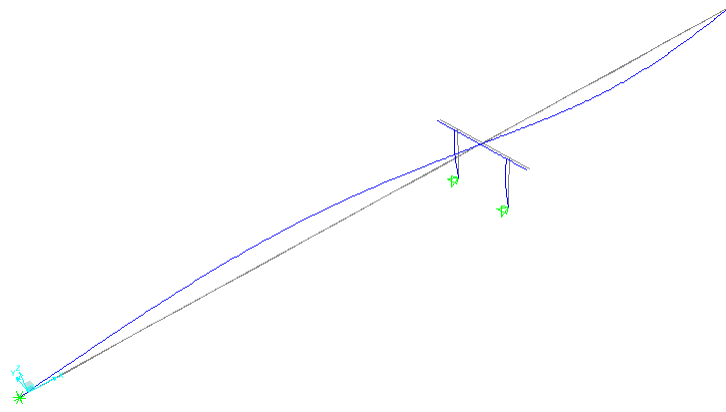
Figure A.7: Mode shape 4 for CSiBridge model of OSB 1 with roller abutments.

(a) Perspective

(b) Profile
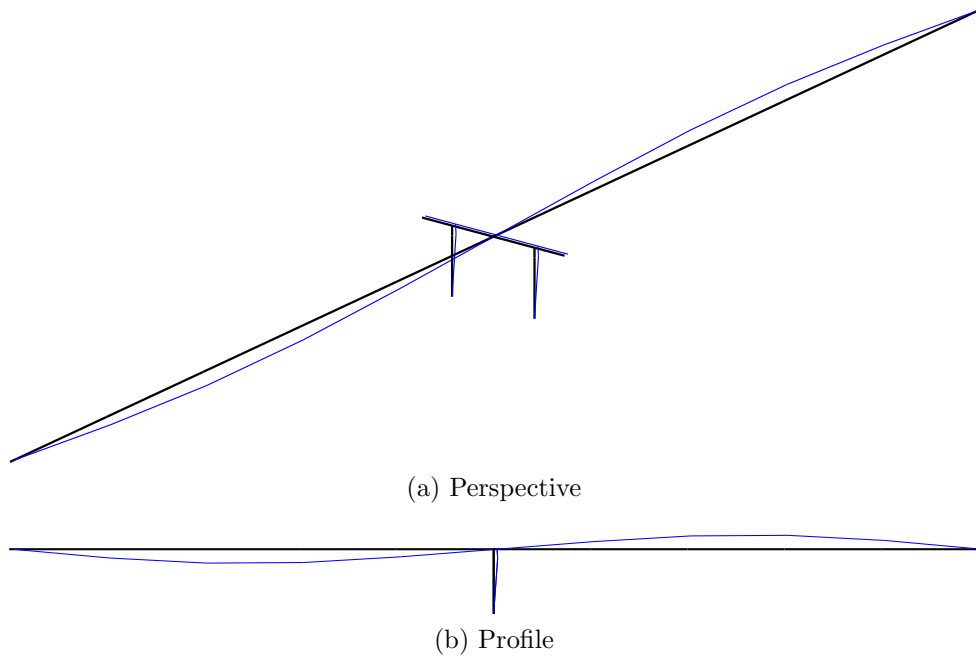
Figure A.8: Mode shape 4 for OpenSees model of OSB 1 with roller abutments.
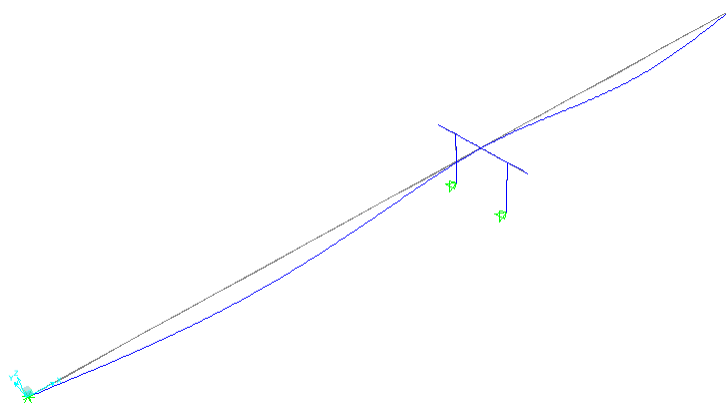
Figure A.9: Mode shape 5 for CSiBridge model of OSB 1 with roller abutments.

(a) Perspective

(b) Profile
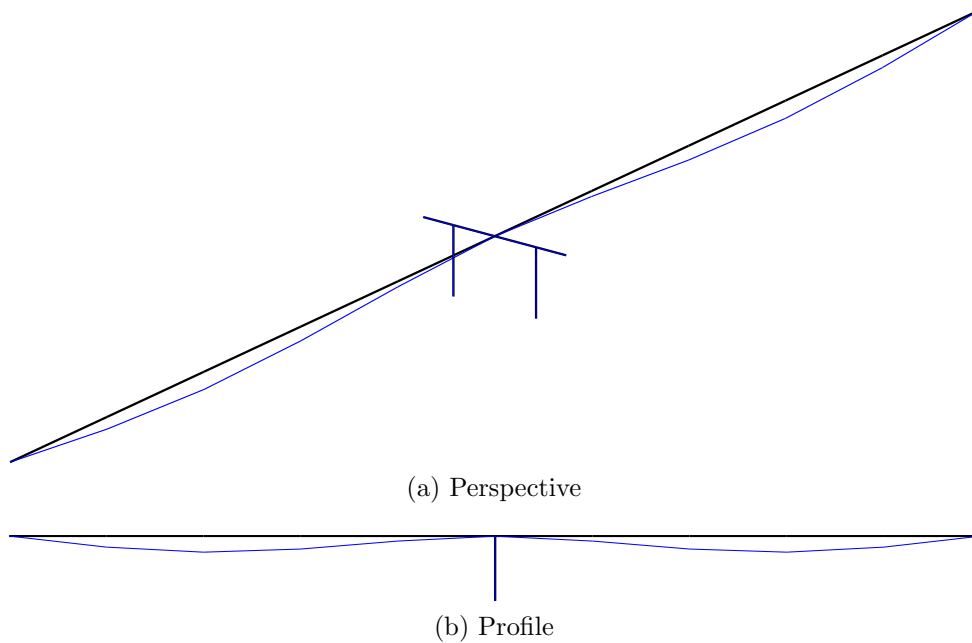
Figure A.10: Mode shape 5 for OpenSees model of OSB 1 with roller abutments.
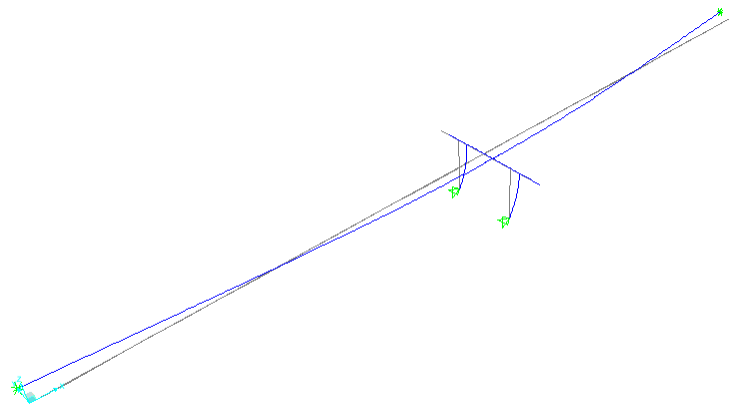
Figure A.11: Mode shape 6 for CSiBridge model of OSB 1 with roller abutments.

(a) Perspective

(b) Profile
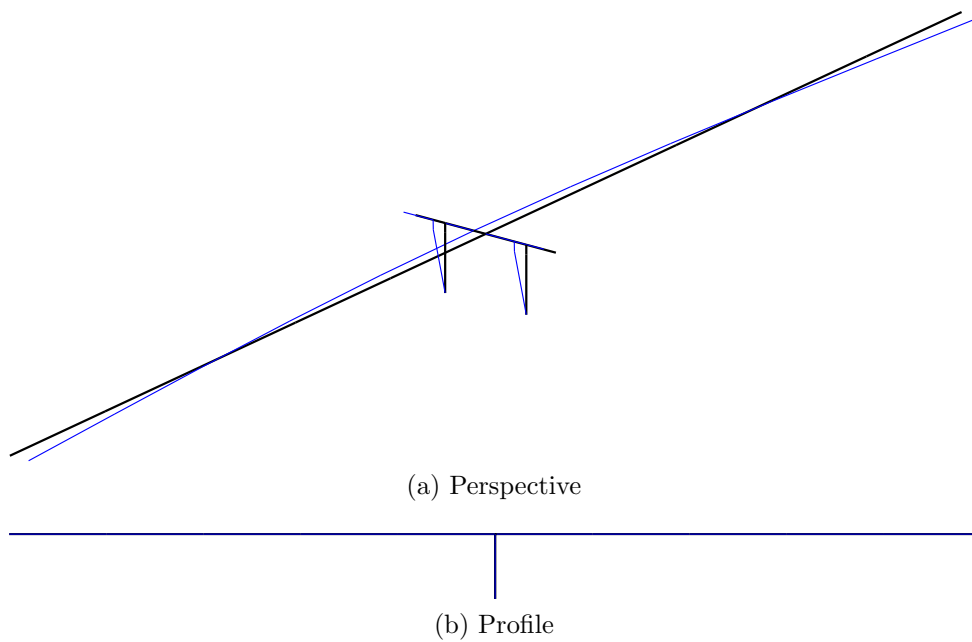
Figure A.12: Mode shape 6 for OpenSees model of OSB 1 with roller abutments.
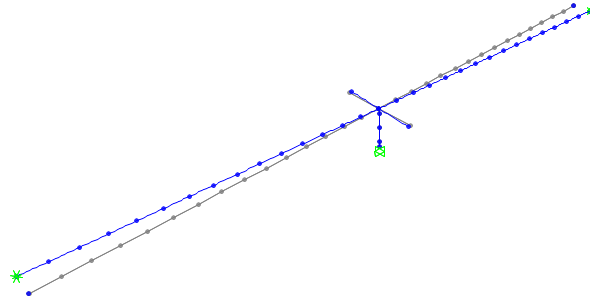
Figure A.13: Mode shape 1 for CSiBridge model of OSB 2 with roller abutments.

(a) Perspective

(b) Profile
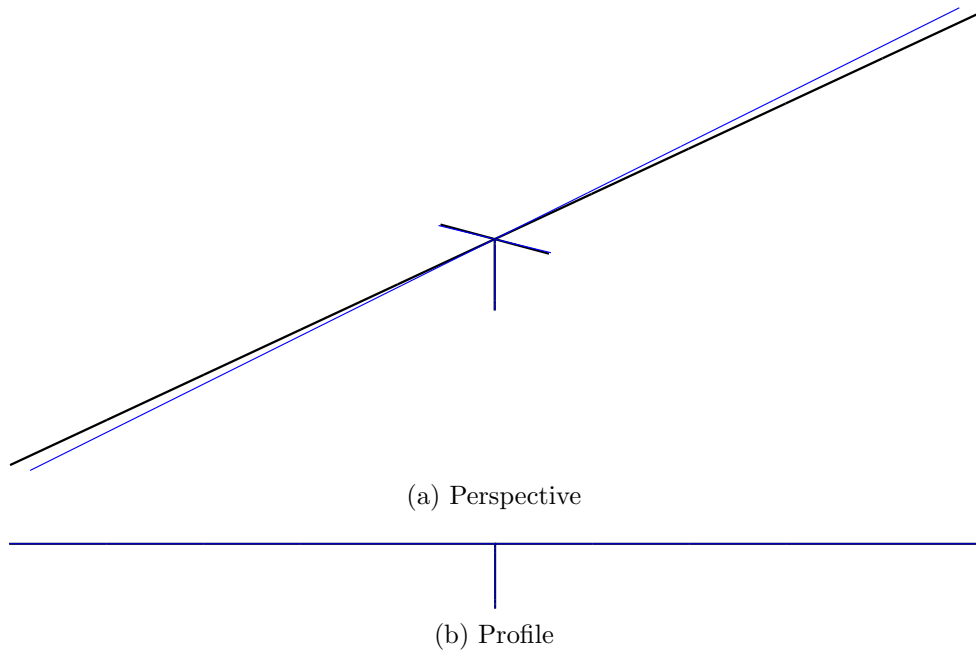
Figure A.14: Mode shape 1 for OpenSees model of OSB 2 with roller abutments.
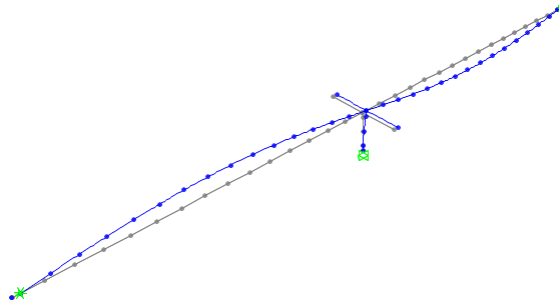
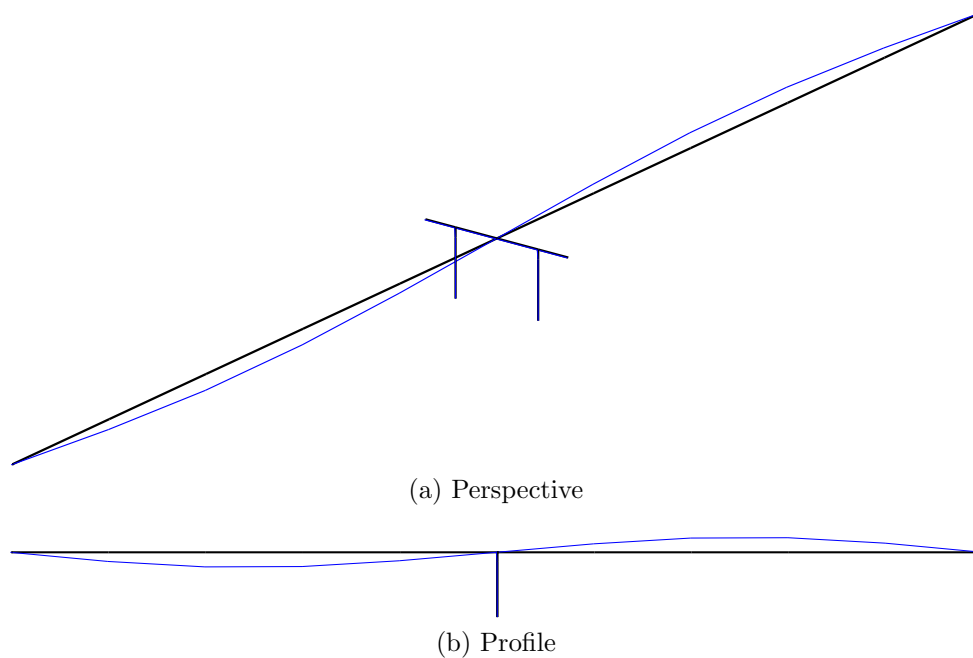Figure A.15: Mode shape 2 for CSiBridge model of OSB 2 with roller abutments.

(a) Perspective

(b) Profile
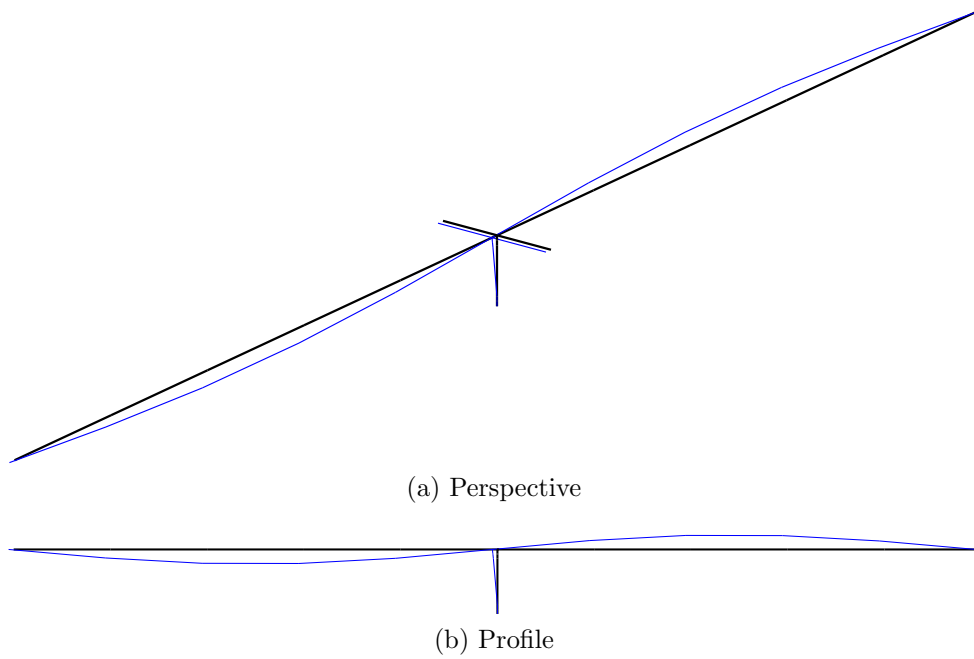
Figure A.16: Mode shape 2 for OpenSees model of OSB 2 with roller abutments.
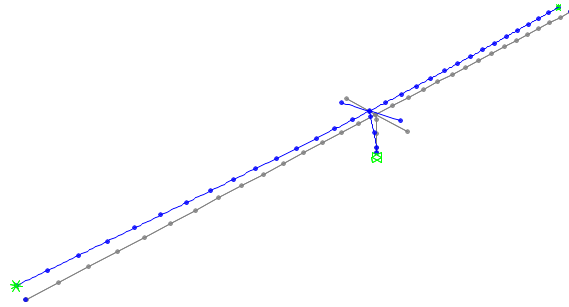
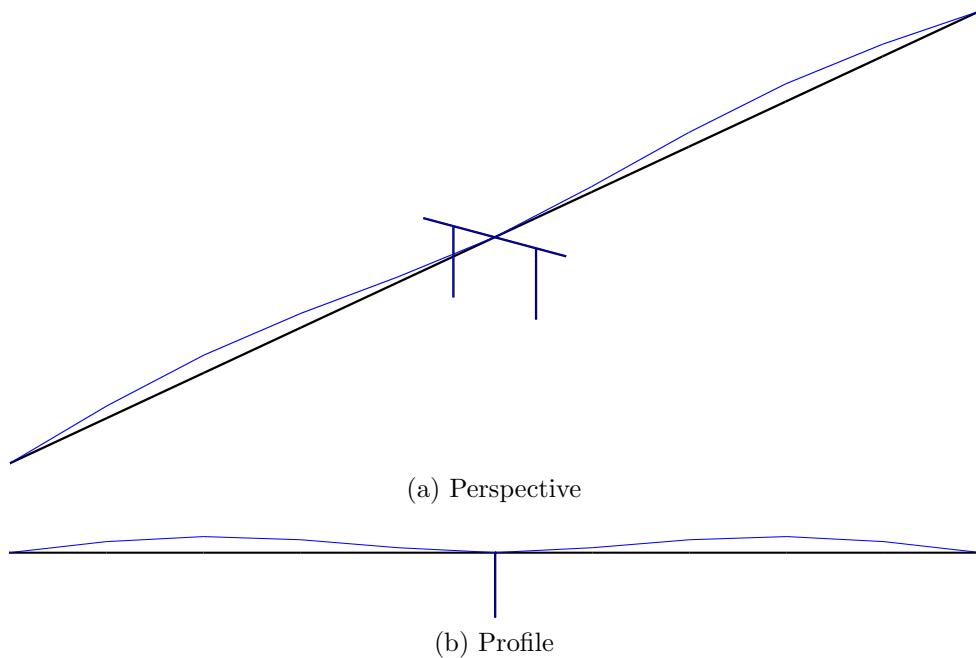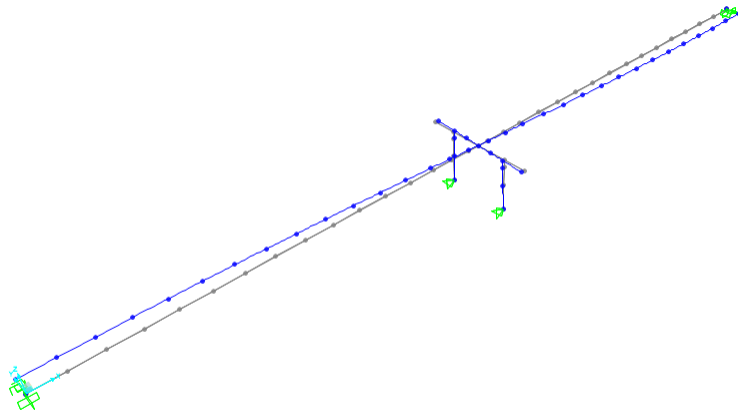Figure A.17: Mode shape 3 for CSiBridge model of OSB 2 with roller abutments.

(a) Perspective

(b) Profile
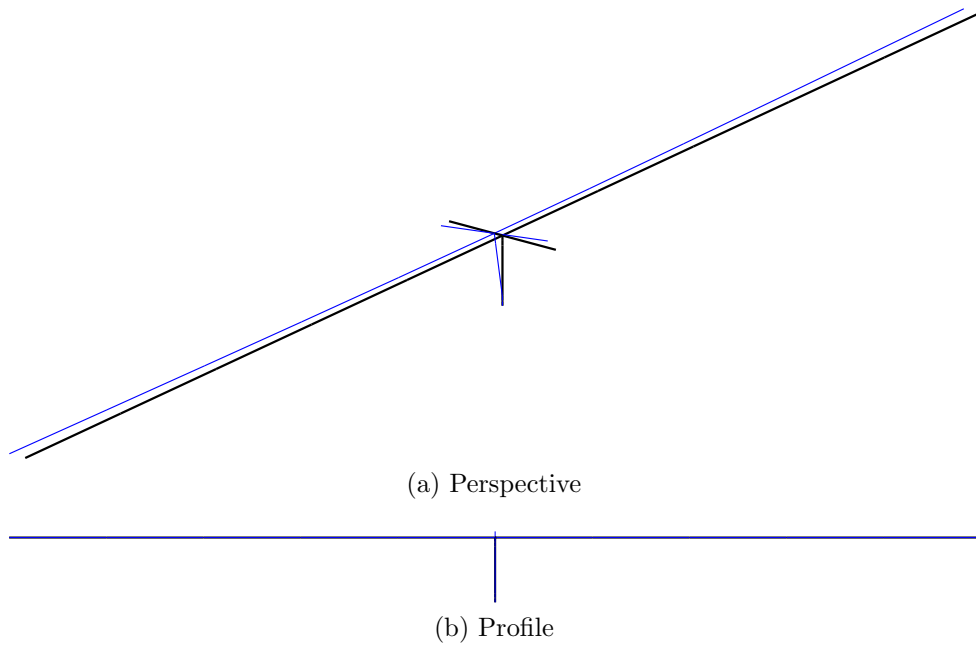
Figure A.18: Mode shape 3 for OpenSees model of OSB 2 with roller abutments.
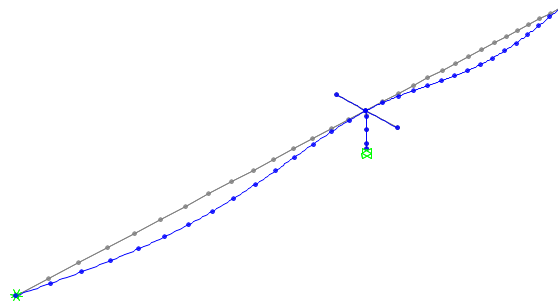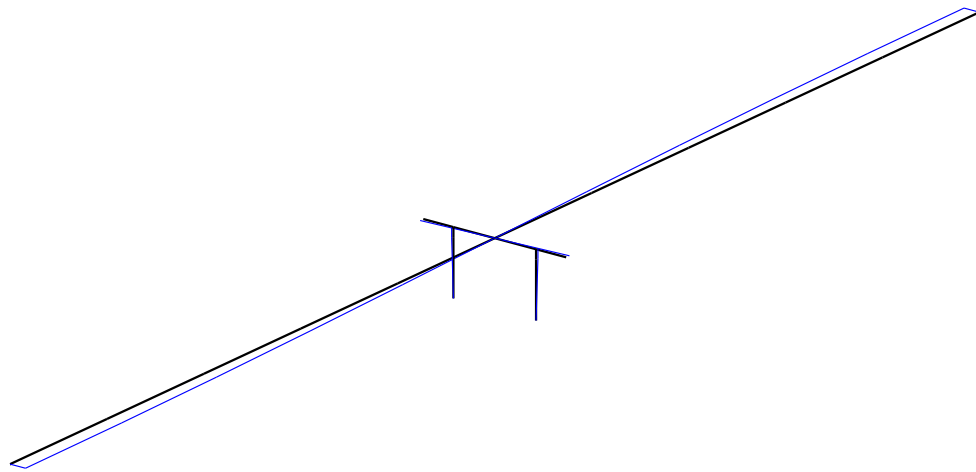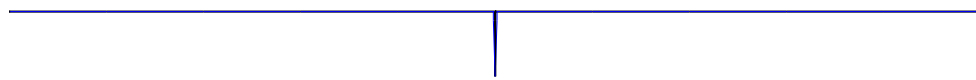
Figure A.19: Mode shape 4 for CSiBridge model of OSB 2 with roller abutments.

(a) Perspective

(b) Profile
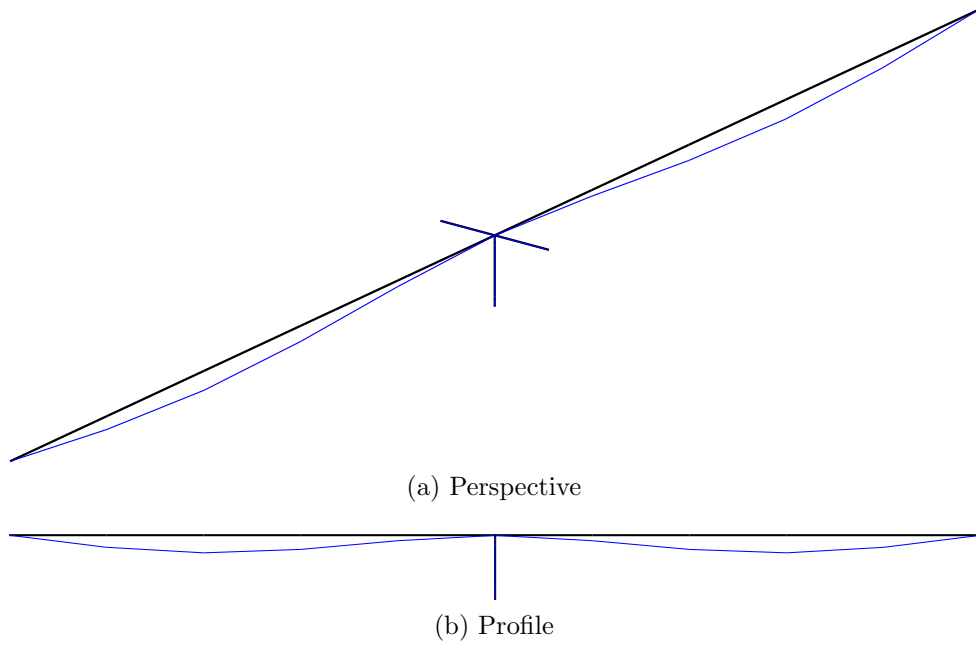
Figure A.20: Mode shape 4 for OpenSees model of OSB 2 with roller abutments.
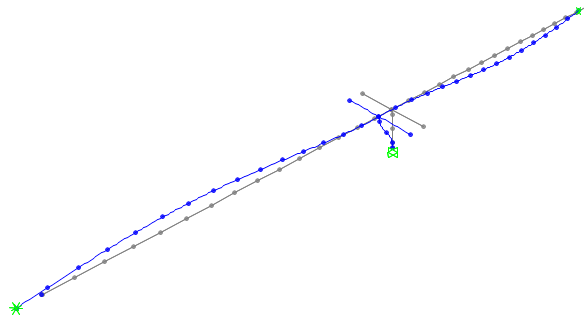
Figure A.21: Mode shape 5 for CSiBridge model of OSB 2 with roller abutments.

(a) Perspective

(b) Profile
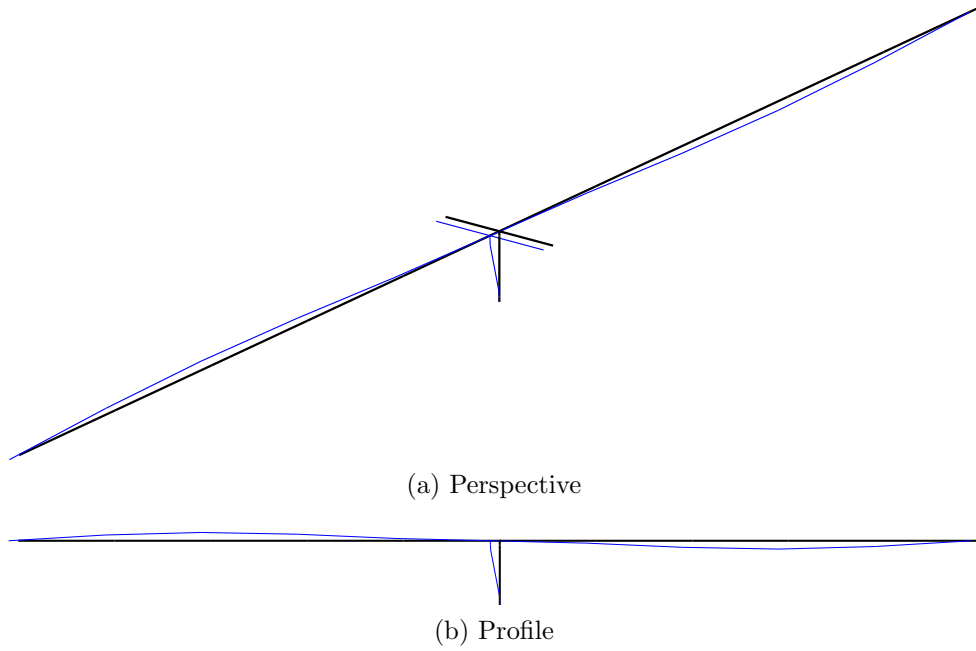
Figure A.22: Mode shape 5 for OpenSees model of OSB 2 with roller abutments.
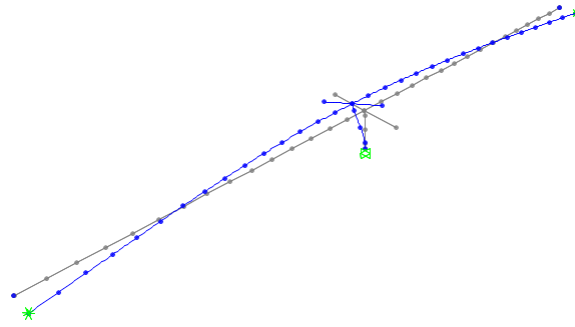
Figure A.23: Mode shape 6 for CSiBridge model of OSB 2 with roller abutments.

(a) Perspective

(b) Profile
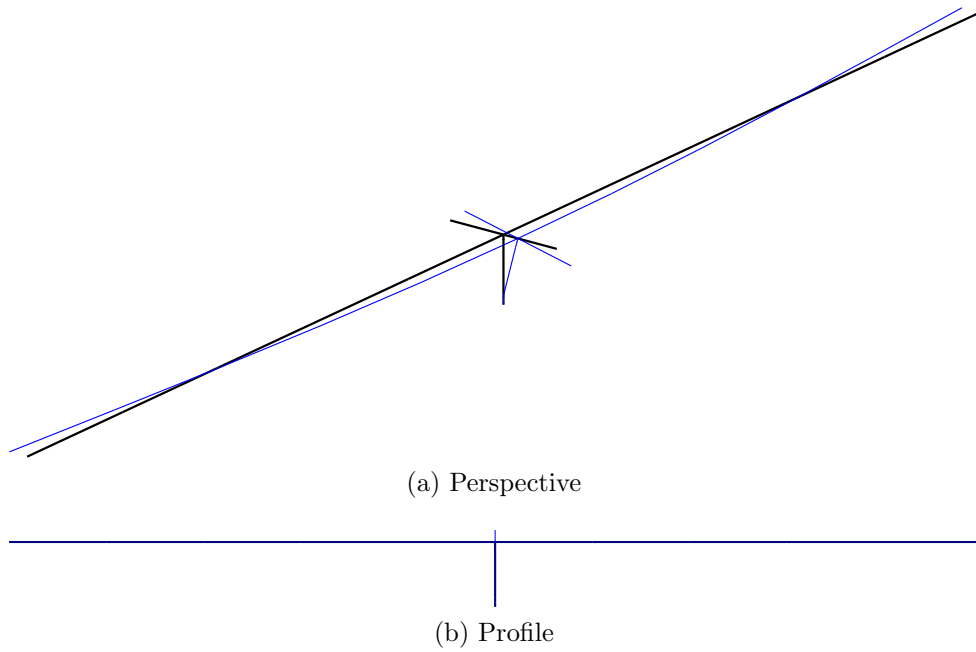
Figure A.24: Mode shape 6 for OpenSees model of OSB 2 with roller abutments.
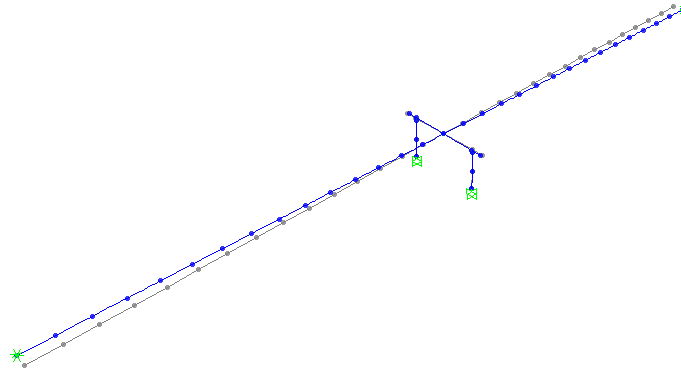
Figure A.25: Mode shape 1 for CSiBridge model of OSB 3 with roller abutments.

(a) Perspective

(b) Profile
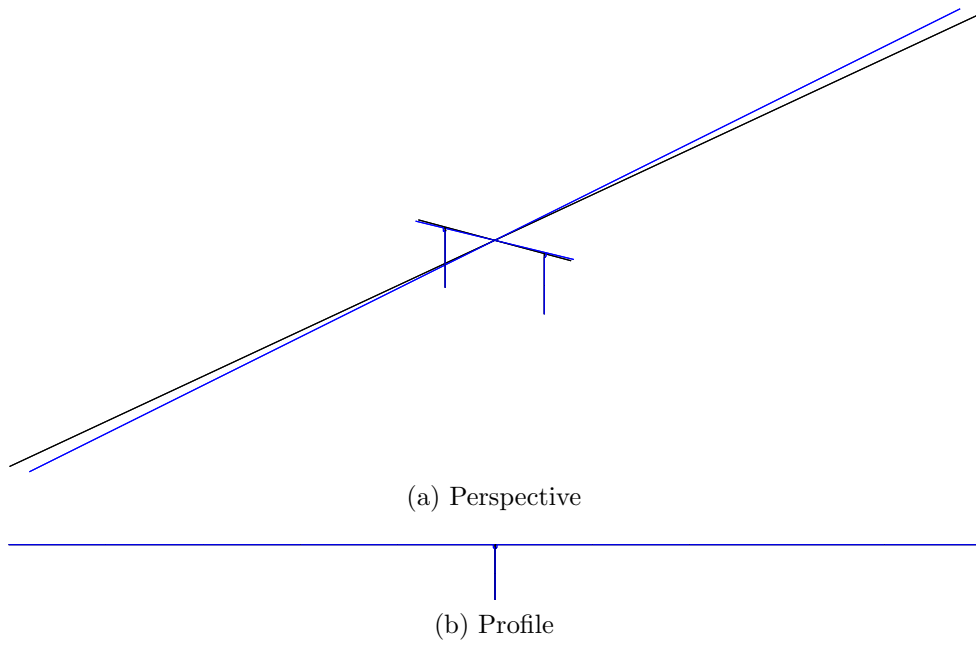
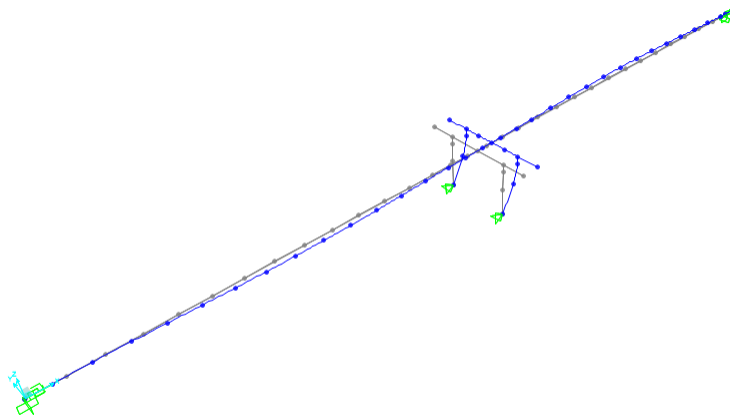Figure A.26: Mode shape 1 for OpenSees model of OSB 3 with roller abutments.
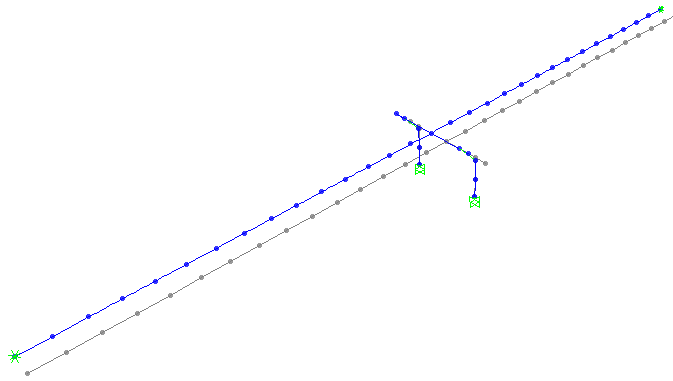
Figure A.27: Mode shape 2 for CSiBridge model of OSB 3 with roller abutments.

(a) Perspective

(b) Profile
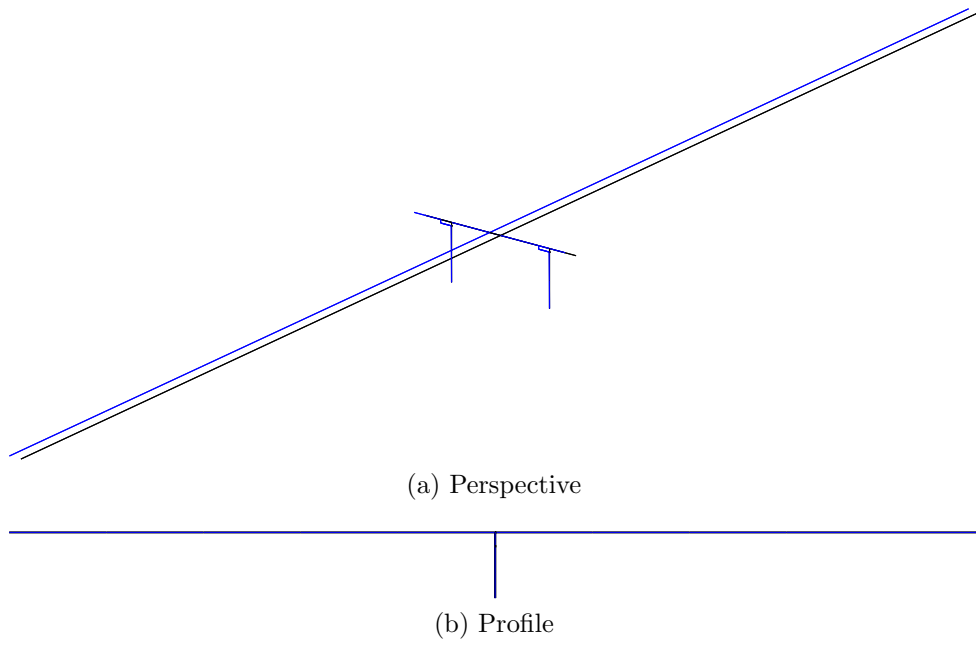
Figure A.28: Mode shape 2 for OpenSees model of OSB 3 with roller abutments.
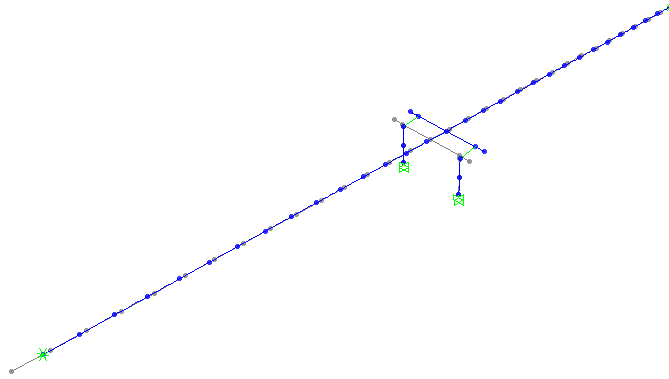
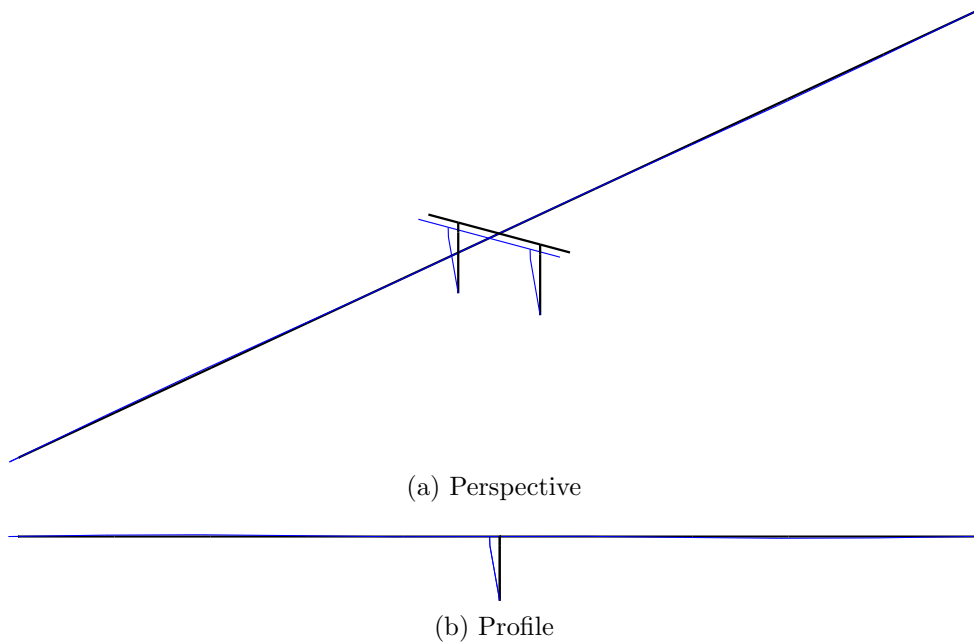Figure A.29: Mode shape 3 for CSiBridge model of OSB 3 with roller abutments.

(a) Perspective

(b) Profile
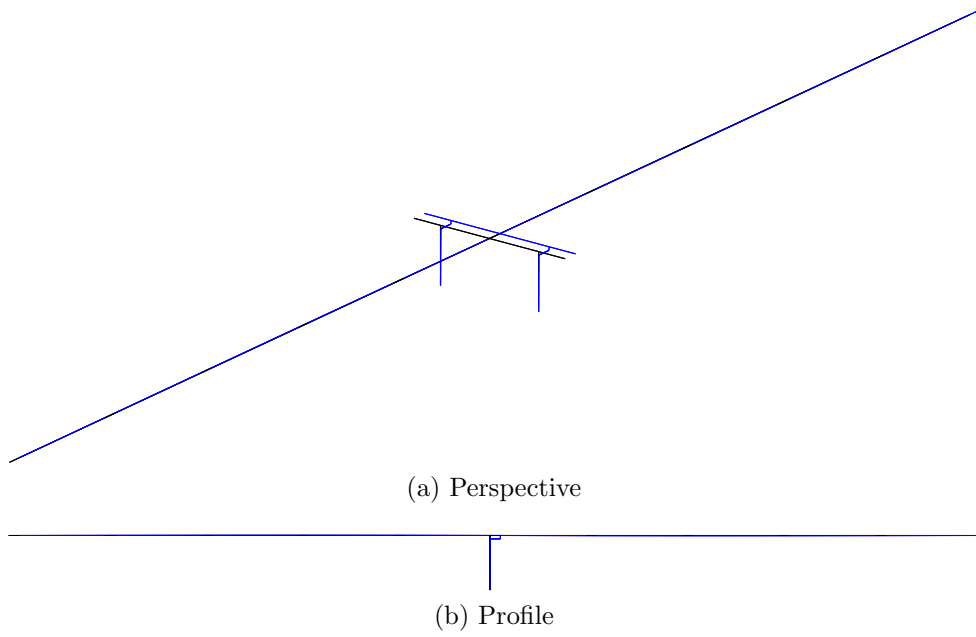
Figure A.30: Mode shape 3 for OpenSees model of OSB 3 with roller abutments.
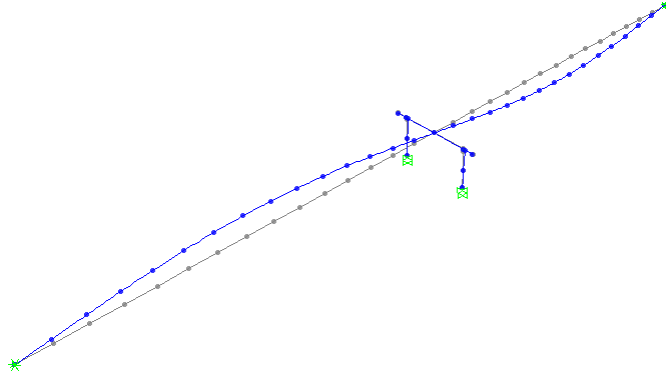
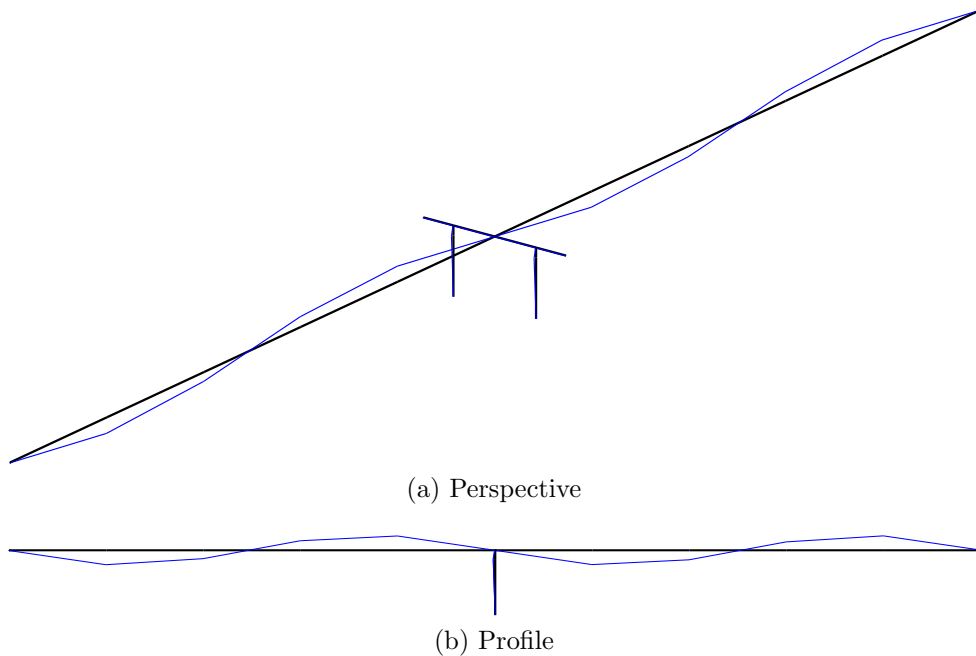Figure A.31: Mode shape 4 for CSiBridge model of OSB 3 with roller abutments.

(a) Perspective

(b) Profile
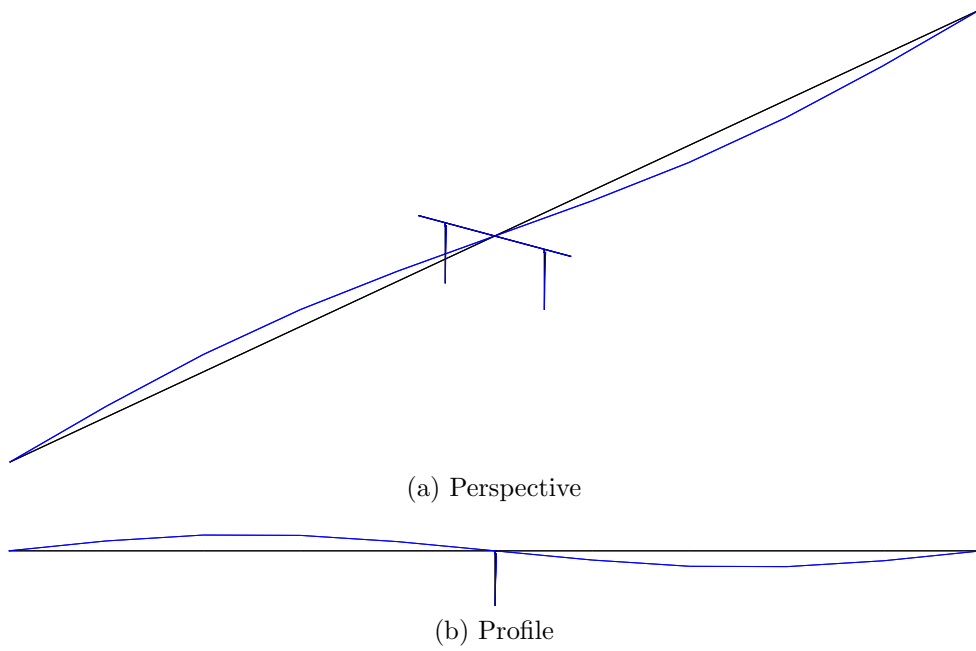
Figure A.32: Mode shape 4 for OpenSees model of OSB 3 with roller abutments.
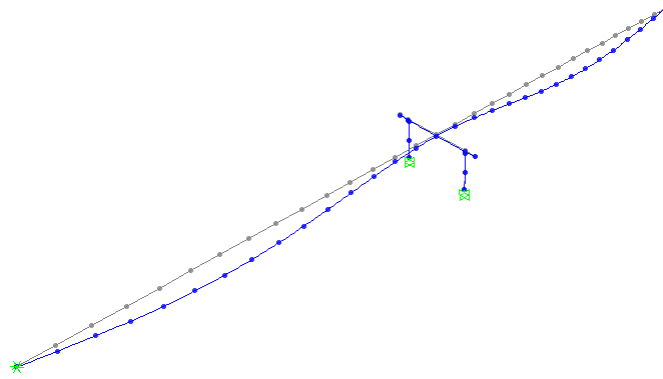
Figure A.33: Mode shape 5 for CSiBridge model of OSB 3 with roller abutments.

(a) Perspective

(b) Profile
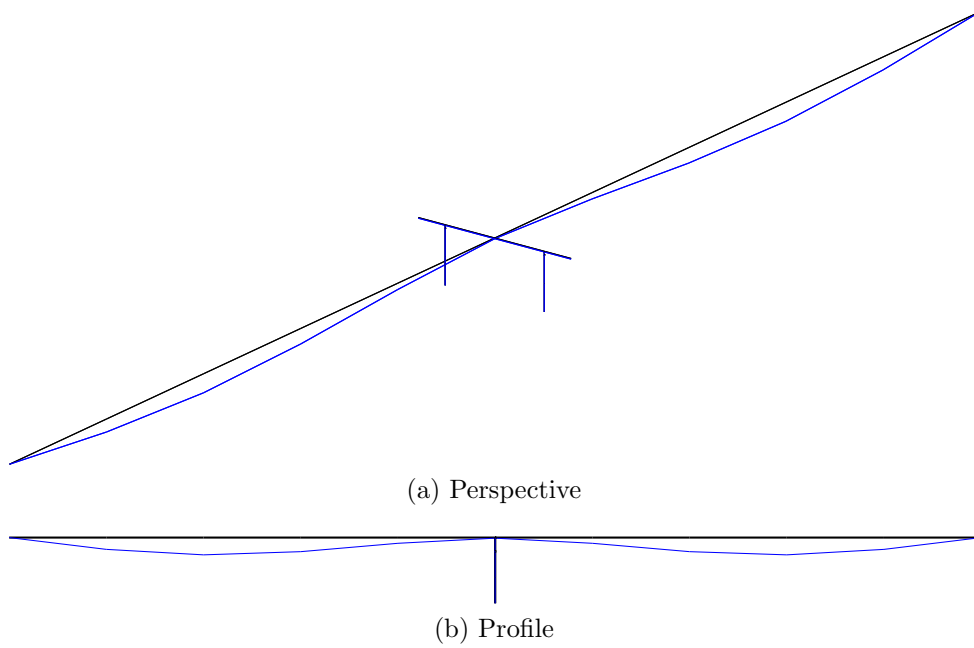
Figure A.34: Mode shape 5 for OpenSees model of OSB 3 with roller abutments.
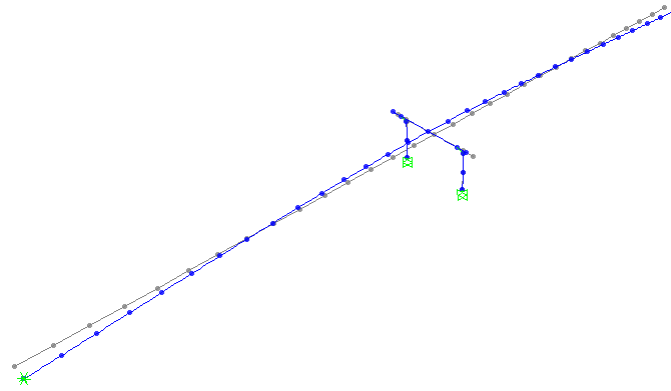
Figure A.35: Mode shape 6 for CSiBridge model of OSB 3 with roller abutments.

(a) Perspective

(b) Profile
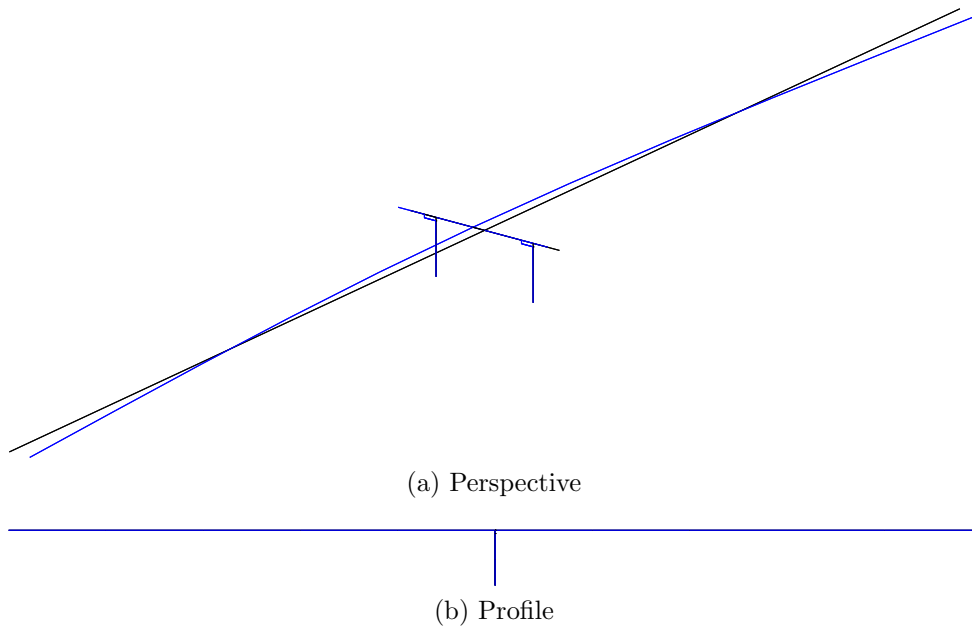
Figure A.36: Mode shape 6 for OpenSees model of OSB 3 with roller abutments.
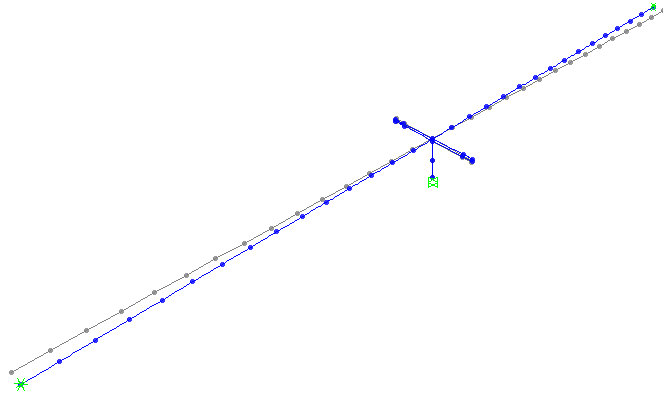
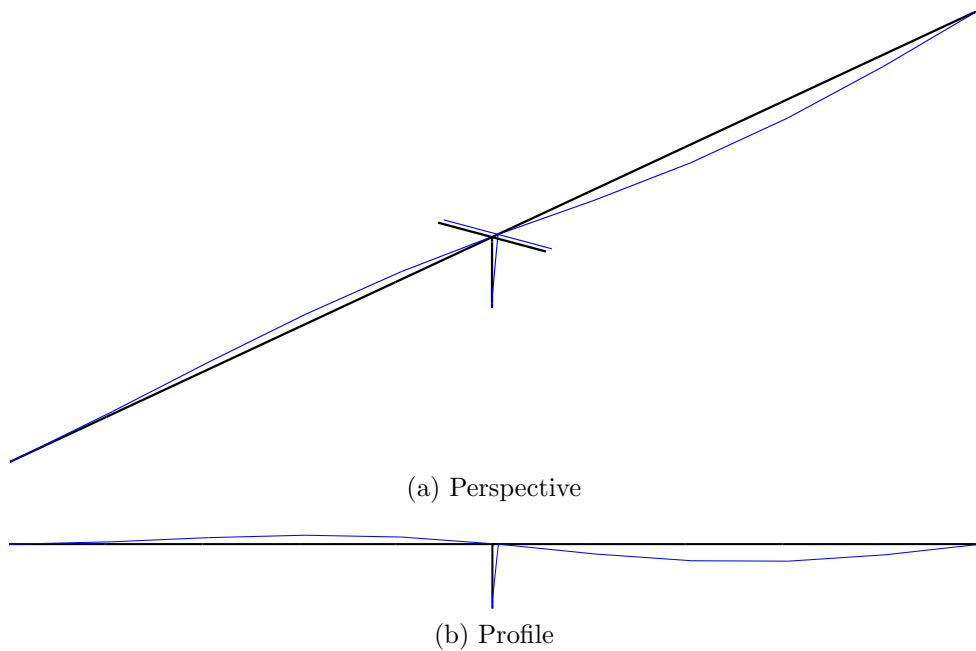Figure A.37: Mode shape 1 for CSiBridge model of OSB 4 with roller abutments.

(a) Perspective

(b) Profile
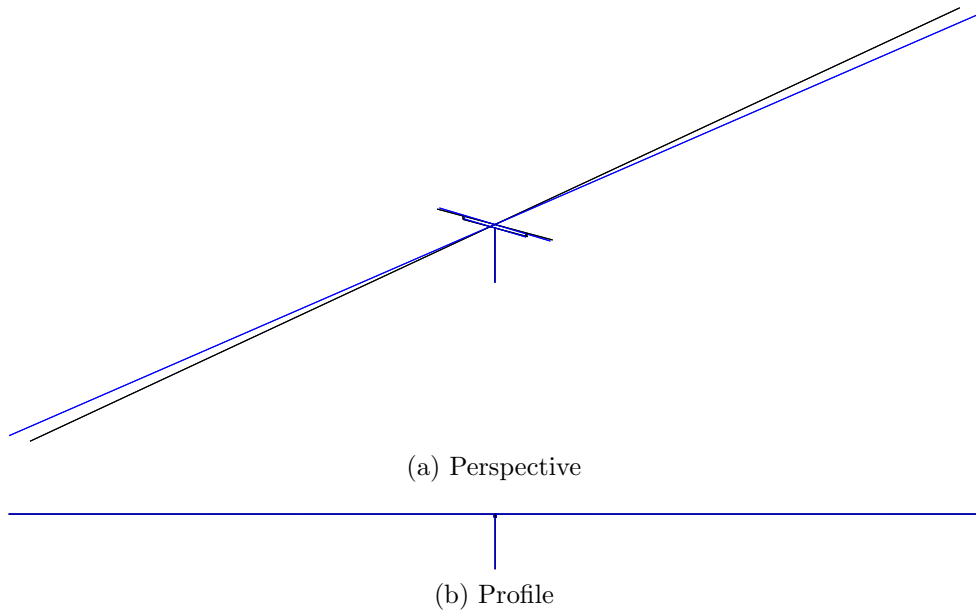
Figure A.38: Mode shape 1 for OpenSees model of OSB 4 with roller abutments.

232
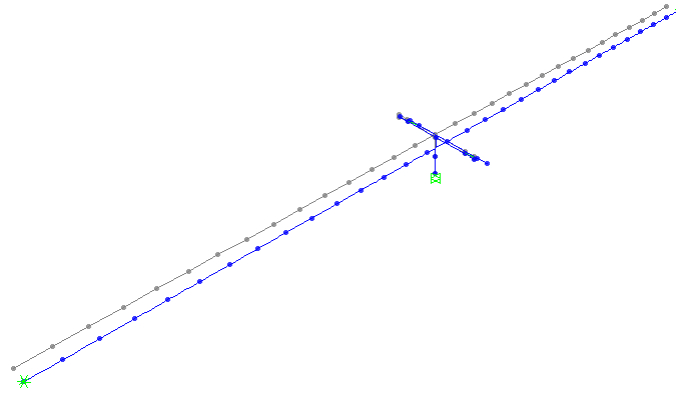
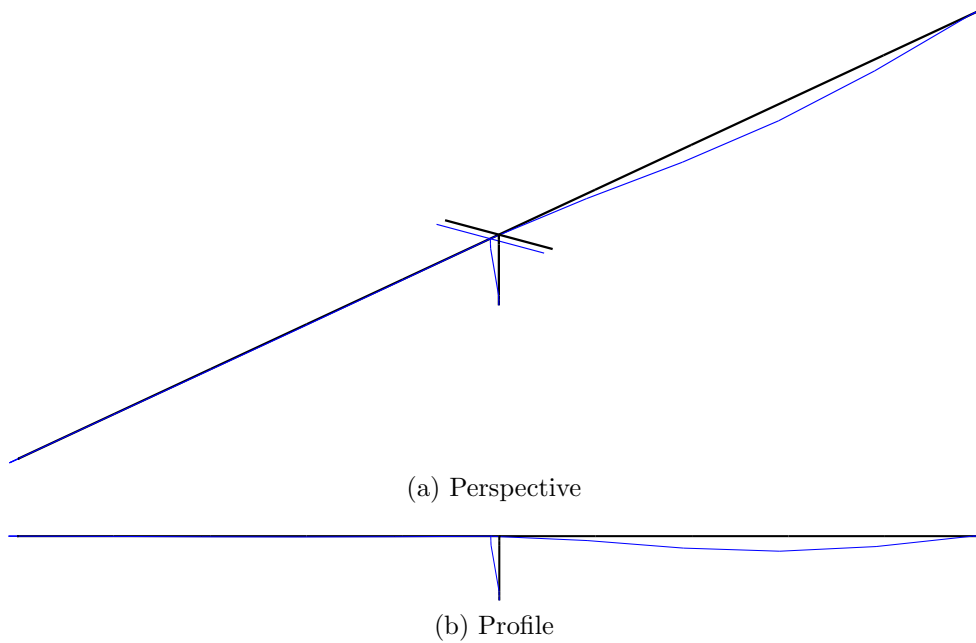Figure A.39: Mode shape 2 for CSiBridge model of OSB 4 with roller abutments.

(a) Perspective

(b) Profile
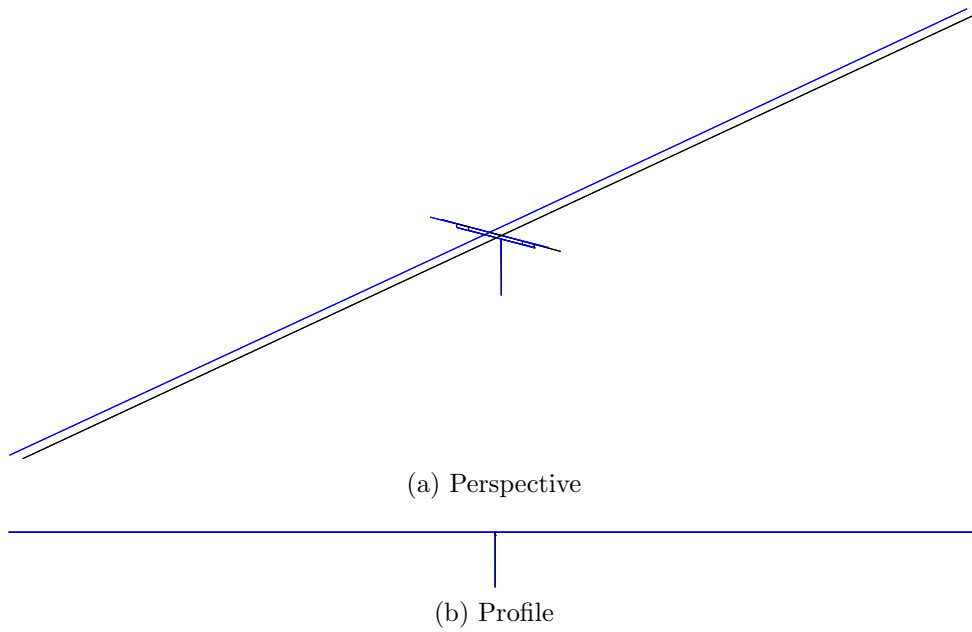
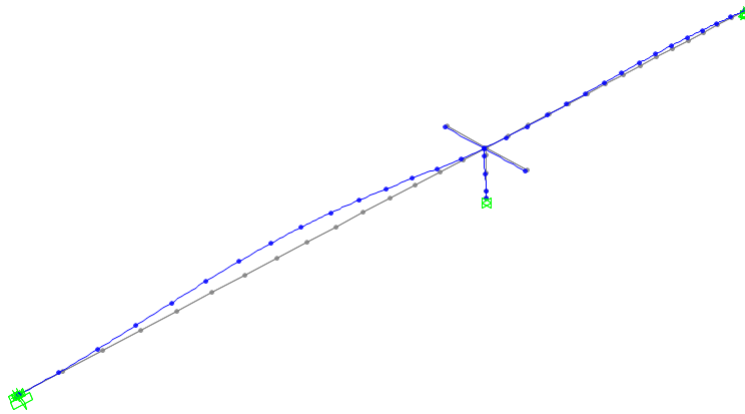Figure A.40: Mode shape 2 for OpenSees model of OSB 4 with roller abutments.

233

Figure A.41: Mode shape 3 for CSiBridge model of OSB 4 with roller abutments.

(a) Perspective

(b) Profile

Figure A.42: Mode shape 3 for OpenSees model of OSB 4 with roller abutments.
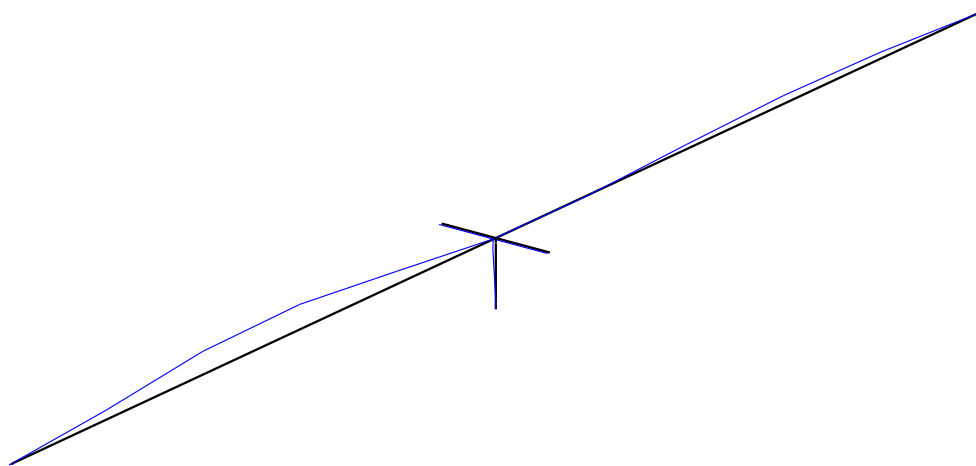
Figure A.43: Mode shape 4 for CSiBridge model of OSB 4 with roller abutments.

(a) Perspective

(b) Profile

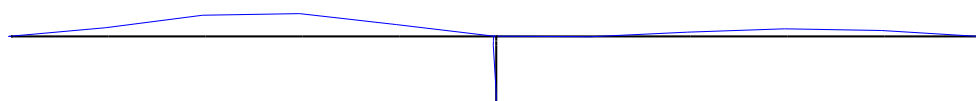Figure A.44: Mode shape 4 for OpenSees model of OSB 4 with roller abutments.

Figure A.45: Mode shape 5 for CSiBridge model of OSB 4 with roller abutments.

(a) Perspective

(b) Profile

Figure A.46: Mode shape 5 for OpenSees model of OSB 4 with roller abutments.

Figure A.47: Mode shape 6 for CSiBridge model of OSB 4 with roller abutments.

(a) Perspective

(b) Profile

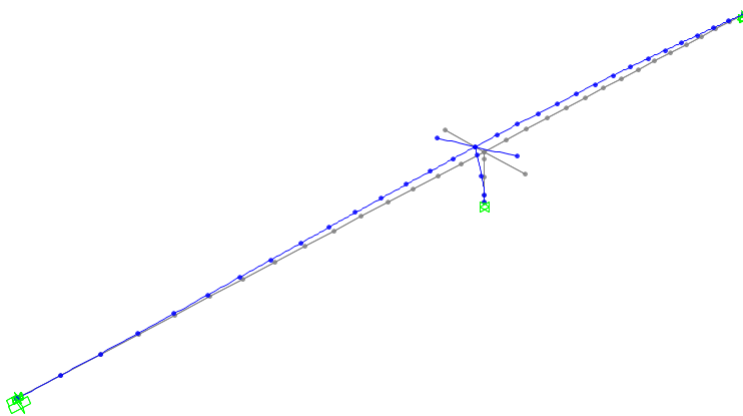Figure A.48: Mode shape 6 for OpenSees model of OSB 4 with roller abutments.

Appendix B

Mode Shapes (Original Abutments)

The first six mode shapes for each OSB with the original nonlinear abutments are presented for both the CSiBridge and OpenSees models.

Figure B.1: Mode shape 1 for CSiBridge model of OSB 1 with original abutments.
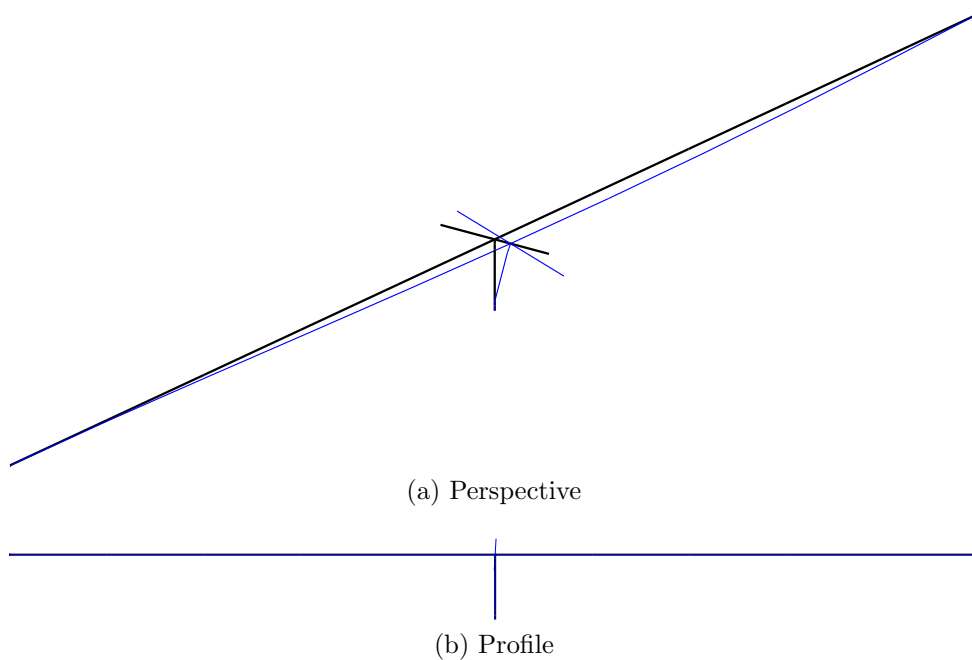

(a) Perspective

(b) Profile

Figure B.2: Mode shape 1 for OpenSees model of OSB 1 with original abutments.

239
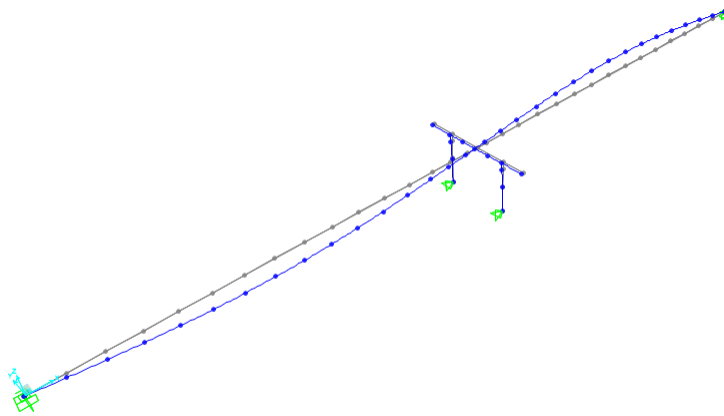
Figure B.3: Mode shape 2 for CSiBridge model of OSB 1 with original abutments.
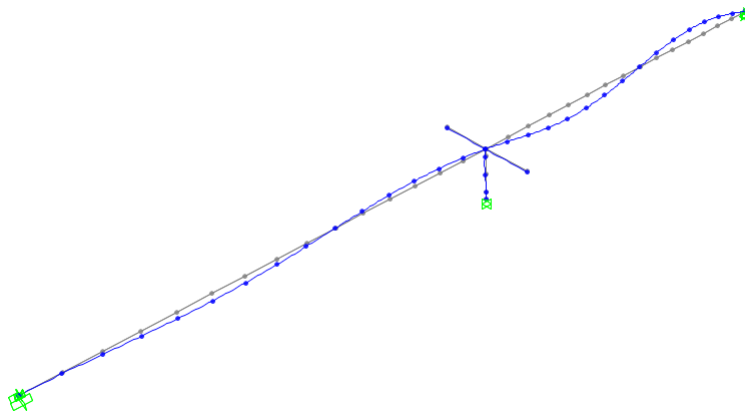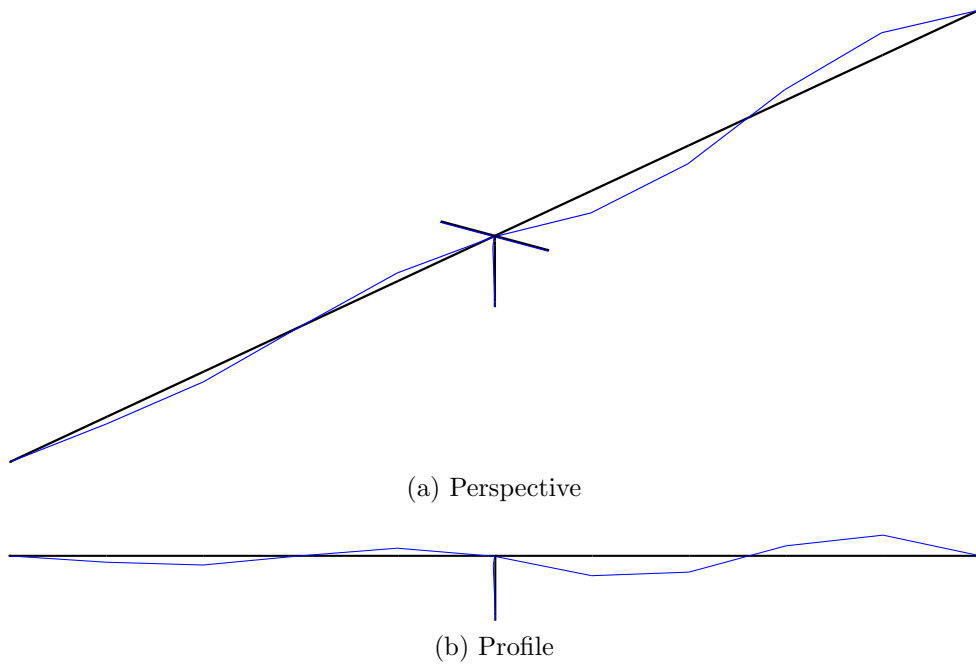

(a) Perspective

(b) Profile

Figure B.4: Mode shape 2 for OpenSees model of OSB 1 with original abutments.
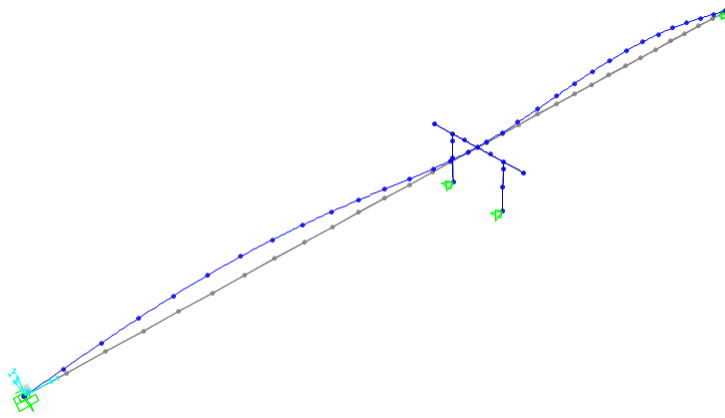
Figure B.5: Mode shape 3 for CSiBridge model of OSB 1 with original abutments.

(a) Perspective

(b) Profile
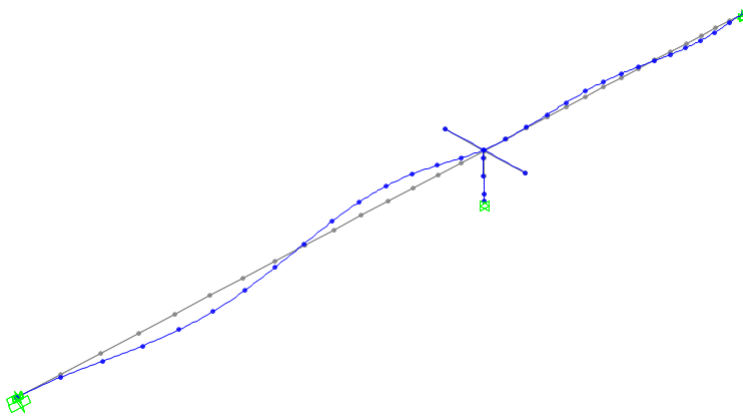
Figure B.6: Mode shape 3 for OpenSees model of OSB 1 with original abutments.

Figure B.7: Mode shape 4 for CSiBridge model of OSB 1 with original abutments.

(a) Perspective

(b) Profile

Figure B.8: Mode shape 4 for OpenSees model of OSB 1 with original abutments.

Figure B.9: Mode shape 5 for CSiBridge model of OSB 1 with original abutments.

(a) Perspective

(b) Profile

Figure B.10: Mode shape 5 for OpenSees model of OSB 1 with original abutments.
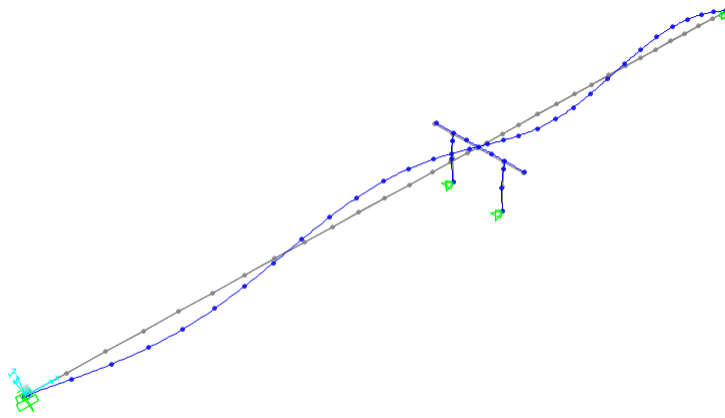
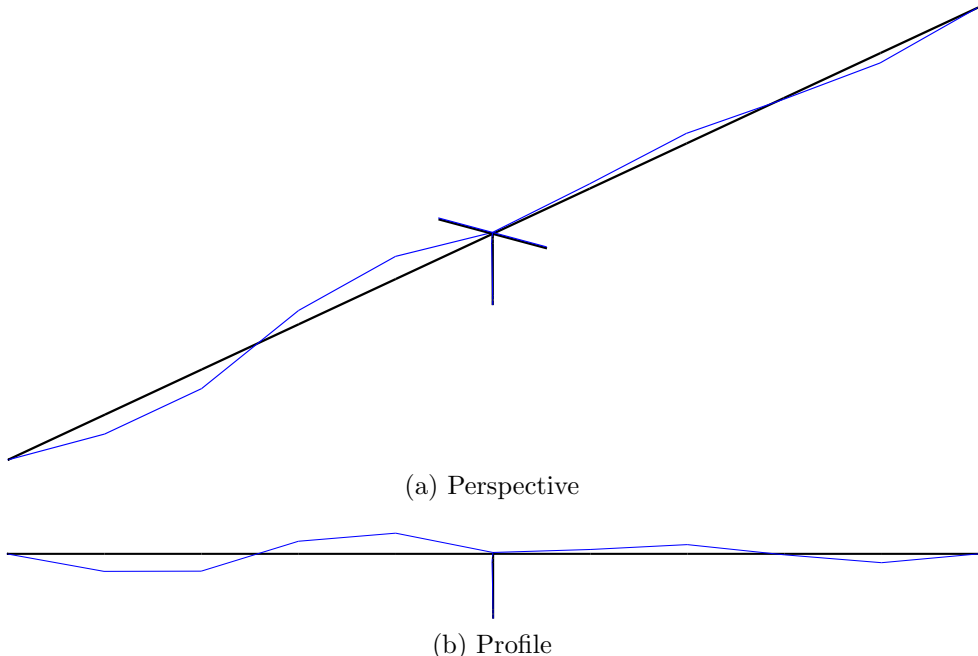Figure B.11: Mode shape 6 for CSiBridge model of OSB 1 with original abutments.

(a) Perspective

(b) Profile

Figure B.12: Mode shape 6 for OpenSees model of OSB 1 with original abutments.
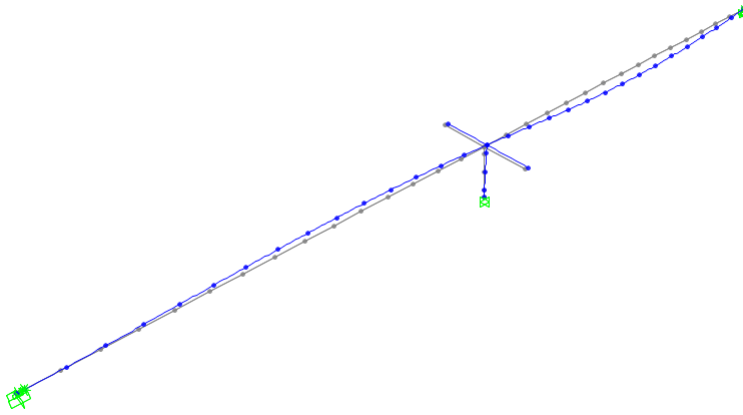
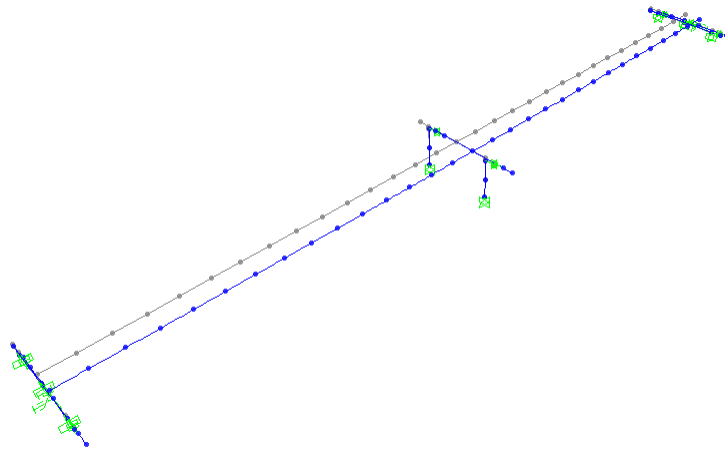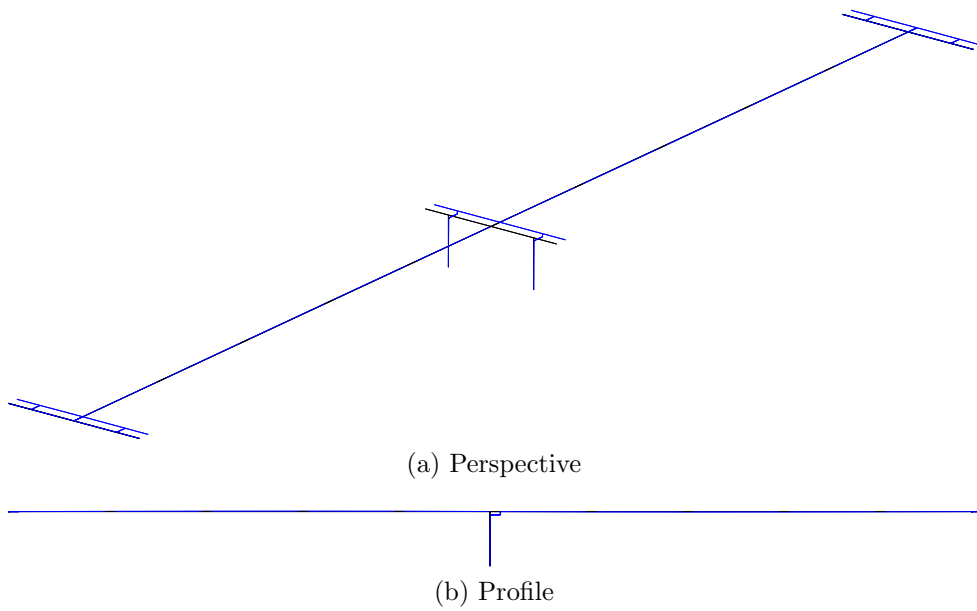Figure B.13: Mode shape 1 for CSiBridge model of OSB 2 with original abutments.

(a) Perspective

(b) Profile

Figure B.14: Mode shape 1 for OpenSees model of OSB 2 with original abutments.
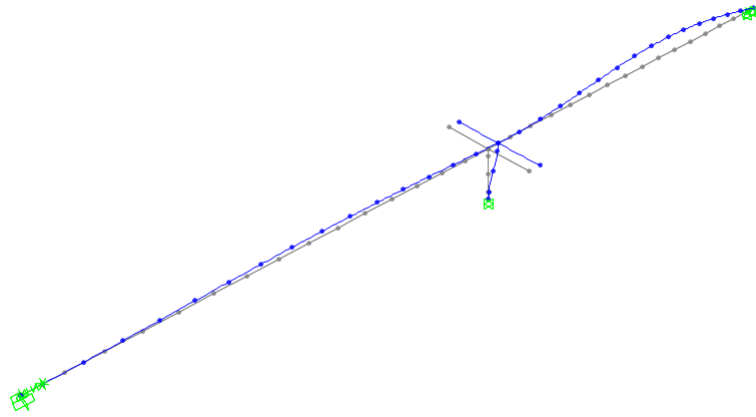
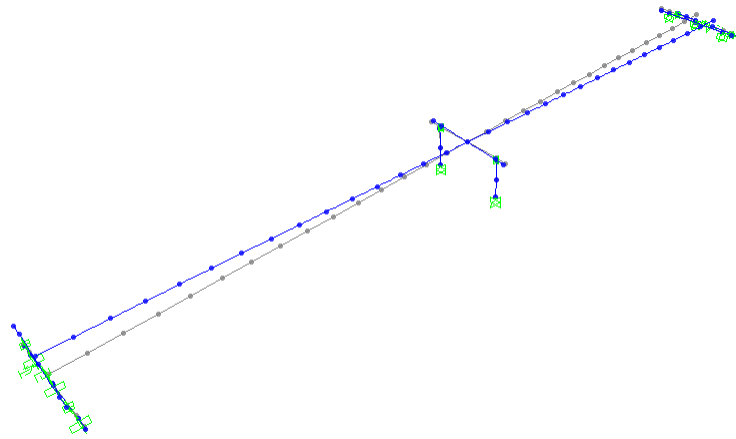Figure B.15: Mode shape 2 for CSiBridge model of OSB 2 with original abutments.

(a) Perspective

(b) Profile

Figure B.16: Mode shape 2 for OpenSees model of OSB 2 with original abutments.

246

Figure B.17: Mode shape 3 for CSiBridge model of OSB 2 with original abutments.
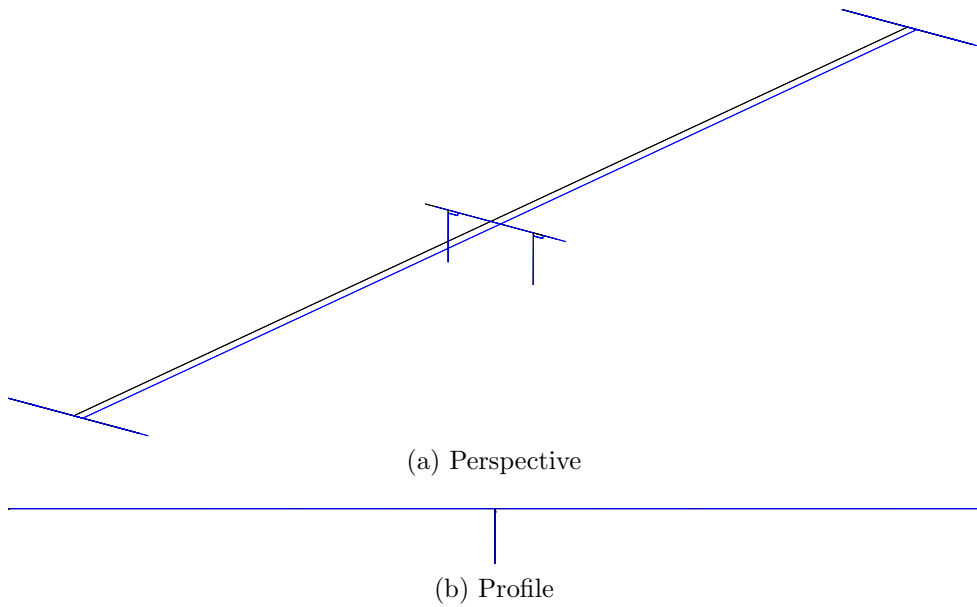

(a) Perspective

(b) Profile

Figure B.18: Mode shape 3 for OpenSees model of OSB 2 with original abutments.

Figure B.19: Mode shape 4 for CSiBridge model of OSB 2 with original abutments.

(a) Perspective

(b) Profile

Figure B.20: Mode shape 4 for OpenSees model of OSB 2 with original abutments.

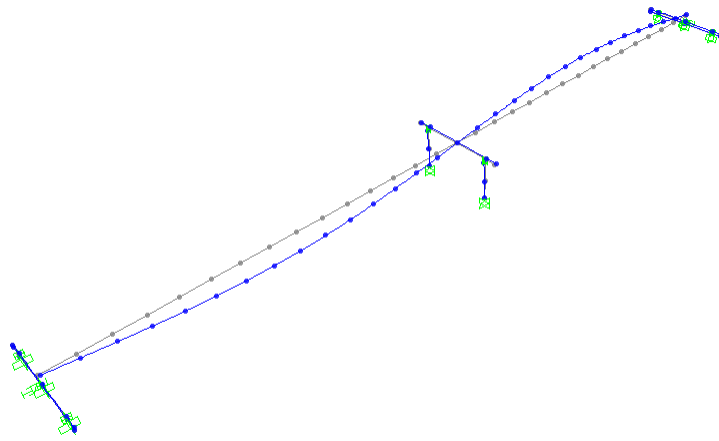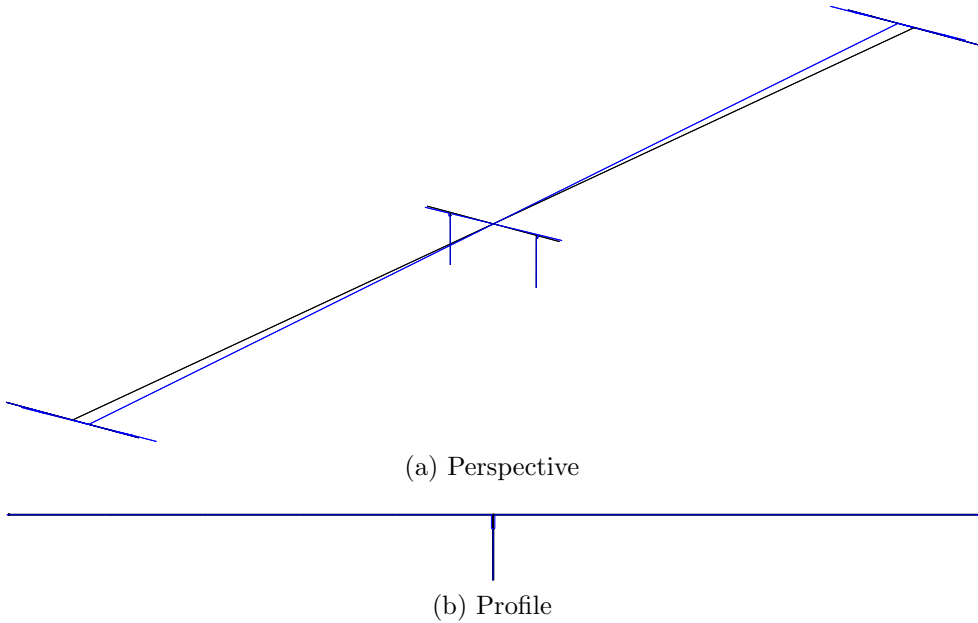Figure B.21: Mode shape 5 for CSiBridge model of OSB 2 with original abutments.

(a) Perspective

(b) Profile

Figure B.22: Mode shape 5 for OpenSees model of OSB 2 with original abutments.

Figure B.23: Mode shape 6 for CSiBridge model of OSB 2 with original abutments.
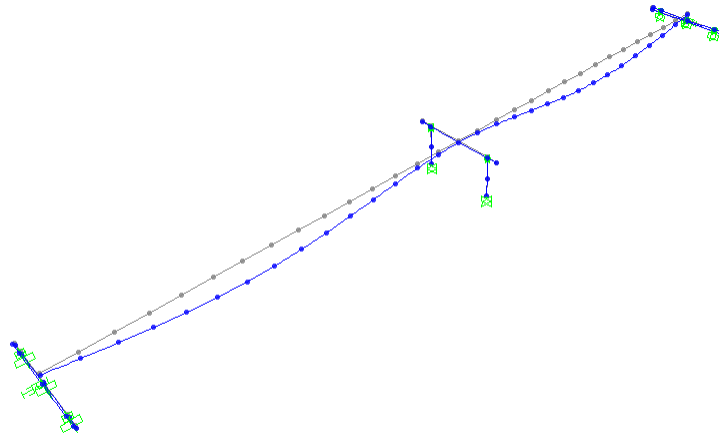

(a) Perspective

(b) Profile
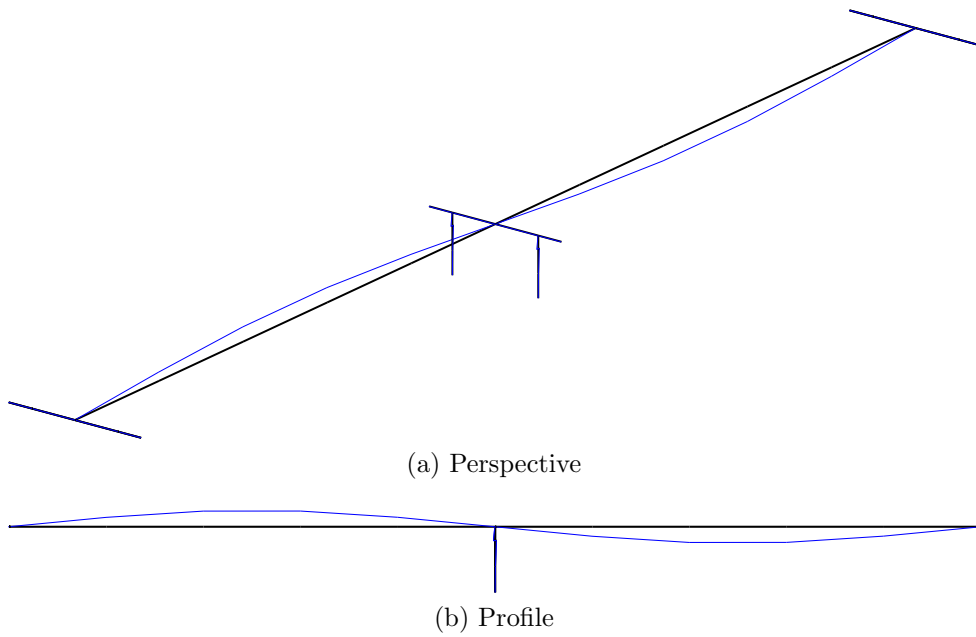
Figure B.24: Mode shape 6 for OpenSees model of OSB 2 with original abutments.

Figure B.25: Mode shape 1 for CSiBridge model of OSB 3 with original abutments.

(a) Perspective

(b) Profile

Figure B.26: Mode shape 1 for OpenSees model of OSB 3 with original abutments.

251

Figure B.27: Mode shape 2 for CSiBridge model of OSB 3 with original abutments.

(a) Perspective

(b) Profile

Figure B.28: Mode shape 2 for OpenSees model of OSB 3 with original abutments.

Figure B.29: Mode shape 3 for CSiBridge model of OSB 3 with original abutments.

(a) Perspective

(b) Profile

Figure B.30: Mode shape 3 for OpenSees model of OSB 3 with original abutments.

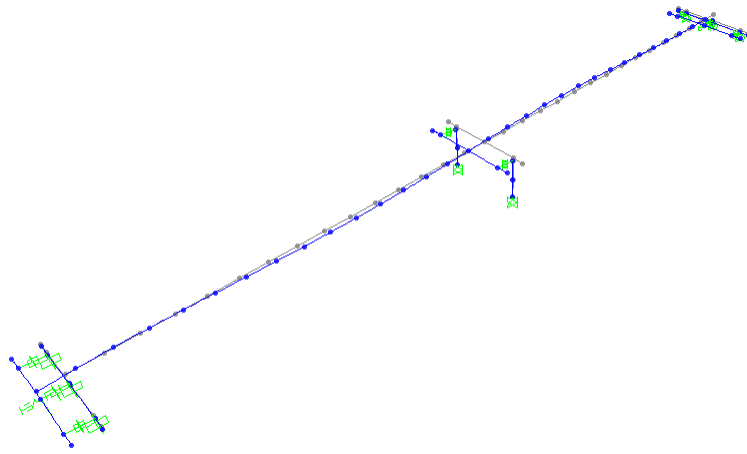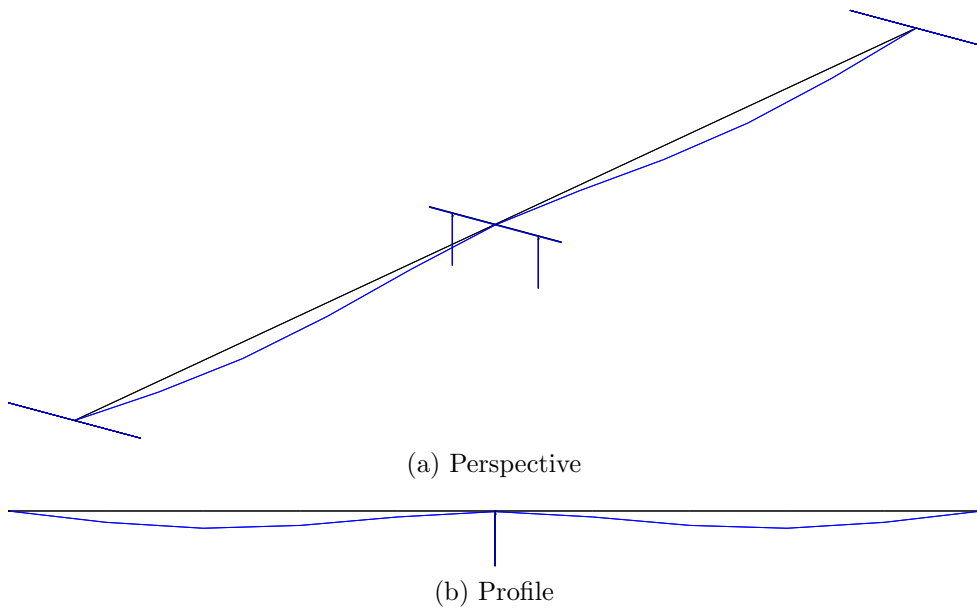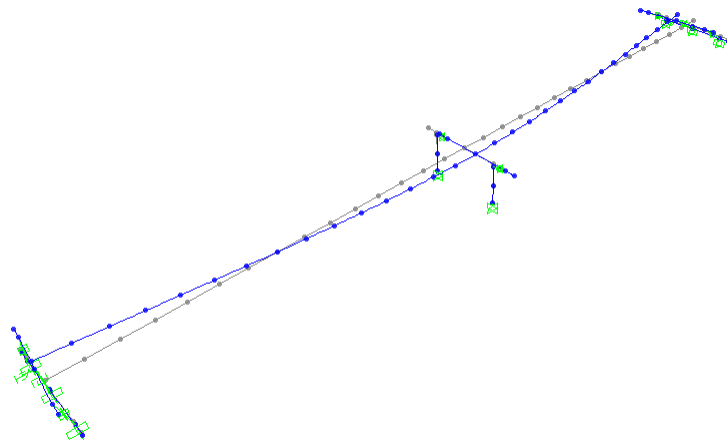Figure B.31: Mode shape 4 for CSiBridge model of OSB 3 with original abutments.

(a) Perspective

(b) Profile

Figure B.32: Mode shape 4 for OpenSees model of OSB 3 with original abutments.

254

Figure B.33: Mode shape 5 for CSiBridge model of OSB 3 with original abutments.

(a) Perspective

(b) Profile

Figure B.34: Mode shape 5 for OpenSees model of OSB 3 with original abutments.

255

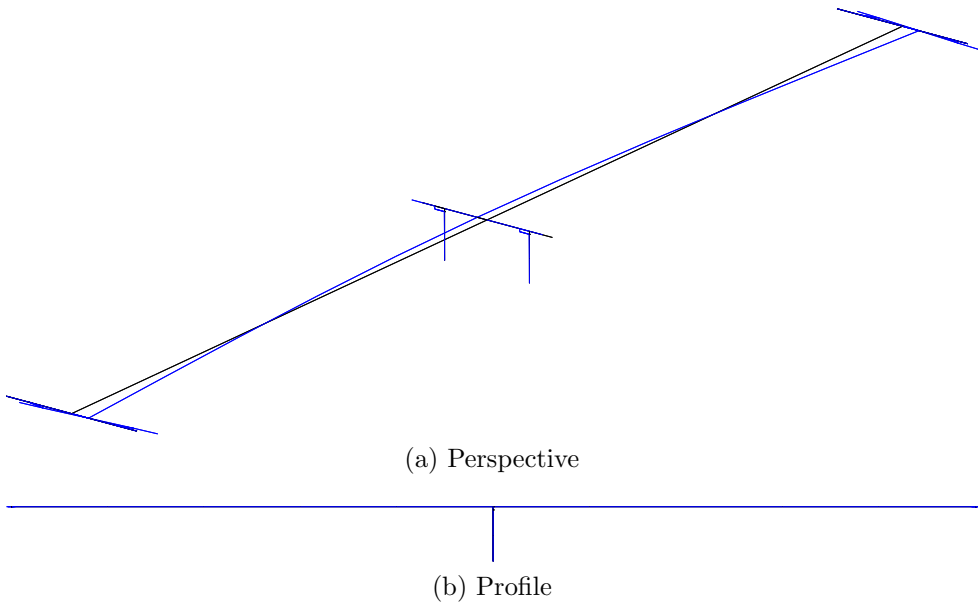Figure B.35: Mode shape 6 for CSiBridge model of OSB 3 with original abutments.

(a) Perspective

(b) Profile

Figure B.36: Mode shape 6 for OpenSees model of OSB 3 with original abutments.

256

Figure B.37: Mode shape 1 for CSiBridge model of OSB 4 with original abutments.
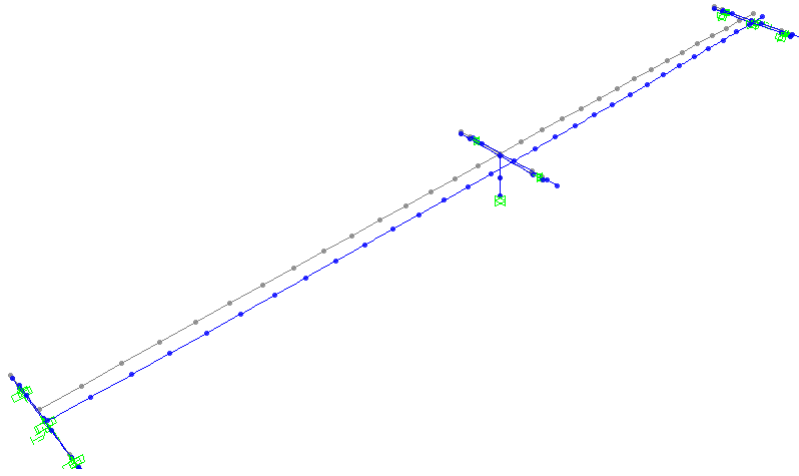
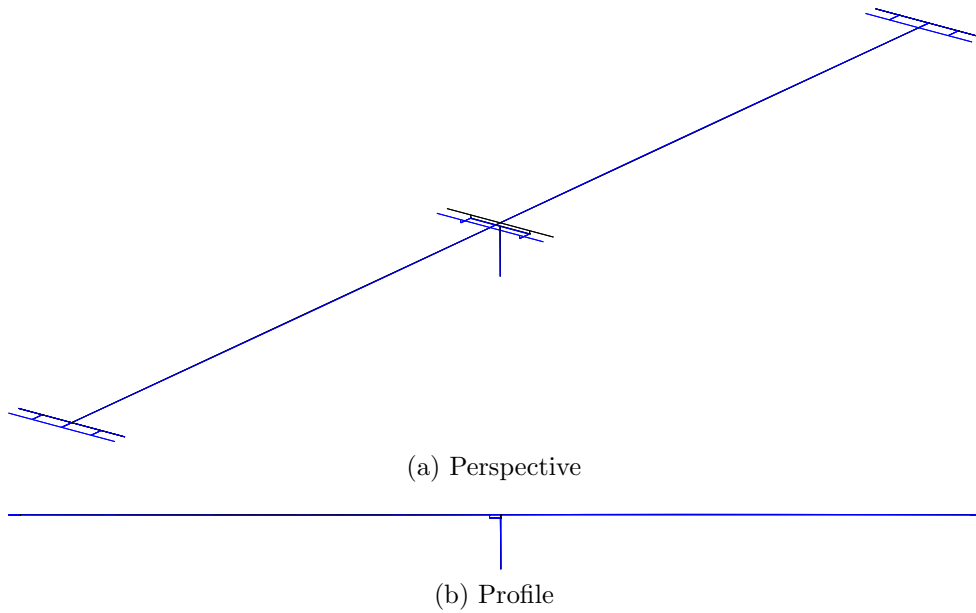

(a) Perspective

(b) Profile

Figure B.38: Mode shape 1 for OpenSees model of OSB 4 with original abutments.

Figure B.39: Mode shape 2 for CSiBridge model of OSB 4 with original abutments.

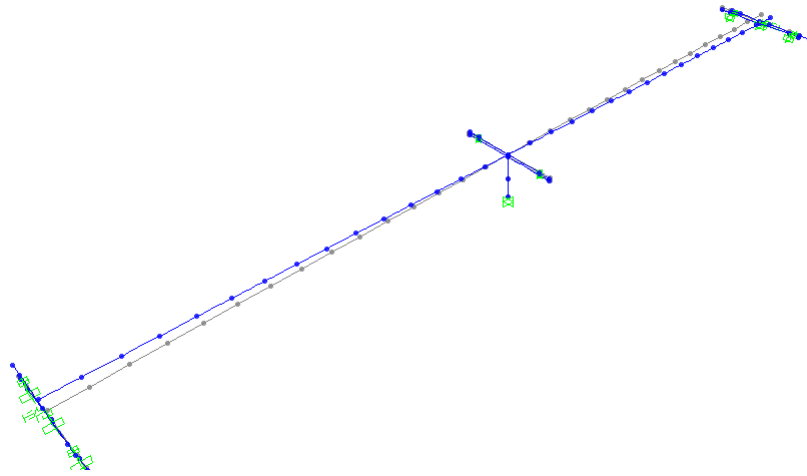

(a) Perspective

(b) Profile

Figure B.40: Mode shape 2 for OpenSees model of OSB 4 with original abutments.

Figure B.41: Mode shape 3 for CSiBridge model of OSB 4 with original abutments.

(a) Perspective

(b) Profile

Figure B.42: Mode shape 3 for OpenSees model of OSB 4 with original abutments.

259

Figure B.43: Mode shape 4 for CSiBridge model of OSB 4 with original abutments.
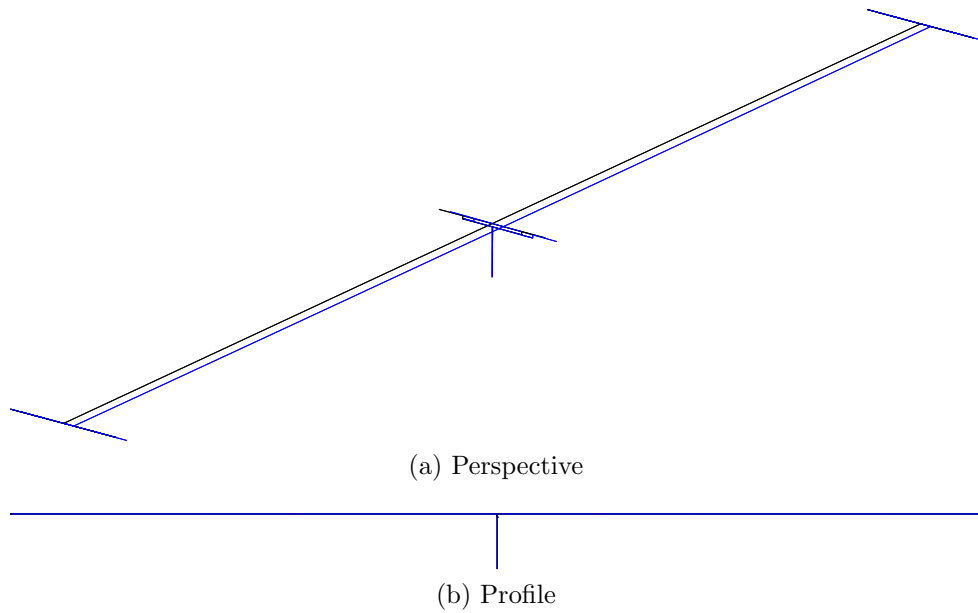
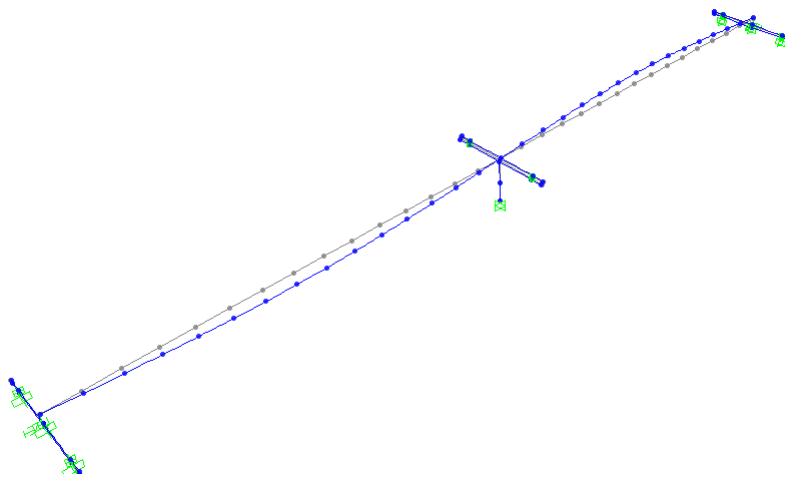

(a) Perspective

(b) Profile

Figure B.44: Mode shape 4 for OpenSees model of OSB 4 with original abutments.

Figure B.45: Mode shape 5 for CSiBridge model of OSB 4 with original abutments.

(a) Perspective

(b) Profile
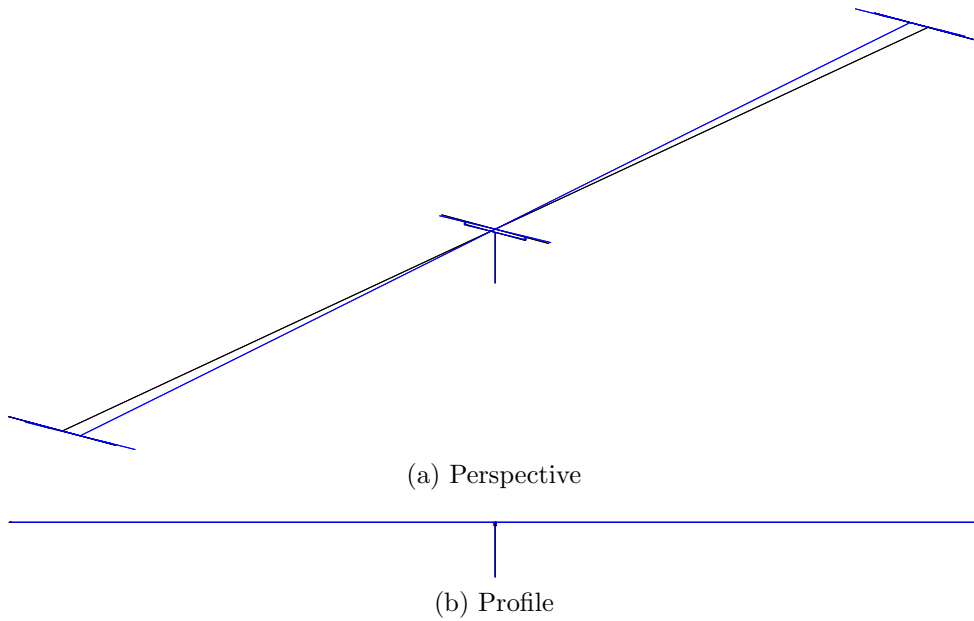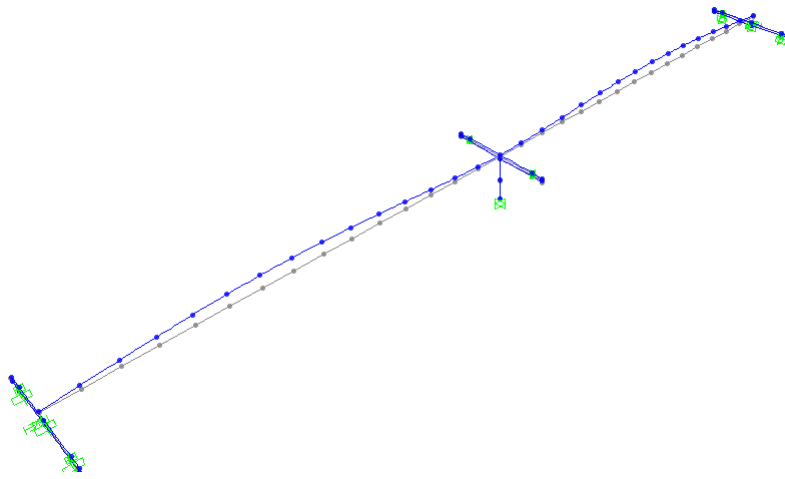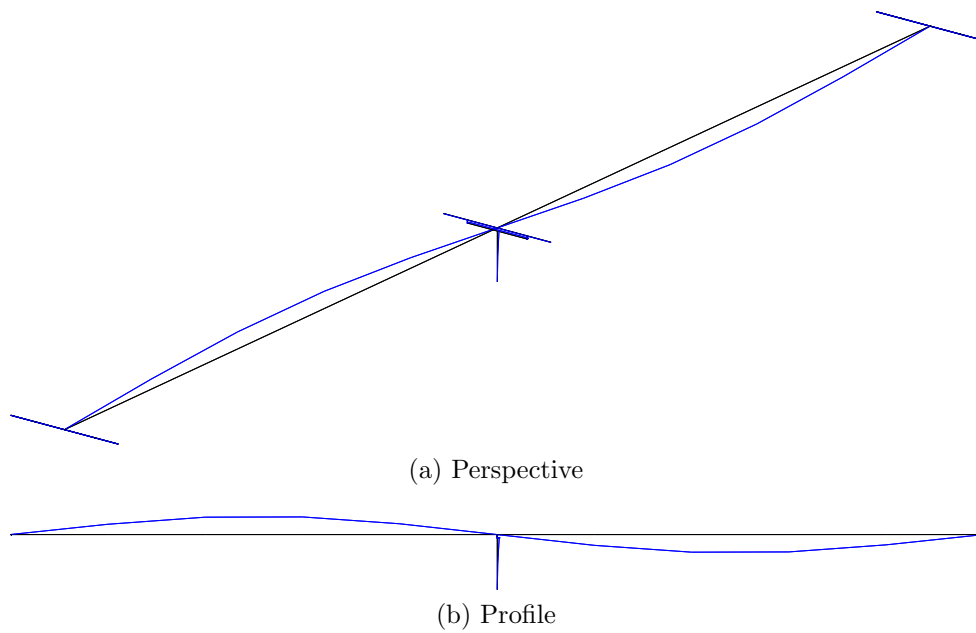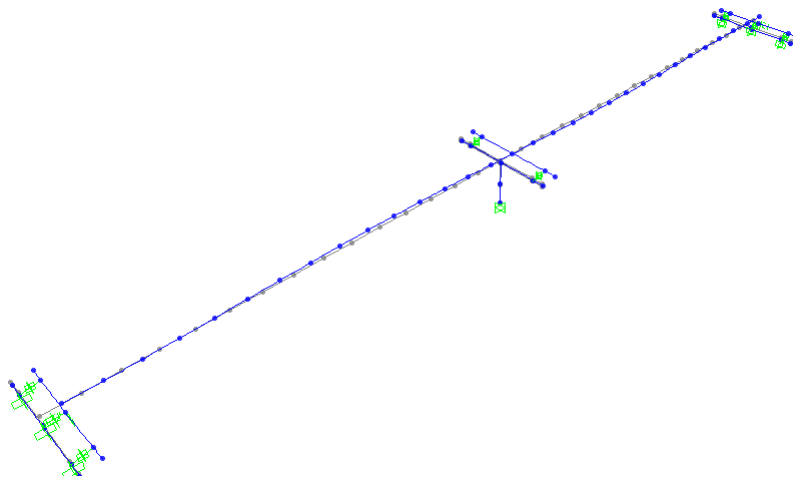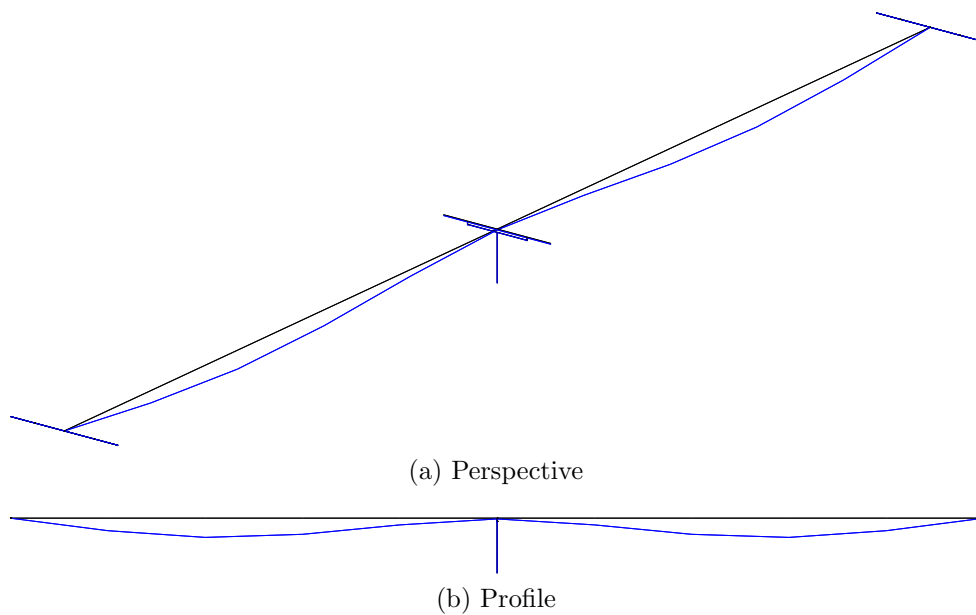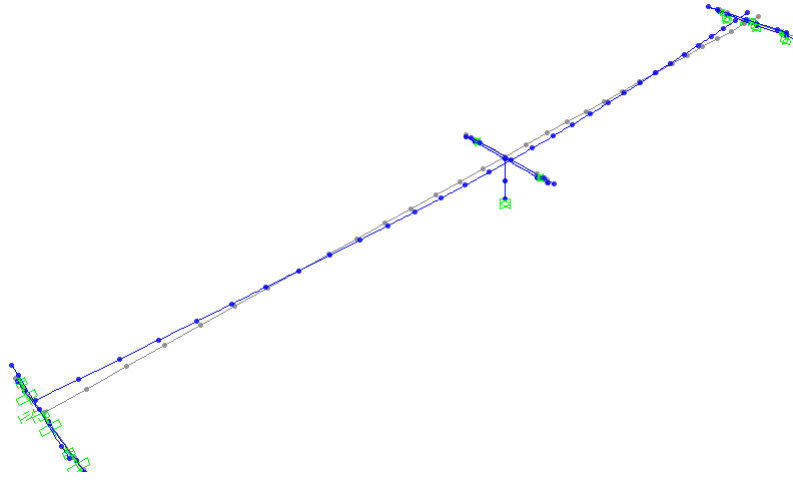
Figure B.46: Mode shape 5 for OpenSees model of OSB 4 with original abutments.

Figure B.47: Mode shape 6 for CSiBridge model of OSB 4 with original abutments.
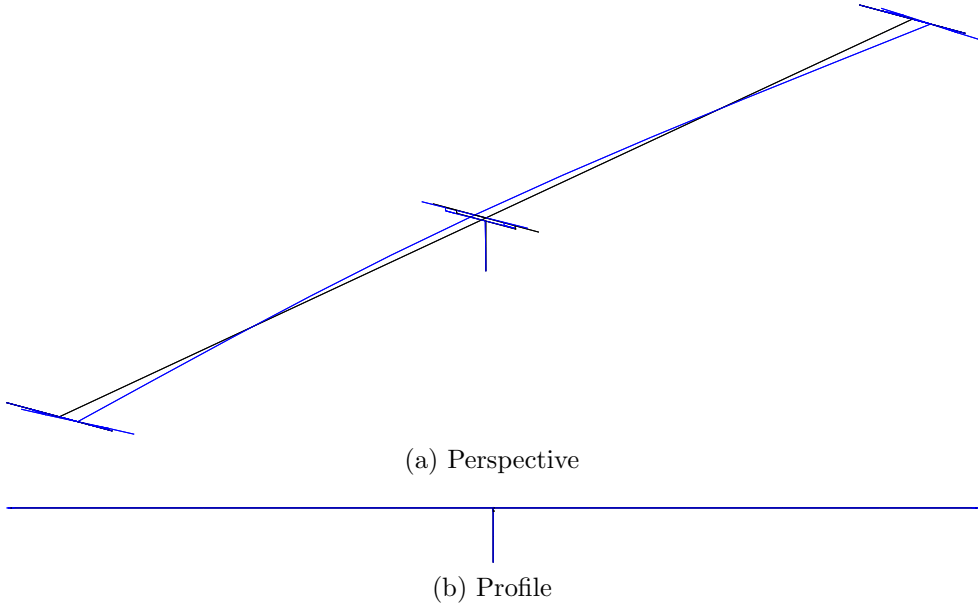

(a) Perspective

(b) Profile

Figure B.48: Mode shape 6 for OpenSees model of OSB 4 with original abutments.

262

Bibliography

[1] A. Aviram, K. R. Mackie, and B. Stojadinovic. Effect of abutment modeling on the seismic response of bridge structures. *Earthquake Engineering and Engineering Vibration*, 7(4):395–402, 2008.

[2] A. Aviram, K. R. Mackie, and B. Stojadinovic. Guidelines for nonlinear analysis of bridge structures in California. Technical Report PEER-2008/03, Pacific Earthquake Engineering Research Center, 2008.

[3] A. Aviram, K. R. Mackie, and B. Stojadinovic. Nonlinear modeling of bridge structures in california. *ACI Special Publication*, 271(1):1–26, 2010.

[4] M. P. Berry and M. O. Eberhard. Performance modeling strategies for modern reinforced concrete bridge columns. Technical Report PEER-2007/07, Pacific Earthquake Engineering Research Center, 2007.

[5] SDC Caltrans. Caltrans seismic design criteria version 1.7. *California Department of Transportation, Sacramento*, 2013.

[6] E. Choi, R. DesRoches, and B. Nielson. Seismic fragility of typical bridges in moderate seismic zones. *Engineering Structures*, 26(2):187–199, 2004.

[7] ACI Committee, American Concrete Institute, and International Organization for Standardization. Building code requirements for structural concrete (aci 318-14) and commentary. American Concrete Institute, 2014.

[8] R. A. Dameron, V. P. Sobash, and I. P. Lam. Nonlinear seismic analysis of bridge structures. foundation-soil representation and ground motion input. In *11th ADINA Conference*, Cambridge, MA, 1997.

[9] S. Erhan and M. Dicleli. Effect of dynamic soilbridge interaction modeling assumptions on the calculated seismic response of integral bridges. *Soil Dynamics and Earthquake Engineering*, 66(11):42–55, 2014.

[10] S. Erhan and M. Dicleli. Comparative assessment of the seismic performance of integral and conventional bridges with respect to the differences at the abutments. *Bulletin of Earthquake Engineering*, 13(2):653–677, 2015.

[11] G. Fenves and M. Ellery. Behavior and failure analysis of a multiple-frame highway bridge in the 1994 northridge earthquake. Technical Report 98/08, Pacific Earthquake Engineering Research Center, 1998.

[12] P. Franchin. Reliability of Uncertain Inelastic Structures under Earthquake Excitation. *Journal of Engineering Mechanics*, 130(2):180–191, 2004.

[13] A. Hajihashemi, S. Pezeshk, and E. Burdette. Effects of different support modeling assumptions on the seismic response of ordinary bridges. In *Structures Congress 2013*, Pittsburgh, PA, 2013.

[14] B. Jeremic, S. Kunnath, and L. Larson. Soil-foundation-structure interaction effects in seismic behavior of bridges. In *13th World Conference on Earthquake Engineering*, Vancouver, B.C., Canada, 2004.

[15] M. Kunde and R. Jangid. Effects of pier and deck flexibility on the seismic response of isolated bridges. *Journal of Bridge Engineering*, 11(1):109–121, 2006.

[16] S. Kunnath, T. Haukaas, B. Jeremi, P. Somerville, M. Berry, M. Eberhard, T. Haukaas, A. Kiureghian, M. Sarraf, and R. Imbsen. Application of the PEER PBEE methodology to the i-880 viaduct. Technical Report 06/10, Pacific Earthquake Engineering Research Center, Sept. 2007.

[17] O. Kwon and A. Elnashai. Fragility analysis of a bridge with consideration of soil-structure-interaction using multi-platform analysis. In *Structures Congress 2007*, Long Beach, CA, 2007.

[18] J. Lu and A. Elgamal. Parametric study of ordinary standard bridges using opensees and csibridge. Technical Report SSRP14/03, Structural Systems Research Project, Jul. 2015.

[19] K. Mackie and B. Stojadinovic. Bridge abutment model sensitivity for probabilistic seismic demand evaluation. In *Proceedings of the Third National Seismic Conference and Workshop on Bridges and Highways*, Portland, OR, 2002.

[20] R. M. Mutobe and T. R. Cooper. Nonlinear analysis of a large bridge with isolation bearings. *Computers and Structures*, 72(1-3):279–292, 1999.

[21] B. G. Nielson and R. DesRoches. Influence of modeling assumptions on the seismic response of multi-span simply supported steel girder bridges in moderate seismic zones. *Engineering Structures*, 28(8):1083–1092, 2006.

[22] R. Omrani, B. Mobasher, X. Liang, S. Gunay, K.M. Mosalam, F. Zareian, and E. Taciroglu. Guidelines for nonlinear seismic analysis of ordinary bridges: Version 2.0. Technical Report CA15-2266, STRUCTURAL ENGINEERING MECHANICS AND MATERIALS, Dec. 2015.

[23] T. Paulay and M. J. N. Priestly. *Seismic Design of Reinforced Concrete and Masonry Buildings.* John Wiley & Sons, Inc., 1992.

[24] A. Rahmani, M. Taiebat, and W. D. L. Finn. Nonlinear dynamic analysis of meloland road overpass using three-dimensional continuum modeling approach. *Soil Dynamics and Earthquake Engineering*, 57:121–132, 2014.

[25] M. Salveson and B. Fell. Effect of abutment shear keys on the seismic response of bridges. In *Structures Congress*, Las Vegas, NV, 2011.

[26] M. H. Scott, P. Franchin, G. L. Fenves, and F. C. Filippou. Response Sensitivity for Nonlinear Beam-Column Elements. *Journal of Structural Engineering*, 130(9):1281–1288, 2004.

[27] M. H. Scott and K. L. Ryan. Moment-rotation behavior of force-based plastic hinge elements. *Earthquake Spectra*, 29(2):597–607, 2013.

[28] A. Shamsabadi, P. Khalili-Tehrani, J. Stewart, and E. Taciroglu. Validated simulation models for lateral response of bridge abutments with typical backfills. *Journal of Bridge Engineering*, 15(3):302–311, 2010.

[29] A. Shamsabadi, T. Ostrom, and E. Taciroglu. Three dimensional global nonlinear time history analyses of instrumented bridges to validate current bridge seismic design procedures. In *Seminar on Utilization of Strong-Motion Data*, Los Angeles, CA, 2011.

[30] A. Shamsabadi, K. Rollins, and M. Kapuskar. Nonlinear soilabutmentbridge structure interaction for seismic performance-based design. *Journal of Geotechnical and Geoenvironmental Engineering*, 133(6):707–720, 2007.

[31] Y. Zhang, Z. Yang, J. Bielak, J. Conte, and A. Elgamal. Treatment of seismic input and boundary conditions in nonlinear seismic analysis of a bridge ground system. In *16th ASCE Engineering Mechanics Conference*, Seattle, WA, 2003.